2017

Multi-Scale Methodologies for Probabilistic Resilience Assessment and Enhancement of Bridges and Transportation Systems

Aman Karamlou
Lehigh University

Multi-Scale Methodologies for Probabilistic Resilience Assessment and Enhancement of Bridges and Transportation Systems

by

Aman Karamlou

Presented to the Graduate and Research Committee

of Lehigh University

in Candidacy for the Degree of

Doctor of Philosophy

in

Structural Engineering

Lehigh University

Bethlehem, PA

January 2017

Approved and recommended for acceptance as a dissertation in partial fulfillment of the requirements for the degree of Doctor of Philosophy.

Date

Dr. Paolo Bocchini
Dissertation Advisor

Accepted Date

Committee Members:

Dr. James Ricles
Committee Chairperson

Dr. Stephen Pessiki
Committee Member

Dr. Clay Naito
Committee Member

Dr. Leonardo Dueñas-Osorio
External Member

Maybe, just maybe, there is no purpose in life. But if you linger a while longer in this world, you might discover something of value in it, like how you discovered that flower. Or, how I discovered you one fateful night.

Lord Orochimaru

*To **Marina** who gave my life a new meaning and purpose*

Acknowledgments

I would like to express my sincere gratitude to my mentor and research advisor, Prof. Paolo Bocchini for his support, advice, and patience during the past few years. I am truly honored to work under his supervision. He has turned this chapter of my life to an amazing experience which I am very proud of. I could have not asked for a better advisor.

I would also like to acknowledge the members of my dissertation committee, Prof. James Ricles the chair of the committee, as well as Prof. Stephen Pessiki, Prof. Clay Naito, and Prof. Leonardo Dueñas-Osorio for their time and effort. Their guidance and suggestions at different stages of this research have improved the quality of this work.

This research has been supported by different institutions and funding agencies. The financial support from the Department of Civil and Environmental Engineering at Lehigh University, P.C. Rossin College of Engineering and Applied Science, ATLSS Engineering Research Center, Pennsylvania Department of Transportation, and Kern Entrepreneurial Engineering Network (KEEN) Initiative is greatly appreciated. The support provided by the National Science Foundation through award CMMI - 1541177 is gratefully acknowledged.

I would like to appreciate Peter Bryan and the specialists at the High Performance Computing Center at Lehigh University including Alex Pacheco and Steve Anthony for their help and technical support.

Many thanks to my good fiends Mr. Hossein Ghodsi and his lovely wife Mrs. Parastoo Fotoohi with whom I started this journey and they have been like my brother and sister ever

since. I would like to thank my uncle Mr. Shahin Heshmat and his wife Dr. Maryam Azizi for all their help and support. Their hospitality made the transition to my new life in the United States very smooth in the first days of my arrival.

Many thanks to my friends and colleges at ATLSS center at Lehigh University; Vasileios Christou, Cristina Cercone, Samantha Sabatino, Georgios Tsampras, Tugce Akbas, Alysson Mondoro and many others. You have been a great source of support and motivation and I have learned a great deal from every single one of you. The memory of the lunch times and the conversations will stay in my mind for eternity.

I would like to express my deepest appreciation to my family. In particular, my mother from whom I learned to be patient, and my father from whom I learned to work hard. Their support and sacrifices are the first reason that I made it this far.

Finally, I would like to thank my beautiful fiancée, Marina, without whom I can not imagine my life. Your patience is embedded in every single word of this dissertation. I look forward to the next chapter of my life with you. The world looks more beautiful through your eyes.

Table of Contents

List of Tables

List of Figures

Notation

Abbreviations

AMIGO	Algorithm with multiple-input genetic operators, page 147
CDF	Cumulative distribution function, page 23
CPM	The critical path method, page 91
CSUS	Central and Southern United States, page 25
DOT	Department of transportation, page 29
EDP	Engineering demand parameter, page 136
FFS	Fragility functionality surface, page 122
FQ-IDCVT	Functional Quantization-Infinite-Dimensional Centroidal Voronoi Tessellation, page 180
IDA	Incremental dynamic analysis, page 22
K-S	Kolmogorov-Smirinov goodness of fit test, page 63
MILP	Mixed integer linear programming, page 90
MOEA	Multi-objective evolutionary algorithms, page 171
MSC	Multi-Span Continuous, page 50
MSSS	Multi-Span Simply Supported, page 50

NSGA	Non-dominated sorting genetic algorithm, page 150
NTHA	Nonlinear time-history analysis, page 22
PDF	Probability distribution function, page 48
PEER	Pacific earthquake engineering research center, page 125
PGA	Peak ground acceleration, page 26
PSDA	Probabilistic seismic demand analysis, page 22
PSDM	Probabilistic seismic demand model, page 23
PSHA	Probabilistic seismic hazard analysis, page 46
PTR	Potential Temporary Repair, page 108
RCPSP	Resource constrained project scheduling problem, page 89
Sa	Spectral acceleration, page 26
Sd	Spectral displacement, page 26
SN	Strike normal, page 132
SP	Strike parallel, page 132
$\overline{\text{SSD}}$	Transitive closure of SSD matrix, page 96
SSD	The start-start distance matrix, page 96
SSS	The serial scheduling scheme, page 92
USGS	United States Geological Survey, page 76

Greek Symbols

α	Model parameter, page 40
β_C	Logarithmic standard deviation of capacity distribution, page 24
$\beta_{D\|IM}$	Logarithmic standard deviation of demand, page 23
β	Model parameter, page 40
δ_{max}	Maximum deformation, page 104
Γ	Network performance index, page 41
Γ^0	Network performance index for the cases where all the bridges are out of service, page 41
Γ^{100}	Network performance index for the cases where all the bridges are in service, page 41
γ_D	Cost balancing factors associated with the distance traveled by the passengers, page 41
γ_T	Cost balancing factors associated with the time spent by the passengers, page 41
λ	Lognormal distribution parameter (mean of the associated normal distribution), page 56
$\lambda_X(x)$	Mean annual frequency of exceeding the random variable X, page 125
$\lambda_{IM}(im)$	Mean annual frequency of exceeding the intensity measure *im*, page 125
μ	Mean value, page 56
μ_c	Maximum curvature ductility ratio, page 57
$\nu(i)$	The priority value of task j, page 92

$\Phi[\cdot]$ Standard normal cumulative distribution function, page 23

$0\tilde{\rho}_b$ Bridge restoration priority, page 173

πBr_{rt} The number of resources of type r available at time t, page 92

ρ_i Resilience factor, page 36

σ standard deviation, page 56

θ Angle of seismic incidence, page 134

Θ_t The set of tasks being executed at time t, page 92

ζ Lognormal distribution parameter (standard deviation of the associated normal distribution), page 56

Roman Symbols

a Power model regression parameter, page 22

a_d Decay control parameter, page 36

Ab_{Ad} Abutment maximum displacement in active direction, page 57

Ab_{Pd} Abutment maximum displacement in passive direction, page 57

b Power model regression parameter, page 22

Br_i Availability of resource type i, page 89

br_{ij} The amount of resource j required for the execution of task i, page 89

$Brdg$ Bridge *Meta-Component*, page 138

c_{ij}^0 Time to cover the segment ij at free flow, page 40

c_b^d The minimum time required to cover the detour of bridge b, page 40

c_{ij} Time to cover the segment ij, page 40

C_i Capacity with respect to limit state i, page 21

CO_c Construction cost of the structure, page 46

CO_{dir} Expected direct loss, page 46

$\hat{c}_b(r_b)$ The cost of retrofitting the bth bridge considering the selected retrofit technique r_b, page 178

CET_c Restoration end time of component c, page 97

Cs Conjunction set, page 94

$CW_{\hat{p}}$ Weighting factor reflecting the importance of fixing the connectivity between the nodes pair $\hat{p}$, page 158

$\tilde{d}_i$ An upper bound for LFT_i, page 95

D Demand of the investigated component or system, page 21

d_b^d Detour length of bridge b, page 41

d_i Demand realization of the ith sample in PSDA, page 23

d_{ij} Length of the highway segment ij, page 41

DR_d Damage ratio associated with the damage state d, page 46

DS Damage (limit) state, page 45

t_s Time when the effects of the disruptive event is stabilized, page 37

ndc Bridge damage configuration, page 131

Dec_i The decision set at stage i of SSS, page 92

Δl_{greedy}	The number of tasks added to the partial solutions at each step of the greedy algorithm, page 153
dls_i	Damage limit state threshold i, page 21
DM	Damage measure, page 125
dm	Damage measure threshold, page 125
D_n	Kolmogorov-Smirinov goodness of fit parameter, page 66
Ds	Disjunction set, page 94
$DS0$	Zero (initial) damage state, page 97
$DS_c(t)$	Damage state of cth component at time t, page 97
dsc_d	dth bridge damage scenario, page 99
DV	Decision variable, page 125
dv	Decision variable threshold, page 125
e^j	Disruptive event j, page 37
E_i	Event i, page 24
EDP	Engineering demand parameter, page 57
EFT_i	The earliest finish time of task i, page 92
Ep	Set of precedence relations, page 89
EST_i	The earliest start time of task i, page 91
f	Generic resilience function, page 34
$F(t)$	Performance function, page 37

f_{ij}^{c} Practical flow capacity of segment ij, page 40

F_0 Performance of the system at its original state, page 36

f_b^d Practical capacity the detour of bridge b, page 40

F_d Performance of the system immediately after the disruption, page 36

F_r Performance of the system at a new stable level, page 36

f_{ij} Flow of segment ij, page 40

$F_{ls}(im)$ Fragility at intensity meaure value of im and for limit state ls, page 21

fb_d Fixed bearing maximum deformation, page 57

$FFS_{fls}(t,im)$ Fragility functionality surface with respect to the functionality limit state fls at time t and given the level of the intensity measure im, page 123

fls A functionality limit state, page 123

FM Functionality measure, page 126

$fm(t)$ Time variant functionality measure value, page 126

FT_i The finish time of task i, page 92

GD General distance measure, page 171

H Vector of discrete time steps, page 91

HP12a Level2 solution for probabilistic seismic demand analysis, page 57

HP12 Level3 solution for probabilistic seismic demand analysis, page 57

HP1 Level1 solution for probabilistic seismic demand analysis, page 57

hp1 Lognormality assumption, page 45

hp2a	Power model assumption, page 45
hp2b	Constant dispersion assumption, page 45
HResc	High level resource availability for restoration, page 114
I	Set of all nodes of the network, page 41
IM	Intensity measure, page 21
im	Realization of intensity measure, page 21
nIM	Total number of values of intensity measures, page 45
IF_{ij}	The influence factor of the segment ij, page 182
IF_{total}	The total influence factor, page 182
IMmaps	Intensity measure maps, page 180
J	Subset of nodes connected to node i, page 41
l	Lower bound of the uniform distribution, page 56
l^0_{greedy}	The length of initial partial solutions used for greedy algorithm, page 153
LAb	Bridge left abutment, page 102
LAbAP	Left abutment-approach *Meta-Component*, page 138
LAbF	Bridge left abutment foundation, page 102
LAp	Bridge left approach slab, page 102
LBnt	Left bent *Meta-Component*, page 138
LC	Bridge left column, page 102

LCF	Bridge left column foundation, page 102
Learnall	Learn-all scheduling scheme, page 88
Learnot	Learn-not scheduling scheme, page 89
LR	Bridge left fixed bearings, page 102
LFT_i	The latest finish time of task i, page 91
$\bar{l}_{ij}$	The length of the segment ij influenced by the functionality of its bridges, page 182
l_{ij}	The total length of the segment ij, page 182
lo^s	The last task in trial solution $\mathbf{x^s}$ that starts and has an impact on the objective(s), page 152
$L_{\hat{p}}$	The level of the connectivity between node pair $\hat{p}$, page 159
LR	Bridge left rocker bearings, page 102
LResc	Low level resource availability for restoration, page 114
LST_i	The latest start time of task i, page 91
m	Number of resource types, page 89
MR	Bridge middle fixed bearings, page 102
MR	Bridge middle rocker bearings, page 102
N	Number of samples, page 23
n	number of project tasks, page 89
nc	Number of components of a system, page 34

nDS	Total number of damage states defined for the system, page 45
nb	The total number of bridges in the network, page 178
nd	Number of bridge damage scenarios considered, page 99
nDC	Number of unique bridge damage configurations, page 131
NHP	Level0 solution for probabilistic seismic demand analysis, page 57
$n\hat{p}$	The number of node pairs which need to be connected urgently, page 158
nr_b	Total number of retrofit techniques applicable to bridge b, page 178
NSA_{max}	Number of simultaneous activities, page 149
obj_i	The value of the i objective, page 151
$\hat{p}$	A node pair whose highway connectivity has priority, page 158
$P[\cdot]$	Probability, page 21
p_i	Duration of task i, page 89
pd_i	The shortest Euclidean distance between the member i from PF_{known}, and members of PF_{true}, page 171
$PF_{current}$	Pareto front solutions obtained at the end of each generation, page 172
PF_{known}	A set of Pareto optimal solutions, page 171
PF_{true}	Global Pareto optimal solutions, page 171
PF_{true}	Global Pareto optimal solutions, page 171
PI_i	The set of all immediate predecessors of task i, page 92
$popsize$	Population size, page 151

$Prep$	Preparation tasks, page 86
PRF	Probabilistic resilience failure, page 178
Ps	Parallelity set, page 94
P_V	The space of all possible permutations of vector V, page 150
$\acute{Q}_{ij}$	The contribution of the segment ij to the functionality of the system, page 181
$\bar{Q}$	Loss of functionality, page 123
$\check{Q}$	Expected functionality, page 45
$\hat{Q}(t)$	Total bridge functionality at time t (before application of the window function), page 100
$Q(t)$	Time variant measure of the system functionality, page 34
$Q_c(t)$	Functionality of cth component, page 34
$Qflow$	Transportation network functinality metric based on traffic flow, page 41
qA_i	Functionality assigned to task i, page 99
$QA_i(t)$	Bridge functionality with respect to ith task at time t, page 99
$Qconn$	Connectivity-based transportation network functionality metric, page 158
$Qcons(t)$	Bridge functionality at time t considering all construction tasks, page 100
$qdsc_d$	Functionality assigned to dsc_d, page 99
$Qdsc_d(t)$	Bridge functionality with respect to dsc_d at time t, page 99
QS_{ij}	The functionality of segment ij, page 182

$Qsft(t)$ Bridge functionality at time t considering all safety damage scenarios, page 99

$\bar{R}$ Loss of resilience, page 34

$\tilde{r}_i$ A lower bound for EST_i, page 95

R Resilience, page 35

rb_d Rocker bearing maximum deformation, page 57

$RP(t)$ Real performances of the system at time t, page 35

RAb Bridge right abutment, page 102

RAbAP Right abutment-approach *Meta-Component*, page 138

RAbF Bridge right abutment foundation, page 102

RAp Bridge right approach slab, page 102

r_b Integer number reflecting the retrofit technique assigned to bridge b, page 178

RBnt Right bent *Meta-Component*, page 138

RC Bridge right column, page 102

rc_{cl} The replacement cost of bridge b, page 162

$\overline{rc}_{cl}$ Mean replacement cost of class cl bridges, page 162

RCF Bridge right column foundation, page 102

R_{cr} Critical resilience threshold, page 178

Reg Regular tasks, page 86

RR Bridge right fixed bearings, page 102

RR	Bridge right rocker bearings, page 102
Rsc	Set of renewable resources, page 89
$\check{S}$	The schedule vector representing the start time of the activities of the project, page 149
S_c	Median of capacity, page 24
S_D	Median of demand, page 22
S_p	Speed of recovery, page 36
Sch_i	The scheduled set at stage i of SSS, page 92
$ssd_i j$	Component ij of the SSD matrix, page 96
$ssd_i j$	Component ij of the transitive closure of SSD matrix, page 96
ST_i	Start time of task i, page 94
T	Upper bound for project duration, page 91
t_0	Occurrence time of the disruption, page 34
t_δ	Slack time, page 36
t_h	Time horizon, page 35
t_r	Time of full restoration, page 34
t_r^*	Time to complete initial recovery actions, page 36
$TP(t)$	Target performances of the system at time t, page 35
$t_{cl,rc_b}^{DS0}(Q_b)$	Time required to restore functionality Q_b of bridge b of class cl (major or conventional) with initial damage state $DS0$ and restoration cost of rc_b, page 162

t_e	Time of occurrence of the disruptive event e^j, page 37
$Temp$	Temporary repair tasks, page 86
TRC	The total retrofit cost of all bridges in the network, page 178
t_s	Restoration initiation time, page 37
TTS	Total travel distance covered by all passengers traveling in the network in one hour, page 41
TTT	Total travel time spent by all passengers traveling in the network in one hour, page 41
u	Upper bound of the uniform distribution, page 56
V	Set of project tasks, page 89
$x_{i,t}$	Binary design variable for solving RCPSP using MILP, page 90
$\mathbf{x^s}$	Array of tasks in a representing a trial solution for the optimization problem solved by *AMIGO*, page 150

Abstract

When an extreme event occurs, such as an earthquake or a tsunami, the amount of socio-economic losses due to reduced functionality of infrastructure systems over time is comparable to or even higher than the immediate loss due to the extreme event itself. Therefore, one of the highest priorities of owners, disaster management officials, and decision makers in general is to have a prediction of the disaster performance of lifelines and infrastructures a priory considering different scenarios, and be able to restore the functionality in an efficient manner to the normal condition, or at least to an acceptable level during the emergency, in the aftermath of a catastrophe. Along the line of this need, academic research has been focused on the concept of infrastructure resilience, which reflects the ability of structures, infrastructure systems, and communities to both withstand against and quickly recover functionality after an extreme event.

Among infrastructure systems, transportation networks are of utmost importance as they allow people to move from damaged to safe areas and rescue/recovery teams to effectively accomplish their mission. Moreover, the functionality and restoration of several other infrastructure systems and socio-economic units of the community is highly interdependent with transportation network performance. Among different components of transportation networks, bridges are among of the most vulnerable and need a particular attention.

To this respect, *this research is mostly focused on* ***quantification****, and* ***optimization*** *of the* ***functionality*** *and* ***resilience*** *of* ***bridges*** *and* ***transportation networks*** *in the aftermath of extreme events, and in particular earthquakes, considering the underlying uncertainties*.

The scope of the study includes: (i) accurate\efficient assessment of the seismic fragility of individual bridges; (ii) development of a technique for assessment of bridge functionality and its probabilistic characteristics following an earthquake and during the restoration process; (iii) development of efficient optimization techniques for post-event restoration and pre-event retrofit prioritization of bridges; (iv) development of metrics and formulations for realistic quantification of the functionality and resilience of bridges and transportation networks.

The evaluation of the damage and its probabilistic characteristics is the first step towards the assessment of the functionality of a bridge. In this regard, a simulation-based methodology was introduced for probabilistic seismic demand and fragility analyses, aimed at improving the accuracy of the resilience and life-cycle loss assessment of highway bridges. The impact of different assumptions made on the demand was assessed to determine if they are acceptable. The results show that among different assumptions, the power model and constant dispersion assumption introduce a considerable amount of error to the estimated probabilistic characteristics of demand and fragility. The error can be prevented using the introduced simulation-based technique, which takes advantage of the computational resources widely available nowadays.

A new framework was presented to estimate probabilistic restoration functions of damaged bridges. This was accomplished by simulating different restoration project scenarios, considering the construction methods common in practice and the amount of resource availability. Moreover, two scheduling schemes were proposed to handle the uncertainties in the project scheduling and planning. The application of the proposed methodology was presented for the case of a bridge under a seismic scenario. The results show the critical impact of temporary repair solutions (e.g., temporary shoring) on the probabilistic characteristics of the functionality of the bridge during the restoration. Thus, the consideration of such solutions in probabilistic functionality and resilience analyses of bridges is neces-

sary. Also, a considerable amount of nonlinearity was recognized among the restoration resource availability, duration of the restoration, and the bridge functionality level during the restoration process.

A new tool called "*Functionality-Fragility Surface*" (*FFS*) was introduced for pre-event probabilistic recovery and resilience prediction of damaged structure, infrastructure systems, and communities. *FFS* combines fragility and restoration functions and presents the probability of suffering a certain functionality loss after a certain time elapsed from the occurrence of the extreme event, and given the intensity of the event. *FFS*s were developed for an archetype bridge to showcase the application of the proposed tool and formulation.

Regarding network level analysis, a novel evolutionary optimization methodology for scheduling independent tasks considering resource and time constraints was proposed. The application of the proposed methodology to multi-phase optimal resilience restoration of highway bridges was presented and discussed. The results show the superior performance of the presented technique compared to other formulations both in terms of convergence rate and optimality of the solution. Also, the computed resilience-optimal restoration schedules are more practical and easier to interpret. Moreover, new connectivity-based metrics were introduced to measure the functionality and resilience of transportation networks, to take into account the priorities typically considered during the medium term of the disaster management.

A two-level simulation-based optimization framework for bridge retrofit prioritization is presented. The objectives of the upper-level optimization are the minimization of the cost of bridge retrofit strategy, and probabilistic resilience failure defined as the probability of post-event optimal resilience being less than a critical value. The combined effect of the uncertainties in the seismic event characteristics and resulting damage state of bridges are taken into account by using an advanced efficient sampling technique, and fragility

analysis. The proposed methodology was applied to a transportation network and different optimal bridge retrofit strategies were computed. The technique showed to be effective and efficient in computing the optimal bridge retrofit solutions of the example transportation network.

Chapter 1

Introduction

1.1 Motivation

The devastating outcome of several events such as 1906 San Francisco, 1925 Santa Barbara, and 1933 Long Beach earthquakes triggered the development of seismic design codes and regulations for California as well as other disaster prone regions. Therefore, many researchers focused on studying and developing resistant structural components and systems, in order to reduce the direct losses and disruptions. Since then, the records have shown that, over time, the overall extent of property losses and causalities per earthquake have declined substantially, due to better design and performance of individual components and structures (Poland 2009a, 2011). However, in many cases, society suffered extensively from the indirect losses and long-term socio-economic disruption, mostly due to poor emergency response and long lasting lack of functionality of the key services such as infrastructures (e.g., hospitals and transportation networks), lifelines (e.g., water pipes and power grids), and businesses. This, in fact, encouraged researchers from several academic fields, as well as disaster officials, to pay paramount attention to the topics of disaster management and restoration activities, to make communities more resilient.

The notion of resilience, which was first propounded by ecologists in 1973, has been adopted and reformed by engineers to study and evaluate the response and recovery of communities from unavoidable losses after natural (e.g., earthquake and flood) or human induced (e.g., terrorists attacks) disasters (Boon 2014; Bruyelle et al. 2014; Bausch et al.

2013). Resilience is defined as the ability of physical or social units to absorb perturbation and recover to a reasonable level of functionality in an efficient manner. During the last decade, the research community has focused its efforts to introduce, define and formulate the concept of disaster resilience, as well as evaluate the resilience of different structures, infrastructure systems, and communities. Today, thanks to the advances in designing and developing disaster (in particular earthquake) resistant structures and systems, casualties can be prevented considerably. Therefore, after fulfilling the life-safety goal, resilience is the next phase in disaster risk reduction and loss mitigation policies. However, still further attention is required from the research community, as well as disaster officials and policy makers to implement this concept in practice.

To be disaster resilient, a community should be able to maintain both its physical (e.g, structures and infrastructure systems) and socio-economic elements (e.g., jobs and businesses) acceptably serviceable and operational after a disruption, and quickly recover from the damage. In this way, the community would be able to restart its natural activities as soon as possible. Nowadays, the life of the modern society is highly reliant on its critical infrastructures, such as healthcare facilities, water and electric suppliers. In particular, transportation networks are of utmost importance, as the operation of other social and physical components of the community is highly interdependent with the functionality of these lifelines (Rinaldi et al., 2001). Regarding the emergency situations, transportation networks are the major backbone to provide goods and emergency aids to the damaged regions. In particular, the presence of a functional transportation network facilitates the emergency activities carried out immediately after an event, and expedites the repair of damage to other structures and infrastructures during the recovery phase. Therefore, transportation networks need particular attention when assessing the resilience of communities. Despite their importance, in several past extreme events, transportation networks in the impacted regions were not able to fulfill their expected function, because of the demand im-

posed to their components (e.g., 1971 San Fernando, 1989 Loma Prieta (EERI, 1994), 1994 Northridge (Hall, 1994), 1995 Kobe (Comartin et al., 1995), and 2011 Christchurch earthquakes (Wilkinson et al., 2011)). The functionality of transportation networks is threatened by different factors (e.g., closure of roads due to collapse-generated debris or landslide), among which damage to the bridges is one of the most common and critical (EERI, 1994; Hall, 1994; Comartin et al., 1995; Wilkinson et al., 2011).

To this respect, the research community has performed extensive research to unfold different aspects of resilience of transportation networks. This includes the quantification, assessment, and improvement of resilience of transportation systems and their components. Along this line, the current research aims to address some of the major missing links in resilience and functionality evaluation and prediction of individual bridges and bridge systems. These include the accurate computation of bridge restoration functions considering the underlying uncertainties in damage and restoration process, and efficient restoration and retrofit prioritization of bridges in transportation networks. The following section discusses the objectives of this research.

1.2 Research Objectives

This research studies different aspects of transportation disaster resilience, at both component and system levels. Throughout this study, transportation systems are considered to be composed of networks of highways and roads, as well as bridges. Considering their vulnerability, and their role in the performance of transportation networks, bridges are considered the main focus of this study. Figure 1.1 shows different aspects and components of transportation resilience studies. These include the assessment of damage, restoration, and functionality of bridges, as well as the quantification, enhancement, and optimization of resilience of transportation networks, considering the underlying uncertainties. The ob-

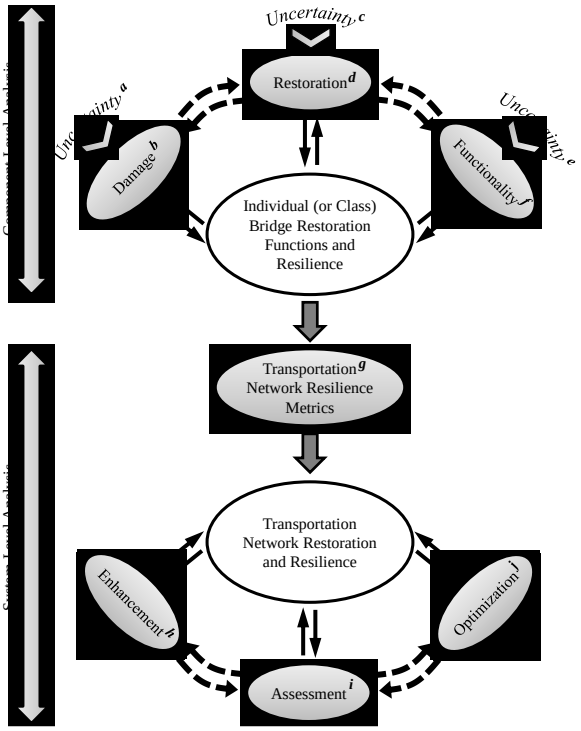

Figure 1.1: Bridge and transportation network resilience assessment diagram

jectives of the current research cover several of the components presented in Figure 1.1. Table 1.1 shows the components of transportation resilience studies (marked by letters in Figure 1.1) addressed by each objective of this dissertation, as discussed in the following. At the component level, the main objectives of this research can be broken down to the following items:

1. To develop a technique to accurately quantify the disaster-induced damage of individual (or class of) bridges, in a probabilistic manner, considering the uncertainties involved in response and capacity of bridge structures.

2. To develop a framework to estimate the recovery functions of individual bridges, in a probabilistic manner, considering the uncertainties involved in the restoration process.

3. To present comprehensive probabilistic formulations and tools to compute the vul-

Table 1.1: Component of transportation resilience addressed by each objective

Objectives	Components covered[1]
Objective-1	*a,b*
Objective-2	*b,c,d,e,f*
Objective-3	*a,b,c,d,e,f*
Objective-4	*g,i*
Objective-5	*h,j*
Objective-6	*a,b,c,d,e,f,g,h,i,j*

[1]Letters refer to the components presented in Figure 1.1

nerability of bridges with respect to loss of functionality in the aftermath of extreme events.

At the system level, the current research aims to achieve the following objectives:

4. To propose metrics and formulations to realistically and efficiently quantify and estimate the functionality and resilience of transportation networks, considering the restoration goals typically considered by disaster managers and communities.

5. To develop an efficient optimization methodology for post-event restoration prioritization of damaged bridge networks, capable of solving large scale real world problems, and considering multiple resilience-based objectives.

6. To develop a framework for optimal proactive resilience improvement of bridge networks, taking into account the uncertainties in seismic hazard intensity and damage level of bridges.

1.3 Research Scope

In the following, a brief overview of the steps taken to achieve the objectives of this research is presented. Also, Figure 1.2 illustrates the connection among these steps.

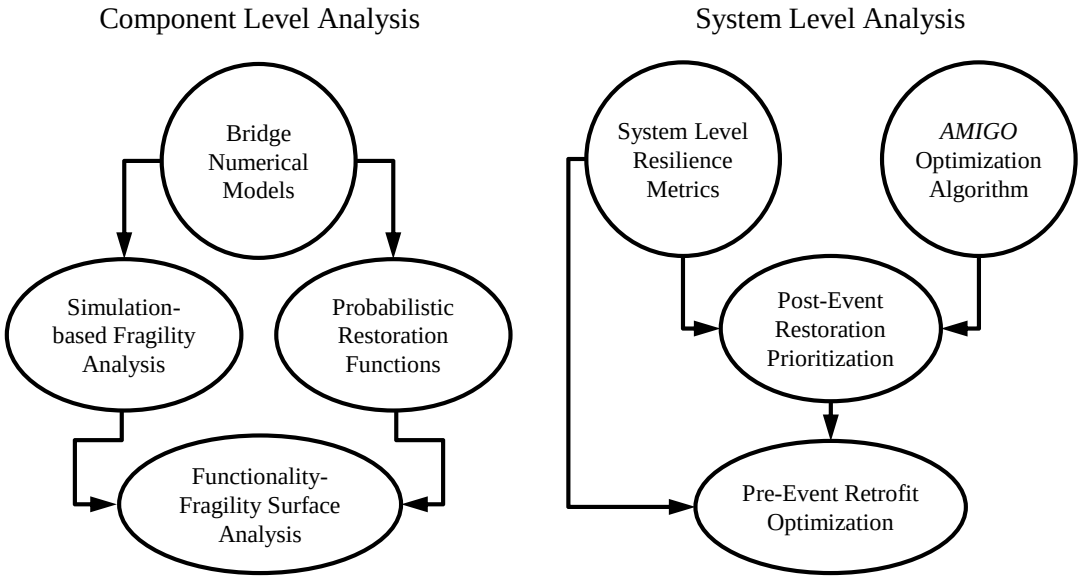

Figure 1.2: Connection between different research tasks in the dissertation

1. **Development of a simulation-based technique for fragility analysis**

   One of the first steps towards the assessment of resilience of transportation systems is the evaluation of damage and vulnerability of bridges, considering the underling uncertainties in the response and capacity of their components (Figure 1.1, items *a* and *b*). This is done by performing probabilistic demand and fragility analyses. Several simplifying assumptions are traditionally made to improve the computational efficiency of estimating demand and fragility. These include demand and capacity lognormality assumption, power model, and constant dispersion assumption. Yet, the impact of such assumptions on the results of fragility analysis has not been fully investigated. To this respect, methodologies typically used for probabilistic seismic demand and fragility analysis of bridges are reviewed and the common assumptions made on the probabilistic distribution of demand parameters are identified. A simulation-based technique is proposed, which avoids such assumptions on the demand. In particular, the approximations introduced to the estimated probabilistic characteristics of demand and fragility by the lognormality assumption, power model, and constant dispersion assumption are prevented using the proposed

methodology. This technique relies on the contemporary computational resources to perform large-scale and extensive simulations.

2. **Bridge numerical model development**

   To showcase the proposed fragility analysis methodology [scope item (1)], and to evaluate the impact of the common assumptions (made on the demand) on the estimated fragility, numerical models of a (bridge) cantilever column, a Multi-Span Simply Supported (MSSS) Steel Girder bridge, and a Multi-Span Continuous (MSC) Steel Girder bridge are developed in the OpenSees platform (McKenna et al., 2000). Detailed models are utilized for different components of the modeled structures to fully capture the sophisticated nonlinear behavior of the materials during the seismic excitation.

3. **Assessment of the accuracy of the common assumptions on the demand**

   Probabilistic seismic demand and fragility analyses are carried out on the developed structural models [scope item (2)], using the most common techniques, as well as the proposed methodology [scope item (1)]. The impact of the common assumptions on the estimated parameters of the demand, probability of failure (fragility), life-cycle loss, and resilience is quantified. The results specify the assumptions which are the major sources of error in the computation of the aforementioned parameters.

4. **Development of a technique for probabilistic restoration curve analysis**

   As shown in Figure 1.1, the assessment of the restoration and functionality of bridges is one of the key components of transportation network resilience analysis. Such information is typically presented in the form of restoration functions, which provide the evolution of the functionality by time, following the extreme event and during the recovery phase. Despite their importance, the currently available bridge restoration functions are too idealized and not fully applicable to individual bridge or network resilience evaluations. Also, many available restoration functions are associated to

bridges with a single damaged component. The transition of such models to restoration functions of bridges with multiple damage configurations is not clear. Several researchers have tried to address this problem by defining system (i.e., bridge) level damage states, which itself adds to the level of complexity of the problem. To this respect, a new simulation-based methodology to estimate probabilistic restoration functions for damaged bridges is developed. The proposed technique computes the functionality of bridges by detailed assessment of the restoration process of the damaged bridge components in a probabilistic way. In particular, the restoration schedule of the bridge is obtained through a mathematical optimization, given the restoration tasks of its components, as well as a number of logical-practical construction considerations and logistic constraints. The proposed methodology is capable of computing the restoration functions for bridges with multiple damaged components and multiple damage configurations. Therefore, the difficulties associated with defining bridge level damage states and their connection with component level damage states are bypassed. Moreover, two scheduling schemes are proposed to handle the uncertainties involved in the project scheduling. The residual functionality of the bridge is obtained from the restoration schedule by taking into account a number of safety- and construction-induced traffic disruptions during the repair process. Samples of bridge restoration functions can be generated using this technique, which can be used to assess the probabilistic characteristics of the functionality at different time steps during the restoration process.

5. **Computation of probabilistic restoration functions**

   To showcase the application of the proposed methodology to compute bridge restoration functions [scope item (4)], the restoration tasks and their properties (e.g., duration distribution, resource consumption, and precedence relations) for different components of the previously modeled MSSS Steel Girder bridge [scope item (2)] are

identified. The bridge is subjected to a ground shaking scenario and the probabilistic restoration functions and repair durations are computed using the proposed technique.

6. **Functionality-fragility surface analysis**

   To integrate all components of bridge resilience analysis (i.e., damage, restoration, and functionality as shown in Figure 1.1), a new tool, called *Functionality-Fragility Surface* (*FFS*) is introduced. *FFS* combines fragility and restoration functions and can be used for pre-event probabilistic prediction of recovery and resilience of structures, infrastructure systems, and communities.

7. **Demonstration of techniques for the computation of *FFS*s**

   To show the simplicity of the computation of *FFS*s using the available data, *FFS*s are computed using available fragility and restoration functions provided by HAZUS (DHS, 2009). Also, a novel technique is presented to compute more accurate *FFS*s, by combining the fragility and restoration curve methodologies developed in this research [in scope items (1) and (4)]. To showcase the application, a complete fragility and probabilistic restoration curve analysis is carried out on a MSSS Steel Girder bridge [scope item (2)], and *FFS*s are computed using the proposed technique.

8. **Network level performance and resilience metrics**

   One of the key steps in the transition from component level to system level resilience analysis is the definition and evaluation of relevant system resilience functions and metrics. Such formulations are used to integrate the functionality and resilience of components (e.g., bridges) and translate them to the system (e.g., transportation networks) resilience (Figure 1.1 item *g*). To this respect, in this scope, two connectivity-based functionality metrics are introduced for the assessment of the performance of transportation networks. Compared to the functionality metrics based on modeling congestion, the proposed metrics are more computationally efficient, which makes

them suitable for large scale applications and extensive iterative computations. Also, they can be used to better reflect the behavior and concerns of disaster managers during different restoration phases.

9. **Development of optimization algorithms for post-event restoration prioritization**

   Resilience of transportation networks can be considerably improved by following a more efficient restoration procedure for their damaged components, in particular bridges. Optimization techniques can be used to find the best restoration process and to maximize the resilience of the system. However, typically solving such optimization problems is computationally expensive, in particular for the case of real-world transportation networks with several damaged bridges. To this respect, a novel evolutionary optimization methodology called "*Algorithm with Multiple-Input Genetic Operators*" (*AMIGO*) for scheduling independent tasks considering resource and time constraints is formulated. The formulations and algorithms of the genetic operators specialized for *AMIGO* are developed. *AMIGO* is designed to be more efficient and can be used for large scale optimization problems, such as bridge network resilience and restoration optimizations.

10. **Demonstration of the application and performance of *AMIGO***

    The application of *AMIGO* [scope item (9)] to multi-phase optimal resilience restoration scheduling of highway bridges is presented and discussed. The quality of the solution and efficiency of *AMIGO* are demonstrated through the application to a large scale real world transportation network subjected to an earthquake scenario. The results are compared to the solutions obtained by other optimization methodologies and formulations. Metrics and formulations developed in this research [scope item (8)] are used to quantify the resilience of the investigated transportation network.

11. **Development of an algorithm for optimal retrofit of resilient transportation net-**

works

In addition to an efficient post-event restoration process [scope item (9)], resilience of transportation networks can be improved by retrofitting the vulnerable bridges in the system. In this scope item, the two solutions are brought together in the form of an optimization problem. To this respect, a two-level simulation-based optimization analysis is presented to obtain different tradeoffs for both pre-event retrofit and post-event restoration of bridges, considering the post-event resilience of the transportation network and pre-event cost of retrofitting as the main objectives of the optimization problem. A Genetic Algorithm with a bi-objective mixed-integer programming formulation is used to compute the optimal retrofit strategies. The proposed framework integrates several aspects of component and system level transportation resilience analysis, and their underlying uncertainties. These include bridge damage (Figure 1.1 item a and b), restoration (Figure 1.1 item d), functionality (Figure 1.1 item f), and transportation system resilience (Figure 1.1 items g, h, i, and j).

12. **Demonstration of the application of the algorithm for retrofit optimization**

    The application of the developed algorithm [scope item (11)] is showcased on an artificial transportation network with 8 bridges. Hazard quantization (Christou and Bocchini, 2015) and fragility curves are used to take into account the uncertainties in hazard and bridge damage. *AMIGO* [scope item (9)] is used for resilient post-event restoration optimization. Metrics and formulations developed in this research [scope item (8)] are used to quantify the resilience of the investigated transportation network.

1.4 Outline of the Dissertation

This dissertation consists of eight chapters. The content of each chapter is summarized in the following.

Chapter 1 presents the overview and motivation of this research, as well as the general objectives and scope of the study. Moreover, the outline of the dissertation is presented in this chapter.

Chapter 2 reviews the background on the different topics covered by this research. This includes the current state-of-the-art techniques and methodologies on probabilistic demand, fragility, functionality, restoration, recovery, and resilience analyses. Considering the focus of this dissertation, more emphasis is placed on the techniques and formulations developed for seismic analysis of bridges and transportation networks.

Chapter 3 investigates the effect of three common assumptions typically made on the probabilistic distribution of engineering demand parameters for the case of seismic fragility analyses of bridges: demand lognormality assumption, power model, and constant dispersion assumption. A simulation-based methodology is proposed, which avoids such assumptions on the demand. The resulting increase in accuracy is estimated on structural models of different complexity (a bridge cantilever column, a Multi-Span Simply Supported Steel Girder bridge, and a Multi-Span Continuous Steel Girder bridge). Most importantly, the quantitative impact of the assumptions is assessed in the context of a life-cycle loss estimation and resilience analysis.

Chapter 4 investigates how the damage induced by the extreme event affects the restoration process and functionality of bridges. To this respect, first a brief review of the shortcomings of the currently available bridge restoration functions for resilience analysis is presented. To overcome the shortcomings, a new comprehensive framework to estimate probabilistic restoration functions for damaged bridges is proposed. The scheduling algorithms and mathematical formulations developed for the proposed methodology are presented in this chapter. This includes the description of the Resource Constrained Project Scheduling Problem (RCPSP) used to model the restoration process of bridges. Also, a Mixed-Integer

Linear Programming (MILP) formulation used to solve RCPSP is presented. To take into account the uncertainties in construction scheduling and also in flow of information, two simulation-based scheduling schemes are presented in this chapter. The proposed scheduling schemes allow to generate samples of the restoration schedule of the bridge, which can be used to generate bridge sample restoration functions. A number of pre-processing algorithms is also presented to improve the computational efficiency of the solution of RCPSP. These are the Critical Path Method, the Serial Scheduling Scheme, and Constraint Propagation technique. The formulations and considerations associated with the assessment of the functionality during the restoration of the bridge is also presented in this chapter. A detailed application of the technique is presented for the case of a MSSS Steel Girder bridge (presented first in Chapter 3), numerically analyzed for a seismic event scenario. The probabilistic restoration functions are computed using different proposed scheduling schemes and considering different levels of restoration resources availability.

Chapter 5 integrates the ideas presented in Chapter 3 and Chapter 4. To this respect, this chapter introduces the "*Functionality Fragility Surface*" (*FFS*), which is a tool for probabilistic functionality and resilience evaluation of damaged structures, infrastructure systems, and communities. The general concept, essential components, and formulation of *FFS* are presented. As an application, *FFS*s are computed for a bridge class using the fragility and restoration curves obtained from HAZUS (DHS, 2009). Moreover, a technique is proposed to compute *FFS* more accurately using the fragility and restoration curve methodologies proposed in Chapters 3 and 4, respectively. A complete set of fragility curves and probabilistic restoration functions are computed for a MSSS Steel Girder bridge, and used to develop *FFS*s.

Chapter 6 presents a system (i.e., transportation network) level restoration and resilience analysis, considering the impact of damaged components (i.e., bridges). To this respect, a novel evolutionary optimization methodology called "*Algorithm with Multiple-*

Input Genetic Operators" (*AMIGO*) is introduced for scheduling independent tasks considering resource and time constraints. The customized solution representation and genetic operators (i.e., initial population generator, mutation and crossover operators) are presented in this chapter. The application of *AMIGO* to multi-phase optimal resilience and restoration scheduling of highway bridges is presented and discussed. Moreover, a new transportation performance metric and bridge restoration model are proposed for a more realistic computation of the resilience. The quality of the solution and efficiency of *AMIGO* are demonstrated through the application to a large transportation network with 238 bridges, subjected to an earthquake scenario. Also, the convergence quality of *AMIGO* is compared to other optimization formulations.

Chapter 7 extends the idea in Chapter 6 from post-event to pre-event analysis. To this respect, a two-level simulation-based optimization analysis is presented to obtain different tradeoffs for both pre-event retrofit and post-event restoration of bridges, considering post-event resilience of the transportation network and pre-event cost of retrofitting as the main objectives of the optimization problem. A Genetic Algorithm with a bi-objective mixed-integer programming formulation is presented to compute the optimal retrofit strategies. Moreover, a new network performance metric is proposed for more computationally efficient calculation of the post-event resilience.

Chapter 8 summarizes the research carried out in this dissertation and provides recommendations for future studies and investigations.

Chapter 2

Research Background

2.1 Introduction

A review of the previous research conduced on the topics covered by the current study is presented in this chapter. The assessment and study of resilience of large systems (e.g., transportation networks) requires several detailed steps and analyses at the level of the components of the system, as well as the system itself. Figure 2.1 illustrates such procedure, schematically. This includes the evaluation of the damage, restoration, and functionality of the components of the system. The aggregation of the results can be used to assess the damage, restoration, functionality, and resilience of the system or system of systems as shown in Figure 2.1.

Considering transportation systems resilience as the main focus of this research, the

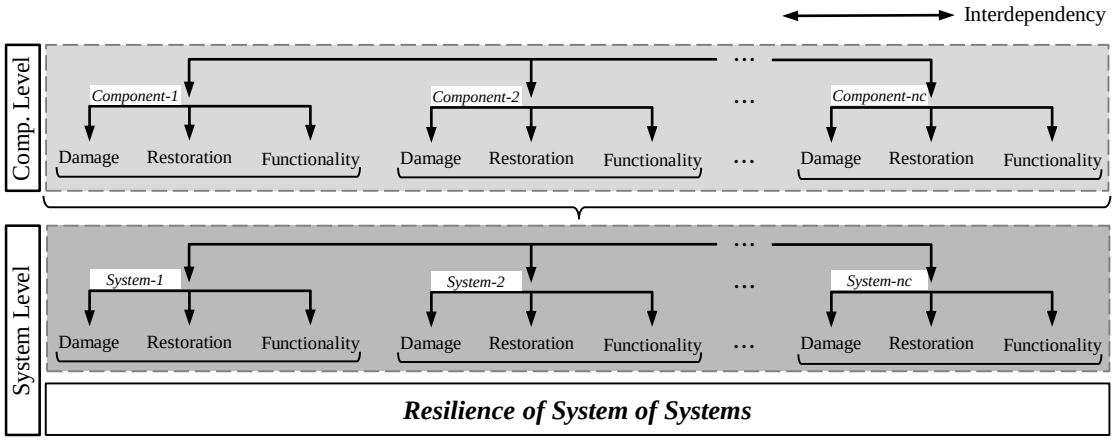

Figure 2.1: General procedure to system resilience assessment from component analysis

presentation of the materials in the current chapter, as well as the rest of this dissertation, follows the same order as discussed above for resilience assessment of a system. To this respect, in the following first a brief overview of the current state-of-the-art techniques on probabilistic seismic demand and fragility analysis is provided. The second section presents a critical review of the currently available restoration functions used for the functionality evolution and resilience analysis of bridge structures. In the third section, the concept of resilience and its application to disaster management are introduced. Also, a review of different metrics and methodologies to measure the resilience of various infrastructure systems is presented. The detailed formulation of such techniques for transportation networks is provided.

2.2 Seismic Fragility Analysis

Seismic performance assessment of structures has gained significant attention from the professional and academic communities. Recent developments of performance-based design techniques allow to not only consider an array of structural performance objectives, but also take into account the uncertainties involved in hazard, response, and capacity of structures and infrastructure systems. Figure 2.2 shows the main modules of probabilistic seismic loss assessment and performance-based design. In such techniques, probabilistic seismic demand analysis (PSDA) and fragility curves play a key role in characterizing the response

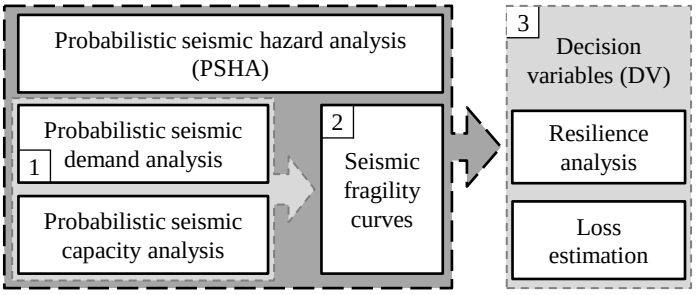

Figure 2.2: Seismic loss assessment framework according to FEMA (2006)

and vulnerability (or resistance) of structures in a probabilistic manner (modules 1 and 2 in Figure 2.2).

Fragility $F_{ls}(im)$ is traditionally expressed as the conditional probability of failure with respect to the limit state ls, given the occurrence of an event with the level of intensity im at the location of the structure, as shown in the following generic equation (Jalayer, 2003):

$$F_{ls}(im) = P[D \geq C_{ls} | IM = im] \tag{2.1}$$

From the terminology point of view, demand (D) represents the statistical characteristics of the *response* of the studied system to the event with intensity im. Examples of demand parameters are the maximum inter-story drift for buildings and deck residual displacement for bridges. Similarly, C_{ls} describes the *capacity* of the system with respect to the limit state ls. Typically, limit states are associated with certain thresholds above which a particular physical damage (e.g., yielding or cracking) takes place, and are often determined through studying the mechanical behavior of the components. Such limit states are referred to as "damage limit states" (dls) in this study.

The first developments and applications of fragility analysis go back to the early 80s, when they were utilized for risk assessment of nuclear power plants (Kennedy et al., 1980; Kennedy and Ravindra, 1984). Since then, several formulations and methodologies have been proposed for the computation and development of fragility curves for different types of structures and infrastructure systems. In general, such techniques can be categorized into four groups. These include *expert-based*, *empirical*, and *experimental* methods which use the available damage data from the past events or conducted experiments. In the the absence of such data, *analytical* methods can be used, which mostly rely on numerical modeling and computational techniques. Several analytical techniques have been proposed for the development of fragility curves, such as Incremental Dynamic Analysis (IDA) (Zhang

and Huo, 2009), Bayesian updating (Gardoni et al., 2003), series expansion (Lupoi et al., 2006), artificial neural networks (Lagaros et al., 2009), and response surface (Franchin et al., 2003). An extensive review of techniques for seismic fragility assessment of bridges is presented by Billah and Alam (2015).

Among the different techniques, Nonlinear Time-History Analysis (NTHA) is the most popular for fragility analysis of bridges. Typically, the first step toward the computation of fragility using NTHA techniques is to perform the probabilistic seismic demand analysis (PDSA) to estimate of the probabilistic characteristics of the structural demand given the occurrence of a certain level of the event intensity measure (*IM*). A seminal work of this line of research is the study carried out by Shome (1999) and Cornell et al. (2002), in which a probabilistic approach was utilized to combine the uncertainty involved in demand and capacity in order to derive a closed-form formulation of the damage given the ground motion intensity measure. The following equation was proposed to relate the demand (D) and *IM* assuming that the structural demand is a linear function of *IM* in a log-log space:

$$S_D(im) = a(im)^b \tag{2.2}$$

where a and b are regression constants, and $S_D(im)$ is the median of the demand at the intensity level im. This assumption, called power model, implies that the demand at each level of *IM* follows a lognormal distribution with median value equal to $S_D(im)$. In order to compute the regression parameters, a detailed numerical model of the structure needs to be created. Samples of the material, geometrical, and mechanical properties of the structure should be generated considering the underlying distribution of each property. The resulting numerical models should be paired with and analyzed subjected to a suite of ground motions that is a representative of the seismicity of the region. The maximum responses of the investigated components of the structure (e.g., ductility, drift, etc.) recorded from each analysis are plotted versus the ground motion *IM*s in the logarithmic scale, and a linear

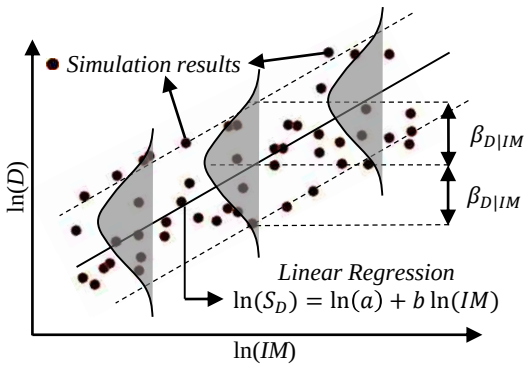

Figure 2.3: Schematic presentation of probabilistic seismic demand model (PSDM).

regression analysis is performed. Figure 2.3 shows a schematic view of this probabilistic demand model.

Regarding the dispersion, typically it is assumed that the logarithmic standard deviation of the demand ($\beta_{D|IM}$) is constant over the investigated range of the IM, and can be computed using the following equation (Jalayer, 2003):

$$\beta_{D|IM} = \sqrt{\frac{\sum_{i=1}^{N}[\ln(d_i) - \ln(aIM^b)]^2}{N-2}} \tag{2.3}$$

in which N is the number of samples, and d_i is the demand of the ith sample model obtained by nonlinear analysis (and Monte Carlo simulation).

Following the mentioned assumptions (lognormality of the demand, power model, and constant dispersion), Cornell et al. (2002) derived the following equation, which presents a closed- form formulation for the conditional probability of exceedance of the demand D, given IM.

$$P[D \geq d|im] = 1 - \Phi\left[\frac{\ln(d) - \ln(S_D)}{\beta_{D|IM}}\right] = 1 - \Phi\left[\frac{\ln(d) - \ln(a(im)^b)}{\beta_{D|IM}}\right] \tag{2.4}$$

where $\Phi[\cdot]$ is the standard normal cumulative distribution function (CDF). If the capacity with respect to limit state ls (i.e., C_{ls}) is a deterministic parameter, Equation 2.4 can be used

to compute the fragility of the components considering $C_{ls} = d$. Otherwise, assuming that the capacity follows a lognormal distribution, Equation 2.4 can be expanded to derive the closed-form fragility function presented in the following equation (Nielson, 2005):

$$P[D \geq C|im] = \Phi\left[\frac{\ln(S_D/S_C)}{\sqrt{\beta_{D|IM}^2 + \beta_C^2}}\right] = \Phi\left[\frac{\ln(im) - \left(\frac{\ln(S_C)-\ln(a)}{b}\right)}{\frac{\sqrt{\beta_{D|IM}^2+\beta_C^2}}{b}}\right] \tag{2.5}$$

in which S_C and β_C are the median and dispersion of the lognormally distributed component capacity. The right-hand-side of Equation 2.5 presents the fragility in the form of a two parameter lognormal cumulative distribution function, with appropriate median and dispersion for each limit state.

While component fragility curves are useful to evaluate the vulnerability of individual members of a structure, system fragility can be computed to assess the overall structure's proneness to damage. Nielson (2005) computed the system fragility curves of bridges by assuming that the vulnerable components of the bridge work in series configuration. Equation 2.6 shows the mathematical formulation of system failure with components in series.

$$P[ls_j|im] = P\left[\bigcup_{i=1}^{N} E_i(ls_j|im)\right] \tag{2.6}$$

where $E_i(ls_j|im)$ is the event in which component i exceeds the limit states j under the intensity measure value im. In this equation the probability of the system to fail with respect to the limit state j ($P[ls_j|IM]$) is defined as the probability of the union of events (E_i) for all components of the bridge. Dueñas-Osorio and Padgett (2011) proposed a more flexible criterion and derived the associated mathematical formulations for bridge system failure. With this definition, a bridge fails with respect to the limit state j not only if any of its components reaches this limit state, but also when a predefined number of critical components exceed limit state $j-1$.

The probabilistic seismic demand and fragility models presented above are among the most popular methodologies and have been used by several researchers for demand and fragility analyses of a wide range of structures and infrastructures, in particular highway bridges. To name just a few, Mackie and Stojadinovic (2001) developed an analytical model for typical highway bridges of California and studied the probabilistic seismic demand of the bridges using the models presented above considering several IMs. Choi (2002) and Nielson (2005) computed fragility curves for different classes of highway bridges typical to Central and Southern United States (CSUS). Padgett (2007) developed fragility curves for bridges typical to CSUS regions considering the effect of different retrofit solutions, such as the use of column steel jackets, restrainer cables, and elastomeric bearings. Zhang et al. (2008) assessed the effect of liquefaction-induced lateral spreading on the fragility of six bridge classes. Ghosh and Padgett (2010) computed time-dependent fragilities by performing probabilistic seismic demand and fragility analyses on bridge components and systems considering several deterioration factors and aging parameters. They found out that accounting deterioration increases the demand and fragility of some components on one hand and decreases these parameters on some other vulnerable components of the bridge. Tondini and Stojadinovic (2012) studied the influence of geometrical parameters (e.g., radius of the deck and column height) on the statistical characteristics of seismic demand for curved bridges. Banerjee and Ganesh Prasad (2013) generated bridge seismic fragility curves in flood-prone regions and evaluated the effect of scour depth on the vulnerability of bridges. Padgett et al. (2013) and Wang et al. (2013a,b) studied the influence of vertical ground motions, soil interaction, and liquefaction on the fragility of bridges. Billah et al. (2013) evaluated the effect of near and far fault ground motions on the fragility of retrofitted bridge multi-column bents. Huo and Zhang (2013) assessed the effect of pounding and skewness on the response and fragility of multi-span highway bridges. AmiriHormozaki et al. (2015) computed the seismic fragility for horizontally curved steel I-girder highway bridges. Pang et al. (2014) developed fragility curves for cable-stayed bridges.

The choice of *IM* is another important step in performing probabilistic seismic demand and fragility analyses. In fact, when using the models discussed earlier, selecting a better *IM* can improve the quality of the estimated probabilistic characteristics of the demand (i.e., median and dispersion), as well as the fragility. Several researchers have worked on this topic, compared the performance of different *IM*s, and proposed new ones. Luco and Cornell (2007), and Giovenale et al. (2004) introduced three criteria to compare the performance of *IM*s: "efficiency", "sufficiency", and "hazard computability". An efficient *IM* results in small amount of dispersion for the estimated demand at a given value of *IM*. A sufficient *IM* is the one that is independent of earthquake magnitude and source-to-site distance. Hazard computability indicates whether hazard curves are available for the selected *IM* or not. Hazard curves are one of the major ingredients of the probabilistic performance and risk assessment framework (see Figure 2.2) as they provide the information on the annual probability exceedance at each level of *IM*. "Practicality" is another metric reflecting the level of correlation between the demand parameter and *IM* (Mackie and Stojadinovic, 2001). Padgett et al. (2008) introduced the "proficiency" of *IM*, which is a metric based on the "efficiency" criterion. While it was shown that the spectral acceleration (Sa) at the fundamental period, and spectral displacement (Sd) are among the most "efficient" *IM*s (Mackie and Stojadinovic, 2001) for general purposes, Padgett et al. (2008) showed that the peak ground acceleration (PGA) is the optimal *IM* for probabilistic seismic demand and fragility analysis of bridge classes and portfolios. As opposed to individual *IM*s, other researchers proposed vector-type *IM*s, composed of multiple *IM*s (Shome and Cornell, 1999; Bazzurro and Cornell, 2002; Baker and Allin Cornell, 2005; Kafali and Grigoriu, 2007; Bojórquez et al., 2012, to name just a few). Also, Shafieezadeh et al. (2012) proposed a new set of *IM*s for probabilistic seismic demand models of highway bridges based on fractional operators and compared their characteristics with conventional *IM*s.

Table 2.1: Summary of the reviewed restoration functions and their features

Model	Class	Damage State	Probabilistic	Type
ATC (1985)	Survey-based	System	×	Discrete
DHS (2009)	Survey-based	System	×	Normal
Porter (2004)	Survey-based	Component	√	Lognormal
Padgett and DesRoches (2007)	Survey-based	Component	×	Stepwise
Shinozuka et al. (2003)	Mathematical	System	√	Linear
Bocchini et al. (2012)	Mathematical	System	√	Multi-types

2.3 Bridge Restoration Functions

Restoration (or recovery) functions provide the functionality of individual infrastructure components or systems in the aftermath of an extreme event. As it will be shown later in this chapter, resilience of a system is typically presented as a function of the restoration functions of its components. Therefore, a detailed analysis of the functionality of the system components is ineluctable for a realistic and reliable infrastructure system resilience assessment. In the case of transportation systems, while most of the proposed methodologies take advantage of very sophisticated and thorough models to capture the behavior of the system, simplified models have usually been assumed for the functionality of the individual bridges during the restoration.

It is generally acknowledged that the development of accurate restoration functions is extremely difficult, due to several uncertainties involved in decisions associated with restoration of damage, as well as closure of a bridge following a disaster. Therefore, a limited number of restoration functions is available in the literature. This section briefly reviews the most popular bridge restoration models and categorizes them based on their characteristics. The categories include survey-based or mathematical models, component or system models, and deterministic or probabilistic models. Table 2.1 highlights the features and properties of the restoration functions reviewed in this section. Survey-based models are the restoration functions that have been developed based on the results of sur-

veys conducted on bridge experts, disaster managers, or decision makers. Instead, mathematical models have been typically developed by assuming a certain mathematical function that satisfies the expected shape of the restoration functions for the investigated structure, or infrastructure system such as highway bridges. Different models provide the restoration functions of bridges for different bridge component damage configurations. In particular, several models provide the functionality evolution of bridges considering only a single damaged component (e.g., column, bearing, etc.). Others, present the restoration functions for the case of bridges with multiple damaged components. Finally, probabilistic models present the functionality as a random parameter by taking into account the uncertainties involved in different aspect, such as initial damage and restoration resources, while deterministic models do not. In the following, examples of the various categories of bridge restoration models are provided. Later in this dissertation (in Chapter 4), the limitations of these models for resilience analysis of bridges are discussed.

ATC-13 presented a set of restoration functions for thirty five different classes (social function classes) of structures and infrastructures, including residential and commercial buildings, water and power distribution supplies, and transportation services (ATC, 1985). These restoration functions, which have been computed using the results of a survey carried out on forty two experts, present the mean value and standard deviation of the time required to restore the functionality of each class to 30%, 60%, and 100% of the normal service level. It is worth noting that since restoration activities immediately after an event are highly impacted by the emergency conditions during the early stages of disaster response, the restoration functions provided by ATC-13 tend to only reflect the long-term restoration. The restoration functions are provided for seven damage states, which are no, slight, light, moderate, heavy, major, and destroyed damage. ATC-13 categorizes the highway bridges into two groups, namely major bridges (with individual spans over 100 feet) and conventional bridges. In case the time to reach a functionality level other than the

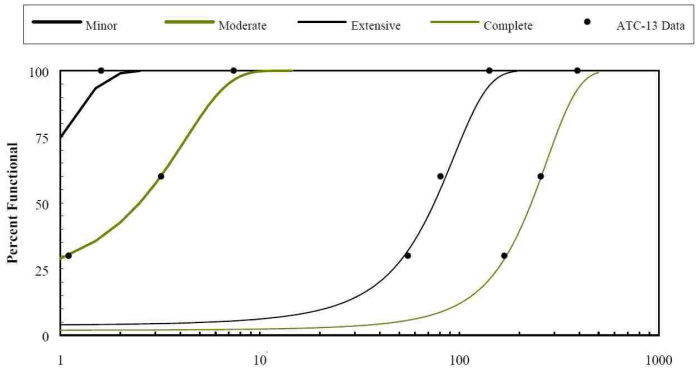

Figure 2.4: HAZUS bridge restoration functions (DHS, 2009)

three reported values (i.e., 30%, 60%, and 100%) is needed, ATC-13 recommends a linear interpolation.

HAZUS (DHS, 2009) developed a set of continuous restoration functions by fitting a normal Gaussian cumulative distribution function (CDF) to the three-point restoration functions provided by ATC-13. In case of bridges, four restoration functions have been computed for four damage states, namely minor, moderate, extensive, and complete damage, by fitting a normal function to ATC-13 restoration data associated with slight, light, moderate, and heavy damage states for conventional bridges, respectively (Figure 2.4).

Porter (2004) surveyed six engineers from different departments of transportation (DOTs) to study bridge damage-closure relationships, in a probabilistic manner. Different component damage measures were included such as the amount of approach settlement, abutment vertical and horizontal offsets, and column crack width. The bridge closure decision associated with the level of damage was divided into four categories: “no closure”, “close 1-3 days”, “close more than 3 days”, and “reduced speed”. The final products were presented in the form of fragility functions relating the component damage and closure decision, probabilistically. More specifically, lognormal CDFs were used to present the conditional probability of exceeding a certain level of closure decision given a component damage measure (e.g., $P[\geq 1 \text{ day closure} \mid \text{settlment} = 2\ in]$, see Figure 2.5).

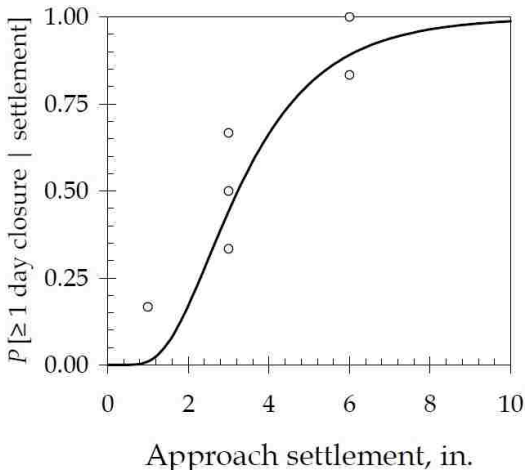

Figure 2.5: Example of a fragility function computed for bridge approach settlement (Porter, 2004)

Padgett and DesRoches (2007) defined four deterministic bridge restoration functions, each corresponding to one component damage state similar to the damage states presented in HAZUS. A probability distribution was assigned to each damage state to characterize the underlying uncertainty in the capacity of the components of the bridge. The parameters of the distributions were computed using the results of a survey involving 28 experts. The restoration functions are in stepwise shape. Also, the four models represent the restoration functions of bridges with a single damaged components. These restoration models are assumed to be the same for different bridge types and different (single) damaged components, as long as the damage state of the components are the same. Figure 2.6 illustrates these restoration functions for all four damage states.

Other researchers developed mathematical models with different levels of complexity to represent bridge restoration functions. For instance, Shinozuka et al. (2003) modeled the bridge repair process as a probabilistic distribution function in which the total restoration duration was assumed to be uniformly distributed between the minimum and maximum possible time to complete the restoration (Figure 2.7). The parameters of such distributions were presented for different bridge damage states. Yet, the model does not provide any

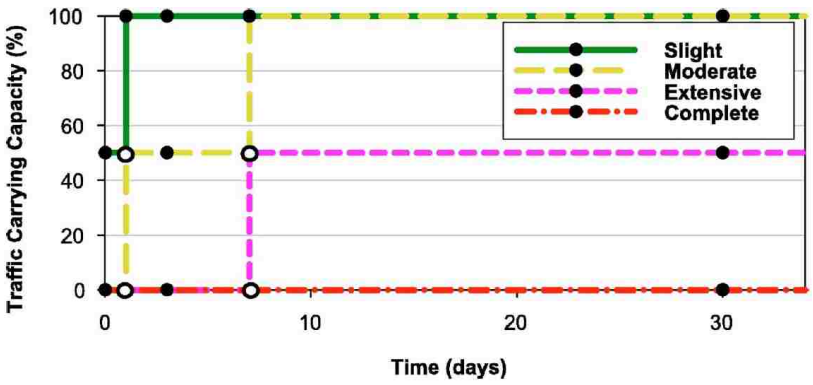

Figure 2.6: Stepwise restoration functions defined for slight, moderate, extensive, and complete damage states (Padgett and DesRoches, 2007)

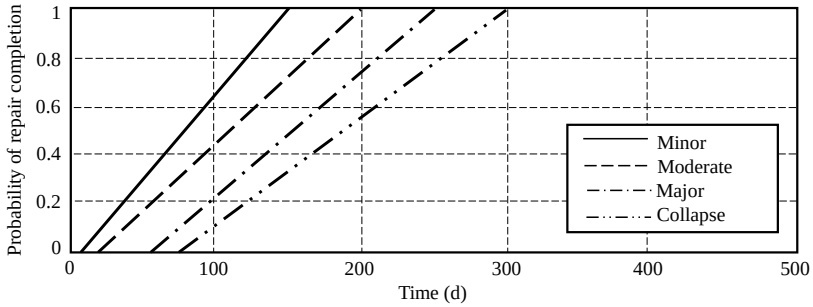

Figure 2.7: Restoration process modeled as uniformly distributed random variable (adapted from Shinozuka et al., 2003)

information on the quality of the functionality of the bridge and its evolution before, during, and after the restoration process.

Bocchini et al. (2012) developed a six-parameter probabilistic recovery model and used it for probabilistic resilience analysis of highway bridges. The recovery functions were characterized by random variables representing the idle time (i.e., time between the extreme event and restoration initiation), post-event residual functionality, restoration duration, and target functionality. By adjusting the parameters, the proposed model is capable of producing restoration functions with different forms, such as linear, positive and negative exponential, and sinusoidal (surrogate of stepwise). Figure 2.8 illustrates a schematic view of the proposed model and its parameters.

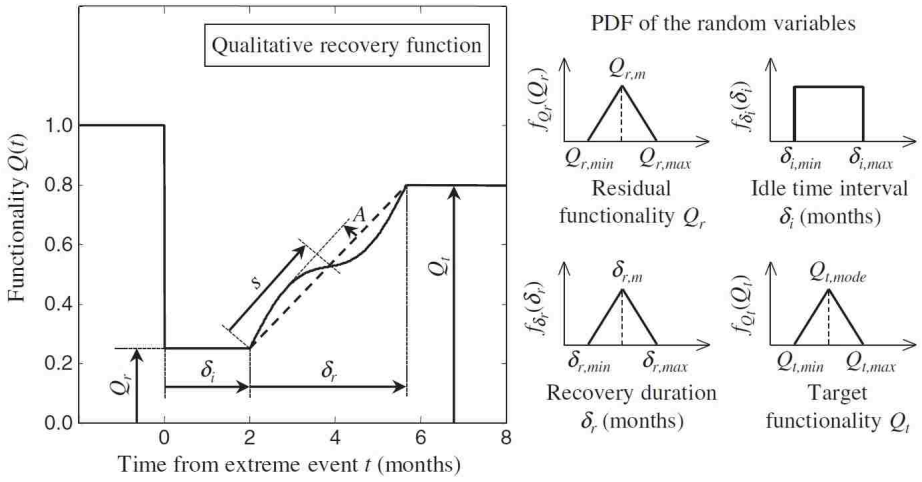

Figure 2.8: Schematic view of the six-parameter probabilistic recovery model, and the probability distribution functions used for different model parameters (Decò et al., 2013)

2.4 Resilience Analysis

Ecologists were the first to adopt the notion of resilience to study large-scale ecological disturbances (Holling 1973). They described resilience as the reorganizing capability of ecological systems after a disturbance to a new stable state (Ludwig et al. 1978). Currently, resilience is one of the most popular topics among researchers of various fields and disciplines. Reviews of the available literature show the emphasis of the research and professional communities on this notion (Bergström et al., 2015; Hosseini et al., 2016). In fact, Hosseini et al. (2016) showed that the number of research papers published every year on the topic of resilience has increased about ten times in four years since the year 2000 (Figure 2.9).

Righi et al. (2015) categorized the research studies conducted on resilience into six areas. These include “theory development”, “identification and classification”, “safety management tools”, “analysis of accidents”, “risk assessment”, and “training”. The research community has contributed to expanding the knowledge in each of these categories and in different areas, such as healthcare, military, construction, electricity distribution, trans-

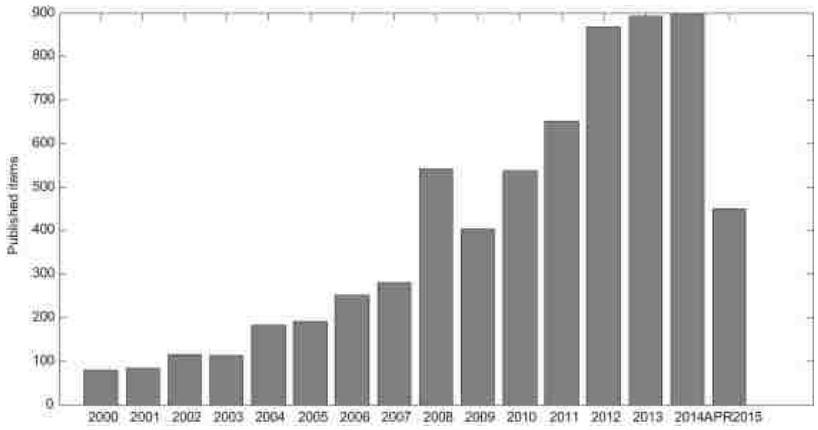

Figure 2.9: Distribution of papers by year of publication, as of April 2015 (Hosseini et al., 2016)

portation, financial services, and natural disasters.

Resilience has different definitions across different fields and domains, such as social, economic, organizational, and engineering. Social resilience is defined as "ability of groups or communities to cope with external stresses and disturbances as a result of social, political, and environmental change" (Adger et al., 2005). In economy resilience can be expressed as the "inherent ability and adaptive response that enables firms and regions to avoid maximum potential losses" (Rose and Liao, 2005). Vogus and Sutcliffe (2007) described organizational resilience as "the ability of an organization to absorb strain and improve functioning despite the presence of adversity". In engineering fields, resilience is defined as the intrinsic ability of a system to adjust its functionality in the presence of a disturbance and unpredicted changes (Hollnagel et al., 2007). Bruneau et al. (2003) recognized four fundamental properties (i.e., robustness, redundancy, resourcefulness, and rapidity), and four dimensions (i.e., technical, organizational, social, and economic) for resilience. Today, the White House defines resilience as the ability to prepare for, withstand, and rapidly recover from a disruption, and adapt to changing condition (Presidential Policy Directive, 2013).

While several formulations have been proposed to quantify the resilience of different

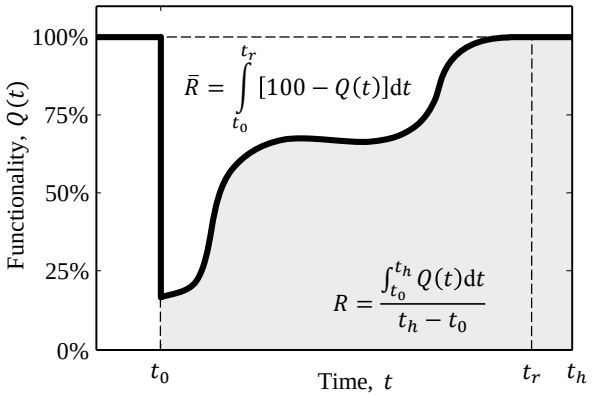

Figure 2.10: Schematic presentation of probabilistic seismic demand model

systems, the majority of them are in the following form:

$$Resilience = f[Q_1(t), Q_2(t), \ldots, Q_{nc}(t)] \tag{2.7}$$

where $Q_c(t)$, $c \in \{1, \ldots, nc\}$ and nc are the time-dependent functionality of the c-th component, and the total number of the components of the system, respectively. f is the function that maps the functionality of the components to the resilience of the system. An extensive review of different resilience metrics is presented by Hosseini et al. (2016). In the following a selected number of such metric is discussed.

Bruneau et al. (2003) presented the first conceptual framework for the assessment of community seismic resilience and proposed the following equation to quantify the loss of resilience:

$$\bar{R} = \int_{t_0}^{t_r} [100 - Q(t)]dt \tag{2.8}$$

where $\bar{R}$ is the loss of resilience, and Q is the time variant measure of the system functionality, which should be defined based on the characteristics of the system. t_0 and t_r are the times corresponding to the occurrence of the disruption (e.g., earthquake) and full functionality restoration of the system ($Q(t_r) = 100\%$), respectively.

Reed et al. (2009) revised the metric presented in Equation 2.8 and proposed the fol-

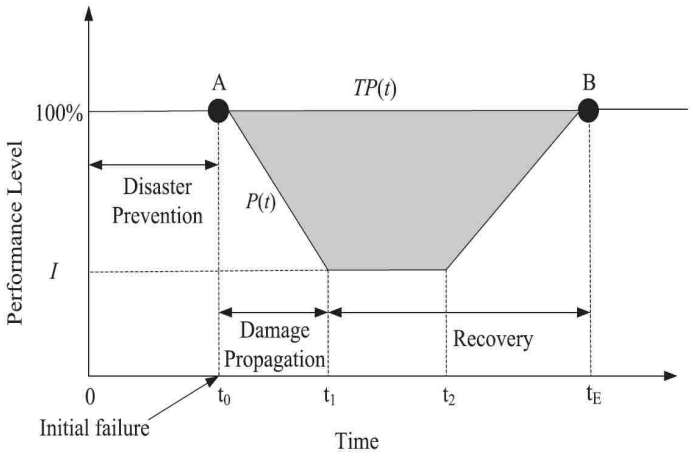

Figure 2.11: Schematic performance curve and parameter definition for Equation 2.10 (Ouyang and Dueñas-Osorio, 2012)

lowing equation to quantify resilience:

$$R = \frac{\int_{t_0}^{t_h} Q(t)dt}{t_h - t_0} \tag{2.9}$$

in which t_h is the end of the investigated time horizon. Figure 2.10 shows the parameters of Equations 2.8 and 2.9, schematically.

Ouyang and Dueñas-Osorio (2012) proposed a time dependent formulation for resilience of urban infrastructure systems which is shown in the following equation:

$$R(t_h) = \frac{\int_0^{t_h} RP(t)dt}{\int_0^{t_h} TP(t)dt} \tag{2.10}$$

where $RP(t)$ and $TP(t)$ are real and target performances of the system at time t (see Figure 2.11). This formulation allows accounting for the changes in system performance as well as the target performance during the investigated time horizon (period) t_h for estimating the resilience.

Francis and Bekera (2014) proposed a resilience metric that incorporates the three capacities of resilience, namely absorptive, adaptive, and restorative capacities. To this re-

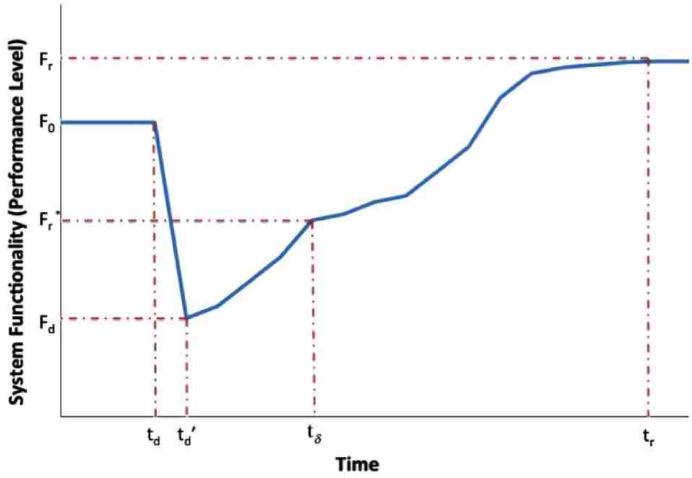

Figure 2.12: Schematic performance curve and parameter definition for Equation 2.11 (Francis and Bekera, 2014)

spect, the resilience factor ρ_i is defined as follows:

$$\rho_i(S_p, F_r, F_d, F_0) = S_p \frac{F_r F_d}{F_0 F_0} \tag{2.11}$$

where S_p reflects the speed of recovery, F_r is the performance at a new stable level, F_d is the performance level immediately after the disruption, and F_0 is the original stable system performance level (see Figure 2.12). The speed of recovery S_p was defined as:

$$S_p = \begin{cases} (t_\delta / t_r^*) \exp[-a_d(t_r - t_r^*)] & \text{for } t_r > t_r* \\ (t_\delta / t_r^*) & \text{otherwise} \end{cases} \tag{2.12}$$

in which t_δ represents the slack time (the maximum time to achieve acceptable recovery). t_r and t_r^* are the time to final recovery (i.e., new equilibrium state) and time to complete initial recovery actions, respectively. a_d is a parameter to control decay in resilience until a new equilibrium is achieved.

Henry and Ramirez-Marquez (2012) expressed resilience as the ratio of recovery to loss

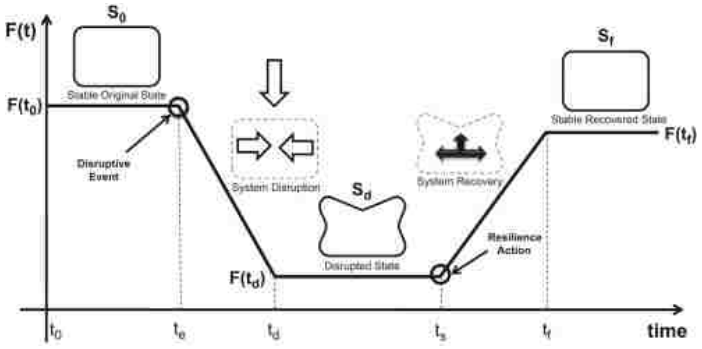

Figure 2.13: Performance curves and system state definitions used in Equation 2.13 (Henry and Ramirez-Marquez, 2012)

as presented by the following equation:

$$R(t|e^j) = \frac{F(t|e^j) - F(t_d|e^j)}{F(t_0) - F(t_d|e^j)} \tag{2.13}$$

This definition categorizes the status of the system into five states: "stable original", "system disruption", "disrupted", "system recovery", and "stable recovered". The stable original state is between times t_0 and t_e, which are the origin and the time of occurrence of the disruptive event e^j, respectively The disrupted state is the time between t_d and t_s which are the time when the effects of the disruptive event is stabilized, and the initiation of the restoration process, respectively. Finally, the stable state starts when the system reaches stability (at time t_s) after the restoration phase. $F(t)$ is the performance function. Figure 2.13 illustrates the different states and parameters associated with Equation 2.13.

In addition to the definition of general metrics, several studies focused on the development of methodologies for the assessment of the resilience of different structures and infrastructure systems. For example, Ouyang and Dueñas-Osorio (2012), and Ouyang et al. (2012) proposed a three-stage resilience analysis framework and studied the resilience of the power transmission grid in Harris County, Texas, USA, and evaluated the effect of different post-blackout improvements, situational awareness enhancements, demand management, and distributed generators integration. Cimellaro et al. (2010a,b) developed a com-

prehensive conceptual model to quantify resilience and applied it to assess the resilience of a hospital building typical of California, as well as a network of hospitals located in Memphis, Tennessee, USA. Omer et al. (2009, 2012) presented a model for measuring the resilience of networked infrastructures, and presented its application to trans-oceanic telecommunication cable networks and maritime transportation systems. A three-objective optimization model was presented by Piratla (2016) to evaluate the design of water distribution systems and assess the different tradeoffs by including sustainability and resilience as the design objectives. Cimellaro et al. (2014) developed a resilience metric to measure the capacity of gas distribution networks to maintain a desired performance level and illustrated the application to the gas distribution network of Introdacqua and Sulmona in Italy, damaged due to the 2009 earthquake. Petrini et al. (2013) presented a multi-scale framework for resilience assessment of large scale urban infrastructures considering the interdependencies among the components of the system. The application of the proposed technique was presented for electric and hydraulic supplies.

Recently, several researchers recognized the similarities between sustainability and resilience, and presented integrated frameworks to address the two concepts. Along this line, Bocchini et al. (2013) reviewed the common aspects of resilience and sustainability. Moreover, a unified approach was proposed to address resilience and sustainability of civil infrastructures in a quantitative manner. The application of this approach was illustrated for the case of a viaduct. Different approaches to address resilience and sustainability of cities are presented by Asprone and Manfredi (2013). Mackie et al. (2015) presented a methodology to compute the sustainability of design and resilience of bridges using carbon footprint, repair cost, and repair time. Rodriguez-Nikl (2015) proposed a conceptual framework for resilience and sustainability assessment and studied the case of a town subjected to extreme events such as sea-level rise and storm.

Similar to many other structures and infrastructure systems, the quantification, assess-

ment, and optimization of resilience of bridges and transportation networks have been also the subject of several studies and researches. For example, Chang et al. (2012b) presented a framework and an optimization formulation to maximize the post earthquake evacuation capacity of transportation networks, considering the effect of damaged bridges in the performance of the system, and applied to the transportation network of Memphis, TN, USA. Vugrin et al. (2014) presented a bi-level optimization model and solution approach for resilient transportation network recovery. Venkittaraman and Banerjee (2014), and Chandrasekaran and Banerjee (2015) evaluated different retrofit strategies for highway bridges and studied the optimal retrofit solution considering resilience as the criterion. Decò et al. (2013), and Biondini et al. (2015) proposed techniques for probabilistic resilience assessment of bridges. Soltani-Sobh Soltani-Sobh et al. (2015, 2016) proposed a model to quantify reliability and improvement in resilience of transportation networks considering the uncertainties in travel demand and link capacity following catastrophic events.

Bocchini and Frangopol (2012a,b) proposed metrics and a framework for resilience evaluation and optimization of highway networks with damaged bridges. Since some of the formulations and methodologies presented by Bocchini and Frangopol (2012a,b) are utilized further in this study, a brief review is presented herein. In this technique, the impact of damaged bridges on the performance of transportation networks is quantified through traffic analysis on the damaged network, which is carried out by solving the well-known traffic distribution and assignment problems (Evans, 1976). To this purpose, transportation networks are modeled in the form of directed graphs, in which nodes represent population centers (e.g., cities, business or residential centers) or road intersections and edges represent the connecting road segments. Solving the traffic distribution and assignment problem is an iterative procedure through which two fundamental sets of information about the traffic characteristics of the network are computed. In particular, traffic distribution uses a gravitational model presented by Levinson and Kumar (1994) to estimate the number of

trips between each pair of nodes. Traffic assignment distributes the generated and attracted trips to the roads by means of Wardrop's user equilibrium model (Sheffi, 1985), which provides the traffic flow (f_{ij}) and travel time (c_{ij}) for each road segment in the network. More details about the computational algorithm used for traffic analysis can be found in Bocchini and Frangopol (2011); Saydam et al. (2013).

In the case of an extreme event, the damage induced by the disaster, safety considerations, or restoration activities might require to partially or fully close some bridges of the transportation network. Using the following equation, Bocchini and Frangopol (2012a,b) modeled the impact of this loss of functionality on the traffic characteristics of the network as an increase in the travel time of the road segments whose bridges are damaged.

$$c_{ij} = c_{ij}^0 \cdot \left[1 + \alpha \left(\frac{f_{ij}}{f_{ij}^c}\right)^\beta\right] + \sum_{b \in ij} (1 - Q_b) \cdot c_b^d \cdot \left[1 + \alpha \left(\frac{(1 - Q_b) \cdot f_{ij}}{f_b^d}\right)^\beta\right] \tag{2.14}$$

The first part of Equation 2.14 is actually the BPR latency function (Bureau of Public Roads, 1964), that accounts for the time required to cover a highway segment in regular conditions (i.e., when all bridges of the segment are fully in service). In this part, f_{ij} and c_{ij} are the traffic flow and the time needed to cover segment ij, respectively. c_{ij}^0 is the time to cover the segment at free flow and f_{ij}^c is the practical flow capacity of the segment. α and β are model parameters set equal to 0.15 and 4.0, respectively (Bureau of Public Roads, 1964). The second part (summation) takes into account the additional time required by the traffic to bypass the damaged bridges. Parameters f_b^d and c_b^d are the practical capacity and the minimum time required to cover the detour of bridge b, respectively. Q_b is the functionality of bridge b, typically represented by the fraction of the total number of lanes of segment ij which is open to traffic. For instance, the value of Q_b is 0 when a bridge is closed (out of service), 0.5 when half of the lanes are open (partially in service), and 1.0 when the bridge is fully open to the traffic (fully in service).

Equation 2.9 was used to compute the resilience of the transportation network. Thus, a flow-based time-dependent functionality indicator ($Qflow$), shown in the following equation, was proposed to quantify the functionality of the bridge networks, at each investigated time step (e.g., before extreme event, after the event and during the restoration phase).

$$Qflow(t) = \frac{\Gamma(t) - \Gamma^0}{\Gamma^{100} - \Gamma^0} \tag{2.15}$$

where $\Gamma(t)$ is the network performance index at time t. Γ^{100} and Γ^0 are the performance indices corresponding to the cases where all the bridges are in service ($Q_b = 1\ \forall b$), or out of service ($Q_b = 0\ \forall b$), respectively. In fact, $Qflow$ measures the normalized performance difference between the post- and pre-event of the network. The performance index $\Gamma(t)$ at each time instance is computed as follows:

$$\Gamma(t) = \frac{1}{\gamma_T \cdot TTT(t) + \gamma_D \cdot TTD(t)} \tag{2.16}$$

in which TTT and TTD are the total travel time spent and distance covered by all passengers traveling in the network in one hour, respectively. γ_T and γ_D are cost balancing factors associated with the time spent and the distance traveled by the passengers, measured in time^{-1} and distance^{-1}, respectively. The values of TTT and TTD are computed using the following equations, along with the procedure discussed earlier in this section:

$$TTT(t) = \sum_{i \in I} \sum_{j \in J} f_{ij}(t) \cdot c_{ij}\left[f_{ij}(t)\right] \tag{2.17}$$

$$TTD(t) = \sum_{i \in I} \sum_{j \in J} \left[f_{ij}(t) \cdot d_{ij} + \sum_{b \in ij} f_{ij}(t) \cdot (1 - Q_b) \cdot d_b^d \right] \tag{2.18}$$

where I is the set of all nodes of the network, and J is the subset of nodes connected to node i. d_{ij} is the length of the highway segment ij, and d_b^d is the detour length of bridge b.

In addition to the presented metric, other formulations have been also used for the computation of resilience of transportation networks and bridges. Reviews of such metrics can be found in (Faturechi and Miller-Hooks, 2014; Ghosn et al., 2016).

2.5 Concluding Remarks

In this chapter, a review of the major components of functionality and resilience analyses of bridges and transportation networks has been provided. These are fragility analysis, restoration function analysis, resilience quantification, and transportation network resilience assessment and optimization.

Fragility analysis needs to be carried out to characterize the demand and failure of bridges, in a probabilistic fashion. However, the assumptions typically made the probabilistic characteristics of demand can introduce a considerable amount of approximation to the computed fragility. The level of such approximations and the impact of each of the common assumptions made on the probability distribution the demand need to be evaluated, systematically.

Restoration functions are required for resilience analysis of bridges and transportation systems in order to evaluate the evolution of functionality during the restoration process. However, the shortcomings of the currently available bridge restoration functions prevent their application for resilience analysis. In particular, the literature is currently missing probabilistic restoration functions (i.e., accounting the uncertainties in damage and restoration scheduling) that are developed for individual bridge structures (as opposed to regional recovery curves). Also, in order to carry out a comprehensive assessment of the resilience of bridges and transportation networks with respect to a wide range of scenarios, bridge restoration functions for different damage configurations need to be available.

In order to effectively improve the resilience of transportation networks, comprehensive methodologies are required which are appealing to asset managers, take advantage of rigorous computations, and consider different priorities of disaster managers. In particular, such techniques need to provide results that are easy to interpret, yet calculated based on advanced computational tools (e.g., structural analysis, reliability, optimization, resilience). Also, the proposed techniques should be computationally efficient and capable of solving large-scale real-world problems in a timely manner. Finally, network resilience metrics and formulations reflecting different phases of disaster management activities should be developed and used for the analysis.

Chapter 3

Critical Comparison of Seismic Fragility Techniques for Resilience and Loss Estimation of Bridges

3.1 Introduction

This chapter considers the typical assumptions made on the marginal distribution of the demand by PSDMs and investigates their veracity. Then, it quantifies how the approximations introduced by these assumptions propagate to seismic fragility (Module 2 in Figure 2.2), resilience, and expected loss (Module 3 in Figure 2.2) computed for bridges. Moreover, as reference solution, a simulation-based approach which does not require any assumption on the distribution of the demand is used to perform the entire analysis, all the way through resilience and life-cycle loss. Studies on three classes of structures with different levels of complexity have been performed and the results in terms of fragility, resilience and loss analyses using the proposed and the conventional methodologies are compared. The methodologies and results presented in this chapter are based on papers by Karamlou and Bocchini (2014b, 2015).

For resilience analysis and regional loss estimation, it is customary to consider and study entire stocks of structures, as opposed to an individual structure. Therefore, among different probabilistic seismic demand and fragility analysis techniques reviewed in Section 2.2, only the methodologies that can handle entire bridge classes are considered herein, which typically rely on a set of assumptions discussed earlier. For convenience, these assumptions namely hypothesis-1 (hp-1), hypothesis-2a (hp-2a), and hypothesis-2b (hp-2b)

are summarized in the following:

- The marginal distribution of demand is lognormal (lognormality assumption-hp1).
- The median of such distribution (S_D) is presented as a power function (Equation 2.2) of the seismic *IM* of choice (power model assumption-hp2a).
- The dispersion of such distribution ($\beta_{D|IM}$) is constant (Equation 2.3) over the considered range of the *IM* (constant dispersion assumption-hp2b).

The name tags shown above (i.e., hp1, hp2a, and hp2b) will be used throughout this chapter to refer to each assumption.

3.2 Probabilistic Resilience Analysis and Life-Cycle Loss Assessment of Bridges

In this chapter, Equation 2.9 is used for the computation of bridge resilience. To this purpose, the expected functionality of the structure at each time instant t after an extreme event can be estimated by using an approach based on the total probability theorem. If a collection of events with a limited range of *IM*s are of interest, Equation 3.1 can be used to compute the expected functionality $\check{Q}(t)$:

$$\check{Q}(t) = \sum_{im=1}^{nIM} P(IM = im) \sum_{d=1}^{nDS} P(DS = d|IM = im) \cdot Q(t|DS = d) \tag{3.1}$$

in which $Q(t|DS = d)$ is the functionality recovery function of the structure at time t with an initial damage level d. In the case of highway bridges, functionality is usually presented in the form of the percentage of traffic carrying capacity in normal conditions (ATC, 1985). $P(DS = d|IM = im)$ is the conditional probability of being in the damage state d given the event scenario with *IM* equal to *im*, computed by any fragility analysis technique

like the methodologies presented in Section 2.2. Finally, $P(IM = im)$ is the probability of occurrence of extreme events generating intensity *im*, computed by a standard probabilistic seismic hazard analysis (PSHA) performed on the region where the bridge is located (FEMA, 2006).

Along this line, the economic loss due to the earthquake induced damage can be estimated probabilistically using the system fragility curves and probabilistic seismic hazard analysis. In this study, the expected direct loss ($\check{CO}_{dir}$) related to the cost of rehabilitation or reconstruction of the structure is calculated using the following equation (Bocchini et al., 2013):

$$\check{CO}_{dir} = CO_c \sum_{im=1}^{nIM} P(IM = im) \sum_{d=1}^{nDS} P(DS = d|IM = im) \cdot DR_d \tag{3.2}$$

in which CO_c is the construction cost of the structure, and DR_d is the damage ratio associated with the damage state d.

3.3 Proposed Technique for Probabilistic Seismic Demand and Fragility Analysis

3.3.1 Probabilistic Seismic Demand Model

The conventional PSDM presented in Section 2.2 allows using all the samples together for the estimation of the demand distribution parameters, as if it was a single random variable through the entire range of *IM*s. This means that the distributions assumed for the demands by this PSDM at every level of *IM* are identical, but only translated as illustrated in Figure 2.3. In another word, in log-log space, the medians are shifted along the regression line and the dispersion is assumed to be constant. The fundamental idea behind this approach is that the maximum structural responses are linearly amplified (in a log-log scale) as the

structure is subjected to a stronger ground motion. However, for many cases the behavior of the structure is much more complicated and this simple model cannot capture it properly. Therefore, the following procedure can be followed for such cases.

1. A suite of ground motions which well represents the seismicity of the site is chosen. The ground motion records of this suite can be clustered into several bins in a way that each bin contains a set of records with similar ground motion characteristics such as magnitude, distance, and frequency content (Shome, 1999). Then, an appropriate number of records should be selected from each bin. Having a collection of records that come from different bins allows to account for the uncertainty inherent in the characteristics of ground motions in the analysis. The selected ground motions can then be scaled properly to several levels of *IM* to obtain a new suite of ground motion records that covers the investigated values of the *IM*. Care should be taken when scaling ground motions. Intensity of ground motions are highly correlated to their other characteristics such as frequency content and duration. However, by scaling the intensity, other characteristics of the ground motion stay unchanged. If deemed necessary, in order to prevent applying large scaling factors to the records, different sets of ground motions can be selected and used for scaling to each investigated level of the *IM*.

2. Samples of material and geometrical properties of the class of structures are generated, for instance by Latin Hypercube (McKay et al., 2000) sampling. Each set of sample parameters define a sample structural model.

3. At each level of *IM*, structural samples are paired with the ground motions. Therefore, the total number of simulations will be equal to:

$$N_{simulations} = N_{samples} \times N_{levels\ of\ IMs} \times N_{ground\ motions\ at\ each\ level\ of\ IM} \tag{3.3}$$

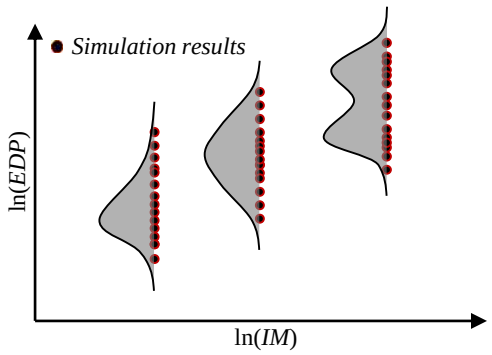

Figure 3.1: Schematic presentation of the proposed probabilistic seismic demand model.

In this way, there is a sufficient number of simulations to estimate the characteristics of the distribution of the demand parameter at each selected level of IM. The number of samples ($N_{samples}$) and ground motions ($N_{ground\ motions\ at\ each\ level\ of\ IM}$) can be specified considering the desired level of confidence in the computed probability of failure.

4. Time-history analysis is performed on each pair of structure and ground motion, and the maximum demand of the vulnerable components of the structure is recorded.

5. The underlying distribution of the demand at each IM can be obtained independently either by fitting the best distribution to the data, or computing the empirical probability distribution function (PDF) of the data using a non-parametric technique, such as kernel smoothing (Bowman and Azzalini, 1997) (see Figure 3.1). The correlation among different component demand parameters is also computed.

This proposed methodology is computationally more expensive than the traditional PSDM, and it may have been impractical 20 years ago, with the resources normally available at that time. However, the fast development of the computational resources readily available to companies and institutions has made these analyses possible today with perfectly reasonable computational times.

3.3.2 Fragility Curves

Following the probabilistic demand analysis discussed in the previous section, the fragility of the vulnerable components as well as the bridge system fragility can be calculated numerically by means of large-scale Monte Carlo simulation, together with the methodology presented in Section 2.2. The following steps can be performed to compute the component fragilities.

1. An adequate number of samples of the demand at each value of the IM is generated. These samples can be generated from the closed-form or empirical distributions previously fitted to the demand at each level of IM.
2. The same number of samples is generated for the capacity for each limit state.
3. The ratio of the negative safety margins is calculated by subtracting demand and capacity of the corresponding component, for every investigated damage state.
4. If the fragility needs to be presented in the form of a continuous CDF, a curve fitting to the available discrete fragility points can be performed.

The above process is the same for both component and system fragility curves. However, as mentioned earlier, for the case of the system fragility curves the correlation between the demand of different components should be taken into account for the generation of the samples at each level of IM (Nielson, 2005) using a technique for multi-variate non-Gaussian simulation (Iman and Conover, 1982).

The analysis is then completed with resilience and loss estimation exactly as explained in Section 3.2. It should be mentioned that the entire process that leads to the computation of fragility curves and resilience relies on a broad array of assumptions. These include simplifications and approximations typically made on structural modeling, finite element

techniques, and structural analysis. This chapter focuses on the errors introduced by a subset of these assumptions, which in many cases are responsible for substantial inaccuracy. A comprehensive analysis of all these assumptions is beyond the scope of this study.

3.4 Numerical Application

Nielson (2005) classified the bridges of the US National Bridge Inventory database (FHWA, 2002) into 11 categories. Multi-Span Simply Supported (MSSS) Steel Girder and Multi-Span Continuous (MSC) Steel Girder bridges are two of the most common bridge classes in the US, accounting for more than 11% and 13% of the total bridge population, respectively. These bridges are typically characterized by concrete decks and steel girders, circular reinforced concrete columns, multi-column concrete bents, high type fixed and rocker (expansion) bearings, and pile bent type abutments (Nielson, 2005). The majority of them have 3 spans, with small skew angle (less than 30 degrees). Most of these bridges are not designed according to seismic standards, due to their age. In fact, they usually have less than 1% of longitudinal reinforcement and low confinement in their columns or bents and use high type bearings which make them vulnerable against seismic loadings (Padgett and DesRoches, 2009). In this study, three structural models with different levels of complexity are analyzed using the OpenSees platform (McKenna et al., 2000) and probabilistic seismic demand, fragility, resilience, and expected life-cycle loss analyses are carried out. These include 2 dimensional finite element models of a MSSS Steel Girder bridge and a MSC Steel Girder bridge, and a cantilever concrete column with properties similar to that of MSSS and MSC Steel Girder bridge columns. Details of the numerical models, as well as the results of the analysis are presented in the following sections.

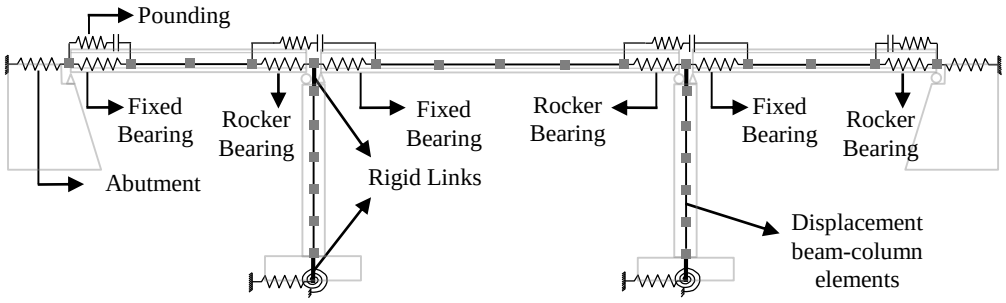

Figure 3.2: MSSS Steel Girder bridge analytical model

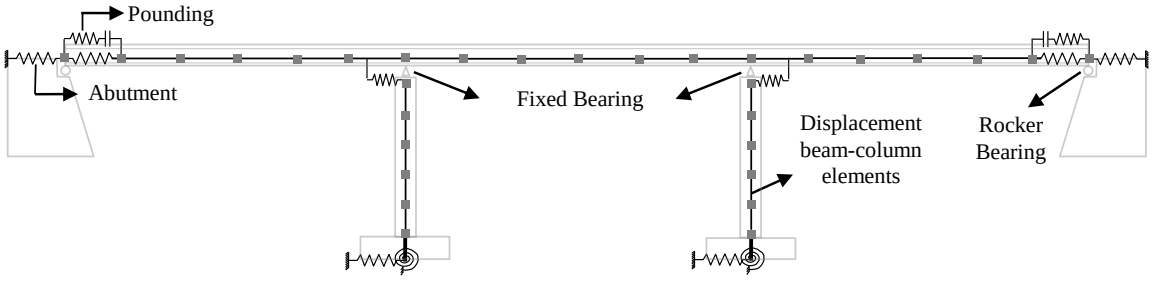

Figure 3.3: MSC Steel Girder bridge analytical model

3.4.1 Finite Element Models

The analytical models developed for this study is inspired by those presented by Nielson (2005) and Choi et al. (2004). A schematic view of the MSSS and MSC Steel Girder bridges and their components are shown in Figures 3.2 and 3.3, respectively. Both bridge models have 3 spans. Regarding the MSSS Steel Girder bridge, the external spans are 12.2 m long and the middle span is 24.4 m long. Unlike the MSSS Steel Girder bridge, the MSC Steel Girder bridge has three spans with the same length equal to 30.3 m. The decks of the bridges are modeled with elastic beam-column elements, because these components are not expected to enter the plastic range during seismic events.

Displacement-based beam-column elements with 5 integration points (with Gauss-Lobatto quadrature) have been used to model the columns. The concrete section of the columns has been discretized employing fiber sections considering different fibers for longitudinal steel

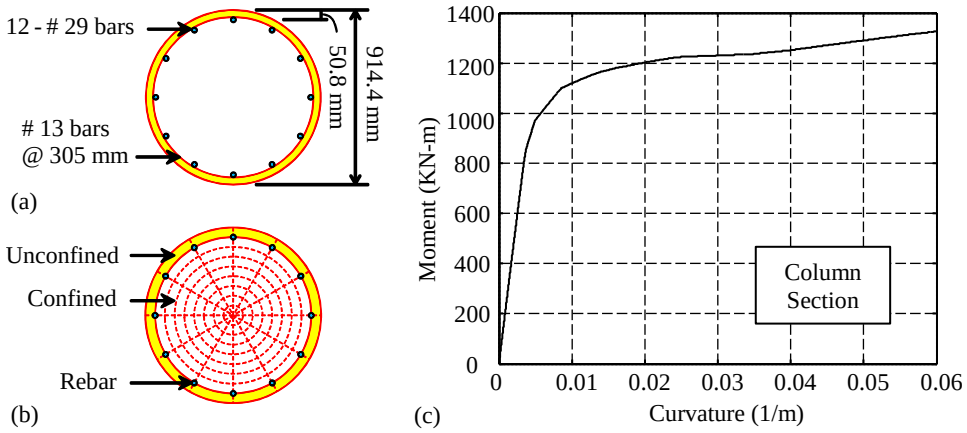

Figure 3.4: Reinforced concrete column: (a) section geometry, (b) fiber section discretization, and (c) moment-curvature behavior (Figures 3.4a and 3.4b adapted from Nielson, 2005)

reinforcements, unconfined concrete in the cover, and confined concrete in the core of the column section. The confined concrete strength was estimated based on the recommendations of Park et al. (1982). Figure 3.4 shows the column section and fiber discretization, along with the result of the moment-curvature analysis of a column section.

As mentioned before, two types of steel high type bearings are typically used in these bridges. Zero-length elements have been used to model these components. The nonlinear force-deformation behavior of the fixed rocker bearings has been modeled following the results of experimental and analytical studies on steel bearings (Mander et al., 1996). The cyclic behaviors of fixed and rocker bearings are illustrated in Figure 3.5.

Zero-length elements and nonlinear springs have been utilized to capture the behavior of the pile bent abutments in the passive and active directions. The passive behavior is considered when the abutment is pushed towards its backfill soil. In this direction, both soil and piles contribute to the stiffness of the abutment. The contribution of the backfill soil is modeled based on the recommendations of Caltrans (1999) and Nielson (2005). Figure 3.6a shows the force-deformation diagram of the soil in the passive direction. The stiffness of the abutment in the active direction is provided only by the piles. The model

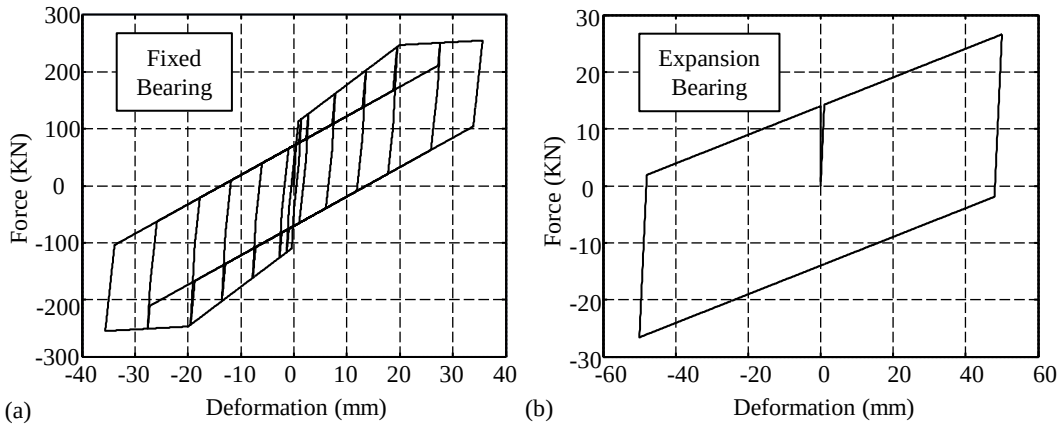

Figure 3.5: Force deformation behavior of bearings: (a) fixed bearing, (b) rocker bearing

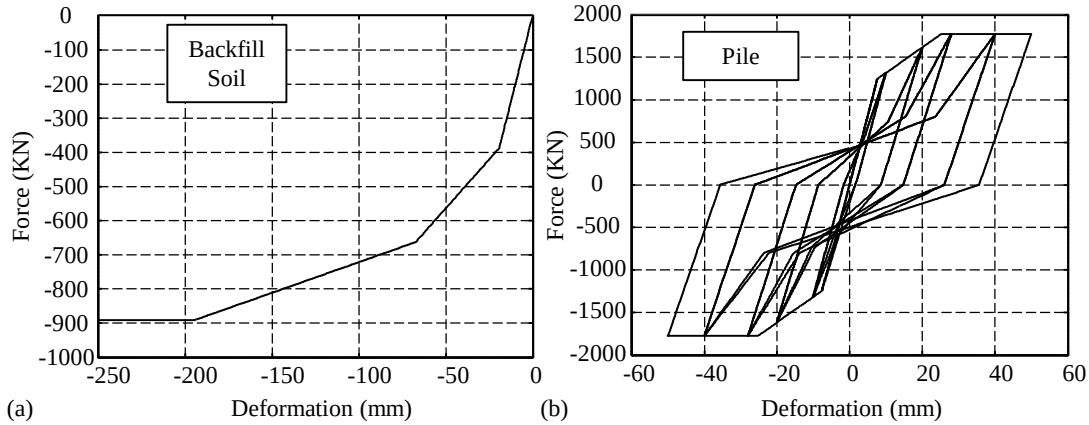

Figure 3.6: Abutment materials: (a) soil behavior, (b) pile behavior

proposed by Choi (2002) has been implemented to capture the nonlinear behavior of the piles in the abutments (Figure 3.6b).

Muthukumar and DesRoches (2005) studied the effect of pounding on the seismic response of the bridges. In fact, the maximum seismic response of the bearings and abutments can be influenced considerably by the pounding effects. In order to model the deck-deck pounding, as well as the abutment-deck pounding, additional dedicated zero-length elements have been employed and an OpenSees impact material model was assigned to these elements.

The column foundations were modeled with linear elastic springs in the longitudinal

and rotational degrees of freedom. The stiffness of the foundations in each direction is affected by the horizontal and vertical stiffness of the foundation piles. For the MSSS Steel Girder bridges modeled in this study, 8 piles support each rectangular (2.44 m $\times$ 2.44 m) foundation at the bottom of the columns. The columns are assumed to be fixed to the ground at the base in the vertical direction.

The mass of the bridges is considered to be concentrated at the deck nodes. Mass and stiffness proportional (Rayleigh) damping has been used to model the effect of damping on the structure. To properly represent the entire class of bridges, most of the materials and modeling characteristics of the bridge elements that have been presented are considered to be random and the underlying distributions and corresponding parameters will be discussed in the following section.

In addition to the MSSS and MSC Steel Girder bridge models discussed above, a 2 dimensional model of a cantilever column has been developed in OpenSees. The cantilever column model has the same properties as the columns of the complete bridges. At the foundation, the cantilever column is attached to the ground through linear elastic springs in longitudinal and rotational directions, similar to the column foundations of the complete bridges. The column was assumed to carry a concentrated mass at its tip. The value of the mass is computed considering the weight transfered from the supper structure of a MSSS Steel Girder bridge to one of its columns.

The three models used in this study each represent a structure with different levels of complexity in their modeling and behavior. In this way, the results obtained and the observations made are more general rather than being specific to a type of structure.

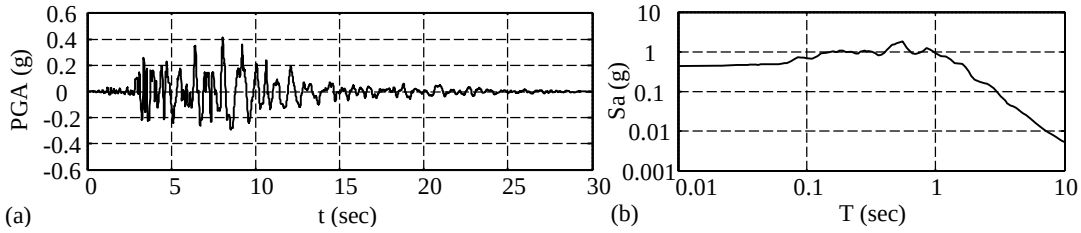

Figure 3.7: Ground motion: (a) acceleration record, (b) spectral acceleration

3.4.2 Probabilistic Seismic Demand Analysis

Probabilistic seismic demand analysis has been performed on the presented finite element models. In this application only one record has been selected from the PEER data base (, PEER) and scaled to the desired levels of *IM*. The ground motion employed for this analysis is one of the 1994 Northridge earthquake records with magnitude 6.69 and distance 11.79 Km from the epicenter. Figure 3.7 shows the acceleration time history as well as the spectral acceleration of this ground motion. In order to have a suite of ground motions with different levels of *IM* (here peak ground acceleration), the mentioned record was scaled to obtain seven ground motion records with PGAs from 0.1g to 0.7g. It is worth noting that this chapter focuses on the variability of the response and fragility caused by the uncertainty in the material and modeling parameters. However, for complete fragility and probabilistic seismic demand analyses, the uncertainty in the response of the structures caused by ground motion record variability should be also taken into account. Such variability is considered later in this dissertation by selecting a suite of ground motions for the complete bridge fragility analysis presented in Chapter 5.

Latin Hypercube sampling (McKay et al., 2000) has been performed in order to account for the variability across different bridges of the same class and the uncertainty in the parameters. In total, 16 properties of the models have been considered to be random variables, with distributions assessed by previous analytical or experimental studies. Unconfined concrete compressive stress (Hwang and Jaw, 1990), damping ratio (Fang et al., 1999), and

Table 3.1: Random variables and underlying distributions considered for PSDA

Random variable	Distribution	Parameter-1	Parameter-2	Units
Steel yield stress	Lognormal	λ=6.13	ζ=0.08	MPa
Concrete compressive strength	Normal	μ=33.8	σ=4.3	MPa
Piles' horizontal stiffness	Uniform	l=3.5	u=10.5	kN/mm/pile
Piles' vertical stiffness	Uniform	l=87.5	u=262.5	kN/mm/pile
Abutment active stiffness	Uniform	l=3.5	u=10.5	kN/mm/pile
Abutment passive stiffness	Uniform	l=11.5	u=28.8	kN/mm/m
Unit weight of middle deck (MSSS)	Uniform	l=46.8	u=57.2	kN/m
Unit weight of end deck (MSSS)	Uniform	l=35.1	u=42.9	kN/m
Unit weight of deck (MSC)	Uniform	l=61.47	u=75.13	kN/m
Damping ratio	Normal	μ=0.045	σ=0.0125	-
Fixed bearing Coef.[1] of friction (long.[2])	Lognormal	λ=-1.56	ζ=0.5	-
Rocker bearing Coef. of friction (long.)	Lognormal	λ=-3.22	ζ=0.5	-
Deck-deck gap (MSSS)	Normal	$\mu = 25.4$	$\sigma = 4.32$	mm
Deck-abutment gaps (MSSS)	Normal	$\mu = 38.1$	$\sigma = 5.84$	mm
Deck-abutment gaps (MSC)	Normal	$\mu = 76.2$	$\sigma = 24.1$	mm
Bearings initial stiffness coefficient	Uniform	l=0.5	u=1.5	-

[1]Coefficient, [2]longitudinal

internal gaps (Choi, 2002) were assumed to follow a normal distribution. Instead, lognormal distributions were assumed for the steel yield stress (Ellingwood and Hwang, 1985) and coefficient of friction of the steel bearings (Mander et al., 1996). For the rest of the random parameters, since there is not enough data in the literature, uniform distributions have been assumed, as recommended by Nielson (2005). It is worth noting that, the random variables associated to the material properties of abutments, and bearings are only relevant for the full bridges and not applied to the cantilever column model. A complete list of these variables is presented in Table 3.1, along with the associated probability distributions and corresponding parameters. One thousand samples were generated for each of the mentioned parameters and assigned to the model to have one thousand different bridge and one thousand cantilever column models.

For probabilistic seismic demand analysis, each sample structure (cantilever column or bridge) was paired with every ground motion record discussed earlier and time history anal-

Table 3.2: Hypotheses for each solution. $\surd$ = included; $\times$ = not included

Solutions		**Hypotheses**		
Levels	Name tags	hp1 Lognormality of demand distribution	hp2a Power model	hp2b Constant dispersion
Level 0	NHP	$\times$	$\times$	$\times$
Level 1	HP1	$\surd$	$\times$	$\times$
Level 2	HP12a	$\surd$	$\surd$	$\times$
Level 3	HP12	$\surd$	$\surd$	$\surd$

yses were performed on the models. A Matlab (The Mathworks Inc., 2014) script has been developed to execute the resulting seven thousand time history analyses and post-process the outputs in parallel using a Linux workstation equipped with 2 Xeon E5-2620 processors and 64 GB RAM. For the case of the complete bridge models, the time required to perform the analyses for all pairs of bridge samples and ground motions (7000 time history analyses in total) was about 15 hours using the mentioned machine. In the post-processing phase of the analysis, the maximum responses of the selected key components of the modeled structures have been recorded. For the case of the cantilever column, these responses (or *EDP*s) include the maximum curvature ductility (ratio of the maximum and yield curvature) of the column (μ_c). For complete bridges, in addition to μ_c, the maximum deformation of the fixed and rocker bearings (fb_d and rb_d), and the maximum displacement of the abutments in both passive and active directions (Ab_{Ad} and Ab_{Pd}) were also recorded.

The focus of this section is on the approximations introduced to the results of the probabilistic seismic demand and fragility analyses by the common assumptions made on the marginal distribution of the demand, namely lognormality assumption, power model, and constant dispersion (see Section 2.2). For this purpose, wherever applicable, three sets of results with different levels of assumptions are presented for each analysis. Table 3.2 shows the hypotheses considered in each solution set and the name assigned to them.

Figures 3.8 to 3.11 present the normalized histogram of the maximum recorded demands on the cantilever column and some of the key components of the MSSS Steel Girder

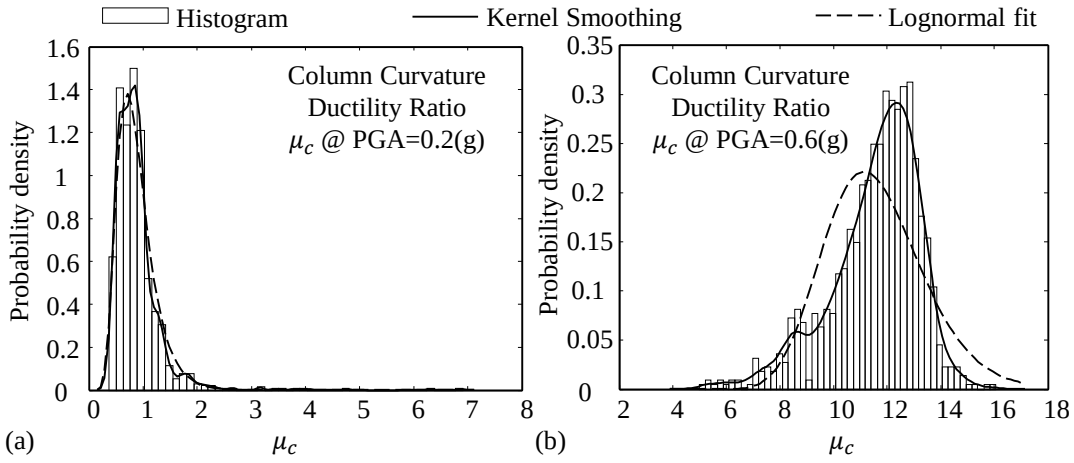

Figure 3.8: Cantilever column curvature ductility: (a) probability distribution at 0.2(g), (b) probability distribution at 0.6(g)

bridge. These include the column curvature ductility (for both the cantilever column and MSSS Steel Girder bridge), as well as fixed and rocker bearing deformation demands (for the MSSS Steel Girder bridge) for the case of the model samples paired with the ground motions with PGA equal to 0.2(g) and 0.6(g). Along with each histogram, the empirical distribution of the data obtained by means of kernel smoothing (Bowman and Azzalini, 1997) and the lognormal distribution fitted to the data with the maximum likelihood method are plotted as well. By comparing the lognormal distribution with the empirical PDF, it can be observed that in most cases the distribution of the data does not match the lognormal distribution. Among the selected figures, it can be seen that only for the case of the maximum deformation of the rocker bearings under the PGA of 0.6(g), lognormal distribution can be an acceptable approximation. For the rest of the cases, neither at the peaks, nor at the tails, the lognormal offers a good approximation of the actual distribution of the data. These results are confirmed by the lognormal probability plots presented in Figures 3.9 to 3.11. These figures show in a qualitative manner that in most cases, the lognormal distribution cannot be an ideal model for the data. The same trend was observed for the response of the rest of the demand parameters (e.g., abutment displacement in the active and passive directions) and under other ranges of IM. Also, similar results were obtained from the PSDA

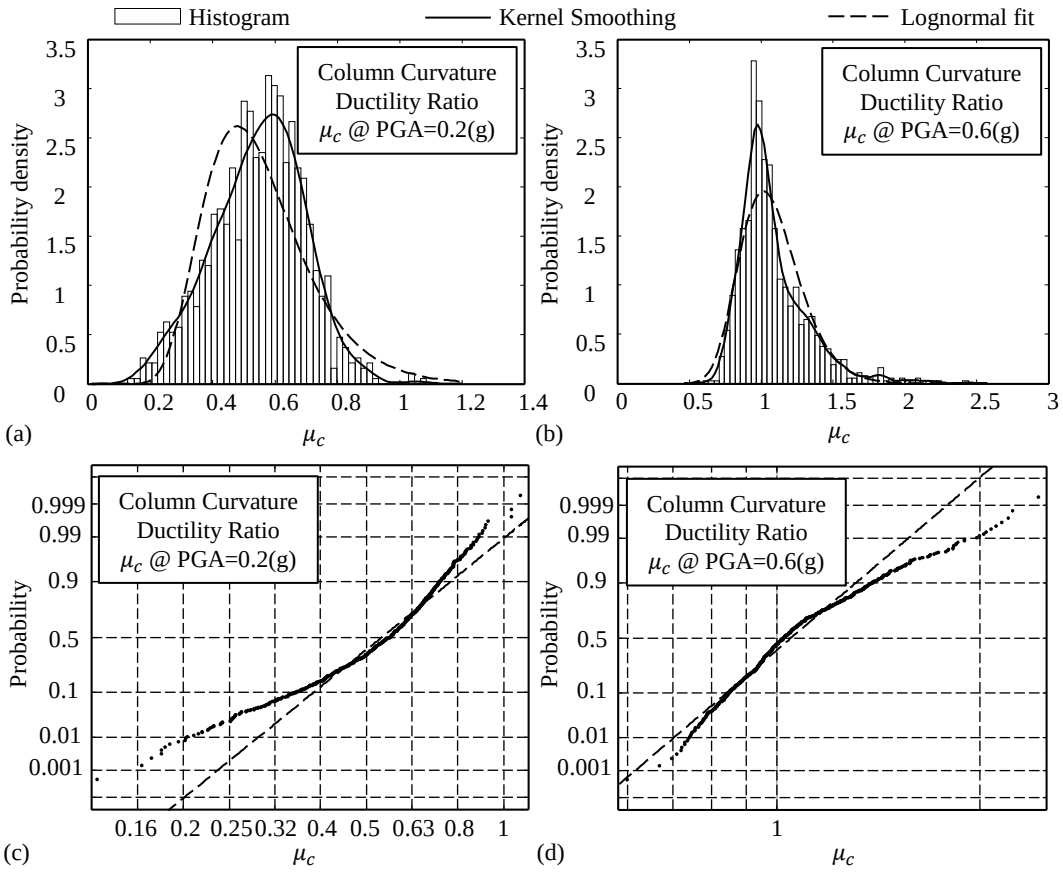

Figure 3.9: MSSS Steel Girder bridge column curvature ductility: (a) probability distribution at 0.2(g), (b) probability distribution at 0.6(g), (c) probability paper plot at 0.2(g), (d) probability paper plot at 0.6(g)

of the MSC Steel Girder bridge model. A more quantitative evaluation on lognormality assumption will be presented later by means of a goodness of fit test.

To verify the number of samples selected to estimate the probabilistic characteristics of demand parameters, a convergence analysis were carried out. As an example, Figure 3.12 shows the result of such analysis on the mean and standard deviation of the MSSS Steel Girder bridge column curvature ductility ratio demand at 0.6(g). The results show that the selected number of samples (1000) was adequate for this analysis. The same results have been obtained for other demand parameters at various levels of the *IM*.

As previously mentioned, the primary role of a PSDM is to connect *IM* and *EDP*.

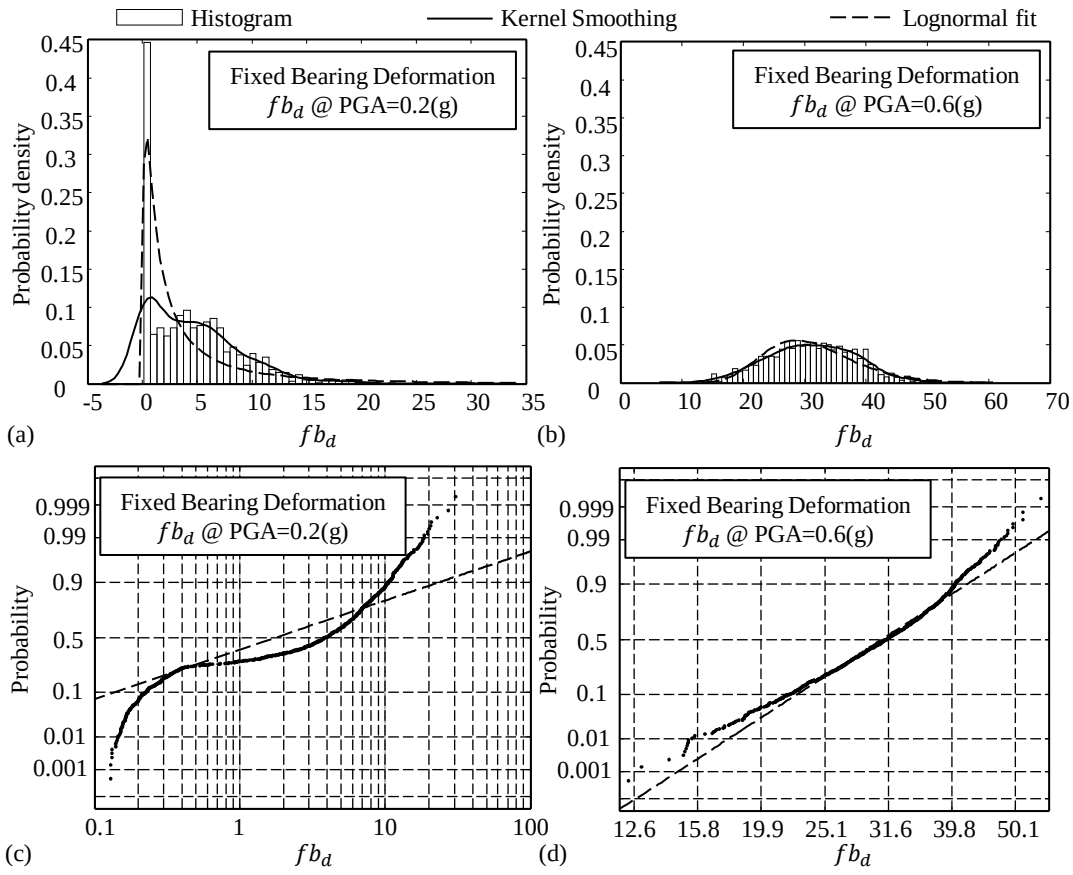

Figure 3.10: MSSS Steel Girder bridge fixed bearing deformation: (a) probability distribution at 0.2(g), (b) probability distribution at 0.6(g), (c) probability paper plot at 0.2(g), (d) probability paper plot at 0.6(g)

Thus, assuming that the demand follows a lognormal distribution (hp1), the power model (hp2a) implies that the medians of the demand (S_D) lie on a line (see Figure 2.3) at any level of *IM* in log-log space. Figure 3.13 presents the PSDM for the curvature ductility demand of the cantilever column. Similarly, Figures 3.14 to 3.18 shows the PSDMs for the MSSS Steel Girder bridge demand parameters considered in this study. Also, Figure 3.19 illustrates the PSDM for the rocker bearings demand of the MSC Steel Girder bridge. The circular markers are demands resulting from the 7000 time history analysis performed on the columns and bridges. Solid lines show the results of a linear regression on these 7000 points, following the popular probabilistic seismic demand analysis methodology utilized in several other studies (Mackie and Stojadinovic, 2001; Nielson, 2005; Choi et al., 2004;

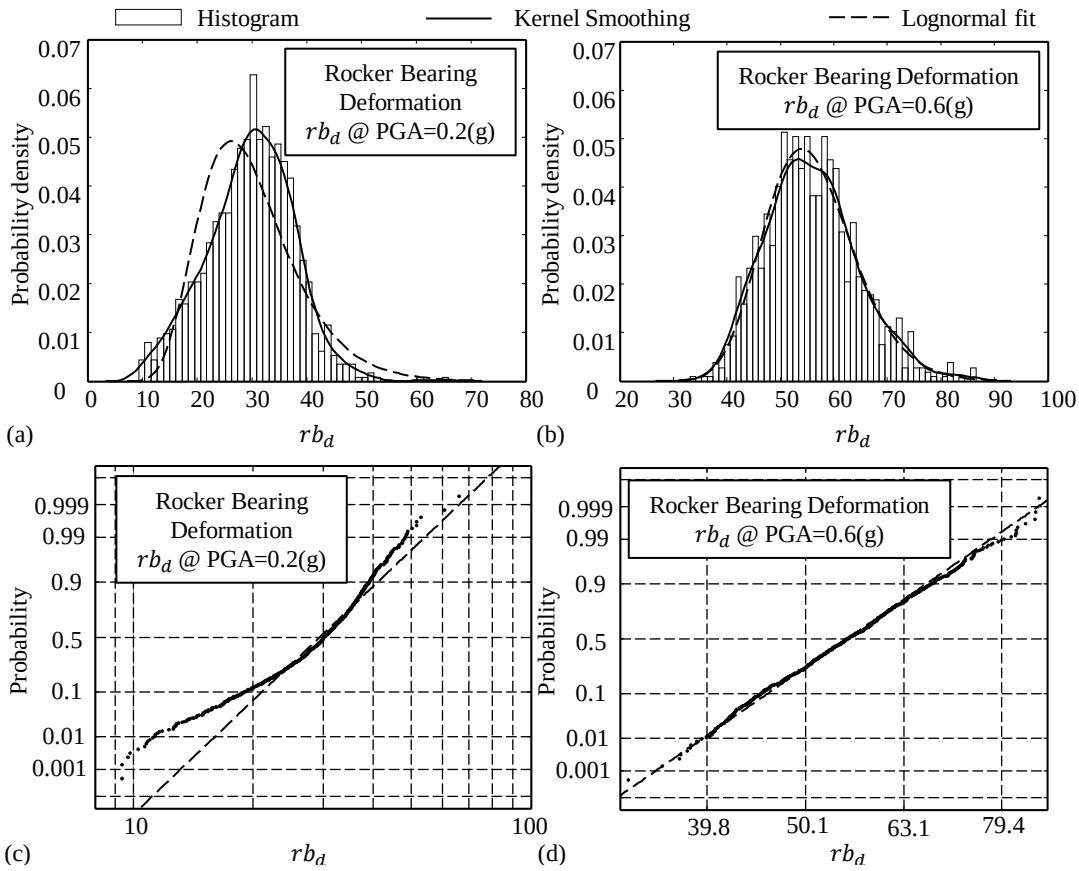

Figure 3.11: MSSS Steel Girder bridge rocker bearing deformation: (a) probability distribution at 0.2(g), (b) probability distribution at 0.6(g), (c) probability paper plot at 0.2(g), (d) probability paper plot at 0.6(g)

Padgett, 2007). These lines are supposed to estimate the medians of the demand at each level of IM. Dashed lines connect the medians of the demand at each IM, as obtained by large-scale simulation. These graphs show that the power model which has been one of the fundamental assumptions of many PSDMs does not yield a good approximation of the medians. In some cases, the difference between the median of the data at some IMs and the regression line is as high as 63%.

The last considered simplifying assumption commonly made in the probabilistic seismic demand analysis is that the dispersion of the demand ($\beta_{D|IM}$) is constant. Assuming that the distribution of the demand is lognormal (hp1), with medians located on the regression line (hp2a), this assumption (hp2b) allows the lognormal standard deviation of the demand

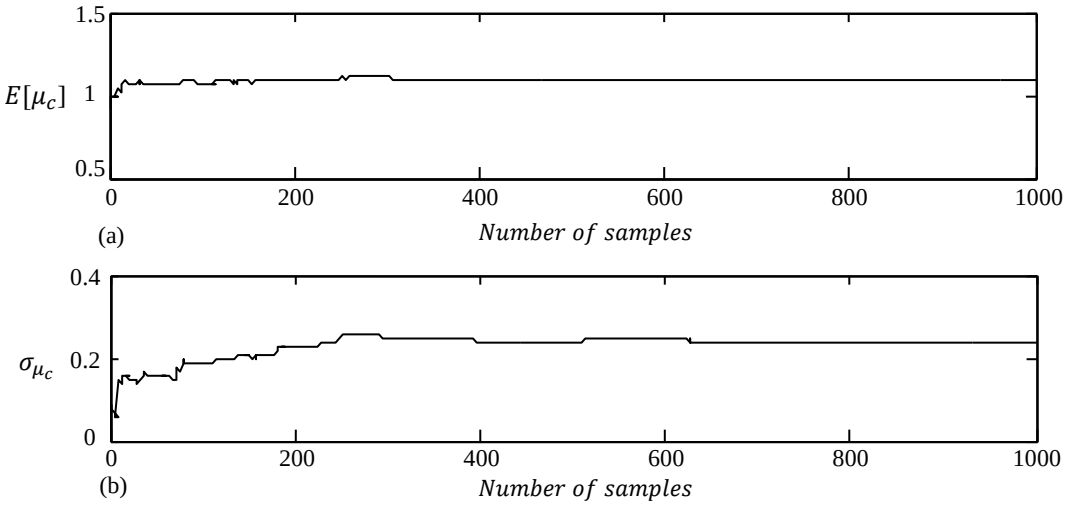

Figure 3.12: Convergence analysis for (a) mean and (b) standard deviation of the MSSS Steel Girder bridge column curvature ductility ratio demand

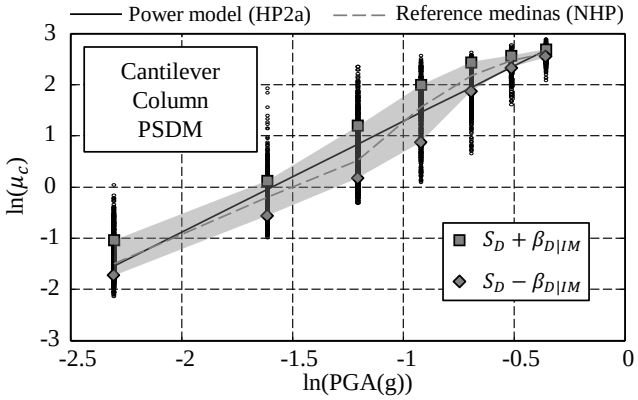

Figure 3.13: Probabilistic seismic demand analysis for cantilever column

to be approximated by Equation 2.3 as regression residuals of the demand parameters combined for all values of *IM*, as if they belonged to the same distribution. In Figures 3.13 to 3.19, the shaded areas show the enclosed region between the mean plus and minus one standard deviation of the associated normal distribution of the data. For most of the demand parameters, the actual dispersion is clearly not constant, changing from one level of *IM* to another. Moreover, when the power model is a bad approximation of the median (as for the PSDMs of column curvatures and bearing responses), then also Equation 2.3 is not a good estimator for the dispersion. On the contrary, in the case of the abutment active response

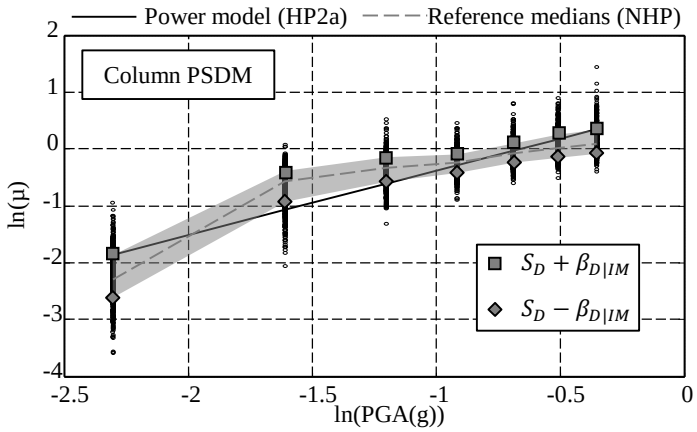

Figure 3.14: Probabilistic seismic demand analysis for MSSS Steel Girder bridge column curvature ductility

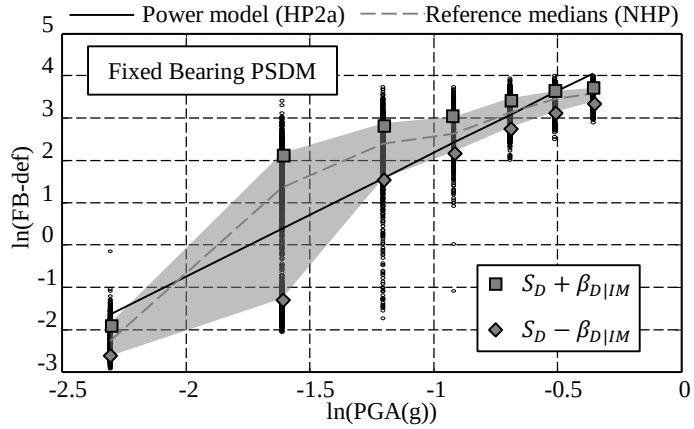

Figure 3.15: Probabilistic seismic demand analysis for MSSS Steel Girder bridge fixed bearing deformation

shown in Figure 3.17 the power model provides a good approximation of the medians of the demand and consequently the dispersion calculated by Equation 2.3 provides a reasonable approximation of the logarithmic standard deviation of the demand parameters.

The effect of each of the common assumptions on the statistical characteristics of the demand was evaluated also in a quantitative manner. The Kolmogorov-Smirinov (K-S) goodness of fit test (Ang and Tang, 2006) has been utilized to quantify the detrimental effect of each assumption on the demand. Figure 3.20 shows parameter D_n which is the absolute value of the maximum difference between the empirical cumulative distribution

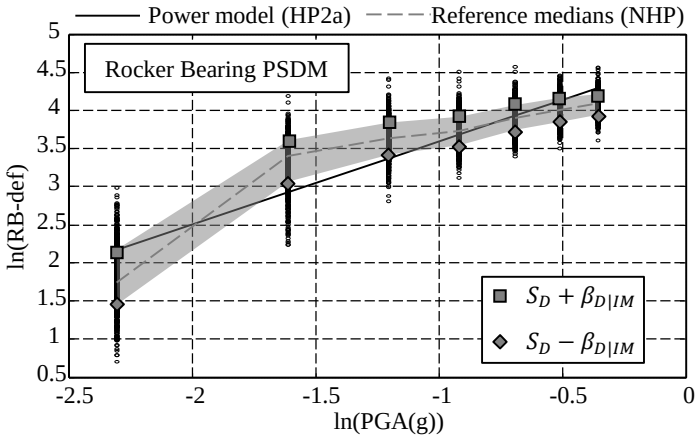

Figure 3.16: Probabilistic seismic demand analysis for MSSS Steel Girder bridge rocker bearing deformation

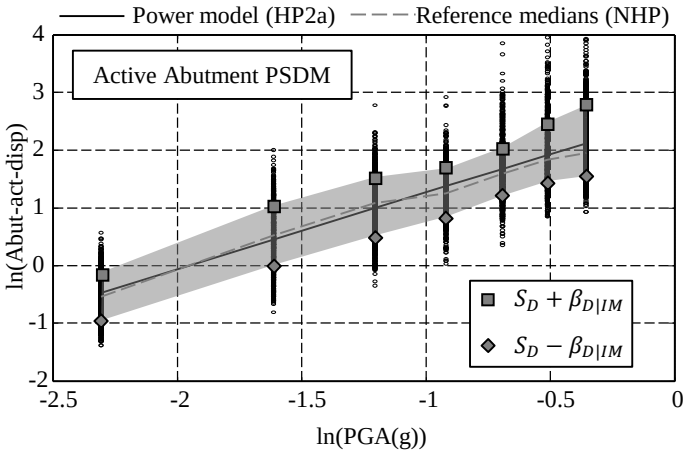

Figure 3.17: Probabilistic seismic demand analysis for MSSS Steel Girder bridge abutment active displacement

function of the demand parameter and its analytical model at each level of *IM*, associated with the analysis on the MSSS Steel Girder bridge model. Lower values of this parameter mean less discrepancies between the predicted and reference distributions. The square markers indicate the cases where the assumed distributions pass the K-S test with 10% significance level. Three different distributions have been tested. In HP12 all the assumptions have been imposed. In HP12a the dispersion of the demand about its assumed median has been calculated for each level of *IM* independently (instead of being constant). Finally, HP1 assumes only the lognormality of the demand, but the parameters were computed in-

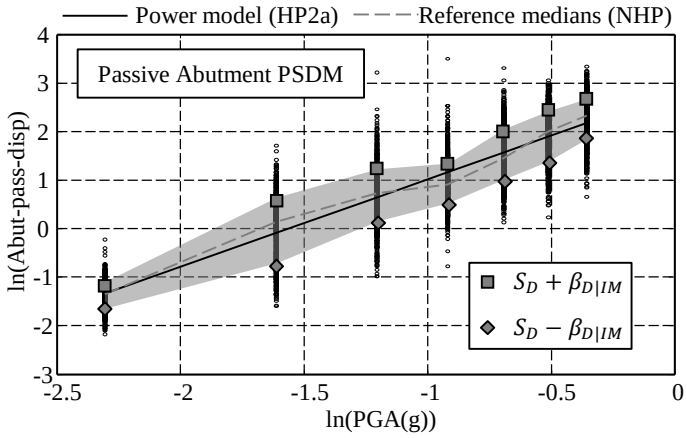

Figure 3.18: Probabilistic seismic demand analysis for MSSS Steel Girder bridge abutment passive displacement

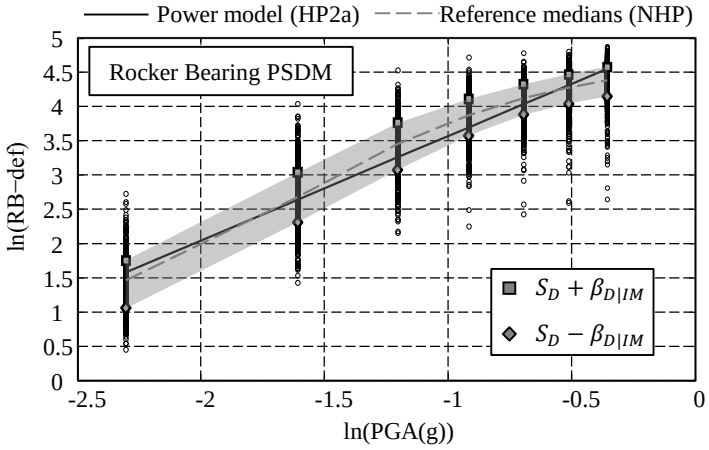

Figure 3.19: Probabilistic seismic demand analysis for MSC Steel Girder bridge rocker bearing deformation

dependently at each *IM* level, without any further assumption (see Table 3.2). As these figures show, the parameter D_n is considerably larger for solutions HP12a and HP12 compared to HP1 for almost all cases and at every level of *IM*. It can be seen that most of the discrepancy introduced in estimating the distribution of the demand is due to assumptions hp2a and hp2b, whereas lognormality alone can be considered acceptable for estimating the distributions. The results obtained from analyzing the response of the cantilever column and MSC Steel Girder bridge models showed a similar trend.

The results presented in this section show that in many cases the current PSDM does

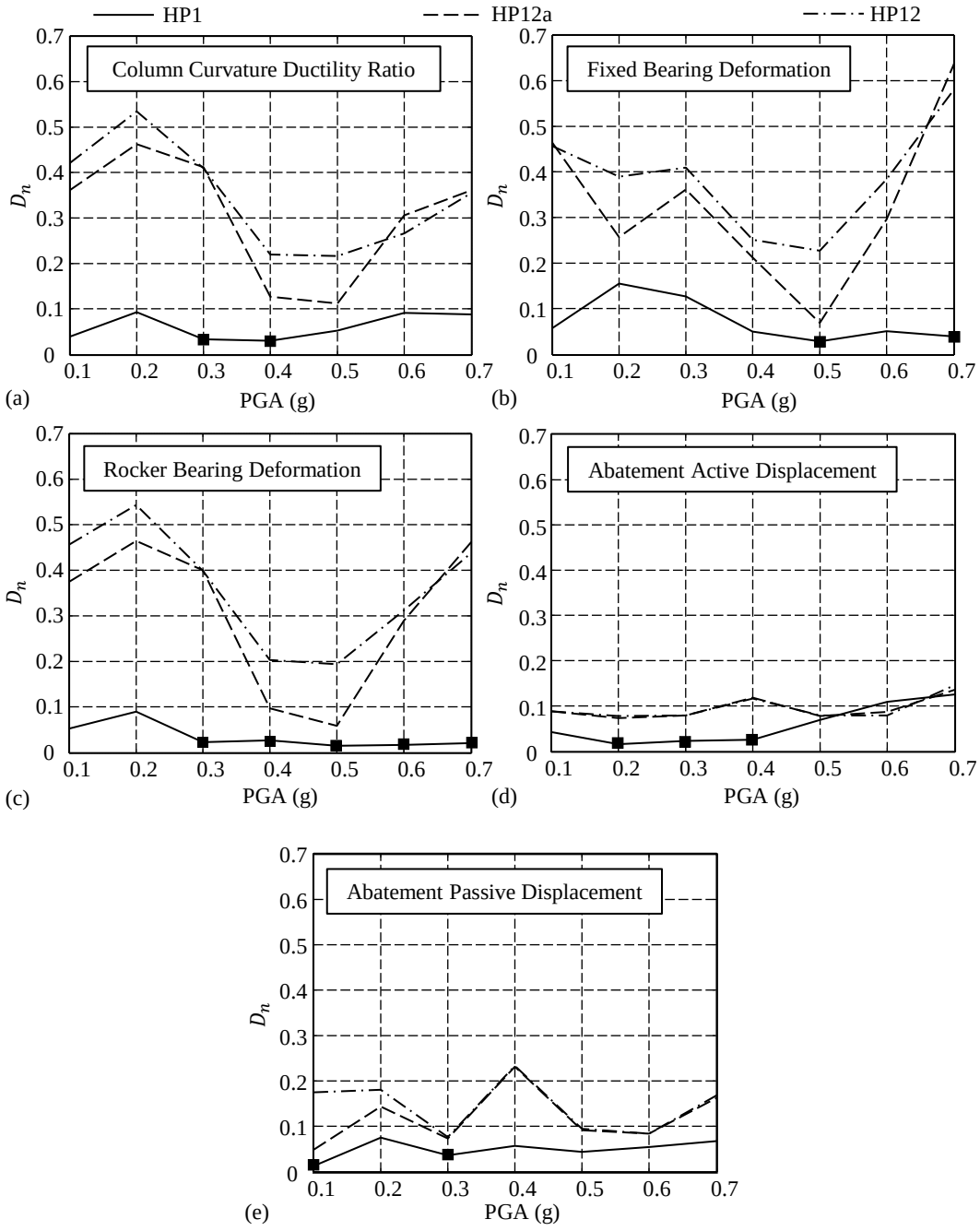

Figure 3.20: K-S goodness of fit test for MSSS Steel Girder bridge: (a) column curvature ductility ratio, (b) fixed bearing deformation, (c) rocker bearing deformation, (d) abutment active displacement, (e) abutment passive displacement

not provide a good approximation of the probabilistic characteristics of the demand. In particular, a considerable amount of error is introduced due to power model and constant dispersion assumptions. As mentioned earlier, the power model assumes that the demand increases as a certain function of the intensity of the ground motion, which can be true in some cases. However, in many other cases the structure and its behavior are much more complex and this simple rule does not necessarily reflect the characteristics of the demand. In particular, for the case of the studied bridge classes, due to irregularities and asymmetry in the geometry and material behavior (e.g., bearings, abutments, and poundings), the current PSDM model fails to capture the probabilistic characteristics of the demand. In the next sections it will be described how the error introduced to the estimation of the demand propagates to the probabilities of failure, resilience, and life-cycle loss.

3.4.3 Fragility Analysis

The probabilistic seismic demand analysis presented in Section 3.4.2 evaluated the statistical characteristics of the demand. Similar knowledge about the uncertainty on the capacity of the vulnerable components of the structure is also needed for fragility analysis. For this study the distribution of the capacity of the cantilever column and components of the bridge models for different limit states was assumed to follow a lognormal distribution based on the study and assumptions presented by Nielson (2005) and Padgett and DesRoches (2007). The lognormality assumption for the capacity is also made mostly for convenience and compatibility with the assumptions of the closed-form fragility function of Equation 2.5. The assessment and validation of the distributions of capacity for different limit states requires extensive experimental analyses that go beyond the scope of this study. In this section, fragility curves of the cantilever column and the bridge classes (components and system) will be presented and the effect of each assumption (made on the marginal distribution of the demand) on the fragilities will be evaluated.

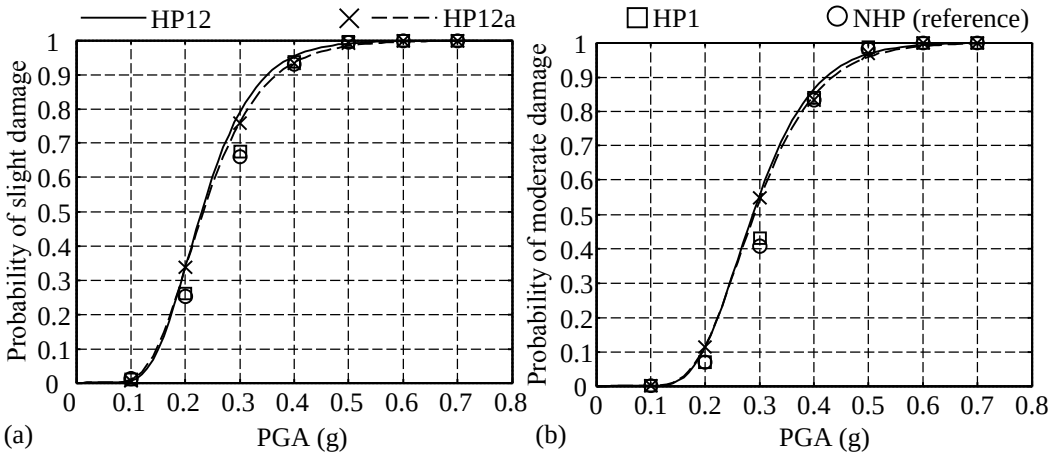

Figure 3.21: Cantilever column fragility curves: (a) slight, and (b) moderate damage

Figure 3.21 illustrates the fragility curves of the cantilever column for slight and moderate damage states. Similarly, Figures 3.22 and 3.23 show the fragility curves of the columns and rocker bearings for all four limit states: including slight, moderate, extensive and complete damage. Also, 3.24 shows the fragility curves of the rocker bearings for all four limit states of the MSC Steel Girder bridge. The continuous lines represent the fragilities generated by Equation 2.5 considering all assumptions (solution HP12), following the same technique presented by Nielson (2005). The cross markers represent fragilities calculated by removing assumption hp2b (solution HP12a). For this purpose, the logarithmic dispersion ($\beta_{D|IM}$) has been computed at each level of IM separately using Equation 2.3 and substituted into Equation 2.5 to calculate the probability of exceedance. The dashed lines represent lognormal cumulative distribution functions fitted to these points. The rest of the fragility values in these figures are computed by means of the proposed methodology presented in the Section 3.3. The square markers indicate fragilities computed considering only the lognormality assumption (solution HP1). In this case, 10^5 samples were generated by Latin Hypercube for capacity and demand. For the demand, the samples have been generated based on the parameters of the lognormal distributions fitted to the data at each level of IM. Probabilities of failure have been calculated by computing the ratios of negative safety margins, obtained comparing samples of capacity and demand. Circular markers

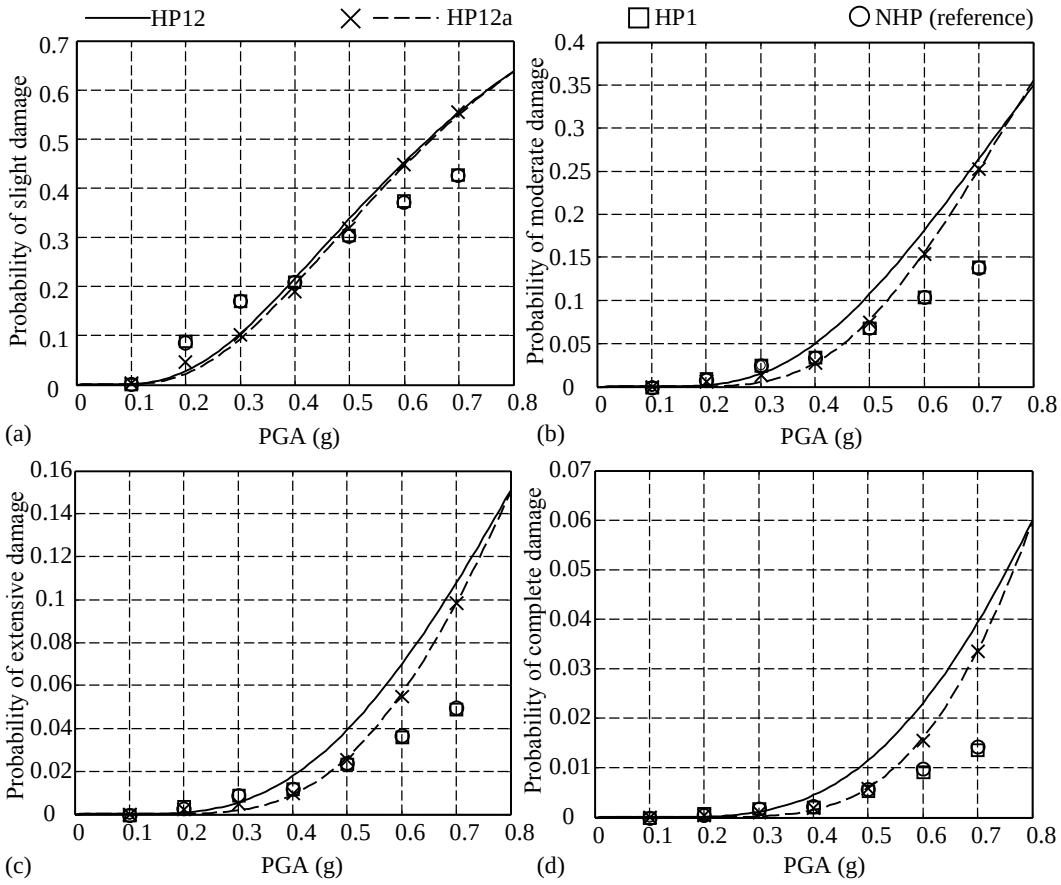

Figure 3.22: MSSS Steel Girder bridge column fragility curves: (a) slight, (b) moderate, (c) extensive, (d) complete damage

show the reference fragilities by removing all the common assumptions (solution NHP). In this case, 10^5 samples of the demand have been generated using the empirical CDF computed at each level of *IM* and classic translation theory (Grigoriu, 1998); ratios of safety margin have been computed as before.

An overall review of the results shows that in most cases NHP and HP1 fragility points are very close. This is consistent with the findings of Section 3.4.2 and means that satisfactory results can be obtained by only assuming that the demand follows a lognormal distribution. The other two assumptions (hp2a and hp2b) introduce a considerable amount of error on the component fragility curves. In fact, at some levels of *IM* the percent error of the probabilities of failure (compared to NHP solutions) considering these two assump-

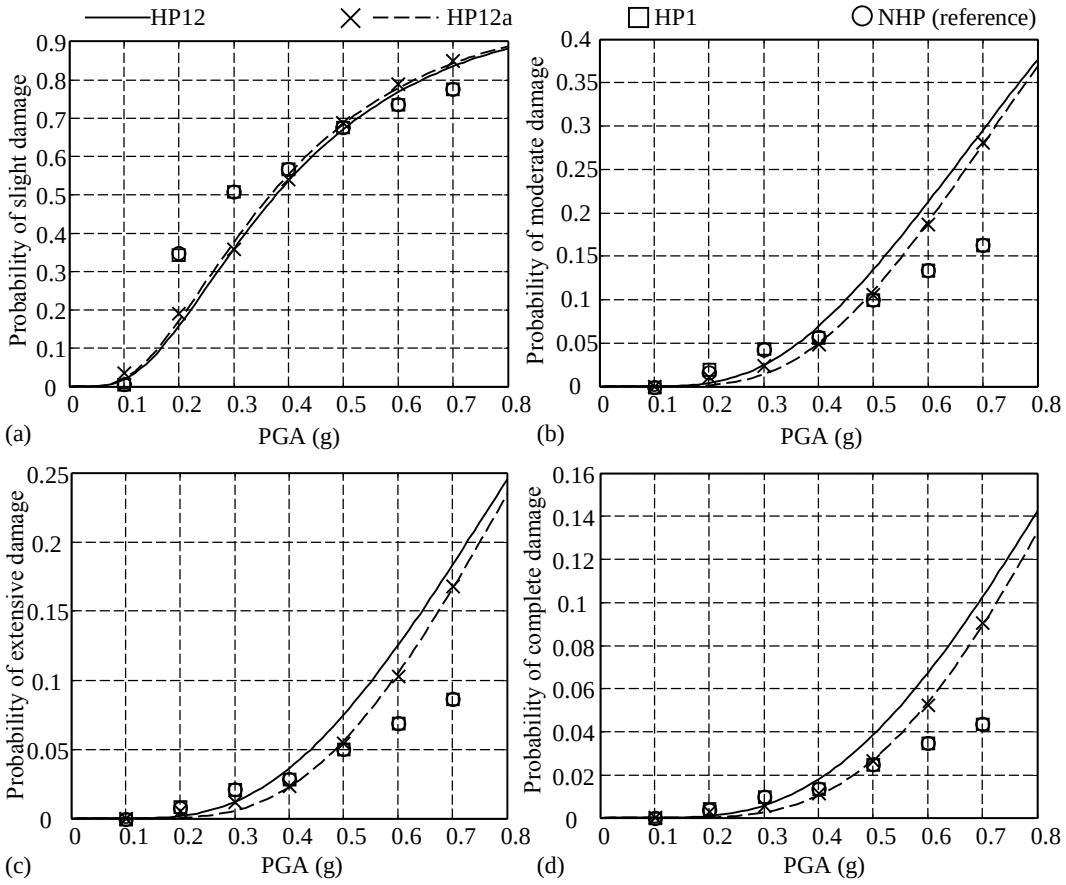

Figure 3.23: MSSS Steel Girder bridge rocker bearing fragility curves: (a) slight, (b) moderate, (c) extensive, (d) complete damage

tions reaches 150%. As expected, the approximations introduced to fragilities by each of the common assumptions follow a similar trend to that of the parameter D_n. For instance, based on the values of this parameter (D_n), Figures 3.20a and 3.20c show that the distribution of the demand by considering HP1, HP12a, or HP12 is close to the actual distribution of the demand at PGAs equal to 0.4(g) or 0.5(g), while HP12a and HP12 are substantially less accurate for other levels of IM. Similarly, by looking at the MSSS Steel Girder bridge column and rocker bearing fragility figures (Figures 3.22 and 3.23), it can be observed that at 0.4(g) and 0.5(g) all fragility points coming from different solutions are relatively close to the reference values (circles), while there is considerable discrepancy from the reference values for fragilities HP12 and HP12a at other levels of IM. The fragility curves of all

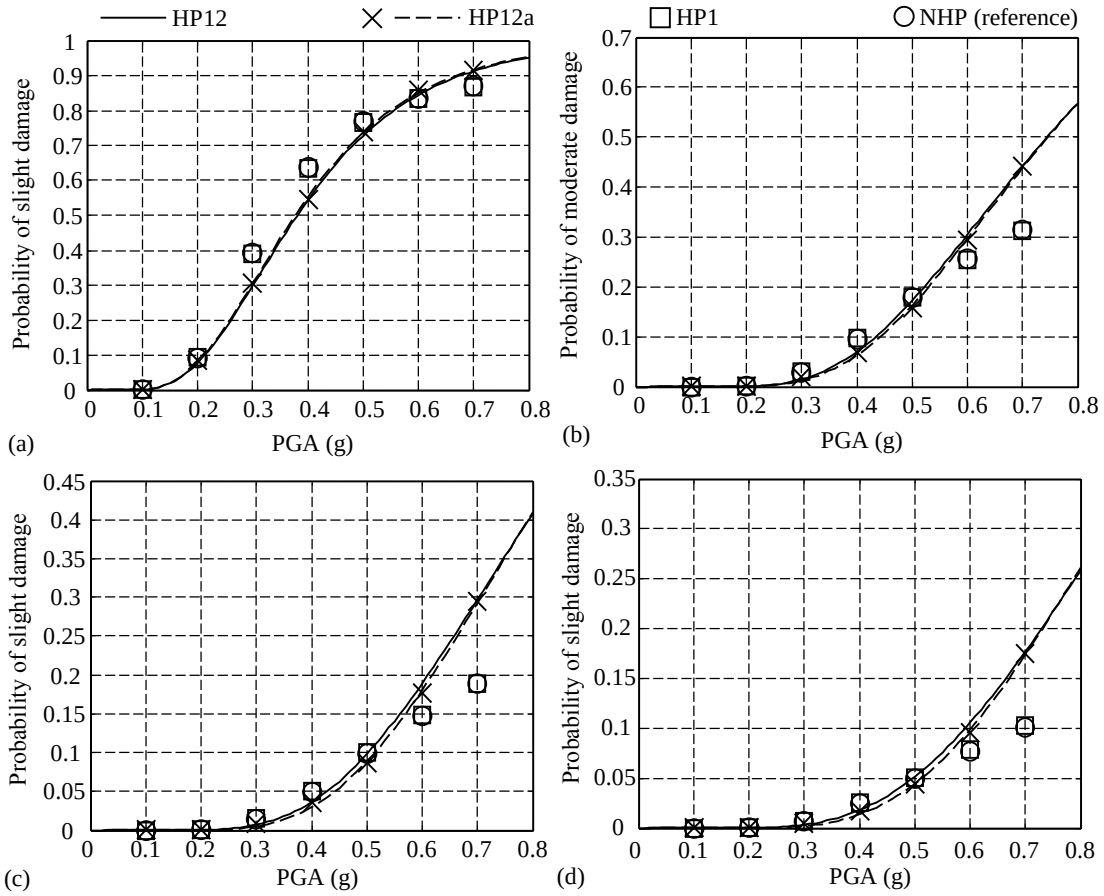

Figure 3.24: MSC Steel Girder bridge rocker bearing fragility curves: (a) slight, (b) moderate, (c) extensive, (d) complete damage

other investigated components of the MSSS and MSC Steel Girder bridges follow almost the same trend as the column and rocker bearing fragility curves presented in Figures 3.21 to 3.24.

The distribution of capacity at each limit state and its amount of overlapping with the distribution of the demand is another important factor that influences the final values of probability of exceedance in fragility curves. Using the results of the analysis performed on the cantilever column and bridge models, it was found that the effect of the form of the distribution of the capacity can be negligible when the probability of failure is either very small or very large, while for intermediate values this effect can be more significant. For example, Figure 3.25 shows the distribution of the cantilever column ductility ratio demand

Table 3.3: MSSS Steel Girder bridge system probabilities of failure and difference with reference values NHP in parentheses

	Probability of moderate damage [%]				Probability of extensive damage [%]			
IM	HP12	HP12a	HP1	NHP	HP12	HP12a	HP1	NHP
0.1(g)	0.0(0.0)	0.0(0.0)	0.0(0.0)	0.0	0.0(0.0)	0.0(0.0)	0.0(0.0)	0.0
0.2(g)	0.2(-0.5)	1.3(0.6)	2.0(1.3)	0.7	0.1(-0.2)	0.7(0.4)	1.1(0.8)	0.3
0.3(g)	1.8(-2.4)	2.8(-1.4)	5.3(1.1)	4.2	0.8(-0.6)	1.3(-0.1)	2.4(1.0)	1.4
0.4(g)	7.6(1.3)	4.7(-1.6)	6.5(0.2)	6.3	3.6(1.5)	1.6(-0.5)	2.2(0.1)	2.1
0.5(g)	16.1(-0.3)	15.6(-0.8)	16.3(-0.1)	16.4	9.3(3.2)	5.7(-0.4)	6.0(-0.1)	6.1
0.6(g)	24.1(0.5)	26.6(3.0)	23.6(0.0)	23.6	16.7(6.2)	15.2(4.7)	10.4(-0.1)	10.5
0.7(g)	30.5(3.6)	31.5(4.6)	26.9(0.0)	26.9	23.9(10.1)	24.5(10.7)	13.7(-0.1)	13.8

(solid lines) at three levels of IM, namely 0.1(g), 0.3(g), and 0.6(g). The distribution of the cantilever column capacity for moderate damage limit state has also been plotted within each figure (dashed lines). For the cases shown in Figures 3.25a and 3.25c where the overlapping area of the two distributions (i.e., demand and capacity) is small, neither the probabilistic characteristics of the demand, nor the capacity have a significant effect on the probability of failure. However, for the case illustrated in Figure 3.25b, a change in the distribution of the demand or capacity might have a considerable effect on the probability of failure.

System fragility curves have been generated for the bridge models with the methods discussed in Sections 2.2 and 3.3.2. Latin Hypercube sampling has been used to generate 10^6 samples of demand and capacity at each level of the IM. Estimates of the probabilities of exceedance have been calculated by assessing the ratio of negative safety margins. As done for the component fragilities, 4 sets of system fragilities have been generated considering different assumptions on the marginal distribution of the demand. Figure 3.26 depicts system fragilities for each limit state for the MSSS Steel Girder bridge. Also, Table 3.3 presents the system probabilities of failure for two limit states, namely moderate and extensive damage, computed with different solutions. The values in the parentheses are the absolute errors associated with the probabilities of failure of solutions HP12, HP12a, and HP1, with respect to the reference solution (NHP). Due to the contribution of all compo-

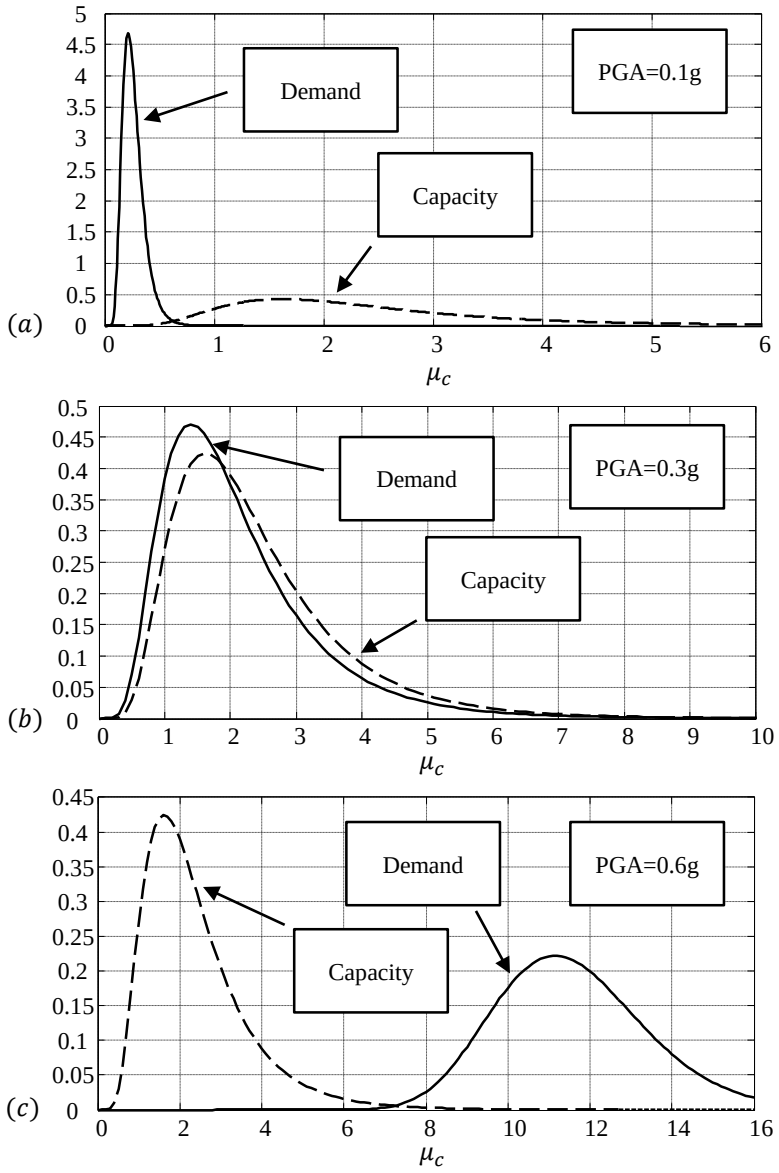

Figure 3.25: Effect of the relative location of the distribution of the demand and capacity on the sensitivity of the probability of failure to their probabilistic characteristics: comparison of moderate damage state capacity distribution and cantilever column ductility demand distribution at (a) 0.1(g), (b) 0.3(g), and (c) 0.65(g)

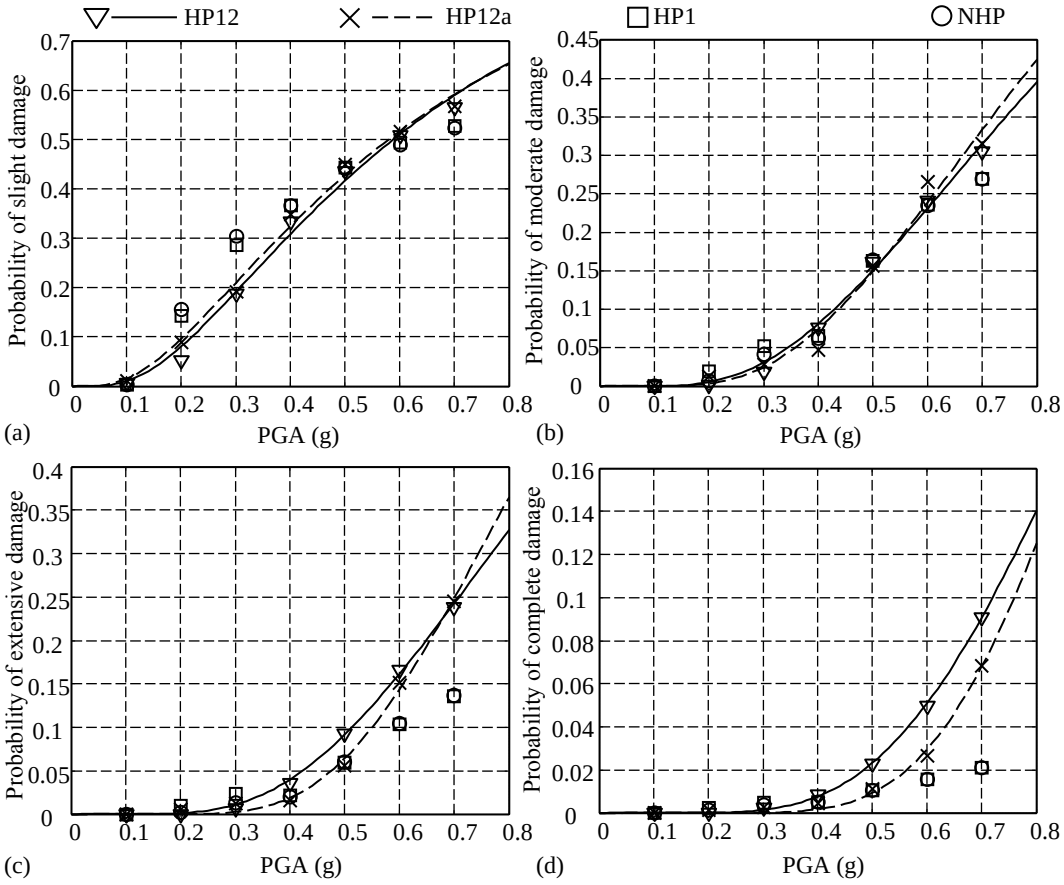

Figure 3.26: MSSS Steel Girder bridge system fragility curves: (a) slight, (b) moderate, (c) extensive, (d) complete damage

nents' demand and capacity, it is very difficult to analyze the effect on the system fragility curves of each assumption made on the distributions of the individual components' demands. However, also in this case the results show the relatively acceptable performance of the solution HP1 compared to other solutions with more assumptions. Similar results were obtained from the system fragility curves computed for the MSC Steel Girder bridge model.

In order to prevent the propagation of the errors due to the mentioned approximations made in the PSDM to the fragility values, the proposed simulation-based technique (i.e., NHP solution) presented in this chapter can be used to compute the probabilities of failure at appropriate levels of the *IM*. Then, if a continuous fragility curve is required for

Table 3.4: Characteristics of the selected bridge for resilience assessment

Year built	Latitude	Longitud	Soil type
1963	34.411669	-119.698329	D
Number of spans	**Maximum span length**	**Width**	**Length**
3	22 (m)	16.7 (m)	42 (m)

subsequent analyses (e.g., loss estimation or resilience) the best closed-form probabilistic distribution can be fitted to the available data.

3.4.4 Probabilistic Resilience and Life-Cycle Los Assessment

The system fragility curves computed in the previous section have been used to calculate the resilience of MSSS Steel Girder bridge following the methodology presented in Section 3.2. For this analysis, the geographic location of the bridge has been selected to be in Santa Barbara, California, USA, where one bridge belonging to the MSSS class is actually located. This bridge is categorized as concrete, multi-column bent California bridge with conventional (non-seismic) design (DHS, 2009). Table 3.4 presents some of the specifics of the bridge. The functionality recovery functions from ATC-13 (ATC, 1985) have been adapted to compute resilience. As discussed in Section 2.3, these recovery profiles have been computed on the basis of experts surveys, and are presented in the form of the mean time required to reach 30, 60, and 100% of the normal functionality of the structure. The selected functions are associated with the recovery profiles of Social Function Class 25c, which corresponds to conventional highway bridges. The damage states 2 through 5 presented in ATC-13 are assumed to be the corresponding damage states associated with slight through complete damage (DHS, 2009). The functionality recovery function for each limit state used in this study is shown in Figure 3.27a.

The probabilities of exceeding the damage states at each level of IM, computed by means of the system fragilities (Figure 3.26), have been used to calculate the corresponding

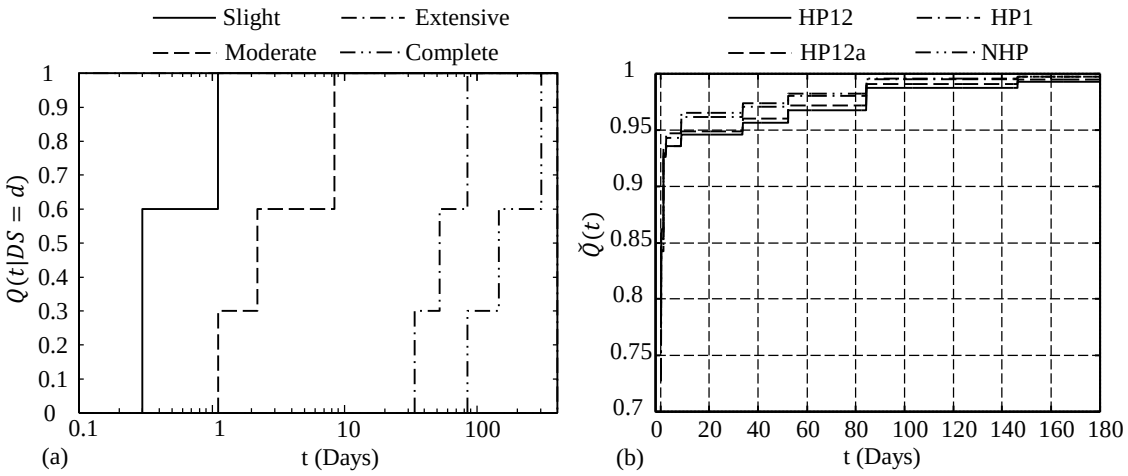

Figure 3.27: (a) Functionality recovery profiles, (b) Expected functionality of the bridge

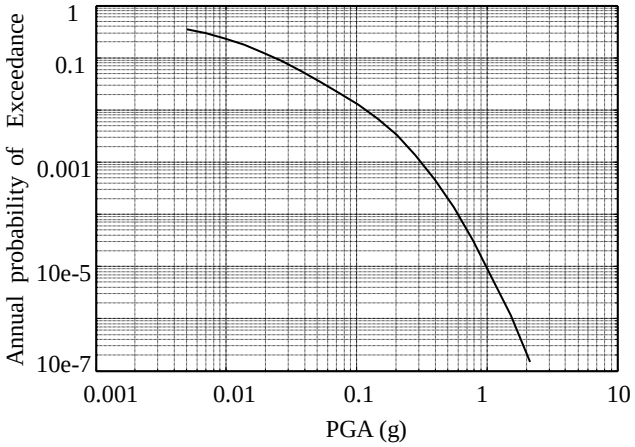

Figure 3.28: The hazard curve associated with the location of the bridge

limit state probabilities of occurrence. A probabilistic seismic hazard analysis has been performed on the site of the location of the bridge based on the United States Geological Survey (USGS) hazard curves (USGS, 2013). Figure 3.28 shows the computed hazard curve. The probabilities of occurrence of each investigated *IM* have been assessed from the hazard curve assuming a life of 100 years for the bridge. Eventually, the expected functionality of the bridge has been computed using Equation 3.1 for the time horizon of 180 days. Figure 3.27b illustrates the expected functionality recovery profile of the bridge. Four profiles presented in the figure account for the consideration of different assumptions made in the distribution of the demand during the fragility analysis. The results show that

Table 3.5: Bridge event and expected resilience and relative error in parentheses

	Expected resilience index [%]			
Ground motion *IM*	HP12	HP12a	HP1	NHP
0.1(g)	100 (0.00)	99.99 (-0.01)	100 (0.00)	100
0.2(g)	99.94 (0.17)	99.66 (-0.11)	99.47 (-0.30)	99.77
0.3(g)	99.56 (0.36)	99.35 (0.15)	98.84 (-0.36)	99.20
0.4(g)	98.24 (-0.63)	99.08 (0.22)	98.81 (-0.05)	98.86
0.5(g)	95.61 (-1.61)	97.26 (0.09)	97.18 (0.01)	97.17
0.6(g)	91.94 (-3.62)	93.39 (-2.10)	95.42 (0.03)	95.39
0.7(g)	87.71 (-6.77)	88.51 (-5.92)	94.11 (0.03)	94.08
All *IM*'s combined	97.27 (-1.14)	97.58 (-0.82)	98.24 (-0.15)	98.39

the functionality profiles obtained considering different levels of assumptions are relatively similar, but those small differences in the recovery can have a large impact on the long-term loss estimation. Following the previous observations of the effect of the assumptions, results of the solutions HP12 and HP12a are the least accurate and HP1 is the most accurate compared to the solution NHP.

Having the evolution of the expected functionality over the time horizon, Equation 2.9 can be used to determine the resilience of the bridge. Table 3.5 presents the resilience of the bridge calculated for each event with *IM*s from 0.1(g) to 0.7(g), as well as the expected resilience considering each assumption made on the distribution of the demand. The values in parentheses are the relative errors associated with the resilience computed for different solutions (HP12, HP12a, and HP1), with respect to the reference solution (NHP). These results show that for several intensities of the ground motion, the reference resilience computed considering the empirical distribution of the demand is considerably different from other approximated values. These discrepancies are more evident for stronger events (with higher *IM*) where the discussed assumptions give worse approximations of the distribution of demand parameters (see Figure 3.20). However, these differences are weighted by the low probabilities of strong events. Thus, the expected resilience of the bridge considering all events is very similar for the four solutions with different assumptions on the demand.

Using the system fragilities illustrated in Figure 3.26, and the probabilistic seismic hazard analysis carried out on the bridge site, Equation 3.2 can be applied to estimate the expected direct loss of the bridge over its life-cycle. The construction cost (CO_c) of the bridge is \$1.34 million (DHS, 2009). The damage ratios (DR_d) are assumed to be 0% for no damage, 3% for slight damage, 8% for moderate damage, 25% for extensive damage, and 100% for complete damage (ATC, 1985). The expected loss of the bridge calculated using the results of the solutions NHP and HP1 are \$30,520 and \$31,960, respectively. On the other hand, the expected loss estimated by solution HP12a is \$40,020 and \$45,060 is the loss resulting from solution HP12. The results show a considerable amount of discrepancies between the expected loss by solutions HP12 and HP12a with the other two solutions. This means that the error introduced to the expected loss by considering all assumptions is about 48% and by considering both hp1 and hp2a is about 31%, respectively. Hypothesis hp1 has a minor impact on the accuracy of the results as it causes only 5% error in the result of the expected loss.

3.5 Concluding Remarks

This chapter presents a simulation-based methodology for probabilistic seismic demand and fragility analyses aimed at improving the accuracy of the resilience and expected life-cycle loss assessment of highway bridges. This methodology allows removing the assumptions usually made on the probability distribution of the demand, and therefore provides more accurate results for computing fragility curves, resilience, and economic loss.

Probabilistic seismic demand and fragility analyses were carried out on the numerical model of a cantilever column, a MSSS Steel Girder bridge class, and a MSC Steel Girder bridge class. The impact of different assumptions made on the demand was evaluated and the results were compared to those of the proposed procedure. The following concluding

remarks have been made from the results of the analysis:

1. A comprehensive analysis has confirmed the general perception that the distribution of the demand is not lognormal. However, the power model and constant dispersion assumption have shown to be the major sources of error for fragility, resilience, and life-cycle loss analyses.

2. The amount of error introduced to the studied metrics depends on the accuracy of the assumptions on estimating the probabilistic characteristics of the demand. The K-S goodness of fit test has been utilized to track the level of accuracy that can be expected form solutions with different levels of assumptions. To this respect, at the values of IM for which the K-S parameter D_s is less than 2.0, the maximum error in the component and system probabilities of failure, and event resilience, has found to be limited to 10, 7, 7%, respectively.

3. The expected life-cycle loss was found to be up to 50% overestimated for the solutions in which power model and constant dispersion have been included. However, the expected resilience is almost the same for all the methodologies (maximum error $\leq 1.14\%$).

The typical level of acceptable error varies significantly depending on the ultimate goal of the analysis. Also, the accuracy yielded by the various assumptions depends on the specific structure. Therefore, the final decision on the applicability of the assumptions should be taken by the analyst. The spectrum of examined cases (i.e., cantilever column, MSSS and MSC Steel Girder bridges) in this chapter is broad enough to make a trend emerge, and a set of recommendations is provided in Table 3.6, as a general rule-of-thumb on whether to use the closed-form solution or perform the simulation.

As a general conclusion, it appears that these assumptions, introduced almost 15 years

Table 3.6: Guidelines on the applicability of closed-form solutions

Analysis type	**Recommendations**
Component fragility	Simulation is recommended if the acceptable error is smaller than 15%
System fragility	Simulation is recommended if the acceptable error is smaller than 10%
Event resilience	Simulation is recommended if the acceptable error is smaller than 10%
Expected resilience	Simulation is recommended if the acceptable error is smaller than 5%
Life-cycle loss	Simulation is always recommended

ago with the aim of simplifying the problem and promote the practical application of these concepts, may be unnecessary today. Contemporary computational resources and improved attention towards probabilistic aspects in the Civil Engineering community allow new approaches to these problems. The proposed simulation-based technique requires some expertise in parallel computing, but is conceptually very simple. Moreover, due to its versatility, it allows to remove other hypotheses and simplifications (such as lognormality assumption of the capacity). The bridge models presented in this chapter will be used in Chapter 4 to assess the restoration and functionality of bridges. Also, the fragility curves computed using the proposed methodology will be utilized in Chapter 5 to perform a fully probabilistic and time-dependent functionality analysis of bridges.

Chapter 4

From Component Damage to System-Level Probabilistic Restoration Functions for a Damaged Bridge

4.1 Introduction

In Section 2.4 several formulations and methodologies for computation of resilience of structures and infrastructure systems were reviewed. While the proposed metrics and techniques address the aspects and dimensions of system resilience in different ways, they typically follow a similar form and present the system resilience as a function of time-dependent functionality of its critical components (Equation 2.7). In regard to resilience assessment of transportation networks, bridges are considered one of the key components whose functionality have direct impact on the performance and resilience of the whole system. However, there are limited number of restoration functions available for bridges. Moreover, many available restoration functions are considerably simplified and do not reflect the expected characteristics of restoration functions for individual bridges (see Section 4.2).

To this respect, this chapter presents a new methodology to evaluate the probabilistic characteristics of functionality of damaged bridges after an extreme event and, more importantly, during the restoration process. In order to have a realistic prediction of the functionality, the restoration process has been modeled in detail, using construction management tools, and considering the uncertainties in scheduling and planning the restoration. The proposed methodology allows to avoid the simplifications and assumptions typically

made in evaluating the bridge system (in this chapter the term "system" refers to the bridge structural system and not to the transportation network) damage state and functionality. This is accomplished by relying on bridge component damage states and restoration, as well as construction logics and logistics. The outcome consists in probabilistic restoration curves with unprecedented level of detail. The application of the methodology is presented through the example of the numerically modeled Multi-Span Simply Supported (MSSS) Steel Girder bridge presented in Chapter 3, subjected to a seismic ground motion scenario. The methodologies and results presented in this chapter are based on a paper by Karamlou and Bocchini (2016a).

4.2 Shortcomings of the Available Bridge Restoration Models

The bridge restoration functions reviewed in Section 2.4 provide valuable information about the post-event functionality of bridges. These include the restoration functions presented by ATC (1985), Shinozuka et al. (2003), DHS (2009), Porter (2004), Padgett and DesRoches (2007), and Bocchini et al. (2012). However, they present a set shortcomings when used for disaster resilience evaluation of individual bridges. In the following, such shortcomings are briefly discussed.

In the majority of these restoration functions, it is not possible to differentiate between the idle time (time between the extreme event and restoration initiation) and restoration time, since they have been calibrated for regional loss analysis rather than for restoration of individual bridges (ATC, 1985; DHS, 2009; Padgett and DesRoches, 2007). This is of great importance, since knowing the idle time is necessary for the assessment of the restoration and resilience of transportation networks.

For the models developed based on component damage states (Porter, 2004; Padgett and DesRoches, 2007), the transition between the component and system damage states is not trivial (Dueñas-Osorio and Padgett, 2011). For the models developed based on system damage states, the damage states definitions are too qualitative and do not encompass all possible component damage scenarios (ATC, 1985; DHS, 2009; Shinozuka et al., 2003; Bocchini et al., 2012). This resolution is usually required when investigating a single structure.

Some of the models do not distinguish between the recovery of different bridge types, as they have been presented only as a function of the initial damage of bridges (ATC, 1985; DHS, 2009; Padgett and DesRoches, 2007).

Bridge restoration functions are more likely to be stepwise, as the functionality of bridges is typically expressed as a fraction of the number of lanes open to the traffic. Discrete models do not provide the evolution of the functionality throughout the restoration process (ATC, 1985), and continuous models seem to be unrealistic when presenting a smooth evolution of the functionality (DHS, 2009). Other limitations can result from temporary reduced speed limits, or reducing the maximum weight of transiting vehicles. Even in these cases, the functionality ends up taking a relatively small set of discrete values.

In case of survey-based models, the number of experts responding to the questionnaires is typically small (ATC, 1985; Porter, 2004; DHS, 2009; Padgett and DesRoches, 2007). On the other hand, the validation of the mathematical models is typically difficult, due to the limited amount of available data (Shinozuka et al., 2003; Bocchini et al., 2012).

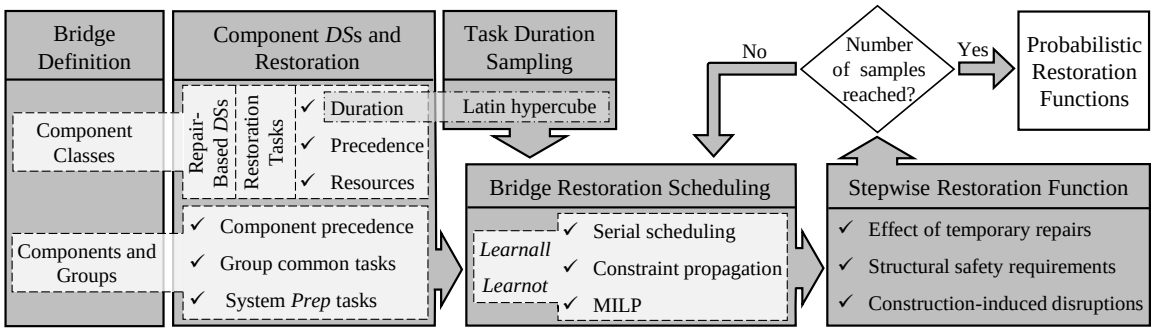

Figure 4.1: Schematic process of the proposed framework for probabilistic bridge restoration function

4.3 Proposed Framework for the Construction of Probabilistic Bridge Restoration Functions

The previously discussed restoration models can provide a general sense of the post-event functionality of damaged bridges. However, this research is aimed at providing a versatile methodology to capture the characteristics of the restoration function for any type of bridge, at any damage state, and considering any level of repair resource availability. The simulation-based nature of the proposed technique allows to consider the uncertainties involved in the restoration scheduling. Figure 4.1 illustrates the flowchart of this methodology, whose components are discussed in the following sections.

4.3.1 Bridge System Definition

The first step is bridge system definition, which consists in the classification of various components of the bridge that need to be considered for the analysis. Typically, these include the subset of components that play important roles in the functionality and stability of the bridge, and take considerable effort to be repaired in case they are damaged (e.g., foundations, columns, abutments, and approach slabs). This can be done for existing bridges

or bridge types used in regional risk and loss analyses, such as those typical of California (Ketchum et al., 2004) or Central and Southeastern United States (Nielson, 2005).

In addition to component classes, also a set of component groups is defined at this stage. Each group contains the components that share some repair and construction efforts. For instance, in the case of a multi-span bridge, all the structural components of a column bent are assigned to one group. This includes column foundation(s), column(s), and bearings. This categorization helps for later manipulation of the restoration tasks that are common among the components of each group.

4.3.2 Component Damage States and Restoration

The second step consists in defining component damage states and their restoration properties. To this respect, for each component class, relevant repair-based damage states (*DS*) are defined. Compared to different types of damage states in the literature, repair-based damage states directly map the restoration decision of a single damaged component class (e.g., repair or replacement) to its relevant demand parameter (e.g., maximum displacement, residual deformation, etc.). For instance, Mackie et al. (2008) presented such repair-based damage states for several selected component classes of bridges typical of California, based on Caltrans policies. The major construction tasks typically performed for the restoration of each damage state are specified for each component class. A list of repair activities for different components has been reported by Mackie et al. (2008). Additionally, useful information can be found in bridge inspection and maintenance manuals compiled by several departments of transportation such as Ramirez et al. (2000), PennDOT (2010), Bhatt et al. (2012), and HOR (2014).

Based on the common construction methods followed in practice, two levels of restoration precedence relations are specified. These are the precedence relations between the var-

ious restoration tasks of each component, and the precedence relations among the restoration of different components of the bridge. For example, typically the repair construction tasks performed on a column start after finishing the tasks on its foundation. Thus, the restoration of the column is considered to be the successor of the restoration of the foundation on which the column is constructed.

The restoration tasks are categorized into three categories, namely Regular (*Reg*), Preparation (*Prep*), and Temporary Repair (*Temp*). *Prep* tasks include off-site tasks for design and/or fabrication of new parts and components, such as shorings, bearings, and column casings. Typically, these tasks are started at the beginning of the restoration schedule. In case multiple components of the bridge require the same *Prep* task, only one is kept in the list of the tasks and the rest are removed. For example, all temporary shorings need to be designed and approved before installation. However, even if several components of the bridge require such restoration task, only one equivalent item will be included for the restoration of the system. Additionally, such tasks are set to be the predecessor for the restoration of their corresponding components. *Temp*s include the tasks associated with the installation and removal of temporary repairs, such as shorings and steel plates for damaged columns and expansion joints, respectively. Such repairs are made to temporarily restore the functionality of the bridge during the restoration process. However, in many cases temporary repair solutions are the same for different structural components (e.g., shoring for foundations, columns and bearings). In such cases, duplicate *Temp*s are removed from the list of the tasks and the precedence relations among the tasks of the affected components are updated accordingly. The tasks that are not categorized as *Prep* or *Temp*, are considered to be *Reg*.

Two sets of information are paired with each restoration task. The first is the probability distribution of the duration of each task. The duration of construction tasks may vary considerably, due to several factors such as proficiency of crews, efficiency of equipment,

weather conditions, etc. Thus, it is critical to take this uncertainty into account for the computation of the bridge restoration schedule. The distribution of the duration of the tasks can be established by performing surveys on bridge engineers and construction managers. The second information is the type and number of construction resources required for the execution of each task. Examples of such resource types are manpower, construction machineries and facilities.

4.3.3 Task Duration Sampling

Task duration sampling is the third step of the proposed technique. After specifying the bridge components, restoration tasks, and precedence relations, as discussed earlier, samples of the duration of the tasks present in the pool of bridge's restoration tasks are generated. Latin hypercube technique is used for a more effective sampling (McKay et al., 2000). It is worth mentioning that the same procedure can be implemented in case other parameters are considered to be uncertain, such as the amount of resource requirements for each restoration task.

4.3.4 Bridge Restoration Scheduling

In this step, the bridge restoration schedules are computed. Each set of task duration samples, along with their associated resource requirements and precedence relations is utilized to generate one sample bridge restoration schedule using a project scheduling optimization algorithm. The computed project schedules might be relatively different from the schedules developed by taking into account all fundamentals of construction management (Yanev, 2007; Orabi et al., 2009, 2010; O'Brien and Plotnick, 2015). However, it is worth noting that the purpose here is not to obtain the best schedule for the project, but to identify scenarios that are feasible and likely to occur, considering the uncertainties in the duration of restoration tasks and construction planning. Actually, each set of samples represents one

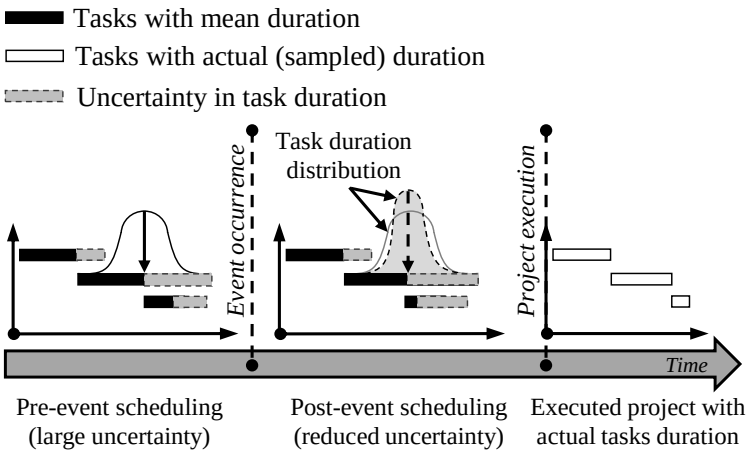

Figure 4.2: The variation of the uncertainty in task duration

possible scenario for the duration of the tasks. The distribution assigned to the duration of each task is determined based on historical data and past experience. Part of this uncertainty is associated with lack of knowledge at the time this analysis is performed (i.e., pre-event) and regarding the anticipated situation of crews, seasonal conditions, etc. at the time of executing the project (i.e., post-event). Some of these aspects become known immediately after the extreme event (e.g., we know in which season the event occurred). Therefore, the amount of this uncertainty is reduced at the time when the restoration project is scheduled (Figure 4.2). However, the quantification of the actual portion of the uncertainty that disappears due to what is learned after the extreme event is extremely difficult. Therefore, the following schemes investigate the two extreme cases: *Learnall* assumes that after the event all the uncertainty on the task duration vanishes; *Learnot* assumes that the uncertainty on the task duration remains exactly the same even after the event.

1. *Learnall*. In this scheme, it is assumed that the durations need to be considered random at the time of the analysis (i.e., pre-event), but the project manager will be able to predict the actual duration of the tasks (i.e., learn their sample realizations) by evaluating the situation immediately after the event, at the time of scheduling the project. Therefore, the project scheduling technique discussed later is used once for

each set of task duration samples, to compute one restoration schedule.

2. *Learnot*. In this scheme, it is assumed that the project manager does not gain any additional knowledge after the extreme event. He still only possesses information on the probabilistic distribution of the duration of the tasks, based on previous experience. Therefore, the actual duration of the tasks (equal to their sample realizations) is not known at the time of scheduling. Thus, the project is planned and started using a baseline schedule computed considering only the mean duration of the tasks. As the project unfolds, the differences between the expected (mean) and actual (samples) durations of the tasks emerge. In these cases, the project schedule is updated, to adjust for the changes. Such update is modeled by re-running the scheduling optimization procedure for all the future tasks, and incorporating the information on the completed and ongoing tasks. In particular, the not-yet-started tasks are rescheduled every time a task finishes earlier than expected, or when it does not finish at its expected completion time. This process is repeated until all tasks of the project are completed.

The restoration schedule for each of the above schemes is computed by solving a resource constrained project scheduling problem (RCPSP). This is an extension of the classic scheduling problem that, in addition to the tasks precedence constraints, takes into account the availability of the required resources for each task. RCPSP is defined by a tuple (V, p, Ep, Rsc, Br, br), where V is a set of n tasks to be scheduled, p is a vector of task durations, Ep is a set of precedence relations so that if $(i, j) \in Ep$ task i is the predecessor of task j, Rsc is a set of m renewable resource types considered in the problem, Br is a vector of resource availability, and br is a matrix of resource consumptions for each task (Artigues et al., 2013). Different objectives can be considered for RCPSP (Neumann et al., 2003). For this research, the minimization of the duration of the project is selected as the objective of the optimization problem.

RCPSP is known to be a *NP-hard* optimization problem in the strong sense. Several researches have proposed different formulations and methodologies to solve large RCPSPs more efficiently (Demeulemeester and Herroelen, 2002; Neumann et al., 2003; Artigues et al., 2013; Brucker, 2002). In this study, a Mixed Integer Linear Programming (MILP) formulation developed by Pritsker et al. (1969) is utilized which is discussed in the following section. Optimality of the solution of this MILP formulated optimization problem is guaranteed by using a branch and bound solution technique.

4.3.4.1 A MILP Formulation for Solving RCPSP

In this formulation, binary design variables $x_{i,t}$ are used, so that $x_{i,t} = 1$ if task i starts at time t, and $x_{i,t} = 0$, otherwise. In addition to the tasks of the project, two dummy tasks $\{0, n+1\}$ are defined with zero duration. Task 0 and $n+1$ are set to be the predecessor and successor of all other tasks, respectively. In this way, 0 and $n+1$ represent the start and end tasks of the project, respectively. The formulation of the problem is as follows:

Find

$$x_{i,t} \quad \forall i \in \{0,1,2,\ldots,n+1\}, \forall t \in \{EST_i, LST_i\} \tag{4.1}$$

so that

$$\sum_{t=EST_{n+1}}^{T} t \cdot x_{n+1,t} = \text{minimum} \tag{4.2}$$

subjected to the constraints

$$\sum_{t=EST_j}^{LST_j} t \cdot x_{j,t} \geq \sum_{t=EST_i}^{LST_i} t \cdot x_{i,t} + p_i \quad \forall (i,j) \in Ep \tag{4.3}$$

$$\sum_{i=1}^{n} br_{i,k} \sum_{\tau=\max(EST_i, t-p_i+1)}^{\min(LST_i,t)} x_{i,\tau} \leq Br_k \quad \forall t \in H, \forall k \in Rsc \tag{4.4}$$

$$\sum_{t=EST_i}^{LST_i} x_{i,t} = 1 \quad \forall i \in \{0,1,2,\ldots,n+1\} \tag{4.5}$$

$$x_{i,t} \in \{0,1\} \quad \forall i \in \{0,1,2,\ldots,n+1\}, \forall t \in \{EST_i, LST_i\} \tag{4.6}$$

where EST_i and LST_i are the earliest and latest start time of task i, and T is an upper bound for the duration of the project, which can be computed by preprocessing. $H = \{0,1,\ldots,T\}$ is the set of discrete time steps considered.

This formulation involves $\sum_{i=1}^{n+1}(LST_i - EST_i + 1)$ design variables and $|Ep| + (T+1)m + n + 1$ constraints, where $|Ep|$ is the total number of precedence relations among the tasks. Therefore, the number of variables and constraints, and consequently the computational cost of the optimization are highly dependent on T and the time window of each task (i.e., $[EST_i, LFT_i]$ where LFT_i denotes the latest finish time of task i computed as $LST_i + p_i$). In order to reduce this variability, a set of preprocessing algorithms has been utilized: the Critical Pass Method (Section 4.3.4.2), the Serial Scheduling Scheme (Section 4.3.4.3), and the Constraint Propagation technique (Section 4.3.4.4). The final solution of the RCPSP is typically computed using a branch and bound technique.

The optimization solution provides (a realization of) the start time of each task, which is used to build (a sample of) the full restoration schedule of the bridge. This schedule is utilized to determine (a sample of) the functionality of the bridge during the restoration, as discussed later in Section 4.3.5.

4.3.4.2 The Critical Path Method

The Critical Path Method (CPM) is a well-known technique to compute the time window of the tasks of a project only considering the precedence relations among the tasks. The time window for task i is defined to be the interval $[EST_i, LFT_i]$. To this respect, a *forward*

pass analysis is carried out to compute EST_i and EFT_i (the earliest finish time of taks i) of each task i. This follows with a *backward pass* analysis to compute LST_i and LFT_i for all of the tasks. Details and examples of CPM can be found in the literature (for example see O'Brien and Plotnick, 2015). The values of LST_i and LFT_i are used to facilitate the operation of the Serial Scheduling Scheme discussed in the following.

4.3.4.3 The Serial Scheduling Scheme

The second preprocessing technique used in this study to facilitate solving the RCPSP is the Serial Scheduling Scheme (SSS). SSS is an efficient priority-rule-based heuristic method consisting of $n+2$ steps (i.e., total number of task considering the dummy tasks 0 and $n+1$). In each step a partial solution is generated. A partial solution is an schedule in which only a subset of tasks has been assigned a start (or finish) time. To perform the SSS, first the tasks of the project are sorted in topological order. This means that $i < j$ if $(i, j) \in Ep$. Two disjoint sets of tasks are defined and updated at each stage of the process. Sch_i is the *scheduled set* that contains the tasks which have been included in the partial solution generated at step i. Dec_i is the *decision set* which contains all unscheduled tasks whose immediate predecessors are in Sch_i. At each step, one task is selected considering a priority rule and moved from the decision set to the scheduled set. The selected task is scheduled at its earliest precedence and resource feasible start time. Then Sch_i and Dec_i are updated accordingly for the next step of the process. This process is continued until all tasks of the project are scheduled.

Algorithm 4.1 illustrates a formal presentation for SSS as formulated by Kolisch (1996). In this algorithm, $|Sch_i|$ is the size of the scheduled set at stage i. PI_j is the set of all immediate predecessors of task j. πBr_{rt} and Θ_t are the number of resource type r available, and the set of tasks being executed at time t, respectively. FT_i is the finish time of task i. $v(j)$ is the priority value of task j, which is defined based on the selected priority rule. The

Algorithm 4.1 Serial scheduling scheme for resource constrained project scheduling

1: **Initialization**:
2: $i \leftarrow 0$
3: $Sch_i \leftarrow \phi$
4: **while** $|Sch_i| < (n+1)$ **do**
5: $\quad Dec_i = \{j | j \notin Sch_n, PI_j \subseteq Sch_n\} \quad \forall j \in \{0, n+1\}$
6: $\quad \pi Br_{rt} = Br_k - \sum_{j \in \Theta_t} br_{jk} \quad \forall t \in \{0, T\}, \forall k \in Rsc$
7: $\quad j^* = min(\text{or } max)_{j \in D_n}\{j | \nu(j)\}$
8: $\quad EFT_{j^*} = max\{FT_j | j \in PI_{j*}\} + p_{j*}$
9: $\quad FT_{j^*} = min\{t | EFT_{j^*} \leq t \leq LFT_{j^*},\ br_{j^*k} \leq \pi Br_{r\tau} \quad \forall \tau \in \{t - p_{j^*} + 1, t\},\ \forall k \in Rsc\}$
10: $\quad Sch_i + 1 = Sch_i \cup \{j^*\}$
11: $\quad i = i + 1$

results of CPM discussed earlier are used for LFT_j. Algorithm 4.1 can be implemented to run in $O((n+2)^2 m + (n+2)\sum_{i=1}^{m} Br_k)$ time (Brucker and Knust, 2006).

Several priority rules have been proposed by the research community (Kolisch, 1996). Depending on the type of the priority rule, the task with the highest (or lowest) priority value (i.e., $\nu(j)$) among the tasks in the decision set is selected at each step of SSS. In the current study, a priority rule based on the latest start time has been utilized. The associated priority value for this rule is computed as follows:

$$\nu(j) = LFT_j - p_j \tag{4.7}$$

Based on this rule, the eligible task with the lowest value of ν has the highest priority.

SSS provides an upper bound (T) and a feasible solution for the problem. The computed feasible solution is utilized as an initial point to improve the computational efficiency of the branch and bound optimization used as the main solver of the RCPSP, as discussed in Section 4.3.4.1. The computed upper bound T is used to facilitate the operation of the Constraint Propagation technique discussed in the following.

4.3.4.4 Constraint Propagation

Constraint propagation consists in a set of techniques to impose additional restrictions to the given time window of the tasks of the project. Considering the MILP formulation presented in Section 4.3.4.1, constraint propagation techniques can be used to facilitate the convergence of the branch and bound solver by decreasing the number of design variables and shrinking the size of the search domain. a detailed presentation of constraint propagation techniques is beyond the scope of this research and more information can be found in the literature (see for example Brucker, 2002; Brucker and Knust, 2006). In the following, only a brief description of the technique is provided.

To initiate the process, each pair of tasks is categorized considering a set of three relations: *conjunction*, *parallelity*, and *disjunction*. (i, j) are in *conjunction* relation (*Cs*) if task i is completed before task j starts (i.e., $i \rightarrow j$). This indicates that:

$$ST_i + p_i \leq ST_j \iff i \rightarrow j \tag{4.8}$$

where ST_i and ST_j are the start times of tasks i and j, respectively. (i, j) are in *parallelity* relation (*Ps*) if the execution of tasks i and j overlaps (i.e., $i \parallel j$), indicating that:

$$[ST_i + p_i > ST_j \wedge ST_j + p_j > ST_i] \iff i \parallel j \tag{4.9}$$

Finally, *disjunction* (Ds) relation is defined as the complementary of the *parallelity* relation as shown in the following:

$$[ST_i + p_i \leq ST_j \vee ST_j + p_j \leq ST_i] \iff i - j \tag{4.10}$$

The *conjunction*, *parallelity*, and *disjunction* sets are formed at the beginning and updated

in a stage-wise fashion using a series of constraint propagation techniques. As shown in the following equations, the initial members of the *conjunction* and *disjunction* sets can be specified using the problem precedence and resource constraints, respectively.

$$i \rightarrow j \Longleftarrow (i,j) \in Ep \tag{4.11}$$

$$i - j \Longleftarrow \{\exists k \in \{1,\cdots,m\} : br_{ik} + br_{jk} > Br_k\} \tag{4.12}$$

Brucker (2002) showed that an initial *parallelity* set can be formed considering the following relations:

$$i \parallel j \Longleftarrow \{p_i + p_j > max(\tilde{d}_i, \tilde{d}_j) - min(\tilde{r}_i, \tilde{r}_j)\} \tag{4.13}$$

where $\tilde{r}_i$ and $\tilde{d}_i$ are a lower bound for EST_i and an upper bound for LFT_i, respectively. To compute these values, the problem (i.e., RCPSP) is formulated as an activity-on-node graph. The value of $\tilde{r}_i$ is computed as the length of the longest path from the vertex of dummy task 0 to the vertex of task i. $\tilde{d}_i$ is computed as follows:

$$\tilde{d}_i = T - \tilde{q}_i \tag{4.14}$$

where T is an upper bound for the problem (here obtained through the SSS). $\tilde{q}_i$ is the length of the longest path from the vertex of task i to the vertex of the dummy task $n+1$. In this study, the Bellman Ford algorithm has been used to compute the longest path for $\tilde{r}_i$ and $\tilde{q}_i$ (Ahuja et al., 1993). To this purpose, Bellman-Ford algorithm is applied to the graph with all edge weights negated. $[\tilde{r}_i, \tilde{d}_i]$ is the time window of task i used in the formulation presented in Section 4.3.4.1. Tighter task time windows are derived from the updated *conjunction*, *parallelity*, and *disjunction* sets by using a set of constraint propagation techniques discussed in the following.

After the initial formation of the *conjunction*, *parallelity*, and *disjunction* sets, a matrix called SSD (Start-Start Distance) is formed. SSD is a matrix of size $(n+2)\times(n+2)$ with the components computed as follows:

$$ssd_{ij} = \begin{cases} 0 & \text{if } i = j \\ p_i & \text{if } i \rightarrow j \\ -(p_j - 1) & \text{if } i \parallel j \\ p_i - T & \text{otherwise} \end{cases} \tag{4.15}$$

Brucker (2002) showed that the components of the first row and last column of the SSD matrix are indeed $\tilde{r}_i$ (i.e., $ssd_{1i} = \tilde{r}_i$) and $\tilde{q}_i$ (i.e., $ssd_{j(n+1)} = \tilde{q}_j + p_j$) values, respectively. As discussed earlier, these two values can be used to form the time window of each task.

A series of constraint propagation techniques are applied to replace the components of the SSD matrix, as well as expanding the *conjunction*, *parallelity*, and *disjunction* sets. The first technique is to replace the SSD matrix with its transitive closure ($\overline{\text{SSD}}$), which can be computed using the Floyd-Warshall algorithm (Ahuja et al., 1993). The process is continued with checking the feasibility of the $\overline{\text{SSD}}$ matrix. To this respect, it was shown that if there is any $\overline{ssd}_{ii} > 0$, there is no feasible project schedule with total duration less than (or equal to) the previously computed upper bound (i.e., T). If the SSD matrix is feasible, the conjunction and parallelity sets can be updated as follows:

$$i \rightarrow j \Longleftrightarrow \tilde{d}_{ij} \geq p_i \tag{4.16}$$

$$i \parallel j \Longleftrightarrow [\tilde{d}_{ij} \geq -(p_j - 1) \ \wedge \ \tilde{d}_{ji} \geq -(p_i - 1)] \tag{4.17}$$

The *disjunction* set can be updated using the following relation:

$$i - j \Longleftarrow [\exists(i,j,k) : k \parallel i \wedge k \parallel j] \tag{4.18}$$

Several other constraint propagation techniques has been presented by Brucker and Knust (2006). Finally, the *conjunction* set is updated considering the following relation (*direct conjunction*):

$$i \rightarrow j \Longleftarrow [i - j \wedge \tilde{d}_{ij} \geq -(p_j - 1)] \tag{4.19}$$

A new SSD matrix is computed using the updated *conjunction*, *parallelity*, and *disjunction* sets. The process continues until the SSD matrix is unchanged or infeasible. At this point, the first row and last column of the last feasible SSD matrix are used to compute the time window of each task. Algorithm 4.2 shows the constraint propagation process as implemented in this research.

4.3.5 Bridge Restoration Function

Finally, the bridge restoration functions are computed, as discussed in the following. From the schedule provided by following *Learnall* or *Learnot* schemes, the execution time-window of each task is extracted and used to specify the damage state of each component throughout the project using the following equation:

$$DS_c(t) = \begin{cases} DS_c(t_0) & \text{if } t < CET_c \\ DS0 & \text{if } t \geq CET_c \end{cases} \tag{4.20}$$

where $DS_c(t)$ is the damage state of component c at time t after the initiation of the restoration process. t_0 and CET_c are the bridge restoration start time and the restoration end time of component c, respectively. $DS0$ indicates the zero damage state (no damage). Other

Algorithm 4.2 Constraint propagation procedure

input: n, p, Ep, Rsc, br, Br, m, T
output: EST_i, LFT_i $\quad \forall i \in \{0, n+1\}$

Form initial *conjunction*, *disjunction*, and *parallelity* sets:
$Cs \leftarrow \{i,j|(i,j) \in Ep\}$ $\quad \forall i,j \in \{0,n+1\}$ and $i \neq j$
$Ds \leftarrow \{i,j|\exists k \in \{1,\cdots,m\} : br_{ik} + br_{jk} > Br_k\}$ $\quad \forall i,j \in \{0,n+1\}$ and $i \neq j$
$Ps \leftarrow \{i,j|\{p_i + p_j > max(\tilde{d}_i, \tilde{d}_j) - min(\tilde{r}_i, \tilde{r}_j)\}$ $\quad \forall i,j \in \{0,n+1\}$ and $i \neq j$
Form the initial SSD matrix:
$ssd_{ij} \leftarrow 0$ if $i = j$
$ssd_{ij} \leftarrow p_i$ if $\{i,j\} \in Cs$
$ssd_{ij} \leftarrow -(p_j - 1)$ if $\{i,j\} \in Ps$
$ssd_{ij} \leftarrow p_i - T$ otherwise
$\widehat{ssd}_{ij} \leftarrow ssd_{ij}$ $\quad \forall i,j \in \{0,n+1\}$ and $i \neq j$
$\overline{ssd} \leftarrow$ compute transitive closure of ssd
while $\overline{ssd} \neq ssd$ **and** $\nexists\, i : \overline{ssd}_{ii} > 0$ **do**
$\widehat{ssd}_{ij} \leftarrow ssd_{ij}$ $\quad \forall i,j \in \{0,n+1\}$ and $i \neq j$
$Cs \leftarrow \{i,j|\overline{ssd}_{ij} \geq p_i\}$ $\quad \forall i,j \in \{0,n+1\}$ and $i \neq j$
$Ps \leftarrow [\tilde{d}_{ij} \geq -(p_j - 1) \wedge \tilde{d}_{ji} \geq -(p_i - 1)]$ $\quad \forall i,j \in \{0,n+1\}$ and $i \neq j$
$Ds \leftarrow [\exists (i,j,k) : k \parallel i \wedge k \parallel j]$
$Cs \leftarrow [(i,j) \in Ds \wedge \tilde{d}_{ij} \geq -(p_j - 1)]$
$\overline{ssd}_{ij} \leftarrow 0$ if $i = j$
$\overline{ssd}_{ij} \leftarrow p_i$ if $\{i,j\} \in Cs$
$\overline{ssd}_{ij} \leftarrow -(p_j - 1)$ if $\{i,j\} \in Ps$
$\overline{ssd}_{ij} \leftarrow p_i - T$ otherwise
$\overline{ssd} \leftarrow$ compute transitive closure of ssd
$ssd_{ij} \leftarrow \widehat{ssd}_{ij}$ $\quad \forall i,j \in \{0,n+1\}$ and $i \neq j$
$EST_i \leftarrow ssd_{1,i}$ $\quad \forall i,j \in \{0,n+1\}$ and $i \neq j$
$LFT_i \leftarrow T - ssd_{i(n+1)} + p_i$ $\quad \forall i,j \in \{0,n+1\}$ and $i \neq j$

intermediate damage states can be easily considered, if applicable. Then, the following considerations are taken into account to determine the functionality of the bridge at each time step during the restoration process.

1. *The effect of temporary repairs*. The functionality of the damaged components that include temporary repair in their schedule is assumed to be fully restored. Therefore, for such components, the damage state is set to $DS0$ while the temporary repair is in place.

2. *Structural safety requirements*. A set of nd bridge damage scenarios $(dsc_1, \cdots, dsc_{nd})$ is defined in the form of damage state combinations of multiple (or single) bridge components, and a functionality level is assigned to each scenario. These damage

state scenarios can be determined by specifying the minimum structural requirements needed to maintain a certain level of functionality. For example, the allowable traffic is reduced to 0% if at least one column in a multi-column bent has failed, or 50% if all columns are extensively cracked. The time dependent functionality of the bridge with respect to each damage scenario $Qdsc_d(t)$ is computed at each time step using the following equation:

$$Qdsc_d(t) = \begin{cases} qdsc_d & \text{if } dsc_d = \text{true at } t \\ 100\% & \text{otherwise} \end{cases} \tag{4.21}$$

where $qdsc_d$ is the functionality level assigned to the bridge in case the damage configuration of the components matches the dth damage scenario (dsc_d). Therefore, the bridge functionality at time t considering all safety damage scenarios $Qsft(t)$ is computed as:

$$Qsft(t) = \min[Qdsc_1(t), \ldots, Qdsc_{nd}(t)] \tag{4.22}$$

3. *Construction-induced traffic disruption*. The execution of many restoration tasks requires the bridge to be closed completely or at least partially. This can be due to the construction activities or crew safety considerations. Thus, for each task, the functionality of the bridge at each time step accounting for such disruptions $QA_i(t)$ is computed as follows:

$$QA_i(t) = \begin{cases} qA_i & \text{if } ST_i \leq t < FT_i \\ 100\% & \text{otherwise} \end{cases} \tag{4.23}$$

where qA_i is the functionality of the bridge during the execution of task i, considering construction-induced traffic disruptions. Thus, the total functionality considering all

construction tasks $Qcons(t)$ can be computed as:

$$Qcons(t) = \min[QA_1(t), \ldots, QA_n(t)] \tag{4.24}$$

Finally, (a sample of) the functionality at each time step is set equal to the minimum of the functionalities computed by equations 4.22 and 4.24 as follows:

$$\hat{Q}(t) = \min[Qsft(t), Qcons(t)] \tag{4.25}$$

This procedure is repeated for all sample durations and the value of the functionality at each time step from all sample schedules is collected and utilized to compute the probabilistic characteristics of the functionality. This provides the probabilistic restoration function for the bridge, which can be presented in several forms, including the probability of delivering any level of functionality at every time step during the restoration process. The total number of sample durations and simulations required to compute the probabilistic restoration functions depend on the complexity of the problem and in particular the variability of duration of the tasks.

It is worth mentioning that the proposed methodology is independent of the type of hazard. While modeling (or detecting) damage and corresponding component restoration solutions might be different for different types of catastrophic events, as long as the required data are available, the presented model can be utilized to develop the restoration functions of the damaged bridge. Such information can be acquired from construction engineers and bridge experts. A detailed application of the discussed methodology for the case of a seismically damaged bridge is presented in the next section.

Table 4.1: Deterministic modeling parameters and material properties used for MSSS Girder bridge (adapted from Nielson, 2005)

Parameter	Value	Units
Steel yield stress	6.13	MPa
Concrete compressive strength	27.6	MPa
Piles' horizontal stiffness	7.0	kN/mm/pile
Piles' vertical stiffness	175.0	kN/mm/pile
Abutment active stiffness	7.0	kN/mm/pile
Abutment passive stiffness	20.2	kN/mm/m
Middle deck unit weight	52.0	kN/m
End deck unit weight	39.0	kN/m
Deck-deck gap	38.1	mm
Deck-abutment gap	25.4	mm
Damping ratio	0.05	-
Fixed bearing Coef. of friction	0.21	-
Rocker bearing Coef. of friction	0.04	-
Bearings initial stiffness coefficient	1.0	-

4.4 Application

The probabilistic restoration curves have been computed for a Multi-Span Simply Supported (MSSS) Steel Girder bridge to demonstrate the application of the proposed methodology. Details of the numerical model, restoration data, and the simulation procedure to compute restoration functions are presented in the following.

4.4.1 Bridge Numerical Model

For the purpose of this study, a detailed finite element model of a MSSS Steel Girder bridge similar to the model presented in Section 3.4.1 was developed in the OpenSees platform (McKenna et al., 2000). Figure 4.3 shows a schematic view of the bridge and its components used for this application. The material properties and modeling parameters of the bridge was considered to be deterministic. The values of such properties and parameters are presented in Table 4.1.

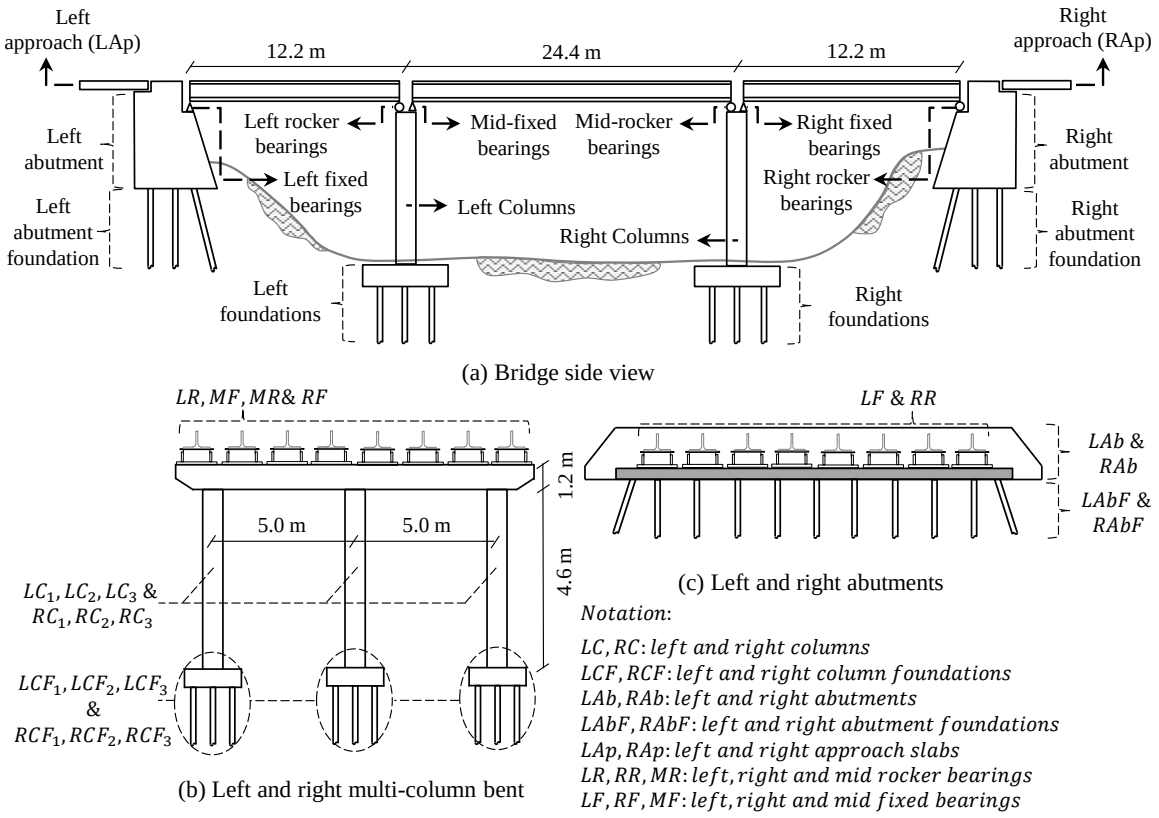

Figure 4.3: MSSS Steel Girder bridge and components

Nielson (2005) conducted a statistical analysis on CSUS bridges and showed that the median age of MSSS Steel Girder bridges was about 50 years and 90% of these bridges were constructed before 1990, which means that no seismic provisions were applied in their design. Thus, these bridges are considerably vulnerable to seismic loadings. In particular, low confinement concrete columns and high-type bearings (prone to toppling or overturning) contribute to the seismic vulnerability of this bridge class. Moreover, these bridges have the lowest deck and substructure condition rates among the bridge classes of the CSUS, mostly due to their age (Nielson, 2005; FHWA, 2013). Among several aging and deterioration factors, corrosion is the most common in bridges. This includes the corrosion of concrete reinforcement and steel bearings. To account for aging effects on the behavior of the bridge, reinforced concrete columns and bearings have been modeled con-

sidering the effect of chloride-induced corrosion deterioration, assuming that the bridge is 50 years old. In the case of the columns, the reduction of the cross-sectional area of the longitudinal and transverse reinforcements due to corrosion has been computed based on the model presented by Enright and Frangopol (1998), which results in the reduction of the confined concrete ultimate strength and column lateral load capacity. The behavior of the rocker bearings is affected by the accumulation of rust due to corrosion, which increases the friction between the bearing and its masonry plate (Fan and McCormick, 2015; Mander et al., 1996; Barker and Hartnagel, 1998). This increase has been modeled based on the recommendations of Mander et al. (1996) and Ghosh and Padgett (2010). Regarding the fixed bearings, the reduction of the cross-sectional area of the anchor bolts due to corrosion affects the behavior and strength of the bearings. This reduction has been computed in the same way as for the column reinforcing bars, and the effect on the ultimate strength of the bearings has been applied accordingly.

4.4.2 Bridge Damage and Restoration Data

Table 4.2 presents the repair-based damage states of the components of the bridge considered for this study (Barker and Hartnagel, 1998; Mander et al., 1996; Nielson, 2005; Hwang et al., 2001; Mackie et al., 2008; Aygün et al., 2010; Ledezma and Bray, 2008). These include the columns, bearings, abutments, approach slabs, and foundations. For each damage state of each component, a set of restoration tasks and their associated properties (e.g., precedence relations, resource requirement) is specified. In this chapter, only the component restoration details associated with the component damage states of the bridge subjected to the investigated scenario will be presented. Details of the restoration tasks for all damage states and components and their associated properties is presented in Chapter 5 and Appendix A.

Table 4.2: Component damage states

DS0	DS1	DS2	DS3	DS4
Column (*LC,RC*)				
$\mu_c \leq 1.58$	$1.58 < \mu_c \leq 3.22$	$3.22 < \mu_c \leq 6.84$	$\mu_c > 6.84$	-
no damage	Cracking	Cover spalling	Bar buckling	-
Fixed bearing (*LF,RF,MF*)				
$fb_d \leq 20$	$20 < fb_d \leq 40$	$40 < fb_d \leq 250$	$fb_d > 250$	-
no damage	Anchor bolt damage	Toppling potential	Unseating	-
Rocker bearing (*LR,RR,MR*)				
$rb_d \leq 50$	$50 < rb_d \leq 100$	$100 < rb_d \leq 150$	$150 < rb_d \leq 250$	$rb_d > 250$
no damage	Damage to pins	Unstability	Toppling	Unseating
Abutment (*LAb,RAb*)				
$Ab_{Pd} \leq 100$	$100 < Ab_{Pd} \leq 120$	$120 < Ab_{Pd} \leq 150$	$Ab_{Pd} > 150$	-
no damage	Damage to joint seal	Backwall cracking	Failure	-
Approach slab (*LAp,RAp*)				
$Ab_{Ad} \leq 200$	$200 < Ab_{Ad} \leq 435$	$Ab_{Ad} > 435$	-	-
no damage	Moderate settlement	Extensive settlement	-	-
Pile foundation (*LCF,RCF,LAbF,RAbF*)				
δ_{max}[1] ≤ 86	$86 < \delta_{max} \leq 115$	$\delta_{max} > 115$	-	-
no damage	Piles moderate damage	Piles extensive damage	-	-

[1] δ_{max} is the maximum deformation. For the case of column foundations, δ_{max} is the maximum displacement of the foundation. For the case of abutment foundations $\delta_{max} = max\{Ab_{Ad}, Ab_{Pd}\}$.

4.4.3 Component Response, Damage, and Restoration Data

In the absence of strong ground motion records for the CSUS regions, synthetic time histories are typically utilized for response and vulnerability evaluation of infrastructure and lifeline systems. The ground motion record used in this study to assess the potential damage to the MSSS Steel Girder bridge shown in Figure 4.3, has been selected from the suite of ground motions generated by Rix and Fernandez-Leon (2004) for Memphis regions. This record, shown in Figure 4.4, has a peak ground acceleration (PGA) of 0.65g, associated with an event with a magnitude and distance of 7.5 and 20 km, respectively.

The bridge model has been subjected to the selected ground motion and a nonlinear time-history analysis has been carried out. Figure 4.5 illustrates the load-deformation re-

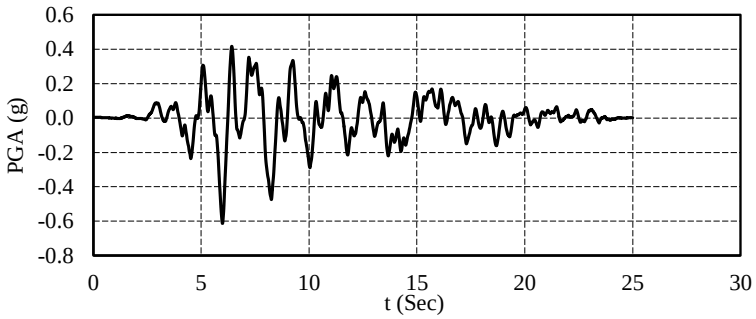

Figure 4.4: Selected synthetic ground motion

Table 4.3: Bridge component demand and damage states

Component	Demand measure	$DS_c(t_0)$
LC_1, LC_2, LC_3	$\mu_c = 1.93$	DS1
RC_1, RC_2, RC_3	$\mu_c = 2.01$	DS1
LF	$fb_d = 73.51\ mm$	DS2
LR	$rb_d = 38.82\ mm$	DS1
MF	$fb_d = 4.57\ mm$	DS0
MR	$rb_d = 27.13\ mm$	DS0
RF	$fb_d = 1.28\ mm$	DS0
RR	$rb_d = 65.32\ mm$	DS1
LAp	$Ab_{Ad} = 4.31\ mm$	DS0
RAp	$Ab_{Ad} = 0.65\ mm$	DS0
LAb	$Ab_{Pd} = -9.96\ mm$	DS0
RAb	$Ab_{Pd} = -9.95\ mm$	DS0
LCF_1, LCF_2, LCF_3	$\delta_{max} = 2.75\ mm$	DS0
RCF_1, RCF_2, RCF_3	$\delta_{max} = 2.71\ mm$	DS0
$LAbF$	$\delta_{max} = 9.96\ mm$	DS0
$RAbF$	$\delta_{max} = 9.95\ mm$	DS0

sponse of different components of the bridge obtained from this analysis. The damage state of each component has been specified by comparing the component maximum response and the criteria shown in Table 4.2. Based on these results (presented in Table 4.3), all six columns of the bridge are cracked. Also, the fixed bearings mounted on the left abutment are prone to toppling due to extensive displacement. Finally, the rocker bearings mounted on the left bent beam and right abutment are damaged to some extent.

Table 4.4 presents all unique tasks involved in the restoration of the damaged components, and their type. Table 4.5 shows the properties of each task used in the proposed

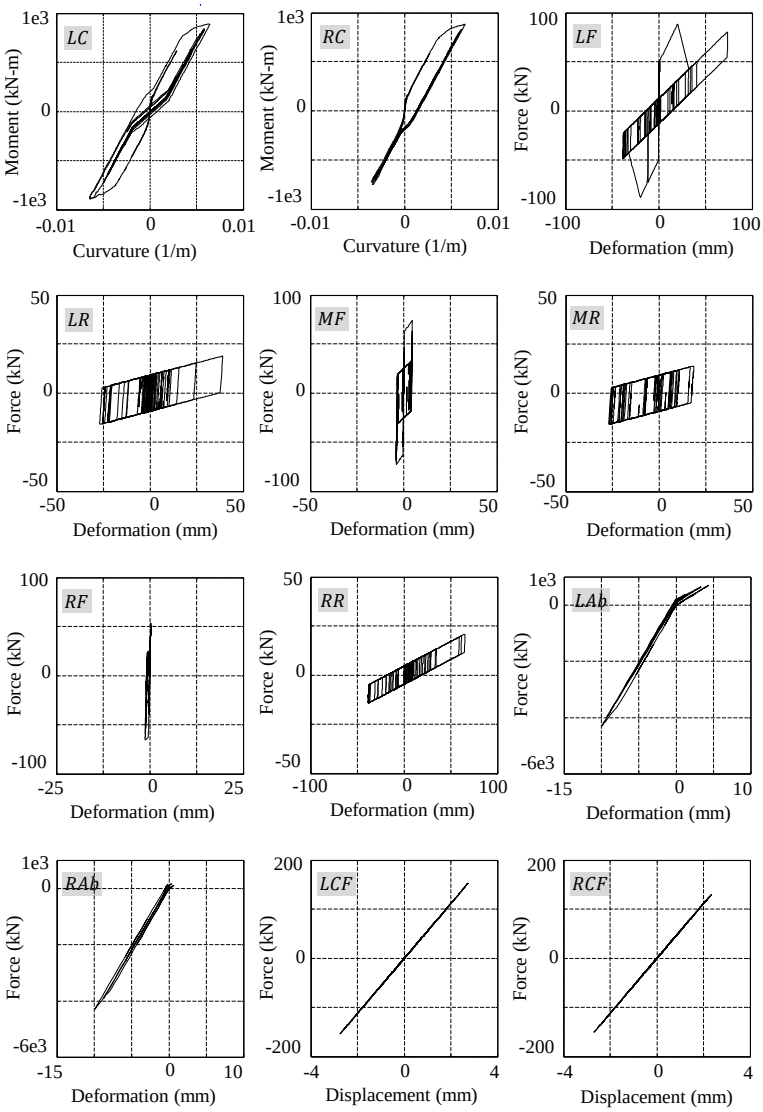

Figure 4.5: Bridge component response

technique: the functionality during the tasks execution (i.e., qA), duration probability distributions, and resource requirements (see Appendix A for the complete list of component damage states and their associated restoration tasks). As shown in table 4.5, in this study three major categories of resources are considered for the analysis, namely manpower, crane, and concrete mixer. It is worth mentioning that the tasks shown in Table 4.4 are the major required restoration activities which have the duration of at least one day. If deemed useful, the analysis can be performed with a higher task resolution, by breaking down the

Table 4.4: Pool of relevant restoration tasks

Task ID	Description	Type
A_1	Repair minor spall	*Reg*
A_2	Repair minor cracks with epoxy	*Reg*
A_3	Submit/review shoring plan	*Prep*
A_4	Install column shoring	*Temp*
A_5	Install abutment shoring	*Temp*
A_6	Remove/construct new pedestals	*Reg*
A_7	Cure pedestal concrete	*Reg*
A_8	Install new bearings	*Reg*
A_9	Remove shoring	*Temp*
A_{10}	Realign bearings	*Reg*

Table 4.5: Restoration tasks functionality, duration, and resource requirement properties

Task ID	$qA(\%)$	Duration (days)				Resource requirement		
		Distribution	Mode	Min	Max	Manpower	Crane	Concrete mixer
A_1	100	Triangular	2	1	3	2	0	1
A_2	100	Triangular	2	1	3	2	0	1
A_3	100	Triangular	30	20	40	0	0	0
A_4	0	Triangular	3	2	4	4	1	0
A_5	0	Triangular	2	1	3	4	1	0
A_6	100	Triangular	2	1	3	5	0	1
A_7	100	Triangular	10	7	12	1	0	0
A_8	100	Uniform	-	1	2	5	0	0
A_9	0	-	-	1	1	5	1	0
A_{10}	50	Uniform	-	1	2	5	1	0

major tasks to their respective components. The tasks and their duration properties have been adapted from selected literatures such as Mackie et al. (2008) and PennDOT (2010), as well as consulting with professional engineers expert in the field (Girondo, 2014; Sause, 2014). As shown in Table 4.5, some levels of functionality loss have been considered for four restoration tasks. These include tasks A_4, A_5, and A_9 which are associated with installing or removing temporary shorings (Girondo, 2014; Sause, 2014). During the execution of these tasks, the bridge is typically completely closed as the traffic might cause safety concerns for crews working underneath the deck. For the same reason, the functionality of the bridge during the realignment of the bearings (task A_{10}) is considered to be 50%. This is due to the fact that realignment is first performed for half of the deck and then for the next half. During each phase, the section of the deck on which the crew is

Table 4.6: Component restoration properties

Component	Group	Tasks	Predecessors		PTR
			Task	Component	
LC_1, LC_2, LC_3	Left bent	A_1	-	-	A_4
		A_2	-		
RC_1, RC_2, RC_3	Right bent	A_1	-	-	A_4
		A_2	-		
LF	Left abutment	A_3	-	-	A_5
		A_5	A_3		
		A_6	A_5		
		A_7	A_6		
		A_8	A_7		
		A_9	A_8		
LR	Left bent	A_3	-	LC_1, LC_2, LC_3	A_4
		A_4	A_3		
		A_{10}	A_4		
		A_9	A_{10}		
RR	Right abutment	Similar to LR[1]		-	A_4

[1] RR uses A_5 instead of A_4

working is closed (PennDOT, 2010). The restoration tasks of each component, tasks and components precedence relations, and component groups are presented in Table 4.6. The last column of this table shows the temporary repair tasks that can potentially affect the functionality of a damaged component, although such tasks might not be explicitly present among the restoration tasks of components. For instance, temporary shoring (A_4) installed for bearings of the left bent group is also effective for the columns of the left bent (i.e., LC_1, LC_2, and LC_3).

The tasks presented in Table 4.4 are meant to restore their corresponding components to their undamaged pre-event status. However, in some cases it is possible to look at the necessary restoration process as an opportunity to improve the performance of the structure for future hazards. This can be done by repairing or rebuilding the damaged structure, so that the final product is stronger or more resilient than the original. For example, several studies have shown that high type bearings are one of the major sources of vulnerability for

MSSS Steel Girder bridges (for example see Chapter 3). Therefore, it would be preferable to replace them with less damage susceptible components, such as elastomeric bearings (Padgett and DesRoches, 2009). While the proposed methodology is capable of modeling any type of restoration process, regardless of the final stage of the bridge, such cases are not the focus of the current study and not presented here in this example.

4.4.4 Restoration Curve Development

For the sake of clarity, first the process of generating one sample restoration schedule and its corresponding restoration function is presented here in detail. To this respect, the duration of the restoration tasks is assumed to be equal to the mean value of their corresponding distributions presented in Table 4.5. Regarding the resources, it is assumed that the minimum feasible number of resources is available for the project. This is associated with five workers (manpower), one crane, and one concrete mixer. Considering the precedence constraints (Table 4.6) and tasks resource requirements (Table 4.5), the restoration schedule of the bridge has been computed by implementing the *Learnall* scheme and solving the corresponding RCPSP. The whole process of assembling the input data and forming the variables of the techniques presented in Section 4.3.4 has been coded in the Matlab programming environment (The Mathworks Inc., 2014). To solve the associated MILP problem, Gurobi 6.0.2 has been used, which is a powerful optimization solver (Gurobi, 2015).

Figure 4.6a shows the Gantt chart of the computed restoration schedule. Based on this figure, the duration of the construction process is 51 days. The restoration starts with repairing crack and spall damage in the columns of the bridge due to the ground motion excitation (12 tasks in total). The replacement or realignment of the damaged bearings requires the installation of temporary shoring at the location of bearings (A_4 and A_5). According to Table 4.6, temporary shorings plans should be first submitted and reviewed before the shoring

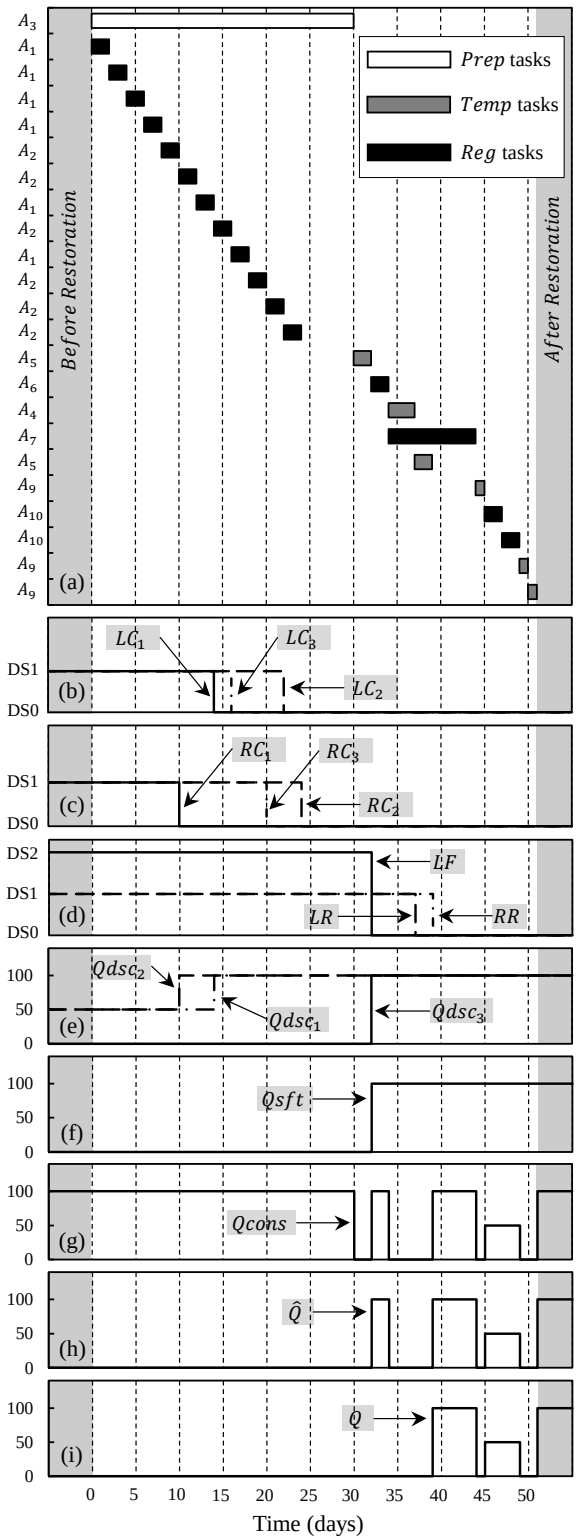

Figure 4.6: (a) Bridge restoration schedule, (b) Left Columns damage states, (c) Right columns damage states, (d) Bearings damage states, (e) Safety scenarios, (f) Bridge functionality considering safety,(g) Bridge functionality considering construction operations, (h) Raw bridge restoration function, (i) Windowed restoration function

Table 4.7: Bridge damage scenarios

Damage scenario	Components states	$qdsc(\%)$
dsc_1	$\bigcap(LC_1$ in DS2, LC_2 in DS2, LC_3 in DS2)	50
dsc_2	$\bigcap(RC_1$ in DS2, RC_2 in DS2, RC_3 in DS2)	50
dsc_3	LF in DS2	0

fabrication and installation (A_3). However, since the type of this task is introduced as *Prep*, only one is included in the schedule and is set as the predecessor of all shoring installation tasks (required for installing the shorings for *LF*, *LR*, and *RR*). This task is carried out in parallel with the restoration of columns as its execution does not consume any of the resources considered for this study (see Table 4.5). Typically, during emergency situations in developed countries unlimited resources can be assumed for design and fabrication tasks (i.e., *Prep*s).

Figure 4.6b-d presents the time-evolution of the damage state for each damaged component [$DS_c(t)$] based on the computed schedule and Equation 4.20. Figure 4.6b-c shows that the initial damage state of each column (DS1) changes to DS0 by completion of the required restoration tasks (A_1 and A_2). However, in the case of the bearings shown in Figure 4.6d, the damage state changes to DS0 before the completion of the bearings restoration tasks, as soon as the temporary repair for each set of bearings is in place (shoring).

The information on the damage state of each component at each time step is used to specify the functionality of the bridge considering safety requirements and based on a set of damage scenarios. Although several of such damage scenarios can be defined, only three dominant scenarios are presented in Table 4.7. A full list of other relevant damage scenarios is presented in Chapter 5. Based on the first and second scenarios, due to assumed structural safety considerations, there is a 50% reduction of the functionality of the bridge in case all columns of a bent are cracked (reduced traffic load). Thus, as shown in Figure 4.6e, $Qdsc_1$ and $Qdsc_2$ show 50% functionality until at least one column in each bent is restored. Full closure of the bridge is assumed for damage scenario dsc_3, due to the fixed bearings being

prone to toppling and instability. In such case it is assumed that the bridge is not safe as the traffic might increase the chance of deck toppling down completely or even unseating. Therefore, Figure 4.6e shows 0% functionality for $Qdsc_3$ as long as this scenario is effective. The total functionality of the bridge, accounting for these safety considerations, is computed by taking the minimum value of the functionality for all $Qdsc_1$, $Qdsc_2$, and $Qdsc_3$ at each time step, following Equation 4.22. For the current application, the results show that the functionality of the bridge is completely dominated by dsc_3, associated with the damaged fixed bearings at the left abutment (LF), as illustrated in Figure 4.6f.

The effect of the traffic disruption caused by construction operations is applied in the next step using qA values specified for each individual task (Table 4.4) and Equation 4.23. Accordingly, the functionality of the bridge during the installation and removal of temporary shorings is set to 0%. Also, due to crew safety considerations, the lanes over which the rocker bearings are being repaired (realigned) are closed. This reduces the functionality of the bridge to 50% during rocker bearings restoration. Considering these restrictions, $Qcons(t)$ is computed based on Equation 4.24 and shown in Figure 4.6g. The total functionality of the bridge $\hat{Q}$ can now be computed by taking the minimum of $Qsft(t)$ and $Qcons(t)$ using Equation 4.25. Figure 4.6h shows that the bridge is fully reopened (i.e., $\hat{Q} = 100\%$) twice, and partially reopened (i.e., $\hat{Q} = 50\%$) once during the restoration process and before the completion of the project.

The functionality profile shown in Figure 4.6h has been computed by taking into account a series of logical structural safety and construction considerations. However, in some cases the results might not necessarily look realistic from a practical point of view. For instance, the computed restoration profile $\hat{Q}$ might indicate that the bridge is fully (or partially) opened and closed several times. Occasionally, openings last for only short periods of time (e.g., 2 or 3 days). This is not the common practice, as opening and closing a bridge to traffic requires extra effort (e.g., installing proper traffic signs, and employing

extra crews for directing the traffic). Therefore, a window filter has been designed that scans the computed restoration function and cuts down the functionality to a lower level in case the time span along which the bridge is fully (or partially) reopened is less that a specified length. In the case of the current problem, since three levels of functionality have been assumed for the bridge (0%, 50%, and 100%), this filter has been applied to the functionality profile of Figure 4.6h twice, once to decrease the unrealistic full reopening of the bridge to partial opening (100% $\rightarrow$ 50%), and once to decrease the unrealistic partial reopening of the bridge to closure (50% $\rightarrow$ 0%). Here, the length of the window has been assumed to be four days. The final stepwise functionality profile (restoration function) is presented as Q and illustrated in Figure 4.6i.

The restoration schedule shown in Figure 4.6 and its corresponding restoration function are only one possible scenario for the recovery of the current bridge example. However, the sequence of tasks, the total duration of the restoration, and the level of functionality of the bridge can vary substantially considering the uncertainties involved in the duration of each individual task, as well as the scheduling of the project. To take these uncertainties into account and obtain the probabilistic characteristics of the functionality at each time step after the extreme event and during the restoration phase, one thousand samples of each task duration were generated using Latin hypercube sampling (McKay et al., 2000). The results of a convergence analysis showed that the selected number of samples is sufficient for accurately estimating the probabilistic restoration functions (the results are presented later in this chapter). These samples were used to compute one thousand restoration schedules and functionality profiles for the MSSS Steel Girder bridge of this study, using both scheduling schemes (i.e., *Learnall* and *Learnot*). To study the effect of resources on the restoration and functionality, this analysis has been performed with two levels of resource availability. These include the low level resource availability (*LResc*) with the minimum feasible number of available resources for each resource type, and high level (*HResc*) with

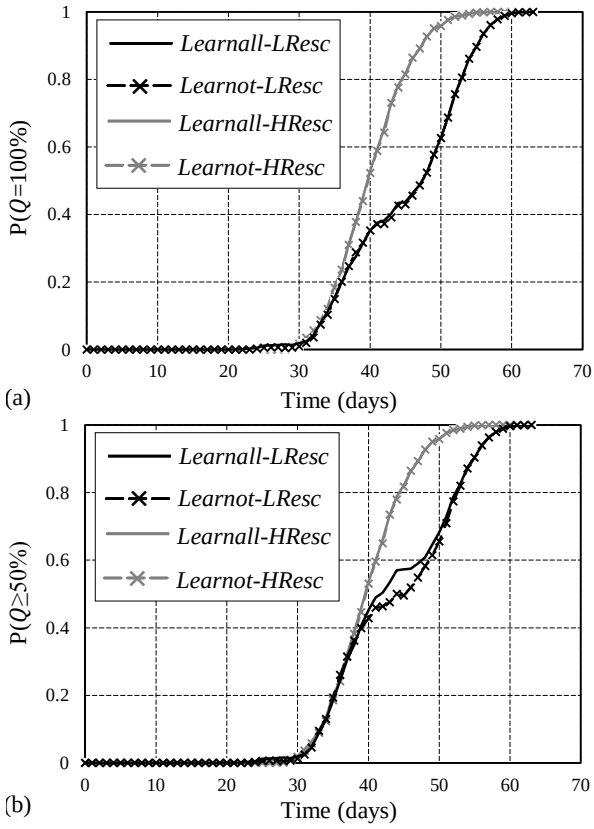

Figure 4.7: Probabilistic restoration functions for (a) full functionality, and (b) at least partial functionality of the bridge

twice the number of minimum resources. Figure 4.7 shows two sets of possible outcomes of the analysis, namely the probabilistic restoration functions of the current bridge for full functionality $P(Q(t) = 100\%)$, and at least partial functionality $P(Q(t) \geq 50\%)$. Regarding the computational efforts, the simulations took about 80 seconds for *Learnall* and 800 seconds and *Learnot* scheme, using a personal computer with 4.00 GB of RAM and Intel i7 2.93 GHz CPU.

Comparing the results related to the analysis with different levels of resource availability, it can be seen that in all cases, an increase in the number of available resources, generally increases the probability of the bridge being fully or at least partially open to traffic. This was expected as with more resources, more tasks can be executed in parallel and the total restoration process can be completed earlier. However, this increase in functionality

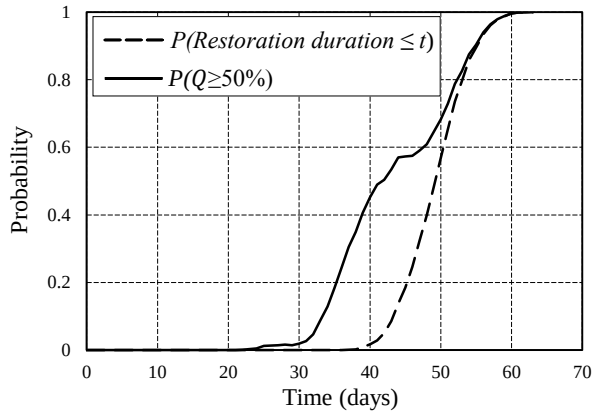

Figure 4.8: Comparison between the CDF of the restoration duration and partial functionality probability for the case of *Learnall-LResc*

probability occurs only after at least 35 days from the beginning of the project.

It is worth noting that a large portion of the functionality probability at many time steps depends on the cases in which the bridge is temporarily (fully or partially) reopened before the restoration project is fully finished. This can be observed by comparing the curves presented in Figure 4.7 with the values of the cumulative distribution function (CDF) of the project duration $P(Restoration\ duration \leq t)$, computed for each scheduling scheme and level of resource availability. As an example, Figure 4.8 shows such comparison for the results computed by the *Learnall* scheduling scheme with *LResc* resource availability. The considerable difference between the values of the two curves confirms the importance of computing and considering the functionality provided by temporary reopening the bridge before the completion of the restoration, in evaluating the probabilistic characteristics of the functionality for damaged bridges. Also, Figure 4.8 shows that after about 55 days, the achievement of functionality is the result of the completion of the restoration process, as the two curves start to overlap. Similar results have been obtained from analyses with the other scheduling scheme and different level of resource availability.

Regarding the methodologies used to deal with the uncertainties in the tasks duration and scheduling, there is a difference between the functionality probability of the bridge

obtained from *Learnall* and *Learnot* schemes, in the case of low resource availability (i.e., *LResc*), in which *Learnot* and *Learnall* provide a lower bound and an upper bound, respectively. This difference is more noticeable for the case of $P(Q(t) \geq 50\%)$, and for the time steps between 40 and 50 days. For the rest of the cases, the results of the two schemes almost overlap.

As mentioned earlier, a preliminary convergence was performed to verify that the number of samples is adequate. Figure 4.9 shows the results of such analysis on the probabilistic restoration functions associated with $P(Q(t) \geq 50\%)$, computed by *Learnall* scheduling scheme and considering low level of restoration resource availability (i.e., *LResc*). The figures present the box-plot of the values of $P(Q(t) \geq 50\%)$ at different time steps, which have been computed by resampling the values of task durations and recomputing the probabilistic restoration functions. This process has been carried out 50 times and for different number of task duration samples. According to the figures, largest dispersion in the computed values for $P(Q(t) \geq 50\%)$ is observed in the range of 40 to 50 days. Figure 4.9a illustrates that such dispersion is relatively large considering only 100 samples for the analysis. On the other hand, Figure 4.9b shows that one thousand samples can result in an acceptable level of dispersion, while the computational cost is reasonably small. For example, the coefficient of variation of the computed values for $P(Q(t) \geq 50\%)$ at 45 days after the initiation of the restoration process is equal to 0.0738 , 0.025, and 0.0071 using 100, 1,000, and 10,000 task duration samples, respectively.

4.4.5 Total Restoration Duration

In addition to the probabilistic restoration functions, other useful information can also be obtained from this analysis, among which the total duration of the restoration project is of great importance. In fact these are the two important pieces of information that can be utilized by disaster managers and decision makers to plan the efficient restoration of damaged

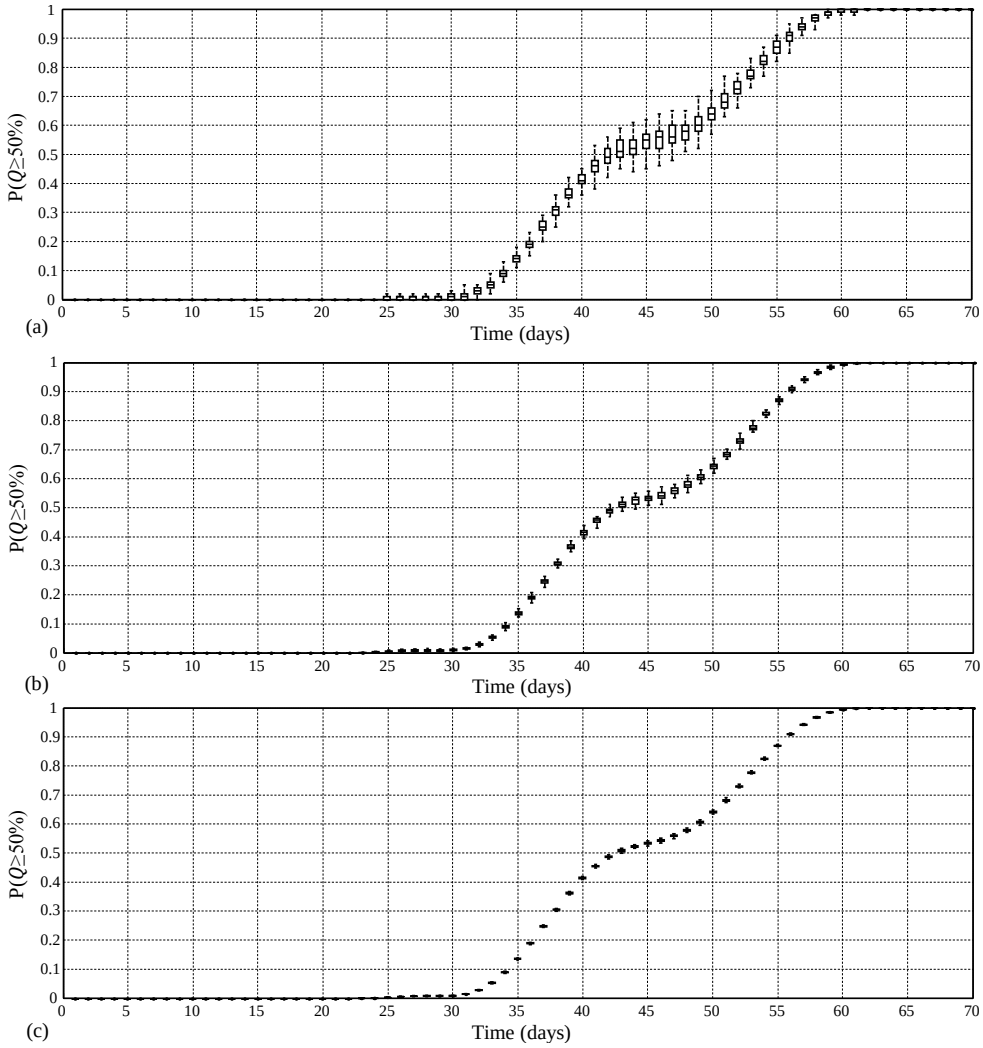

Figure 4.9: Box-plot of the probabilistic restoration curves, considering 50 separate analyses, using (a) 100, (b) 1,000, and (c) 10,000 task duration samples in each one

transportation networks and predict the amount of resources required for the restoration. Figure 4.10 shows the histogram of the total duration of the restoration computed for different resource availabilities and scheduling schemes. The results show that the mean value of the restoration duration decreases only by about 4 days when doubling the available resources. This is because a large portion of the length of the project is allocated to task A_3, which is considered a *Prep* task with no resource requirement. Also, such increase in the number of available resources does not necessarily halve the duration of the rest of the project after the completion of task A_3. The mean values of the total project duration com-

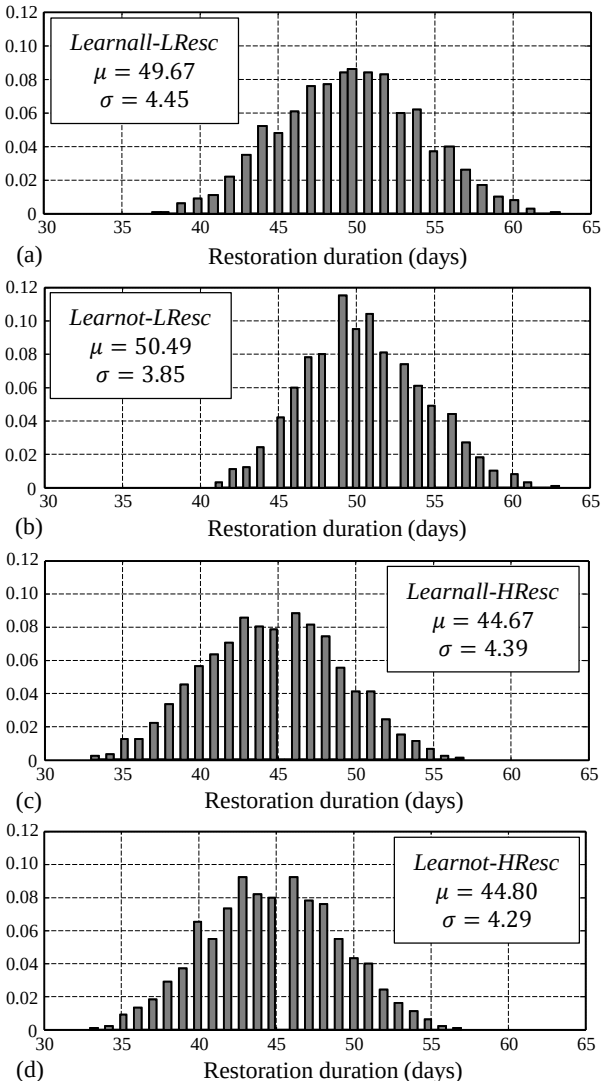

Figure 4.10: Total restoration duration: (a) *Learnall-HResc*, (b) *Learnot-LResc*, (c) *Learnall-HResc*, (d) *Learnot-HResc*

puted by *Learnall* and *Learnot* schemes are close, too. However, the duration computed by *Learnot* and for the *LResc* case shows less variability, as the standard deviation computed for *Learnot* and *LResc* is about 15% less than the case of *Learnall* and *LResc*. This is due to the fact that *Learnot* scheme starts with a baseline schedule (here the mean schedule) and later updates it considering the unexpected changes in the duration of tasks. Therefore, less variability is expected in the project duration of the sample projects.

4.5 Concluding Remarks

This chapter presents a novel technique for the construction of probabilistic restoration functions for damaged bridges. This is accomplished by simulating different restoration project scenarios, considering the construction methods common in practice and the amount of resource availability. Moreover, two scheduling schemes are proposed to handle the uncertainties involved in project scheduling and planning, and capture their reduction as new information becomes available over time. A stepwise restoration function is derived from each restoration schedule by taking into account a number of construction processing logics namely, the serviceability of the bridge considering the damage level of its components, ongoing construction activities, and effects of temporary repair actions.

The probabilistic restoration functions of a MSSS Steel Girder bridge have been computed to showcase the application of the proposed methodology. To this respect, a detailed analytical model of the bridge has been developed and the probabilistic restoration functions have been derived considering a selected seismic scenario. The results showed that there is a considerable nonlinearity in the relationship among the resource availability, total restoration duration, and probability of functionality at each time step after the restoration. In late stages of the restoration, the probability of the bridge being fully (or at least partially) functional mostly depends on the completion of the restoration. However, the temporary reopening of the bridge plays a significant role in increasing such probability after the initiation and in early stages of the restoration process. Therefore, it is of great importance to model the restoration process for a thorough evaluation of the functionality after an extreme event. For the case of the studied bridge, although increasing the amount of resources showed to be ineffective in increasing the functionality probability in early stages of the restoration process, it considerably increased such probability in later time steps.

The methodology proposed in this chapter for the computation of bridge restoration functions is integrated with the fragility analysis technique presented in Chapter 3. The result is presented in the form of a comprehensive framework for fully probabilistic evaluation of the functionality of individual bridges, considering the uncertainties in damage, restoration and functionality discussed in the next chapter.

Chapter 5

Functionality-Fragility Surface

5.1 Introduction

This chapter proposes a tool called "*Functionality-Fragility Surface*" (*FFS*) for pre-event probabilistic recovery and resilience prediction of structures, infrastructure systems, and communities. *FFS* is a way to study and a graphical format to present the evolution of the functionality in a probabilistic manner. Such representation allows to integrate the extreme event intensity and restoration strategies for the computation and presentation of the functionality. This is performed by combining two well-known tools, namely Fragility Curves and Restoration Functions, to present the probability of loss of functionality of a system as a function of the extreme-event intensity, as well as the elapsed time from the initiation of the restoration process. In the following sections, first *FFS* is introduced conceptually and its potential applications for recovery and resilience analysis are briefly discussed. Then, a comprehensive methodology for the computation of *FFS*s for individual bridges is introduced. This methodology combines the techniques presented in Chapters 3 and 4 to compute *FFS*s. A detailed example of such computations for a Multi-Span Simply Supported Steel Girder bridge is presented next. At the end, the summary of the study and conclusions are presented. The methodologies and results presented in this chapter are based on a paper by (Karamlou and Bocchini).

5.2 Functionality-Fragility Surfaces: the Concept

The techniques and methodologies developed for seismic performance assessment and performance-based design of structures and infrastructure systems are going to replace the conventional methods currently being used. Such techniques enable engineers to implement different performance objectives and take into account the associated uncertainties. In general, performance assessment is composed of three major elements: the evaluation of hazard (PSHA), the assessment of the damage (fragility analysis), and the estimation of the corresponding losses (loss assessment) with respect to an investigated performance metric (see Figure 2.2). Among different performance metrics, resilience has become the focal point of disaster performance assessment studies. In fact, resilience is not only a post-event performance metric, but it is also going to be a criterion for the design of new disaster resistant structures, infrastructure systems, and communities (NIST, 2015).

Fragility analysis is one of the key steps in performance-based techniques, providing the information on the probability of failure of the system considering a particular limit state. Due to its importance, fragility analysis has been subjected to an extensive research and several improvements have been made for the computation of the fragility curves of different structures and infrastructure systems (see Section 2.2). Therefore, it would be helpful to use such a powerful tool to assess the probability of failure with respect to resilience-based criteria. However, resilience is typically associated with the evolution of functionality during the recovery process. Therefore, a time-dependent analysis of the functionality is an inseparable part of resilience analysis. In this regard, the notion of *Functionality-Fragility Surface (FFS)* allows to study the vulnerability to the loss of functionality, in a probabilistic fashion. The conceptual formulation of *FFS* evolved from Equation 2.1 is presented as

follows:

$$FFS_{fls}(t, im) = P[\underbrace{\bar{Q}(t)}_{\equiv D} \geq C_{fls}|im] \tag{5.1}$$

where $\bar{Q}(t)$ is the loss of functionality experienced by the system at time t after the occurrence of the extreme event. C_{fls} is the loss of functionality that triggers the functionality limit state fls. For example, immediate occupancy and collapse prevention are two common functionality limit states. Compared to Equation 2.1 (fragility definition), the role of the demand here is taken by the loss of functionality ($\bar{Q}$) and the role of the capacity is taken by pre-defined functionality thresholds (C_{fls}), which may be defined by officials (NIST, 2015). In Equation 5.1, $\bar{Q}$ is a non-stationary random process, as its probabilistic characteristics are not only dependent on the initial damage state of the system, but also change in time considering the restoration strategies following the extreme event. Given the mathematical expression of *FFS* presented in Equation 5.1, a *Functionality-Fragility Surface* is described as the conditional probability of loss of functionality being more than the considered functionality limit state after time t from the extreme event (or initiation of the restoration process), and given the occurrence of an event with intensity *im*. It is worth noting that the loss of functionality threshold C_{fls} presented in Equation 5.1 can be further extended to be probabilistic and time-dependent. For instance, the resilience guidelines prepared for the city of San Fransisco in California (Poland, 2009b) allow for 10 percent loss in roads and highways during the intermediate recovery phase (i.e., $C_{fls}(3 \leq t_{\text{in days}} < 60) = 10\%$) and zero percent during the reconstruction phase (i.e., $C_{fls}(t_{\text{in days}} \geq 60) = 0\%$).

Figure 5.1 shows a schematic view of *FFS*. This figure shows a smooth gradual increase in P with increase in the level of *im*. Similarly, a smooth gradual decrease in P is observed with increase in the time elapsed from the initiation of the restoration (i.e., t). Although this is the expected shape of *FFS*s, the results can change considerably, depending on the type of the studied structure or system, the available data, and the technique utilized to develop such surfaces. Further in this chapter, it will be shown that for individual bridges,

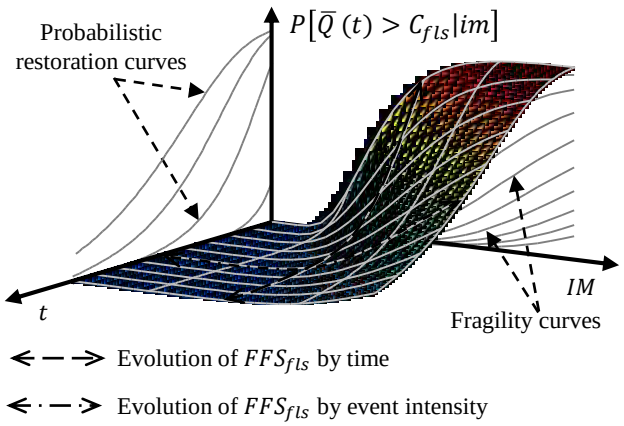

Figure 5.1: A schematic *FFS*.

*FFS*s might show some discontinuities in their shape. Moreover, similar to fragility analysis, multiple types of intensity measure (*IM*) can be used for the development of *FFS*s to improve the results of the computed failure probabilities (see Section 2.2). In such cases, *FFS*s take the form of hyper-surfaces rather than a surface in a three-dimensional space.

The development of *FFS*s requires different procedures and techniques for each type of structure and infrastructure system. Figure 5.2 illustrates a number of the potential ingredients, conceptually. The major elements of *FFS* analysis are fragility and restoration (recovery) curves to address the damage-intensity measure and functionality-time relationships, respectively. In order to relate these two major elements of the analysis, the limit states defined for the development of fragility curves should correspond to a set of restoration strategies from which the recovery curves are developed. In the case of many infrastructure systems, the development of such curves (i.e., fragility and restoration curves) requires rigorous data collection and computational efforts. In particular, for systems with multiple components and sophisticated inter-component relations, translating the damage of the components into the overall functionality of the system is extremely challenging. Moreover, the analysis should be performed probabilistically. Therefore, it is necessary to take into account the relevant sources of uncertainty in both damage and functionality evaluations. These include the uncertainties involved in the response of the system to the extreme

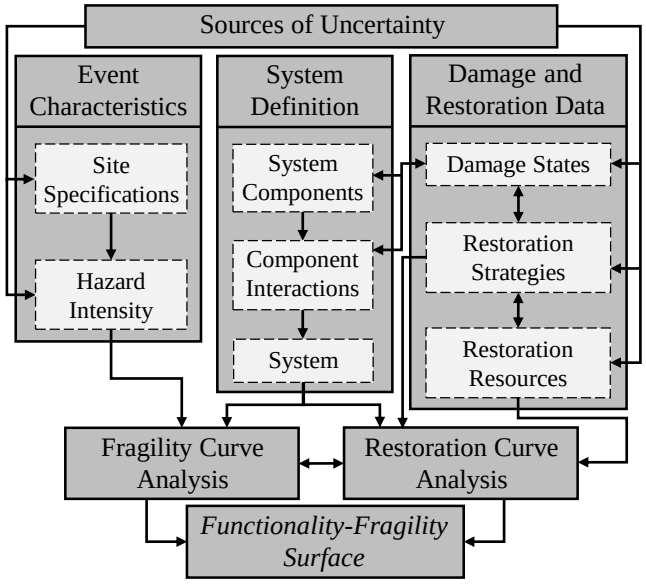

Figure 5.2: Schematic view of the major elements for *FFS* development.

event, as well as the restoration strategies and resources.

In case of seismic hazard, the performance-based earthquake engineering methodology and framework developed by the Pacific Earthquake Engineering Research Center (PEER) have been widely used for loss assessment of different structures and infrastructure systems. The following shows the classic PEER loss estimation equation developed by Cornell and Krawinkler (2000):

$$\lambda_{DV}(dv) = \int_{dm}\int_{im} \underbrace{G_{DV|DM}(dv,dm)}_{\text{Loss model}} \cdot \overbrace{dG_{DM|IM}(dm,im)}^{\text{Fragility model}} \cdot \underbrace{|d\lambda_{IM}(im)|}_{\text{Hazard model}} \tag{5.2}$$

where $\lambda_{DV}(dv)$ and $\lambda_{IM}(im)$ represent the mean annual frequency of exceeding the decision variable dv, and the intensity measure im, respectively. $G_{DV|DM}$ is the cumulative distribution function of the decision variable DV conditioned on the damage measure DM. Similarly, $G_{DM|IM}$ is defined as the cumulative distribution function of the damage measure DM conditioned on the intensity measure IM. Other research efforts have already focused on utilizing the PEER formulation for resilience-based risk assessment (Cimellaro et al.,

2010b; Broccardo et al., 2015). *FFS* can well fit in this framework, considering the loss of functionality as damage measure. In such case, Equation 5.2 can be modified into the following form:

$$\lambda_{DV}(dv) = \frac{1}{t_h} \int_{dm} \int_{t} \int_{im} G_{DV|FM}(dv, fm(t)) \cdot \underbrace{dG_{FM|IM}(\overbrace{fm(t)}^{\bar{Q}(t) \geq C_{fls}}, im)}_{FFS} \cdot dt \cdot |d\lambda_{IM}(im)| \quad (5.3)$$

where $fm(t)$ and t_h are the time variant functionality measure value and the investigated time horizon, respectively. $G_{DV|FM}$ is the cumulative distribution function of the decision variable DV conditioned on the functionality measure FM. Similarly, $G_{FM|IM}$ is defined as the cumulative distribution function of the functionality measure FM conditioned on the intensity measure IM. Considering seismic resilience as decision variable, Equation 5.3 can be revised depending on the functional relationship between the resilience and functionality metrics.

In summary, *FFS* is a tool general enough to be applicable to very diverse components and systems, so enabling a coherent treatment for community resilience studies spanning multiple sectors. Moreover, being completely hazard-agnostic makes *FFS* applicable to any hazard. Thus, it can also be used for life-cycle analyses of components/systems prone to multiple types of hazard. Finally, *FFS* incorporates probability with as much accuracy as the available data allow.

5.3 A Methodology for Developing *FFS* for Bridges

In the aftermath of an earthquake, the damage caused to bridges can extensively downgrade the performance of transportation networks, hinder the post-event emergency activities, and slow down the recovery of other damaged structures and infrastructures. Therefore, restoration of damaged critical bridges is always among the top priorities of decision makers and

disaster managers. Bridge restoration can be quite a lengthy procedure and often the functionality of the bridge fluctuates considerably during the construction process. Thus, the metrics based on the total restoration duration or downtime might not be able to fully reflect the loss associated with the decreased functionality of a damaged bridge. In this regard, *FFS* can be utilized to represent this variability and its associated uncertainty in different ranges of seismic intensity scenarios. Moreover, such data can be used for functionality assessment and optimal disaster management activity planning of infrastructure systems, in particular transportation networks.

For comparison purposes, a first example is provided, where the *FFS* is assessed in a very simple way, using only data available in HAZUS (DHS, 2009) and minimum computations. In its simplest form, a bridge *FFS* can be developed utilizing the fragility curves and restoration functions available in the literature, following the equation shown below, based on the total probability theorem:

$$FFS_{fls}(t,im) = \int_{dm} G_{FM|DM}(fm_{fls}(t),dm) \cdot dG_{DM|IM}(dm,im) = \sum_{\forall dls_i} \underbrace{P[\bar{Q}(t) \geq C_{fls}|dls_i]}_{\text{Restoration function}} \cdot \underbrace{P[D = C_{dls_i}|im]}_{\text{Fragility curve}} \quad (5.4)$$

The summation part in Equation 5.4 is used in case a set of discrete damage limit states (*dls*) is defined for fragility analysis. For instance, Figures 5.3a and 5.3b illustrate fragility curves computed for a bridge of category HWB17 located on soil type D, and their associated restoration curves as presented by HAZUS (DHS, 2009). These curves have been used along with Equation 5.4 to develop a *FFS*, which is shown in Figure 5.3c. The *FFS* illustrated in Figure 5.3c is very simple to assess and uses only data readily available for all bridges in the US. However, it shows some unrealistic trends. The sudden jumps in the values of the *FFS* are mainly due to the fact that the restoration functions presented by HAZUS, as many other available bridge restoration functions (ATC, 1985; Padgett

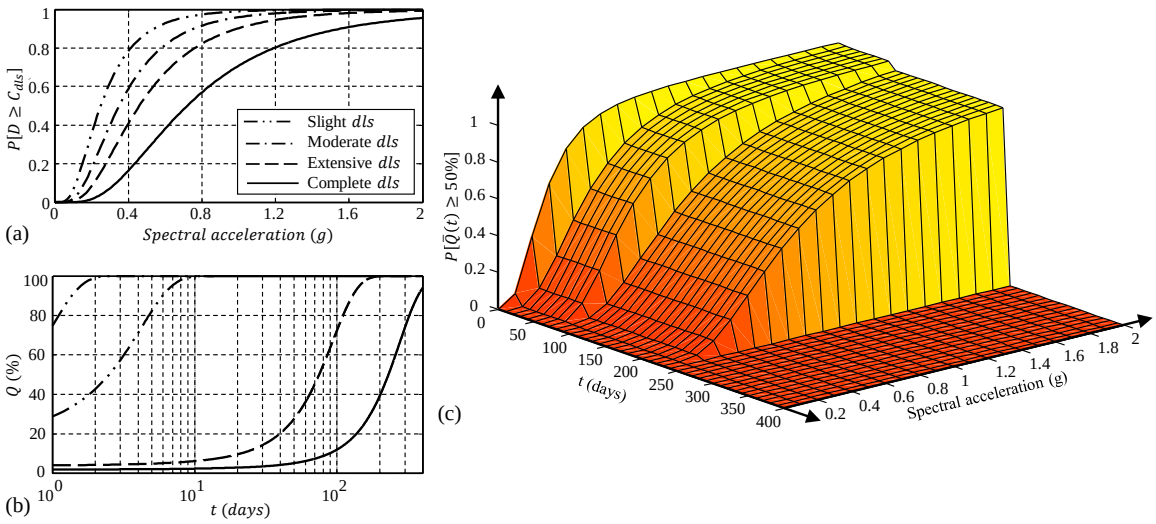

Figure 5.3: HAZUS bridge (a) fragility curves for various limit states, (b) associated restoration curves, and (c) *FFS* for HWB17 bridge type located on soil type D.

and DesRoches, 2007; Shinozuka et al., 2003), are deterministic, rather than probabilistic. Moreover, as mentioned in Section 2.3, the restoration functions shown in Figure 5.3b, and several other similar restoration functions developed through expert opinion surveys (ATC, 1985; Porter, 2004; Padgett and DesRoches, 2007), have been calibrated for regional loss analysis rather than for individual bridge restoration. Therefore, distinguishing the actual pre-restoration idle time and restoration duration is not possible. Finally, the definition of the utilized damage limit states are too qualitative Thus, they are not able to cover all potential component damage combinations.

The methodology proposed in this section to develop *FFS* for individual bridges tends to address the shortcomings mentioned previously. This technique is composed of two major modules:

(a) *Seismic fragility analysis*, which takes into account the effects of uncertainties involved in the ground motion time history, as well as the response and capacity of the structure.

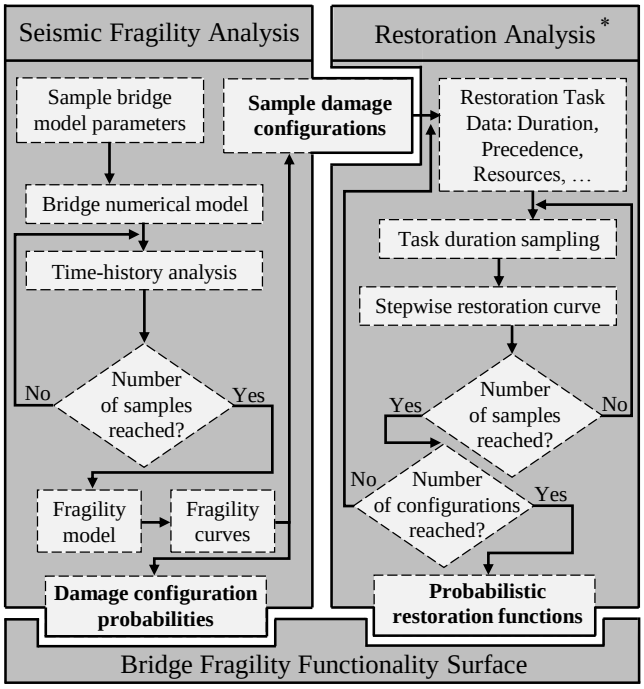

Figure 5.4: Flowchart of the proposed framework for developing bridge FFS (* the Restoration Analysis follows the technique presented in Chapter 4).

(b) *Probabilistic restoration analysis*, which accounts for the uncertainties in the restoration procedure due to the variability in the construction scheduling and resource requirement.

The key element for linking the two modules is a set of repair-based damage limit states for bridge components, which are used consistently in both fragility and restoration analyses. Figure 5.4 presents the flowchart of the proposed technique and its major components, which are discussed in the following section.

5.3.1 Seismic Fragility Analysis

The first step toward developing a bridge *FFS* is to compute fragility curves for the components (e.g., columns, abutments, and bearings) of the studied bridge using an appropriate analytical technique such as Incremental Dynamic Analysis (IDA) or Nonlinear Time-

History Analysis (NTHA). To this purpose, a computational model of the bridge is developed and analyzed, subjected to a suite of ground motions representative of the site on which the studied bridge is located. To specify the damage levels, a set of repair-based damage limit states is defined for each considered component. These limit states are damage thresholds above which a certain procedure is necessary for the restoration of their corresponding components. Similar damage states were presented in Section 4.4 (see Table 4.2) and used to specify the component damage states of the studied MSSS Steel Girder bridge. Using the results of the fragility analysis, samples of the damage states of the components are generated at the selected levels of the intensity measure (sample bridge damage configurations), considering also the correlation among the demand and possibly the capacity of different components.

5.3.2 Probabilistic Restoration Analysis

In this module, the sample bridge damage configurations generated from the fragility analysis are used to develop sample bridge restoration functions. This is carried out using the methodology presented in Chapter 4. The probabilistic restoration functions for each sample bridge damage configuration is then computed by calculating the frequency of negative safety margins at each time step during the restoration process and considering the appropriate functionality limit state. It is worth noting that, since for *FFS* the loss of functionality is identified, rather than the functionality, the complementary values of the computed sample restoration functions are used, following the equation shown below:

$$P[\bar{Q}(t) \geq C_{fls}] = \frac{\sum_{i=1}^{N} FN_i(t)}{N}, \text{ where } FN_i = \begin{cases} 1 & \text{if } [100 - QN_i(t)] \geq C_{fls} \\ 0 & \text{otherwise} \end{cases} \tag{5.5}$$

in which $QN_i(t)$ is the functionality of the bridge at time t, based on the ith realization of the restoration function, and N is the number of sample restoration functions.

5.3.3 Integration of Fragility and Recovery Analyses

Finally, the *FFS* is computed by integrating the results of fragility and restoration curve analysis using the following equation, developed based on the total probability theorem:

$$P[\bar{Q}(t) \geq C_{fls}|im] = \sum_{dc=1}^{nDC} P[\bar{Q}(t) \geq C_{fls}|dc] \cdot P[DC = dc|im] \tag{5.6}$$

where *nDC* is the total number of unique bridge damage configurations resulting from component damage state sampling. $P[DC = dc|im]$ is the probability of occurrence of damage configuration *dc* at the ground motion intensity level *im*.

At the end, it is worth emphasizing that the methodology proposed in this chapter is one possible technique to accurately compute *FFS*s for bridges. Alternative strategies can also be used based on the available information and desired level of accuracy and detail.

5.4 Application: Assessing the *FFS* for a MSSS Steel Girder Bridge

In this section, the procedure for the computation of *FFS*s is presented in detail for the case of an archetype bridge located in a hypothetical seismic region. The bridge studied in this paper falls into the category of MSSS Steel Girder bridges. Figure 5.5 illustrates the studied bridge, its dimensions and major components. Figure 5.6 shows the position of the bridge in its hypothetical site. It is assumed that the seismicity of the region in which the bridge is located is characterized by the two faults shown in the figure. Such characteristics will be further reflected in ground motion selection and the probabilistic seismic demand analysis of the bridge.

In order to perform the fragility analysis, a detailed finite element model of the bridge

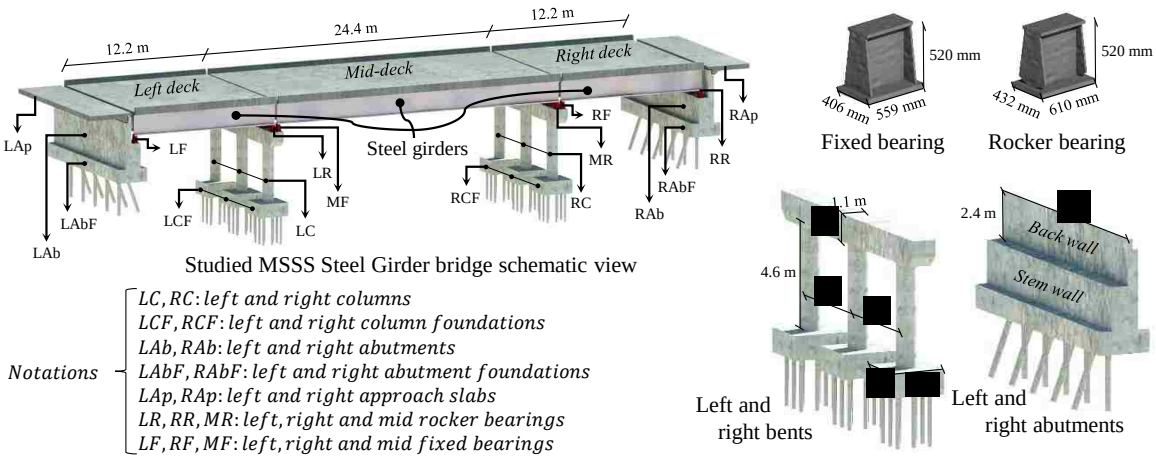

Figure 5.5: Schematic view of the example 3D MSSS Steel Girder bridge.

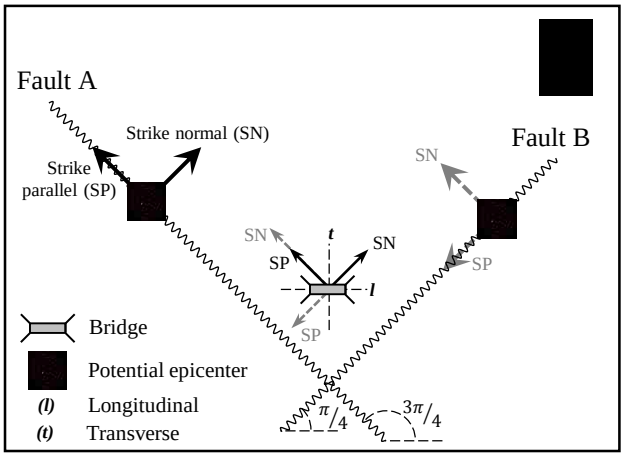

Figure 5.6: Position of the bridge in its hypothetical site.

has been developed in the OpenSees platform (McKenna et al., 2000), considering the decks, bearings, bents, abutments, and pile foundations as the major contributing elements of the model. The finite element model of the bridge is similar to the MSSS Steel Girder bridge models presented in Sections 3.4 and 4.4. However, for this particular application the bridge has been developed in 3D to properly capture the behavior of the bridge considering its asymmetric configuration. More details on the modeling techniques and parameters are presented by Nielson (2005).

As discussed earlier, in order to develop bridge *FFS*s using the proposed approach,

fragility analysis is performed to characterize the component damage probabilities. Several techniques have been proposed for analytical development of bridge fragility curves (see Section 2.2), among which NTHA is one of the most popular. The underlying assumption on the distribution of demand and fragility have been discussed and the approximation introduced to the estimated probability of failure and resilience of bridges has been evaluated in Chapter 3. To avoid such approximations in the current application, the fragility analysis is carried out following the methodology presented in Section 3.3.

The first step towards analyzing the fragility is to perform PSDA to assess the probabilistic characteristics of the bridge component demands at different levels of the selected *IM*. The major sources of demand variability are modeling parameters, material properties, and ground motion characteristics. To take into account the first two, a set of 14 critical random materials and modeling parameters have been identified and samples have been generated using Latin hypercube sampling (McKay et al., 2000). These samples are later assigned to the bridge numerical model to construct sample bridge models. The list of the considered random parameters and their distributions are presented in Table 5.1. This table is similar to Table 3.1 with a number of differences. Since the current bridge is modeled in 3D, a number of additional random variables is included in the list to take into account the variability of the bridge material properties and modeling parameters in transverse direction. These include the coefficient of friction of the bearings in transverse direction. Moreover, unlike the bridge analyzed in Chapter 3, the current bridge is assumed to be an individual bridge rather than a bridge representing a class of structures. Therefore, it is expected that the variability of some of the parameters is lower compared to a representative bridge class. To take this consideration into account, new distributions with less dispersions are assigned to the stiffness of piles (in both horizontal and vertical directions), as well as the abutments (in both active and transverse directions). Also, the stiffness of the abutments in passive direction is assumed to be deterministic and equal to 11.5 kN/mm/m.

Table 5.1: Random parameters and their underlying probability distributions considered for PSDA.

Random variable	Distribution	Param-1	Param-2	Units
Steel yield stress	Lognormal	λ=6.13	ζ=0.08	MPa
Concrete compressive strength	Normal	μ=33.8	σ=4.3	MPa
Piles' horizontal stiffness	Normal	$\mu = 7.0$	$\sigma = 0.46$	KN/mm/pile
Piles' vertical stiffness	Normal	$\mu = 175.0$	$\sigma = 11.66$	kN/mm/pile
Abutment active and transverse stiffnesses	Normal	$\mu = 7.0$	$\sigma = 0.46$	KN/mm/pile
Unit weight of middle deck	Uniform	l=46.8	u=57.2	kN/m
Unit weight of end deck	Uniform	l=35.1	u=42.9	kN/m
Damping ratio	Normal	μ=0.045	σ=0.0125	-
Fixed bearing Coef.[1] of friction (long.[2])	Lognormal	λ=-1.56	ζ=0.5	-
Fixed bearing Coef. of friction (trans[3])	Lognormal	λ=-0.99	ζ=0.5	-
Rocker bearing Coef. of friction (long)	Lognormal	λ=-3.22	ζ=0.5	-
Rocker bearing Coef. of friction (trans)	Lognormal	λ=-2.39	ζ=0.5	-
Deck-deck gap	Normal	$\mu = 25.4$	$\sigma = 4.32$	mm
Deck-abutment gaps	Normal	$\mu = 38.1$	$\sigma = 5.84$	mm

[1]Coefficient, [2]longitudinal, [3]transverse

In the case of highway bridges, due to asymmetric characteristics of the geometry and material behavior properties, the orientation of the seismic ground motion with respect to the bridge axis (i.e., angle of incidence), can have a significant effect on the response and fragility of the structure (Banerjee Basu and Shinozuka, 2011; Torbol and Shinozuka, 2014). Considering the ground motion directionality effects for fragility analysis of classes of structures is not customary, since the relative angles of incidence is not known a priori. However, for the case of the individual bridge in the current application, accounting for such factor can improve the quality of the estimated demand and fragility of the bridge. The values of the angle of seismic incidence and their probabilities depend on several factors, including the characteristics of the ground between the epicenter of the earthquake and the location of the structure, as well as the relative orientation of the structure with respect to the seismic faults of the region. In the case of the current bridge, the angle of seismic incidence (θ) is defined as the angle of the strike normal component of the ground motion with the longitudinal axis of the bridge (see Figure 5.6). Therefore, given the configuration

of the site, and assuming that the soil between the epicenters (located on the faults) and the location of the bridge is homogeneous, two values can be considered for θ. These are $\theta = \pi/4$ and $\theta = 3\pi/4$ for the events originated from faults A and B, respectively. Thus, θ is introduced as another random variable in addition to the parameters shown in Table 5.1, with equal probabilities for the two mentioned values, assuming that the length of the faults A and B are the same.

In order to consider the effect of ground motion variability in the result of the PSDA, a set of representative ground motions has been chosen from the suite of records collected by McGuire et al. (2001). This suite is composed of a number of historical events, characterized by the their event magnitude, distance, and bed conditions (i.e., rock or soil). The records used for the current application have been selected from a set of 144 ground motion records of the suite that have been adjusted to match the soil characteristics of the Central and Eastern United States. Considering the relevant epicenteral distances (Figure 5.6), the ground motions used in the current study have been selected from the bins with event distance ranging from 10 to 100 kilometers (6 bins in total).

The results of preliminary sensitivity and convergence analyses showed that 50 samples of bridge model parameters would be enough to estimate the demand and damage of the bridge components, if factoring out the variability in ground motions. Similarly, 3 ground motions from each bin were found to be sufficient for accurate demand and damage simulations. Thus, following the technique presented in Section 3.3.1, the PSDA has been carried out by scaling the 18 selected ground motions to 7 levels of IM, with values ranging from 0.1g to 0.7g. Each bridge sample has been paired with every scaled ground motion, and time history analyses have been performed. This results in 6300 time history analyses (900 at each level of IM) which have been carried out in parallel using Corona, which is a computing cluster with 66 multi-core nodes located at Lehigh University.

Table 5.2: Recorded EDP for components and their damage limit states.

DS0	DS1	DS2	DS3	DS4
Column (*LC,RC*)				
$\mu_c \leq 1.58$	$1.58 < \mu_c \leq 3.22$	$3.22 < \mu_c \leq 6.84$	$\mu_c > 6.84$	-
no damage	Cracking	Cover spalling	Bar buckling	-
Fixed bearing (*LF,RF,MF*)				
fb_d[1] ≤ 20	$20 < fb_d \leq 40$	$40 < fb_d \leq 250$	-	-
no damage	Anchor bolt damage	Toppling potential	-	-
Rocker bearing (*LR,RR,MR*)				
rb_d^l[2] ≤ 50	$50 < rb_d^l \leq 100$	$100 < rb_d^l \leq 250$	$rb_d^l \leq 100$	$100 < rb_d^l \leq 250$
rb_d^t[3] ≤ 20	$rb_d^t \leq 20$	$rb_d^t \leq 20$	$20 < rb_d^t \leq 40$	$20 < rb_d^t \leq 250$
no damage	Damage to pins	Unstability	Anchor bolt damage	Pedestal damage
Abutment (*LAb,RAb*)				
$Ab_{Pd} \leq 100$	$100 < Ab_{Pd} \leq 120$	$120 < Ab_{Pd} \leq 150$	-	-
no damage	Damage to joint seal	Backwall cracking	-	-
Approach slab (*LAp,RAp*)				
$Ab_{Ad} \leq 200$	$200 < Ab_{Ad} \leq 435$	$Ab_{Ad} > 435$	-	-
no damage	Moderate settlement	Extensive settlement	-	-
Pile foundation (*LCF,RCF,LAbF,RAbF*)				
δ_{max}[4] ≤ 86	$86 < \delta_{max} \leq 115$	$\delta_{max} > 115$	-	-
no damage	Piles moderate damage	Piles extensive damage	-	-

[1]Maximum deformation of both longitudinal and transverse directions (mm), [2]Maximum deformation of rocker bearings in longitudinal direction, [3]Maximum deformation of rocker bearings in transverse direction, [4]Maximum of the absolute displacement of the foundation in all directions

The contribution of two categories of bridge components have been considered when modeling the restoration construction process and functionality of the bridge. The first type are the bridge parts whose restoration requires a considerable amount of construction effort (e.g., time and resources). In this study, these include individual bridge foundation, column, abutment, approach slab, and bearing (24 components in total). The demand and damage level of these components are directly specified using the results of PSDA. Table 5.2 lists these components, along with their repair-based damage states, their associated engineering demand parameters (EDP) recorded and used to specify the damage levels. This table is similar to Table 4.6 presented earlier in Chapter 4. However, the data in this table has been tuned for the case of the current 3D bridge. In particular, the damage states of the

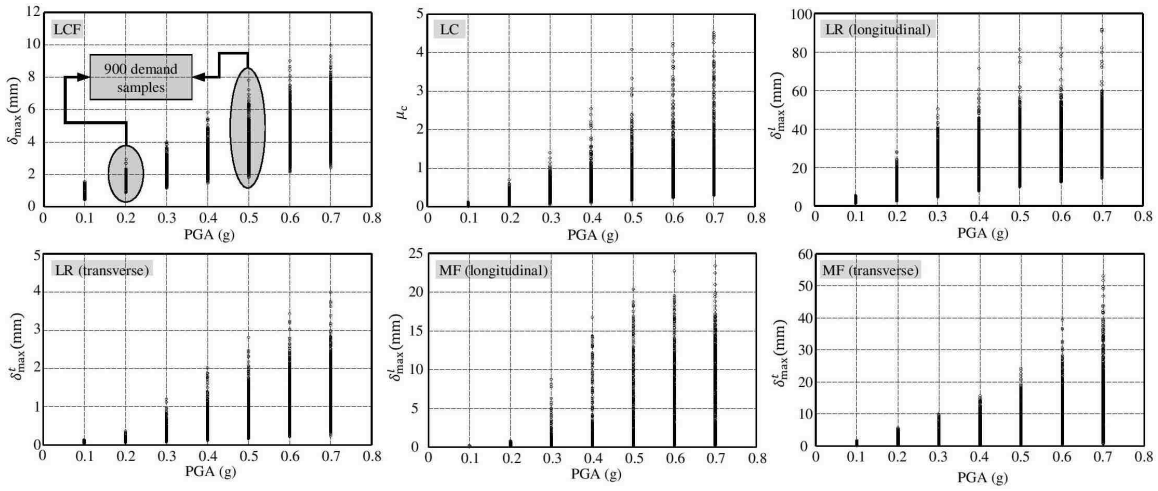

Figure 5.7: Results of the PSDA for left column foundations (LCF), left columns (LC), left rocker (LR) and mid-fix bearings (MF).

rocker bearing have been updated. The damage state criteria of the rest of the components are presented here again for convenience. As shown in this table, for this study the damage thresholds are considered to be deterministic. However, the methodology can handle component capacities with probabilistic features, if applicable.

Figure 5.7 shows the result of the PSDA on the components of the left multi-column bent of the bridge. Such results are utilized to specify the component repair-based damage states (DS) using the limit states presented in Table 5.2. Also, the probability of occurrence of each damage state at each level of *IM* is specified for each component, using the results of this analysis. In case more samples are required to better estimate the demand distribution tails, classic translation theory can be used to expand the number of samples at each level of *IM* through constructing the empirical distribution of the EDPs and considering the correlation among different EDPs (Grigoriu, 1998). Each repair-based damage state shown in Table 5.2 is associated with a restoration solution. The complete list of the restoration solutions, their corresponding restoration tasks, and their properties (e.g., duration, precedence relations, restoration resource requirements, etc.) are reported in Appendix A. Knowing the repair-based damage state of all components for each bridge sample-ground

Table 5.3: *Meta-Component*s.

	Activation condition	Impacted component
$LAbAp$[1]	δ_{max}^{pass}(for LAb) $\geq 150.0(mm)$	LAb, LAp
$RAbAp$[2]	Ab_{Pd}(for RAb) $\geq 150.0(mm)$	RAb, RAp
$LBnt$[3]	$\bigcap$[LC in DS3, $\bigcup$(LR in DS3 or DS4 , MF in DS1 or DS2)]	LC, LR, MF
$RBnt$[4]	$\bigcap$[RC in DS3, $\bigcup$(MR in DS3 or DS4 , RF in DS1 or DS2)]	RC, MR, RF
$Brdg$[5]	$\exists(fb_d \wedge rb_d) \geq 250$[6]$(mm)$	All comps

[1]Left abutment-approach *Meta-Component*, [2]Right abutment-approach *Meta-Component*, [3]Left bent *Meta-Component*, [4]Right bent *Meta-Component*, [5]Bridge *Meta-Component*, [6]Deck unseating damage state.

motion pair, the restoration data associated with all damaged components is combined using the methodology presented in Chapter 4 to construct the probabilistic restoration functions of the bridge. However, in some cases, the repair of components with certain damage combinations requires particular actions which cannot be modeled by aggregating the restoration procedures of each individual damaged components. To address this problem, a set of *Meta-Component*s has been introduced. Each *Meta-Component* is a collection of a number of components. Also, the damage state of each *Meta-Component* is governed by certain damage combinations of components. In case such a damage configuration occurs, the involved components are replaced with their associated *Meta-Component*(s). Table 5.4 presents the five *Meta-Component*s defined for this application. For example, the largest (coarsest) considered *Meta-Component* is the whole bridge itself. In fact, it is assumed that if any of the decks has been unseated, the restoration of the bridge is not modeled by the repair tasks of its individual damaged components. Instead, demolition and reconstruction of the entire bridge is considered as one large restoration task. The complete list of the restoration tasks associated with each *Meta-Component*-damage state presented in Table 5.4, their duration distribution and resource consumptions, and precedence relations can be found in Appendix A.

Table 5.4 presents the complete list of damage scenarios and their associated bridge functionality (i.e., $qdsc$) considered for this application. The data presented in this table is

Table 5.4: Complete list of Bridge damage scenarios

Damage scenario	Components states	$qdsc(\%)$
dsc_1	LAp in DS2	0
dsc_2	$LAbF$ in DS2	0
dsc_3	LAb in DS2	50
dsc_4	LAb in DS3	0
dsc_5	LF in DS2	0
dsc_6	$LAbAP$ in DS1	0
dsc_7	$\bigcap(LCF_1$ in DS2$, LCF_2$ in DS2$, LCF_3$ in DS2$)$	0
dsc_8	$\bigcap(LC_1$ in DS1 or DS2$, LC_2$ in DS1 or DS2$, LC_3$ in DS1 or DS2$)$	50
dsc_9	$\bigcup(LC_1$ in DS3$, LC_2$ in DS3$, LC_3$ in DS3$)$	0
dsc_{10}	LR in DS2 or DS4	0
dsc_{11}	MF in DS2	0
dsc_{12}	$LBnt$ in DS1	0
dsc_{13}	$\bigcap(RCF_1$ in DS2$, RCF_2$ in DS2$, RCF_3$ in DS2$)$	0
dsc_{14}	$\bigcap(RC_1$ in DS1 or DS2$, RC_2$ in DS1 or DS2$, RC_3$ in DS1 or DS2$)$	50
dsc_{15}	$\bigcup(RC_1$ in DS3$, RC_2$ in DS3$, RC_3$ in DS3$)$	0
dsc_{16}	MR in DS2 or DS4	0
dsc_{17}	RF in DS2	0
dsc_{18}	$RBnt$ in DS1	0
dsc_{19}	RAp in DS2	0
dsc_{20}	$RAbF$ in DS2	0
dsc_{21}	RAb in DS2	50
dsc_{22}	RAb in DS3	0
dsc_{23}	RR in DS2 or DS4	0
dsc_{24}	$RAbAP$ in DS1	0

utilized in the technique presented in Chapter 4 to compute the functionality of the bridge considering the safety factors.

Observing the results of the fragility analysis showed that the columns and bearings are the main sources of vulnerability of this archetype bridge. Figure 5.8 illustrates the probability of occurrence of the relevant damage states at each level of *IM* for the components that showed any level of damage during the simulations. Although several component-damage states presented in Tables 5.2 and 5.4 have not occurred in this study, the full range of component damage levels is presented for completeness. Moreover, the results depend on the setup of the problem (e.g., model and loading parameters), and several of the discussed component-damage states occurred in other preliminary studies (e.g., sensitivity and

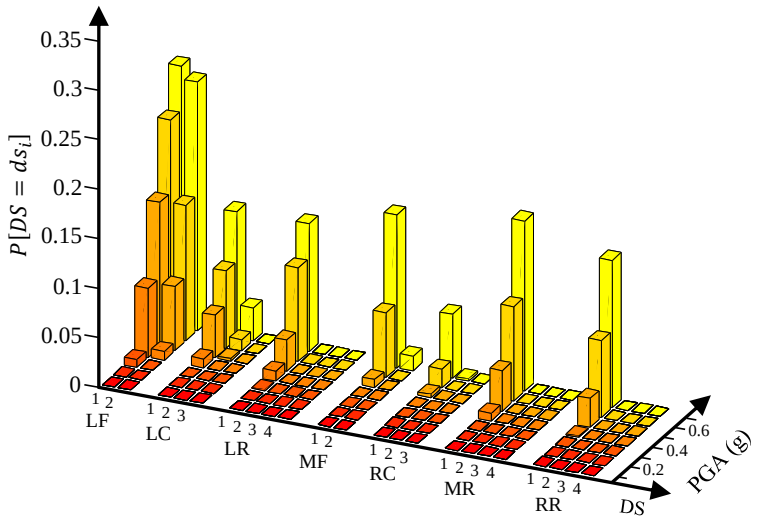

Figure 5.8: Component damage state probabilities (see Table 5.2 for the description of damage states).

convergence analyses) with different bridge parameters and ground motion sets.

The damage state of the components from each time history analysis has been extracted and saved in separate arrays. Each array, here named a *bridge damage configuration*, specifies a certain combination of component damage states. Typically, duplicate damage configurations exists (i.e., the same damage configurations result from several different time history analyses). Thus, first the unique configurations have been filtered from the pool of all damage configurations. A probabilistic restoration function has been computed from each unique damage configuration using the technique proposed in Chapter 4. To this purpose, the restoration tasks, their precedence constraints, and construction resource requirements have been taken into account. For each task, 4 major categories of resources have been considered, namely manpower, crane, concrete mixer, and geomachines. In terms of the resource availability, it has been assumed that 10 units of labors, 2 cranes, 2 geomachines, and 5 concrete mixers are available for executing the required construction tasks. From 6300 time-history analyses performed, the total of 97 unique damage configurations have been recognized, each one with a certain probability of occurrence. Figure 5.9 illustrates the computed probabilistic restoration curves ($P[\bar{Q}(t) \geq C_{fls}]$) for all damage

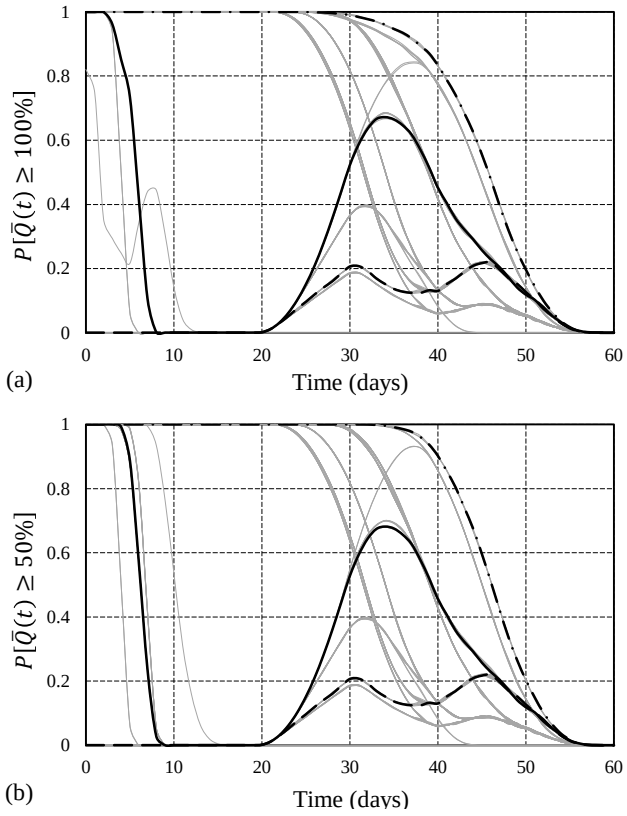

Figure 5.9: The probabilistic restoration functions (presented in terms of loss of functionality) for the computed bridge damage configurations considering two functionality criteria: (a) complete closure, and (b) at least partially closed.

configurations. Restoration curves have been developed using both *Learnall* and *Learnot* scheduling schemes. However, since for most of the damage configurations the functionality bounds computed by the two techniques were very narrow, only the results of *Learnall* are presented herein. The results are shown for two different functionality criteria. These are associated with bridge complete closure ($P[\bar{Q}(t) \geq 100\%]$), and at least partial closure ($P[\bar{Q}(t) \geq 50\%]$). In order to better observe the different shapes of the generated curves, three restoration functions have been highlighted in Figure 5.9. While the dash-dot curves express a monotonic evolution, the other two show some fluctuations. Several factors contribute to the shape of a restoration function. Typically, the monotonic curves (such as the dash-dot curves in Figure 5.9) represent the cases in which the change in the functionality is mostly governed by the full completion of the restoration process. This means that the

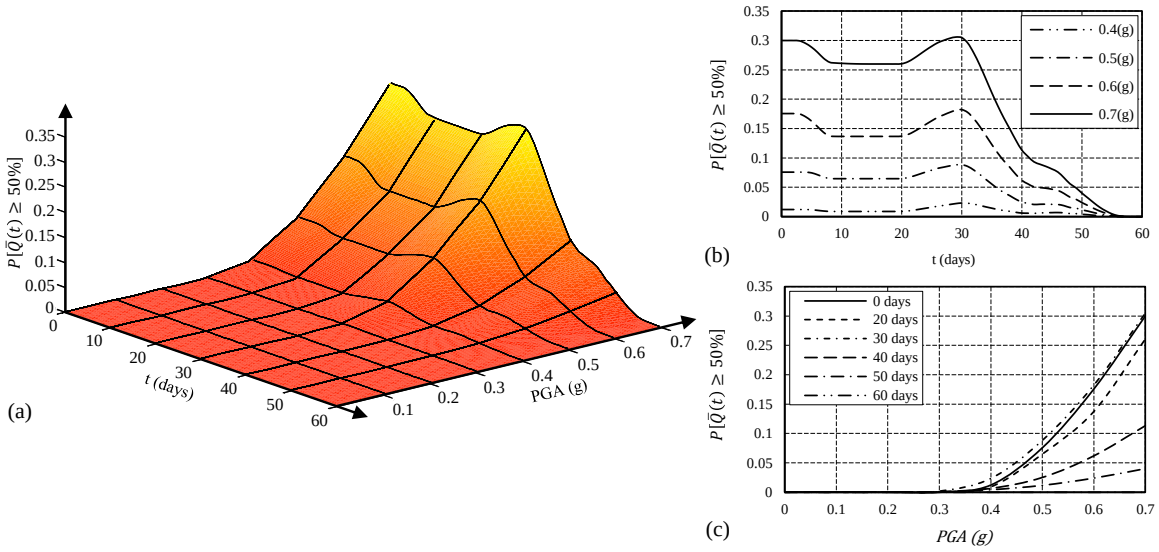

Figure 5.10: (a) *FFS* for the archetype bridge for the limits state of at least partial closure, (b) evolution of *FFS* by event intensity, and (c) evolution of *FFS* by time.

bridge is not completely (or even partially) opened before finalizing the restoration of all damaged components. On the other hand, the fluctuating curves reflect the effect of temporary repairs (e.g., shoring for the restoration of columns or replacement of bearings) on the functionality and temporary reopening of the bridge before completion of the repair process. Each curve shown in Figure 5.9 has a probability of occurrence at each level of the *IM* considered in the study.

Having all the probabilistic restoration functions as presented in Figure 5.9, along with their probabilities at each level of *IM*, Equation 5.6 can be used to compute the *FFS* for the studied bridge considering the fls of interest. Figure 5.10a illustrate the *FFS* computed for the fls associated with the bridge being at least partially closed (i.e., $P[\bar{Q}(t) \geq 50\%]$).

The computed *FFS* shows that the studied bridge would be safe with respect to the considered fls, if subjected to events with intensities less than $0.4(g)$. It is worth noting that this does not mean that restoration is not necessary for any such low intensity events. This rather indicates that the damage configurations for which the initial damage or restoration

require closure of the bridge have considerably small probabilities at $IM < 0.4(g)$. Also, 60 is shown to be the number of days after which the bridge would be at least partially open considering all relevant ground motions intensities and restoration strategies. Compared to the schematic *FFS* presented in Figure 5.1, the *FFS* of Figure 5.10a shows that for the current application, while the values of *FFS* increase monotonically by increasing the level of *IM*, these values do not necessarily follow a decreasing trend with time. To better observe such behavior, Figures 5.10b and 5.10c illustrate the evolution of the values of *FFS* for selected event intensities (here PGA) and time steps, respectively. For example, after 30 days from the initiation of the restoration process, the probability of failure with respect to the studied fls increases from about 2.5% to 35%, by increasing the ground motion intensity from $0.4(g)$ to $0.7(g)$ (see Figure 5.10b). On the other hand, Figures 5.10a and 5.10c show that there is a region of increase in the probability of failure (at about 20 days $< t <$ 30 days), before it starts to decrease monotonically (at about $t = 30$ days). Such behavior is observed since the proposed methodology is able to capture the variation of the functionality during the restoration process in a probabilistic manner, in particular due to potential bridge temporary reopening. Although computed for two different types of bridges and using different sets of data (e.g., fragility and restoration functions), the general trend in the evolution of the *FFS* shown in Figure 5.3 can be compared with the one computed using the proposed method as illustrated in Figure 5.10a. As it can be seen, Figure 5.10a offers a more realistic and reasonable shape with no discontinuities (sudden jumps). This is mainly due to the fact that probabilistic restoration functions have been utilized rather than deterministic functions.

Another set of useful information that can be extracted from *FFS*s is the occurrence probabilities of different relevant functionality limit states, presented as a function of time and event intensity. Such data can be further used for functionality, loss, and resilience assessment of infrastructure systems, such as transportation networks. For the case of the

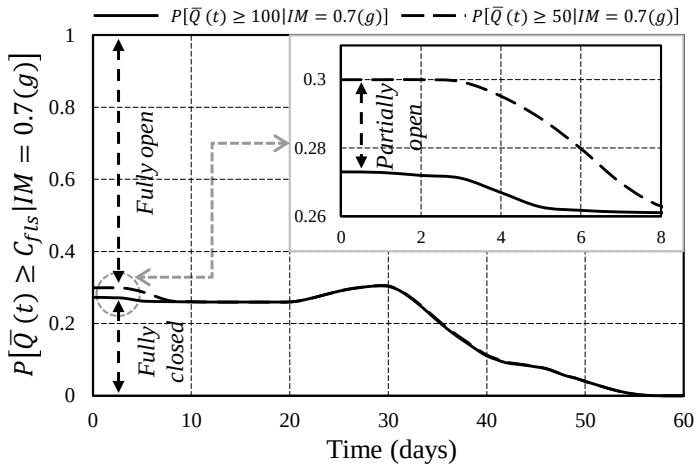

Figure 5.11: Functionality event occurrence probabilities.

studied archetype bridge, three functionality thresholds can be defined, each corresponding to one relevant functionality status of the bridge. These include the bridge being fully open ($C_{fls} = 0\%$), partially closed ($C_{fls} = 50\%$), and fully closed ($C_{fls} = 100\%$). It is worth noting that if relevant, these can be easily generalized to *nDS* (i.e., *n* damage states) or even presented as continuous functionality limit states. Having the two *FFS*s associated with the events $\bar{Q}(t) \geq 50\%$ and $\bar{Q}(t) \geq 100\%$ is enough to fully capture the functionality level sample space. The *FFS* for the former limit state has been shown in Figure 5.10a. The *FFS* for the latter limit state has been computed using the probabilistic restoration curves shown in Figure 5.9a. For clearer observation and evaluation, Figure 5.11 shows the values of the two *FFS*s at different time steps, but only for the level of *IM* equal to $0.7(g)$.

At the end, it is worth noting that although *FFS* has been introduced and formulated as the probability of loss of functionality being more than a threshold ($P[\bar{Q}(t) \geq C_{fls}|im]$), such definition does not bound its application to other functionality measures. In particular, it is likely that for some applications, the assessment of the probability of the level of functionality itself meeting a criterion is more intuitive and useful. In such cases, the *FFS* formulations presented throughout the paper can be revised accordingly, by simply replacing $\bar{Q}(t)$ with $Q(t)$, where $Q(t)$ is the functionality of the system at time t. For

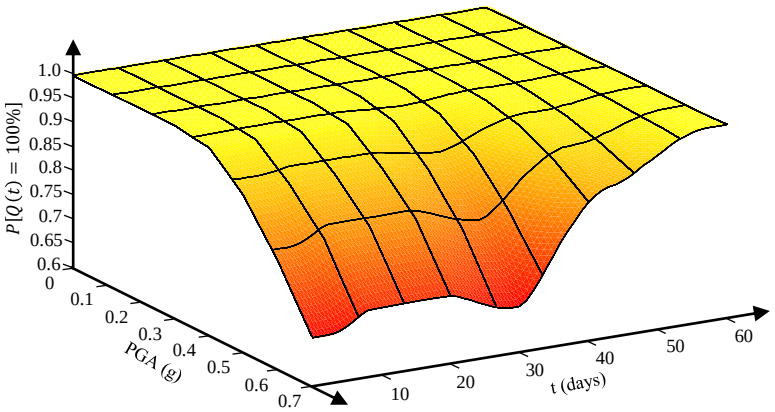

Figure 5.12: *FFS* considering the functionality instead of the loss of functionality.

illustration purposes, Figure 5.12 shows the *FFS* computed for the bridge example of this section, considering the event $Q(t) = 100\%$.

5.5 Concluding Remarks

This chapter introduces "*Functionality-Fragility Surface*" (*FFS*) as a concept for the probabilistic functionality and resilience assessment of individual structures, as well as infrastructure systems and communities. *FFS* is defined as the probability of reaching a particular functionality loss after a certain time elapsed from the occurrence of the extreme event (or from initiation of the restoration process), and given the intensity of the studied extreme event.

*FFS*s can be used as simple visualization tools to present the results of sophisticated and rigorous probabilistic analyses, in particular for functionality assessment of structures, and infrastructure systems. Moreover, *FFS*s are computed by combining two popular and well studied tools typically used for probabilistic damage assessment and functionality evaluation: Fragility Curves and Restoration Functions, typically developed for different types of components, structures, and infrastructure systems. Thus, while *FFS*s provide a new set of information about the probabilistic characteristics of the functionality and its

evolution by time and event intensity, they take advantage of the latest achievements and techniques in fragility and restoration curve development. Moreover, they can become a rigorous and yet simple paradigm that can be applied across multiple infrastructure sectors, multiple scales, and multiple hazards.

Depending on the type of the studied component/system, the importance of its role in the community, and data availability, *FFS*s can be developed using different methodologies with different degrees of accuracy and sophistication. These include, but are not limited to, survey-based, historical data-based, and analytical techniques. To showcase the proposed concept, a simple *FFS* was computed in this chapter for a bridge using the fragility curves and restoration functions provided by the HAZUS database. The computation of *FFS* using the available data from HAZUS showed to be convenient and efficient. However, while the results provided the trend of the functionality evolution over time and event intensity, some unrealistic features were observed. Therefore, to more accurately compute *FFS*s for individual bridges, a novel methodology was presented. The proposed simulation-based technique allows to compute the fragility and probabilistic restoration curves more accurately. The computed *FFS* captured much better trends observed in real applications, compared to the results developed using the simplified methodology.

Chapter 6

Sequencing Algorithm with Multiple-Input Genetic Operators: Application to Disaster Resilience

6.1 Introduction

Considering bridges as critical components of transportation systems, Chapters 3-5 studied the robustness (as defined for resilience analyses), functionality, restoration, and resilience of individual bridges and classes of bridges. In this chapter, restoration and resilience studies are performed at the system level for the case of transportation networks. This is carried out by presenting metrics and methodologies for the resilience-optimal restoration of bridges in transportation networks, in the aftermath of an extreme event.

A new multiple-objective optimization methodology is presented consisting in an evolutionary solution technique for scheduling of independent tasks, considering time and logistic constraints. The optimization solution methodology called *Algorithm with Multiple-Input Genetic Operators (AMIGO)* includes novel genetic operators, which take advantage of auxiliary variables computed during the fitness evaluation process, as well as some global problem parameters, to enhance the search procedure. Figure 6.1 highlights this feature compared to common genetic algorithms. The versatility of the proposed methodology makes it applicable to a variety of scheduling problems common in different fields, such as construction management, production and manufacturing industry, and emergency planning. In particular, in this chapter *AMIGO* is applied to the post-disaster repair and restoration prioritization of damaged highway networks. To this respect, *AMIGO* is tai-

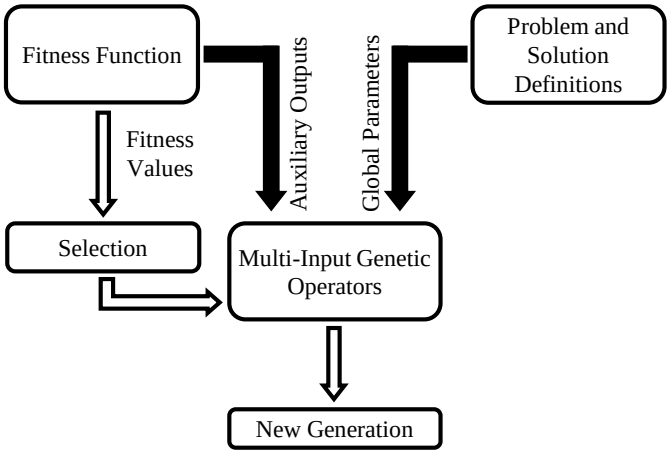

Figure 6.1: Schematic view of *AMIGO*. The highlighted arrows indicate the novel elements of the framework. The use of additional information in the genetic operators enables a much faster convergence to the optimal solution.

lored to find the optimal restoration sequence of the damaged bridges in the context of a highway network. Among several infrastructure system performance criteria, resilience has been selected as the objective of the optimization problem.

In addition to the presentation and application of *AMIGO*, refinements have been performed also on the formulation of post-disaster resilience analysis of bridges and highway networks. These are (1) a new bridge recovery model, and (2) the consideration of different phases of disaster management by introducing a new network connectivity-based resilience metric.

The performance of *AMIGO* is demonstrated through a large-scale numerical example. The highway network serving the port of San Diego has been chosen for this purpose, which contains 238 highway bridges. The proposed methodology has been utilized to find the best restoration strategies for the bridges of the network damaged by an earthquake scenario, selected based on the seismicity of the region. In addition, the efficiency of the proposed formulation has been examined through comparison of the results with previous methodologies.The methodologies and results presented in this chapter are based on papers by Karamlou and Bocchini (2014a, 2016b).

6.2 Proposed Optimization Technique: *AMIGO*

In this section, the framework and solution strategy of the proposed scheduling optimization problem are presented in general terms. Several project scheduling problems have been addressed by the research community, considering different objectives (e.g., project duration, maximum activity lateness, net percent value), and constraints (e.g., precedence, resources, time lag). An extensive review of different problem definitions, formulations, and solution methodologies is presented by Kolisch and Padman (2001), Hartmann and Briskorn (2010), Özdamar and Ulusoy (1995), and Brucker et al. (1999). The optimization problem framework propounded in this study is a version of resource-constrained project scheduling with one renewable resource type, considering a maximum project duration and generic objectives. The problem is formulated as a combinatorial optimization characterized by a triple $(\mathbf{V}, NSA_{max}, t_h)$. Activities (the words "activity" and "task" will be used interchangeably throughout this chapter) of the project are collected in set $\mathbf{V} = \{V_1, V_2, ..., V_n\}$. To take into account logistic constraints (such as man-power, equipments, contractors) typically involved in planning, the number of simultaneous activities at each time step t is limited to NSA_{max}. t_h is the investigated time span (time horizon) of the project. A schedule $\check{\mathbf{S}} = \{\check{S}_1, \check{S}_2, ..., \check{S}_n\}$ is defined as a vector in $\mathbb{R}^n$ such that $\check{S}_i$ is the start time of activity V_i. Finally, the quality of each schedule is determined by its associated fitness, which is a function of the sequence of tasks.

In many cases, the essential components (e.g., fitness functions and constraints) of the problem cannot be formulated in closed-form due to their complexity. This in fact, limits the application of standard optimization methodologies. For such cases, the advancement of heuristic optimization techniques, and evolutionary algorithms in particular, has resulted in high-quality near-optimal solutions for several challenging real-world optimization problems involving industrial, transportation, structural, and infrastructure engineering, among

other fields.

AMIGO belongs to this class of optimization solvers, which are powerful heuristic optimization techniques inspired by the process of natural selection and offer several advantages, such as applicability to almost any type of optimization problem (discrete and continuous), objective functions (differentiable and non-differentiable), and constraints (constrained and unconstrained domains). Moreover, they are particularly convenient for solving multi-objective optimization problems by Pareto-based approaches. Discussion about the fundamentals of evolutionary algorithms is beyond the scope of this study and can be found for instance in (Coello et al., 2002). The main characteristic of *AMIGO* is the fact that it enriches the input of genetic operators with additional information on the outcome of the current individual, allowing for better convergence. Details on the characteristics and implementation of *AMIGO* and its components including a new initial population generator and genetic operators are presented in the following sections. For this study, *AMIGO* and its components have been coded in the Matlab programming environment (The Mathworks Inc., 2014). All subroutines are original, except for two operators (i.e., ranking and selection) extracted from the Elitist Non-Dominated Sorting Genetic Algorithms (NSGA-II) technique (Deb and Goel, 2001; Deb et al., 2002). Figure 6.2 shows the flowchart of *AMIGO* as implemented in this study.

6.2.1 Trial Solution Representation

Let $\mathbf{V}$ be a set containing the n activities of the project. The trial solution of the optimization problem is the array $\mathbf{x^s} = \{x_1^s, x_2^s, ..., x_n^s\}$ such that $\mathbf{x^s} \in P_V$, where P_V is the space of all possible permutations of $\mathbf{V}$. Therefore, the trial solution is a sequence of tasks as shown in Figure 6.3a. In cases where there is only one resource available (i.e., $NSA_{max} = 1$), the activities are simply performed in series. Otherwise, if there are multiple resources (i.e. $NSA_{max} > 1$), the first NSA_{max} tasks are assigned to various resources, then, as soon as one

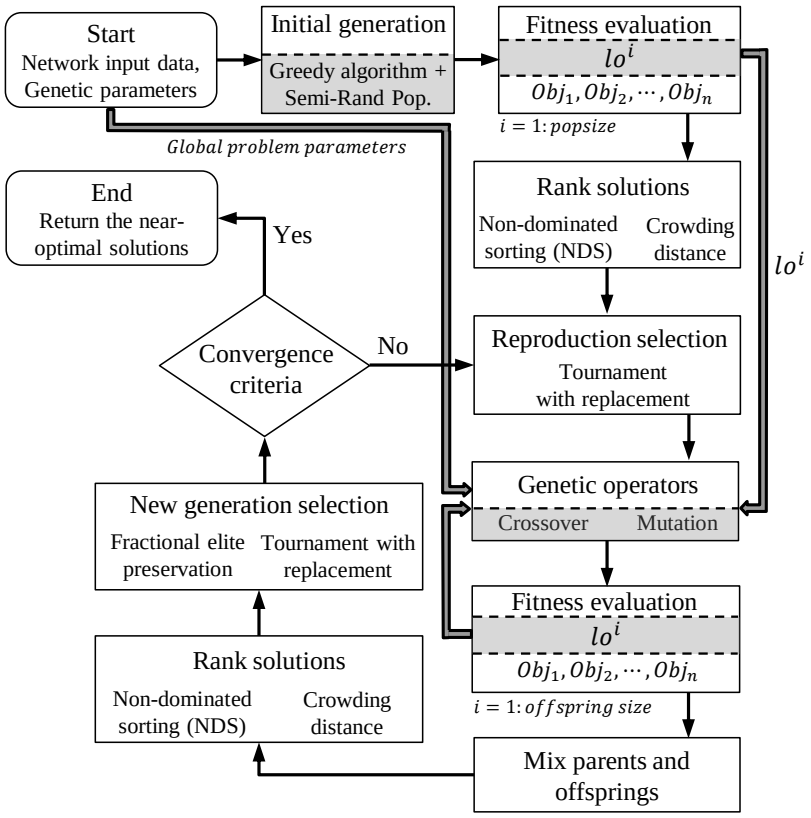

Figure 6.2: Flowchart of *AMIGO* for multi-objective optimization. The highlighted sections and arrows indicate the new aspects of the algorithm. Note that the two selection processes shown in the figure are different and satisfy different purposes: the New Generation Selection is carried out to reduce the size of the mixed population (equal to $2 \cdot popsize$) to the original *popsize*, then the Reproduction Selection is performed to choose parents used in reproduction functions (i.e., mutation and crossover).

activity is completed, the next task in array $\mathbf{x^s}$ is assigned to the resource that has completed its job. In this process, it is assumed that the activities are performed consecutively, without any gap.

The size of the design space seems to be equal to $n!$ (i.e., all possible permutations of n integers). However, there are several redundant solutions representing the same practical outcome. To avoid this redundancy, which would negatively impact the convergence of the evolutionary algorithm, the developed optimization operators interpret the individuals using two additional pieces of information: NSA_{max} and lo^s (Figure 6.3a). The former is a global parameter, whereas the latter is computed by the fitness function for each individual,

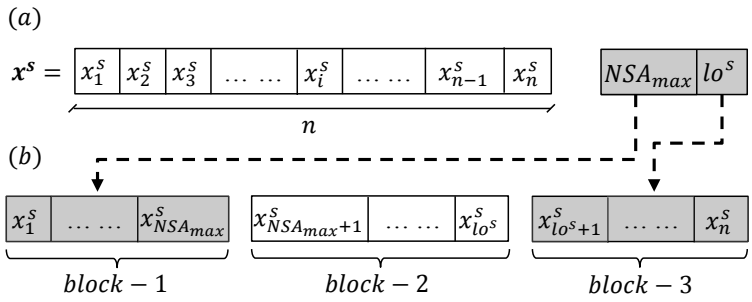

Figure 6.3: Trial solution representation

as part of the assessment of the fitness itself. In many cases, not all activities can be completed during the specified time period (t_h). In this respect, $lo^s \in \mathbf{x^s}$ is defined as the last task in trial solution $\mathbf{x^s}$ that starts and has an impact on the objective(s). With this representation, each trial solution is divided into three blocks, as shown in Figure 6.3b. All activities in block-1 start at the same time (i.e., $t = 0$), then activities in block-2 are performed in sequence, and activities in block-3 are not performed in the investigated time. Obviously, the order of tasks appearing in blocks 1 and 3 is not important in determining the value of the objective(s). Therefore, the fitness of a solution depends only on the tasks that appear in the first block (regardless of their order, so a total number of $C_{NSA_{max}}^n = \frac{n!}{NSA_{max}!(n-NSA_{max})!}$ distinct cases) , and the sequence of the tasks in the second block (for a total number of $(n-NSA_{max})!$ permutations). Thus, the total number of unique solutions is actually:

$$\sum_{s=1}^{C_{NSA_{max}}^n} [(lo^s - NSA_{max})!] \tag{6.1}$$

6.2.2 First Generation

A special subroutine has been developed with the aim of preventing the presence of redundant solutions in the first generation and enhance its quality with a preliminary optimization. To this purpose, block-1 of the individuals (Figure 6.3b) in the initial generation is obtained by randomly selecting one from all $C_{NSA_{max}}^n$ possible sequences of tasks. Then, for

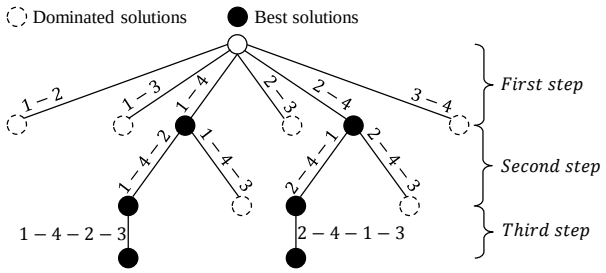

Figure 6.4: Greedy algorithm optimization example for a 4-activity project and $NSA_{max} = 2$.

each individual, the rest of the genes (i.e., block-2 and block-3) are filled by a randomly generated permutation of the remaining activities. It is worth mentioning that at this stage the fitness of the initial individuals is not yet evaluated. Therefore, the value of lo^s for the solutions is not known and not used for the first generation.

In most optimization techniques, the quality of the search process, as well as the optimality of the final results can be improved considerably by selecting a good "starting point". In the case of the current problem, the first generation obtained by the presented procedure is mixed with the result of a customized "greedy algorithm" developed in this research. The greedy algorithm starts considering all possible partial solutions of length $l^0_{greedy} \leq n$ and computes the values of the objective(s) considering the investigated t_h, assuming that only tasks present in the partial solution are accomplished. Then, the best of these solutions are extracted and their associated partial sequences are extended for the next step by adding all possible permutation of Δl_{greedy} of the remaining tasks to the end of each solution. The value of Δl_{greedy} is determined by the available computational capacity (e.g., 2). This process continues until the number of tasks in the optimal sequences reaches $min(n, lo^s)$. Figure 6.4 illustrates the greedy algorithm procedure for the case of a project with 4 activities starting with partial solutions of length $l^0_{greedy} = 2$. The results obtained on several benchmark problems have shown that for small number of tasks the greedy algorithm finds some of the global optima, and for larger instances (e.g., $n > 10$) it can enhance the convergence and reduces the overall computational cost.

Algorithm 6.1 Mutation operator

input: x^p (parent), lo^p, NSA_{max}
output: x^{os} (offspring)

Randomly select a gene $C1 \in [1, n]$
$B1 \leftarrow$ block containing $C1$ in x^p
Randomly select block $B2$ associated with the second gene, with probability $P(B2)$:
if $B1 = 1$ **then**
  $P(B2 = 1) = 0$
  $P(B2 = 2) = \frac{lo^p - NSA_{max}}{n - NSA_{max}}$
  $P(B2 = 3) = \frac{n - lo^p}{n - NSA_{max}}$
else if $B1 = 2$ **then**
  $P(B2 = 1) = \frac{NSA_{max}}{n}$
  $P(B2 = 2) = \frac{lo^p - NSA_{max}}{n}$
  $P(B2 = 3) = \frac{n - lo^p}{n}$
else if $B1 = 3$ **then**
  $P(B2 = 1) = \frac{NSA_{max}}{lo^p}$
  $P(B2 = 2) = \frac{lo^p - NSA_{max}}{lo^p}$
  $P(B2 = 3) = 0$
$C2 \leftarrow$ Randomly select the second gene from the selected block $B2$
$x^{os} \leftarrow$ Swap $C1$ and $C2$ in x^p

6.2.3 Multiple-Input Genetic Operators

The trial solution structure discussed in Section 6.2.1 is a "direct representation", meaning that the phenotype and genotype for the current problem are the same. Therefore, specialized genetic operators need to be developed to properly pass the important properties of the parents to the offspring (Rothlauf, 2006). The operators developed for *AMIGO* take advantage of the two additional data (NSA_{max}, lo^s) shown in Figure 6.3, and search the design space more efficiently by not generating redundant trial solutions.

The novel mutation operator utilized by *AMIGO* is a modified version of "swap mutation", which selects two genes randomly and swaps their contents (Gen and Cheng, 2000). The pseudo-code presented in Algorithm 6.1 shows the proposed mutation scheme. In particular, this procedure guarantees that no offspring is generated just by swapping two genes from block-1 or two genes from block-3.

Algorithm 6.2 Crossover operator

input: x^{p1}, x^{p2} (parents), $lo^{p1}, lo^{p2}, NSA_{max}$
output: x^{os} (offspring)

$os_{blk1} \leftarrow \left(x^{p1}_{1:NSA_{max}} \cap x^{p2}_{1:NSA_{max}}\right)$
$os_{blk3} \leftarrow \left(x^{p1}_{lo^{p1}+1:n} \cap x^{p2}_{lo^{p2}+1:n}\right)$
$x^{p1*} \leftarrow (os_{blk1} \cup os_{blk3})'$ in the order appearing in x^{p1}
$x^{p2*} \leftarrow (os_{blk1} \cup os_{blk3})'$ in the order appearing in x^{p2}
Perform order crossover on $\left(x^{p1*}, x^{p2*}\right)$:
$s1 \leftarrow$ select randomly from $[1, size(x^{p1*})] \in \mathbb{Z}$
$s2 \leftarrow$ select randomly from $[1, size(x^{p1*})] \in \mathbb{Z}$
$os_{blk2}(s1 : s2) \leftarrow x^{p1*}(s1 : s2)$
$[os_{blk2}(1 : s1-1), os_{blk2}(s2+1 : size(os_{blk2}))] \leftarrow x^{p1*}(1 : s1-1) \cup x^{p1*}(s2+1 : size(x^{p1*}))$ in the order they appear in x^{p2*}
$x^{os} \leftarrow$ | os_{blk1} | os_{blk2} | os_{blk3} |

$'$: The prime sign indicates complement

Also a novel crossover operator has been developed for *AMIGO*, based on the well-known "order crossover" (Gen and Cheng, 2000), which keeps a randomly selected array of subsequent genes from one parent, and fills the genes in the offspring by preserving their associated order in the other parent. In the developed crossover, first the common genes which appear in block-1 for both parents are passed to block-1 of the offspring. The same process is repeated on the common genes of the parents in block-3, which will be sent to the end of the offspring. Finally, the order crossover is carried out only on the remaining genes of the parents. The overall crossover procedure is presented in Algorithm 6.2. In the offspring generated by this crossover, the activities that are not performed by any parents have very low chance to be performed by the offspring. Also, the tasks that are carried out at the beginning of the process according to both parents receive higher priority in the offspring as well. Finally, the order crossover applied on the remaining activities will transfer some additional characteristics of the parents to the offspring.

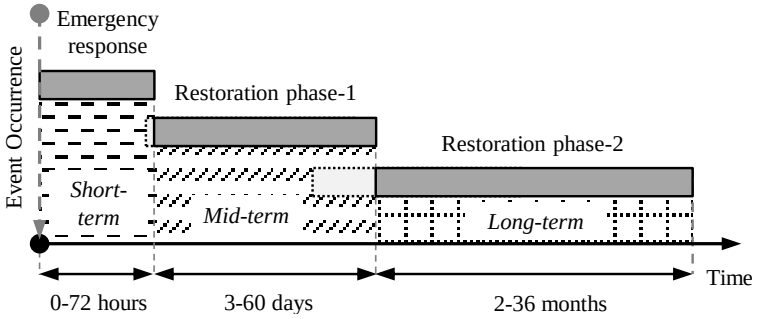

Figure 6.5: Disaster management phases

6.3 Transportation Network Resilience Formulations

The formulation and techniques used in this chapter for computation of resilience of transportation networks are presented in this section.

In real cases, disaster response activities are categorized into different phases based on their priority, as typically evaluated by decision makers and disaster managers (Poland, 2009b; DHS Risk Steering Committee, 2008). These phases, namely short-, medium-, and long-term are schematically shown in Figure 6.5. During the first phase, most of the efforts are focused on emergency and life saving activities, such as sheltering, evacuation, and hospitalization. Therefore, due to high criticality of the situation and short duration, no major restoration is feasible during the first phase and most of the restoration activities are planned for the following two phases. While the full restoration is the ultimate goal during the last stage, a minimum acceptable restoration of critical infrastructures is the main objective of the mid-term response phase. Accordingly, it is necessary to use appropriate functionality and resilience metrics in order to assess the quality of the response of the system with respect to the priorities of each restoration phase. To this respect, two network-level functionality and resilience metrics are utilized in this study which will be discussed in the following sections.

6.3.1 Long-Term Resilience Metric

The formulations and metrics proposed by Bocchini and Frangopol (2012a,b) are utilized in this study to quantify the functionality and resilience of transportation networks. Bocchini and Frangopol (2012a,b) expressed the performance of transportation systems as a function of the total travel time spent (TTT) and total travel distance (TTD) covered by all passengers in the network in one hour, computed using the well-known traffic distribution and assignment problems (Evans, 1976). The effect of damaged bridges and their reduced functionality in increasing the values of TTT and TTD was considered in the proposed formulations. Details of the technique presented by Bocchini and Frangopol (2012a,b) have been reviewed in Section 2.4.

For the purpose of having a fair comparison of the network performance, as done by Equation 2.15, the pre-event traffic demand is applied at all time instants, even though it is well-known that the post-event demand is different. Therefore, the resilience index computed by Equations 2.9 and 2.15 tends to reflect the quality of the response and restoration with respect to the last phase (long-term) of disaster management, whose ultimate goal is the complete restoration to the pre-event conditions.

6.3.2 Proposed Connectivity-Based Medium-Term Resilience Metric

The demand and behavior of traffic is evaluated by means of surveys or analytical models, such as the technique presented in Section 2.4. However, typically there is limited data available on the post-event travel demand. Also, the behavior of traffic in such situations is extremely complex as it is influenced by several socio-economic factors as well as evacuation and emergency policies. Therefore, the majority of analytical models fail to accurately capture post-disaster traffic characteristics. In particular, the models focusing on assessing the congestion by relying on origin-destination demands are not appropriate for

short- or medium-term emergency response evaluations (Chang and Nojima, 2001; Chang et al., 2012a). In this respect, in alternative to Equations 2.9 and 2.15, several other indices have been used in the literature to evaluate and compare the performance and resilience of transportation systems during emergency and recovery phases, among which connectivity- and accessibility-based metrics are probably the most popular (Giovinazzi and Nicholson, 2010; Chang and Nojima, 2001; Sohn, 2006; Tuzun Aksu and Ozdamar, 2014; Bocchini and Frangopol, 2013).

Typically, in each region there are certain locations that are of great importance due to social, economic, or topographic reasons. Emergency shelters, hospitals, airports, schools, and retail services are among these locations. Thus, in addition to their restoration, facilitating the traffic and enhancing the accessibility of these locations is always among the top priorities of disaster managers (after dealing with emergency situations in the first phase of the response). However, since in many cases these locations are not the major origin or destination of traffic in normal conditions, the restoration prioritization on the basis of maximizing the long-term resilience (computed using $Qflow$ using Equation 2.15) is not representative of the second-phase priorities.

The metric introduced in this chapter is a time-variant connectivity-based measure $Qconn(t)$ computed by the following equation:

$$Qconn(t) = \sum_{\hat{p}=1}^{n\hat{p}} CW_{\hat{p}} L_{\hat{p}}(t) \tag{6.2}$$

where $\hat{p}$ is a node pair whose highway connectivity is assumed to have priority. $n\hat{p}$ is the number of node pairs which need to be connected urgently. $CW_{\hat{p}}$ is a weighting factor reflecting the importance of fixing the connectivity between the nodes associated with pair $\hat{p}$, presented in the form of percent of the total functionality ($Qconn$) that is achieved by restoring their connectivity. Therefore, assuming that fully connecting all selected pairs

provides 100% functionality, the following constraint needs to be satisfied regarding $CW_{\hat{p}}$:

$$\sum_{\hat{p}=1}^{n\hat{p}} CW_{\hat{p}} = 1 \tag{6.3}$$

The value of $CW_{\hat{p}}$ is determined based on engineering judgment; an example will be provided in Section 6.5. It is worth noting that the functionality computed using Equations 6.2 and 6.3 is associated with the level of connectivity among the specified urgent node pairs. In this context, full functionality does not necessarily reflect the case in which all the nodes of the network are connected, but only those important for the mid-term recovery. Parameter $L_{\hat{p}}(t)$ determines the level of the connectivity between node pairs. In this respect, node pairs are considered fully or partially connected through network of highways if at least one route exists whose bridges are all fully (i.e., $Q_b = 1.0$) or at least partially (i.e., $Q_b = 0.5$) in service, respectively ("bottle neck assumption"). Accordingly, $L_{\hat{p}}(t)$ is defined and computed at each time step as:

$$L_{\hat{p}}(t) = \begin{cases} 1 & \text{if nodes of pair } \hat{p} \text{ are fully connected} \\ 0.5 & \text{if nodes of pair } \hat{p} \text{ are partially connected} \\ 0 & \text{if nodes of pair } \hat{p} \text{ are not connected} \end{cases} \tag{6.4}$$

While the values of $L_{\hat{p}}(t)$ in Equation. 6.4 have been set as consistent with the bridge functionalities ($Q_b \in \{0.0, 0.5, 1\}$), they can be adjusted for any particular application, based on the utilized bridge functionality model and connectivity considerations. At the end, the resilience computed using Equation 2.9 and Equations 6.2-6.4 addresses the medium-term restoration needs.

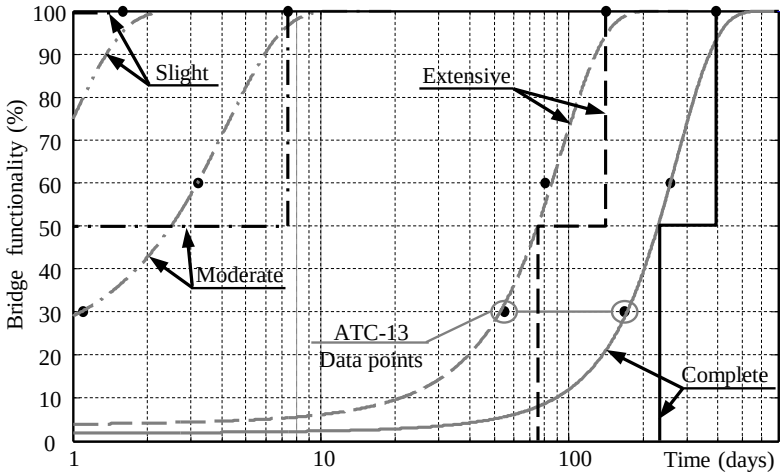

Figure 6.6: Restoration model for carrying bridges: fitted normal CDF (gray curves), stepwise restoration curves used in this study (black lines).

6.4 Proposed Bridge Restoration Model

The restoration model (restoration function) provides the time required to restore a bridge to a certain level of functionality. In this study, the bridge restoration function is assumed to follow a stepwise function, which can be constructed by obtaining the time needed to partially $t(Q_b = 0.5)$ and fully $t(Q_b = 1.0)$ restore a bridge, as well as the replacement cost of the bridge. In general, more intermediate steps can be added, if deemed appropriate for a particular case. In order to obtain these points, a technique similar to the methodology presented in HAZUS-MH (DHS, 2009) has been used. Different restoration functions have been generated considering the functionality of bridges with respect to the carried and crossed traffic. To this purpose, it has been assumed that for bridges that carry the traffic, the desired points lie on normal CDF curves fitted to the discrete mean restoration time values provided by ATC (1985). Therefore, the curve fitting has been carried out for four levels of initial damage states (i.e., slight, moderate, extensive, and complete damage), as well as two classes of bridges, namely SC-25a and SC-25c, associated with major and conventional bridges, respectively. Figure 6.6 illustrates the restoration data from ATC-13 and fitted curves for the class SC-25c.

Table 6.1: Restoration function values for mean cost bridges

$DS0$	$t[Q_b = 0.5]_{in\ days}$		$t[Q_b = 1.0]_{in\ days}$	
	Carried traffic	Crossed traffic	Carried traffic	Crossed traffic
Complete	126	126	304	126
Extensive	46	46	85	46
Moderate	0	0	9	0
Slight	0	0	0	0

Typically, for traffic carrying bridges, after a 50% restoration of the functionality, the major required activities on the substructure are completed and the remaining operations are performed on the superstructure of the bridge. At this point, while half of the lanes are considered to be closed to the carried traffic, it can be assumed that the construction activities would not interfere with the crossed traffic. Therefore, the bridge restoration functions generated considering the functionality with respect to the carried traffic have been modified accordingly, to obtain the associated functionality with respect to the crossed traffic. Additionally, the time required to restore 50% of the carried traffic capacity for moderately damaged bridges is typically very short (e.g., less than a month). Therefore, it has been assumed that moderately damaged bridges are 50% and 100% functional immediately after the extreme event, for traffic carried and crossed, respectively. Moreover, since the restoration of initially slightly damaged bridges does not require major construction activities, the restoration of these bridges has been ignored in this study, by assuming full functionality. Table 6.1 presents the key points of the restoration functions generated as discussed above for conventional bridges.

Based on the way data were collected by ATC-13, it has been assumed that the resulting stepwise curves are representative of the restoration functions of a bridge whose cost is equal to the mean replacement cost of all bridges in the studied region (e.g., California in this study). Therefore, assuming that the restoration time and effort are proportional to the cost of the bridges, an additional scaling factor has been applied to the resulting restoration

times based on the replacement cost for each individual bridge:

$$t^{DS0}_{cl,rc_b}(Q_b) = \frac{rc_b}{\overline{rc}_{cl}} \cdot t^{DS0}_{cl,\overline{rc}_{cl}}(Q_b) \tag{6.5}$$

where $t^{DS0}_{cl,rc_b}(Q_b)$ is the time required to restore functionality Q_b of bridge b of class cl (major or conventional) with initial damage state $DS0$ and replacement cost of rc_b. $\overline{rc}_{cl}$ is the mean replacement cost of class cl bridges in the region.

6.5 Numerical Example

The application of *AMIGO* and the enhanced resilience model is illustrated in this section through a numerical example. The problem statement, input data, and the results of the resilience optimization are presented in the following.

6.5.1 Problem Definition: Port of San Diego Transportation Network

For this application, a portion of the highway network of San Diego (CA) has been considered. The selected region is located in the Southwest of the county, in the vicinity of the Port of San Diego. The Port of San Diego, one of the largest ports in California, has the facilities and equipment for loading, unloading, storage, and shipping a variety of goods, particularly refrigerated commodities, vehicles, and bulk cargoes. Additionally, San Diego port is considered one of the US strategic ports used for transit and accommodation of military equipment and supplies. San Diego is ranked as the 6th and 10th port in California in terms of the value and volume of the shipped cargo, respectively (AAPA, 2013). Its vicinity to major US metropolitan areas, as well as Mexico, and its accessibility to major highways, make the San Diego harbor an important shipping center in the region. The total value of the port's import and export in 2013 have been estimated to be more than $7000 million (AAPA, 2013).

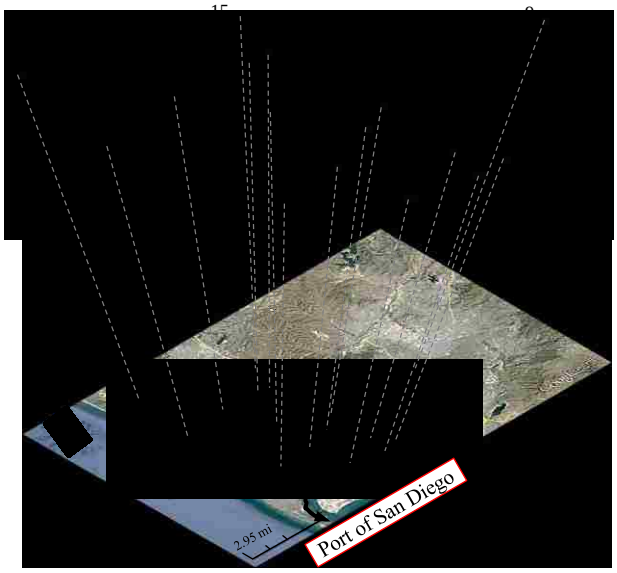

Figure 6.7: Port of San Diego and the modeled transportation network

Figure 6.7 illustrates the San Diego port region along with its major highways used in the transportation model of this study. 16 nodes and 52 links shown in the figure (each highway segment in the figure represents two directed edges of the network graph) are the major intersections and road segments, respectively. However, a technique presented by Bocchini and Frangopol (2012b) has been utilized to fully model the intersection ramps, which increases the number of nodes and edges of the graph to 136 and 282, respectively. The traffic originated from and attracted by each node have been computed for the peak traffic hours following the recommendations presented by Saydam et al. (2013). Also, the practical capacity f_{ij}^{c} of each link has been set to 2000 $\frac{car\text{–}equivalent}{vehicle \cdot hour \cdot lane}$. A detailed discussion about the determination of other traffic parameters can be found in Bocchini and Frangopol (2011).

The network shown in the figure contains 238 highway bridges. The detour distance d_b^d, and replacement cost rc_b of each bridge have been extracted from the National Bridge Inventory (FHWA, 2013). Based on the characteristics of the surrounding secondary roads, the practical capacity of the detours have been set to 1500 $\frac{car\text{–}equivalent}{vehicle \cdot hour \cdot lane}$.

A magnitude 7 earthquake scenario has been simulated using HAZUS-MH. The epicenter of the event has been assumed to be located at latitude 32.78° and longitude -117.15°, as shown schematically in Figure 6.7. A fragility analysis providing the probability of exceeding each damage level (*DS*) has been carried out using HAZUS-MH. In order to conservatively determine a representative damage level (*DS*) based on the results of the fragility analysis, the following assumptions have been made:

$$DS0 = \begin{cases} complete & \text{if } P[DS = complete] \geq 0.15 \\ extensive & \text{else if } P[DS \geq extensive] \geq 0.25 \\ moderate & \text{else if } P[DS \geq moderate] \geq 0.30 \\ slight & \text{else if } P[DS \geq slight] \geq 0.40 \\ no\ damage & \text{otherwise} \end{cases} \tag{6.6}$$

As already mentioned, slight damage does not affect the functionality of the bridges. Hence, the optimization algorithm has to consider only the 80 bridges with at least moderate damage. Table 6.2 presents the properties of these bridges, along with their associated ID (as specified by HAZUS-MH) which can easily be used to track the location and characteristics of each bridge in the network.

It has been assumed that node 1 shown in Figure 6.7 represents the port and, therefore, all business trips associated with the port are originated from or attracted to this node. Also, nodes 9, 15, and 16 act as the gates from which the consignments can be shipped to their major destinations. Thus, it is of great importance to restore connectivity between the gates and the port as soon as possible, in order to facilitate the shipping process from and to the port. Therefore, in addition to the long-term resilience of the transportation network $R(Qflow)$ computed using Equations 2.9 and 2.15, maximizing the resilience associated with connecting the port node and the gate nodes $R(Qconn)$ (medium-term resilience),

Table 6.2: Selected damaged bridges and their properties

No.	Bridge ID	rc_b(M$)	d_b^d(Km)	$DS0$	No.	Bridge ID	rc_b (M$)	d_b^d(Km)	$DS0$
1	CA028824	2.634	3	Extensive	41	CA028616	3.347	2	Moderate
2	CA028460	2.389	2	Moderate	42	CA028619	3.425	2	Moderate
3	CA028416	1.789	2	Moderate	43	CA028462	2.281	2	Moderate
4	CA028580	1.303	4	Complete	44	CA028429	11.749	3	Extensive
5	CA028560	3.307	4	Complete	45	CA029994	7.845	2	Moderate
6	CA028562	0.843	3	Extensive	46	CA029429	9.543	2	Moderate
7	CA028665	1.071	4	Complete	47	CA029433	9.404	2	Moderate
8	CA029857	4.522	3	Extensive	48	CA029436	2.321	2	Moderate
9	CA029207	4.622	4	Complete	49	CA029445	47.168	2	Moderate
10	CA028599	3.906	2	Moderate	50	CA029454	7.384	2	Moderate
11	CA028601	6.276	2	Moderate	51	CA029439	47.168	2	Moderate
12	CA028593	3.138	4	Complete	52	CA029455	3.213	2	Moderate
13	CA028586	2.179	4	Complete	53	CA029777	9.424	2	Moderate
14	CA028828	3.698	4	Complete	54	CA029789	3.323	2	Moderate
15	CA028533	11.257	4	Complete	55	CA028659	4.649	4	Complete
16	CA028531	5.797	2	Moderate	56	CA029780	1.280	2	Moderate
17	CA028527	2.097	4	Complete	57	CA028657	4.413	4	Complete
18	CA028591	5.330	4	Complete	58	CA029791	1.126	3	Extensive
19	CA029343	6.890	3	Extensive	59	CA029784	19.838	2	Moderate
20	CA029341	3.615	2	Moderate	60	CA029351	8.220	2	Moderate
21	CA028921	28.214	2	Moderate	61	CA029332	7.162	2	Moderate
22	CA029352	13.728	4	Complete	62	CA029329	7.162	2	Moderate
23	CA028652	1.590	4	Complete	63	CA029345	2.700	2	Moderate
24	CA028939	1.866	4	Complete	64	CA028954	1.087	2	Moderate
25	CA029478	2.700	4	Complete	65	CA028961	14.371	4	Complete
26	CA028948	6.434	2	Moderate	66	CA028964	1.571	2	Moderate
27	CA028704	1.636	4	Complete	67	CA028962	2.127	2	Moderate
28	CA028605	1.012	2	Moderate	68	CA028965	1.223	2	Moderate
29	CA029308	3.953	2	Moderate	69	CA028845	2.417	2	Moderate
30	CA029306	3.912	2	Moderate	70	CA028955	1.641	2	Moderate
31	CA029312	1.957	2	Moderate	71	CA029361	8.960	2	Moderate
32	CA029698	3.601	2	Moderate	72	CA029861	0.979	2	Moderate
33	CA029305	7.145	2	Moderate	73	CA029859	1.346	2	Moderate
34	CA029191	4.175	2	Moderate	74	CA029358	8.876	2	Moderate
35	CA029199	3.195	2	Moderate	75	CA029860	0.979	2	Moderate
36	CA028475	2.890	2	Moderate	76	CA029865	10.087	3	Extensive
37	CA028617	5.770	4	Complete	77	CA029939	10.200	2	Moderate
38	CA028428	26.183	3	Extensive	78	CA028415	1.286	3	Extensive
39	CA028614	0.658	2	Moderate	79	CA029339	3.125	2	Moderate
40	CA028612	5.063	2	Moderate	80	CA029476	2.676	4	Complete

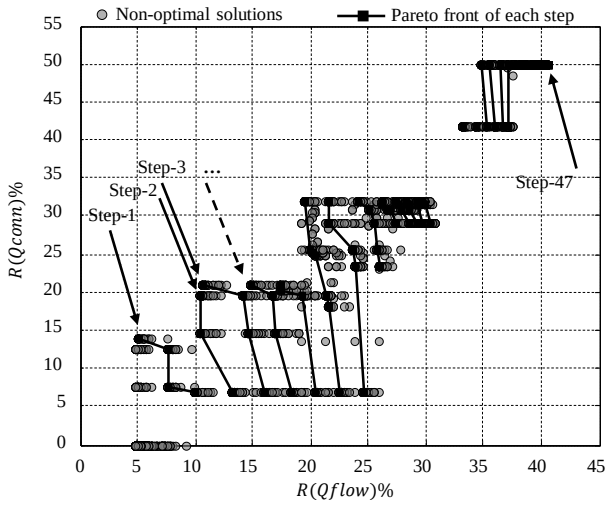

Figure 6.8: Greedy algorithm preliminary optimization

computed using Equation 2.9 and 6.2, has been considered as the objective of this example. Restoration of the connectivity between the port and each gate has been assumed to have the same importance (i.e., $CW_{\hat{p}} = 0.167,\ \hat{p} \in \{1-9,\ 9-1,\ 1-15,\ 15-1,\ 1-16,\ 16-1\}$). In terms of constraints, it has been assumed that 5 major bridge construction companies are available ($NSA_{max} = 5$) to restore the damages in 3 years ($t_h = 36$ months). Resilience computations have been performed with the time step of one month.

6.5.2 Multi-Objective Resilience Optimization Results

The greedy algorithm discussed earlier has been run to determine a convenient initial population. The first level of search has been carried out considering only the restoration of 2 bridges (l^0_{greedy}). For subsequent steps, the partial solutions have been generated by adding one bridge (i.e., $\Delta l_{greedy} = 1$) to the optimal partial solutions obtained from the previous search level. Figure 6.8 shows the values of the two objectives for the examined non-optimal partial solutions along with the Pareto-front of each level. The outcome of the algorithm consists in two restoration schedules with the same values of objectives equal to (40.56%,50.0%) and $lo^s = 47$ (Figure 6.8).

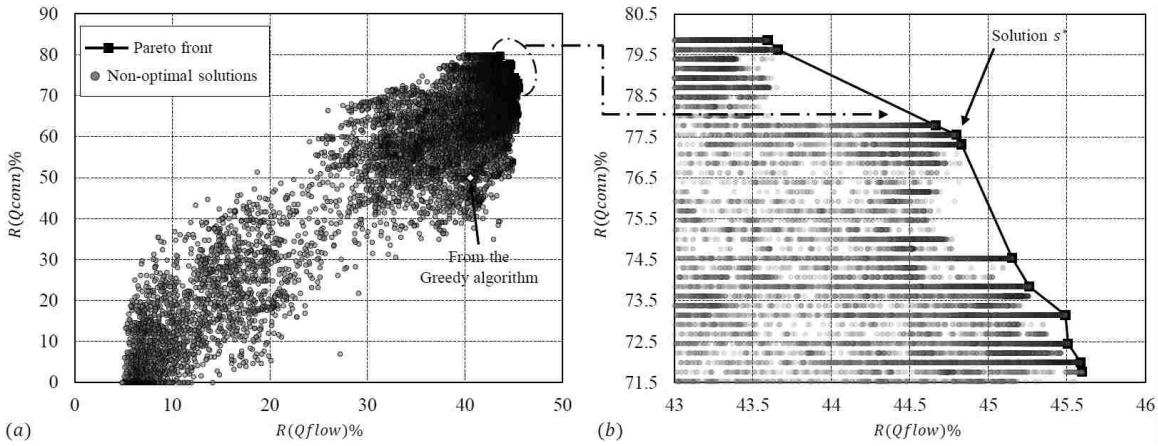

Figure 6.9: *AMIGO* optimization results: (a) Trial solutions, (b) Pareto-front

The individuals obtained from the greedy algorithm have been added to 998 random individuals, for a total of 1000 individuals for the first generation. *AMIGO* converged after 100 generations to a set of Pareto optimal solutions. At each generation, *AMIGO* allows to find a set of trial solutions that have higher objective values compared to those evaluated previously. Figure 6.9 presents the Pareto front as well as the non-optimal solutions evaluated through the process. The diamond marker in Figure 6.9a shows the objective values associated with the solution found my the greedy algorithm discussed on Section 6.2.2. As shown in Figure 6.9b, there is little difference between the values of objectives at different points in the Pareto front. However, even a tiny difference causes considerable impact on the performance and socio-economic losses after an event. These solutions allow different trade-offs between the medium-term (phase-2) and long-term (phase-3) restoration priorities. The Pareto front contains 11 distinct points, but the total number of optimal restoration plans is 128, since for most of the points in the Pareto front more than one trial solution (restoration plan) have been provided by the algorithm. This allows decision makers to select the restoration plan that meets the resilience criteria, while taking into account also other factors (e.g., socio-economic or environmental) which are not considered in the formulation of the problem. As an example, one representative restoration plan

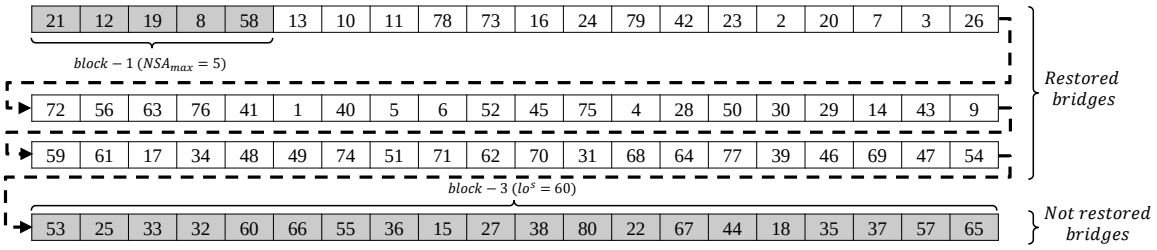

Figure 6.10: Solution s^* (numbers in the sequence are bridge numbers as shown in Table 6.2)

has been selected and will be discussed in detail. Solution s^*, shown in Figure 6.9b with associated objective values of (44.80%,77.55%), has been chosen for this purpose. In total, 7 restoration plans have been provided for this point (with the same objective values). Figure 6.10 shows one of the bridge restoration sequences associated with this solution. According to this solution, the restoration of 60 (out of 80) bridges is feasible ($lo^s = 60$), while the restoration of the rest of the bridges placed in block-3 is either not initiated, or not completed to the level which improves the functionality of the bridge.

In order to evaluate the work flow related to this restoration plan, the associated Gantt chart is illustrated in Figure 6.11. This figure shows the restoration initiation times and the duration of partial and full restorations for the bridges of block-1 and block-2 of the sequence shown in Figure 6.10. The restoration starts simultaneously for all bridges of block-1 (21, 12, 19, 8, 58) and continues whenever a construction company becomes available, considering that $NSA_{max} = 5$. Regardless of the numerical value, that changes for different situations, this constraint provides more realistic results and addresses the issue of the previous technique presented by Bocchini and Frangopol (2012b) in which most of the restorations started immediately after the event (as pointed out by Bocchini (2013) and Vugrin et al. (2014)). The figure shows that the partial restoration of bridge 9 has been completed by the end of month 26 after the initiation of the network restorations. However, completion of the restoration for this bridge is not achievable before the time span. On the

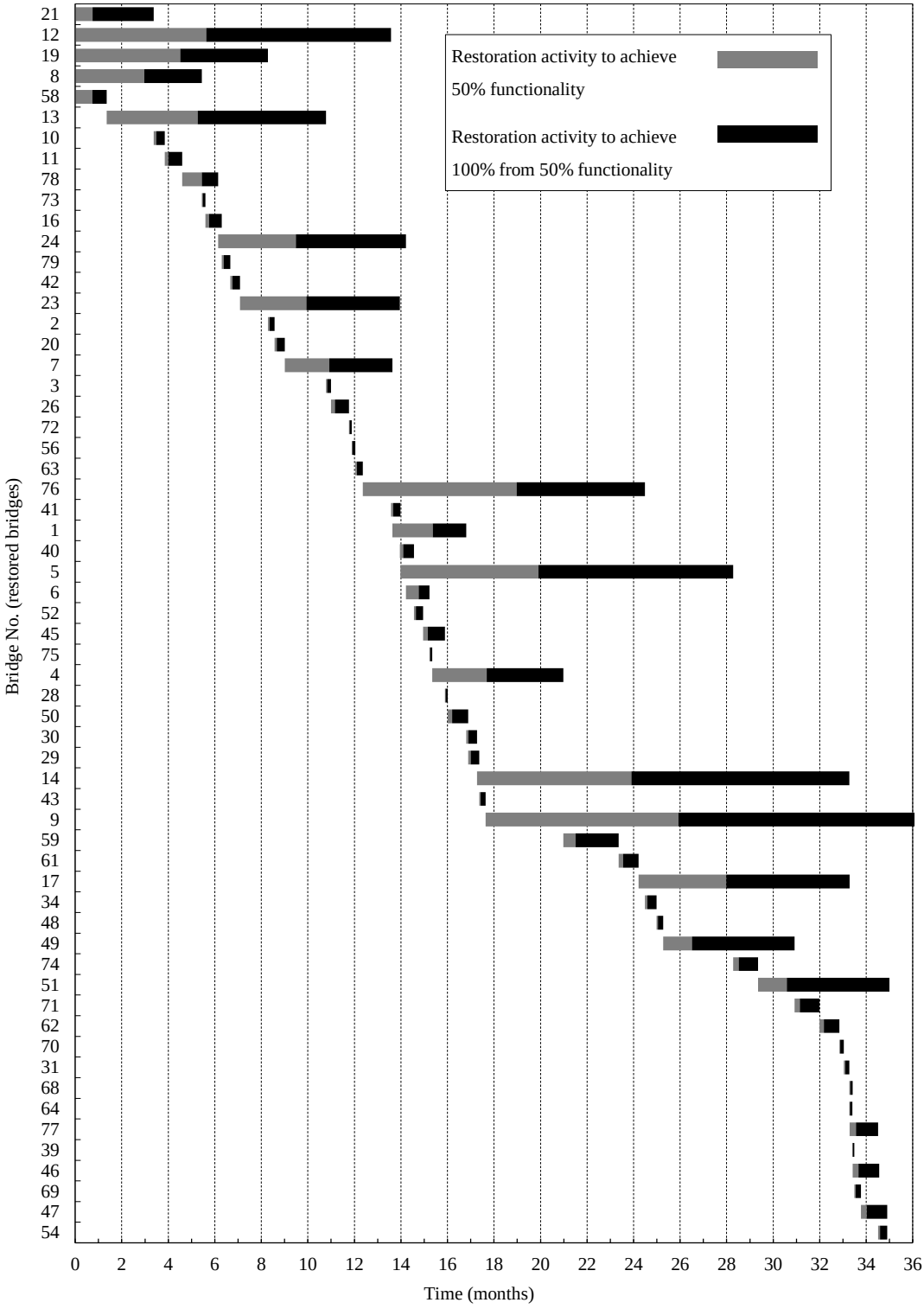

Figure 6.11: Gantt chart for solution s^*

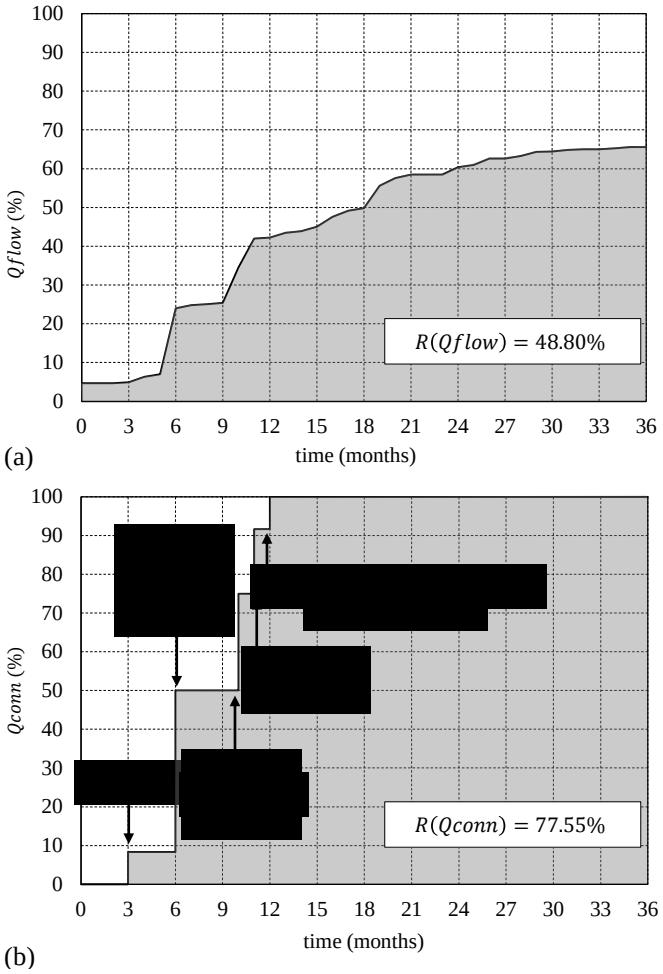

Figure 6.12: Evolution of the two functionality indicators for solution s^*: (a) $Qflow(t)$, (b) $Qconn(t)$

other hand, after the full restorations of bridges 51, 46, 47, and 54 have been completed, there is no bridge whose restoration can be started and at least partially completed. Thus, since any restoration at this point will not have impact on the resilience indices of the network, the restoration schedule of the rest of the bridges have not been illustrated in the figure. However, it is expected that the restoration activities would continue even after the 36 months (t_h).

Figure 6.12 shows the evolution of the two functionality measures $Qflow(t)$ and $Qconn(t)$ for solution s^*, associated with the two resilience objectives. Figure 6.12a illustrates that the long-term functionality of the network has not been revived to its pre-event condition

(i.e., 100%), since the full restoration of all bridges is not possible during 36 months with the available resources. As shown in Figure 6.12b, the highway connection of the critical points of the region (here the port and the gate nodes) has been completely lost immediately after the extreme event (i.e., $Qconn(t_0) = 0$). However, by implementing the restoration plan s^*, it is possible to fully connect these points through highways in 12 months. The major increases in both objectives $Qflow$ and $Qconn$ are observed in months 6 and 10 after the restoration process starts.

6.5.3 Convergence Analysis and Comparison

It is useful to evaluate the performance of evolutionary algorithms by studying the optimality of the final solution, as well as the quality of the convergence to the final solution. In the case of the current example, *AMIGO* converged after evaluating about 100,000 trial solutions, which is a tiny fraction ($1.4e-112$) of all possible sequences (equal to 80!). Also, by observing the distribution of the examined solutions in the design space shown in Figure 6.9a, it can be seen that *AMIGO* has concentrated most of the effort to search the solutions in the neighborhood of the Pareto front. The General Distance (*GD*) measure has been utilized to assess the performance of the developed algorithm and search progress in a quantitative manner. *GD* is a quality indicator for Multi-Objective Evolutionary Algorithms (MOEA) which quantifies the average minimum distance between a set of Pareto optimal solutions (PF_{known}) obtained by the evolutionary algorithm, and the global Pareto optimal solutions (PF_{true}) known a priori (Coello et al., 2002), as follows:

$$GD = \frac{\sqrt{(\sum_{i=1}^{n} pd_i^2)}}{|PF_{known}|} \tag{6.7}$$

where pd_i is the shortest Euclidean distance between the member i from PF_{known}, and members of PF_{true}. $|PF_{known}|$ is the number of the solutions in PF_{known}. For the case of

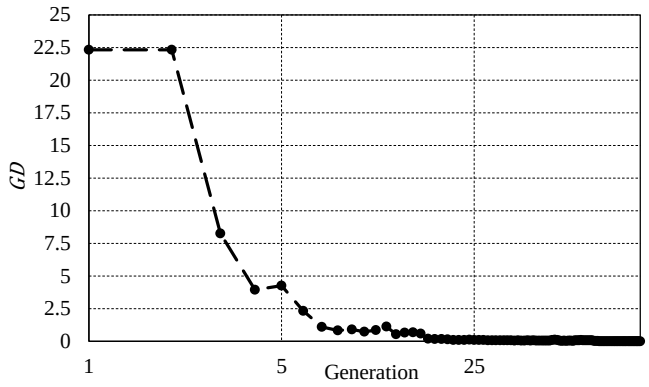

Figure 6.13: Evolution of the *GD* indicator

the current problem, the above indicator has been computed for the Pareto fronts obtained at the end of each generation ($PF_{current}$), assuming that the Pareto front to which *AMIGO* has converged (Figure 6.9) is PF_{true}. In this way, it is possible to monitor the evolution of the objectives through the generations and evaluate the performance of the algorithm for multi-objective problems, although there is no guarantee that the obtained Pareto front is the actual PF_{true}. Figure 6.13 shows that the value of *GD* is large at the beginning, but it decreases quickly during the first 25 generations. This indicates that while the search has started from a region relatively far from the optimal solution, the algorithm managed to approach the neighborhood of the Pareto front shown in Figure 6.9b in a limited number of trials. Although the algorithm continuously provides improved solutions at each generation, the value of *GD* does not show considerable improvements after generation 25. Therefore, in case the amount of available computational capacity is limited, the algorithm can be terminated earlier, when the provided solution is already in close proximity of the Pareto optimal front found after 100 generations. Moreover, the optimality of the solution provided by *AMIGO* has been validated with results given by exhaustive search for simpler problems (see for example Karamlou and Bocchini, 2014a). For all the investigated cases, *AMIGO* was able to converge to the true Pareto front. For the Port of San Diego the total number of possible bridge sequences (including redundant solutions) is too large ($80! > 7e118$) to find the Pareto front by exhaustive search.

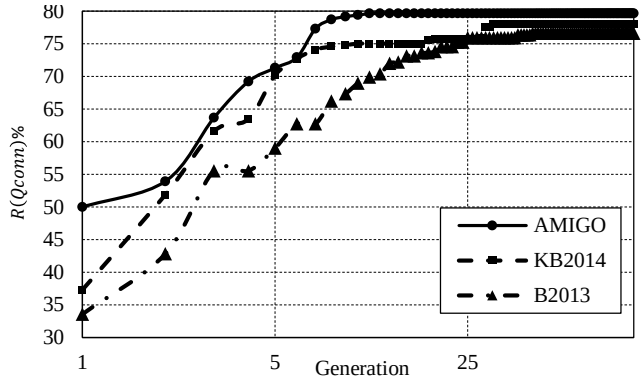

Figure 6.14: Best fitness values at each generation for three optimization methodologies

The overall performance of *AMIGO* has been also compared to two other formulations presented by Bocchini (2013), as well as Karamlou and Bocchini (2014a). Bocchini (2013) formulated the problem in the $\mathbb{R}^{nb}$ domain, by introducing the bridge restoration priority $0 \leq \tilde{\rho}_b \leq 1$ as the design variable of the problem. Karamlou and Bocchini (2014a) used a combinatorial formulation and genetic algorithms with classic swap and order crossovers (Gen and Cheng, 2000). In the following, these two methodologies are called B2013 and KB2014, respectively. It is worth noting that both KB2014, and B2013 are based on a standard implementation of Genetic Algorithms (Goldberg, 1989), meaning that they only use the value of the objective function(s) as a criterion for reproduction and searching the design domain, whereas *AMIGO* adds multiple-input generic operators. Resilience optimization analyses have been carried out on San Diego port transportation network as discussed in this section, considering 1000 populations and 100 generations. To have a clearer comparison and allow the previous methodologies to converge for this large network, the problem has been reduced to single-objective optimization considering $R(Qconn)$ as the objective. Figure 6.14 shows the values of the best fitness after each generation for the three mentioned formulations. The best fitness provided by B2013, KB2014, and *AMIGO* is 76.62%, 78.00%, and 79.63% respectively. Therefore, the results show that in terms of optimality *AMIGO* is superior compared to the other two techniques. It is worth mentioning that the optimum value obtained by *AMIGO* for $R(Qconn)$ is consistent with the maximum

value of this objective computed for the multi-objective optimization problem shown in Figure 6.9b. Additionally, *AMIGO* shows improvement in the convergence rate. The figure shows that the value of the objective decreases continuously and quickly in *AMIGO* and stabilizes in about 10 generations. The overall pace of reduction in B2013 and KB2014 is substantially slower.

6.6 Concluding Remarks

In this chapter, the formulation of a scheduling problem considering resource and time constraints is presented in detail and a novel evolutionary solution methodology is proposed. The proposed optimization algorithm is called *Algorithm with Multi-Input Genetic Operators (AMIGO)* as it takes advantage of the additional data in the genetic operators to make the search process more efficient and expedite the convergence. Several developed optimization operators for *AMIGO*, such as initial population generator, mutation and crossover, are presented for the first time in this chapter. The proposed methodology can be used for solving the optimization problems with any type and number of objective functions.

The application of the methodology to resilience optimal post-disaster restoration intervention of damaged highway bridges is presented. Through this application, a number of enhancements have been made to the framework and formulation of resilience analysis of highway networks. In addition to the long-term resilience metric previously used for resilience evaluation of bridge networks, a connectivity-based resilience indicator is introduced, to take into account the restoration priorities typically considered during the medium-phase of disaster management activities. Moreover, a new bridge recovery model is proposed. Compared to the previous studies, this recovery model is more realistic, as it takes advantage of the available restoration functions obtained by experts surveys and

scaling factors that account for the bridge cost. The San Diego port transportation network was chosen for the demonstration of the performance of the proposed methodology. The number of damaged bridges in this example is considerably higher compared to the previous works (Bocchini and Frangopol, 2012b; Karamlou and Bocchini, 2014a) involving restoration optimization with traffic analysis.

While the total number of feasible solutions for the examined problem is considerably large (80!), the result of a convergence analysis shows that the algorithm managed to find a set of near-optimal Pareto solutions in a small number of trials (about 25 generation). A comparison is made between the performance of the *AMIGO* optimization formulation and previous works presented by Bocchini (2013) and Karamlou and Bocchini (2014a). The results testify the improvement made by the current optimization approach, both in terms of optimality of the solution and convergence rate. This is of great importance, since for large realistic networks, the traffic analysis procedure can be computationally very expensive. Therefore, reducing the number of required generations for convergence can considerably affect the computational cost of the problem and make this approach finally applicable to real-size networks. Compared to previous formulations proposed by Bocchini and Frangopol (2012a,b), the use of operational resource constraints and the new recovery model yield the generation of more realistic schedules.

The technique presented in this chapter was used to study the optimal post-event restoration prioritization of damaged bridges in transportation networks. This methodology will be expanded in Chapter 7 to optimize pre-event retrofitting of vulnerable bridges in transportation networks, considering the uncertainties in regional seismic hazard and fragility of bridges.

Chapter 7

Optimal Retrofit Strategy of Resilient Transportation Networks

7.1 Introduction

Given the definitions and formulations of resilience reviewed in Section 2.4, two general approaches can be followed to improve the disaster resilience of structures and infrastructure systems: reactive and proactive approaches. Reactive approaches are associated with post-event activities, such as a prompt and efficient restoration process following the extreme event. On the other hand, proactive solutions are performed before the occurrence of the event. Increasing the robustness (or decreasing the vulnerability) of the system is a common proactive approach to increase the disaster resilience of structures and infrastructure systems. For instance, Figure 7.1 illustrates these two approaches considering the resilience index formulation proposed by Reed et al. (2009). Each approach increases the area underneath the restoration function, which results in an increase of the estimated resilience.

The methodology presented in Chapter 6 was a reactive approach and is meant to improve the resilience of transportation networks by optimization the post-event restoration process of the damaged bridges. In this chapter, the study is extended to improve the resilience of transportation networks considering both reactive and proactive solutions. Common proactive approaches for transportation networks and their components include strengthening, retrofitting, or rebuilding the vulnerable bridges in the system. However,

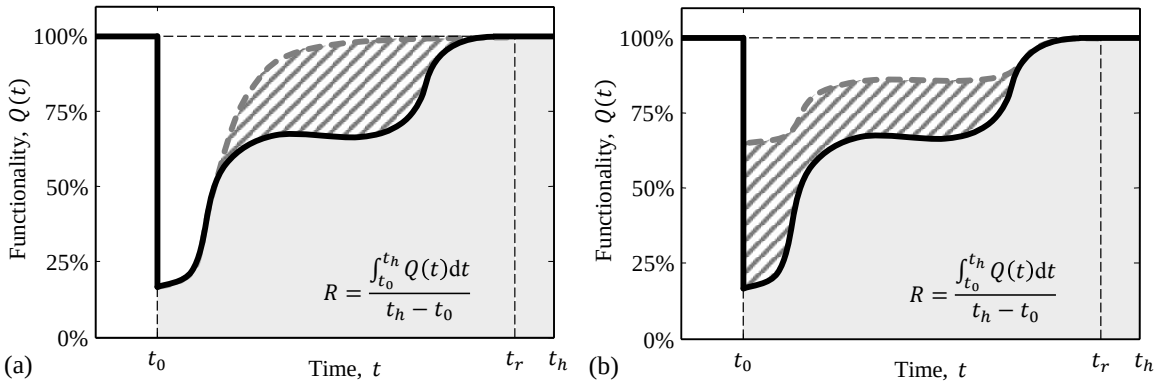

Figure 7.1: Improving resilience through improved (a) restoration process, and (b) robustness

typically due to the financial and logistic constraints, only a limited subset of these actions can be performed in a limited time span. Therefore, it is necessary to prioritize such pre-event disaster management activities.

For the case of the techniques and methodologies dealing with post-event restoration and resilience analyses (such as the one presented in Chapter 6), it is typically assumed that the damage level of the components (e.g., bridges) of the system is known. However, before the event, there is a large amount of variability in the damage that can result from the extreme event which needs to be considered for proactive solutions and predictive studies. This variability is rooted in the uncertainties involved in the characteristics of extreme events, as well as the structural response. The Probabilistic Seismic Hazard Analysis (PSHA) is typically performed to study the variability of seismic events. The uncertainty in the response and damage of structures is addressed by probabilistic seismic demand and fragility analyses (see Chapter 3).

These uncertainties are considered in the following two-level simulation-based optimization framework, which can be used for bridge retrofit prioritization. Moreover, a new transportation network functionality metric is introduced for efficient computation of the post-event resilience. The presented framework is used to compute the optimal retrofit and

restoration strategies of a schematic transportation network. The methodologies and results presented in this chapter are based on a paper by Karamlou et al. (2016).

7.2 Methodology

The proposed framework for bridge retrofit prioritization in this study is formulated as a two-level simulation-based optimization. The use of the two-level optimization framework allows to optimize pre-event retrofit strategies considering the uncertainties involved in the intensity of events, as well as post-event bridge damage and restoration. The formulation of the upper-level optimization is as follows:

Find

$$r_b, \text{ with } r_b \in \mathbb{N} \tag{7.1}$$

so that

$$TRC = \sum_{b=1}^{nb} \hat{c}_b(r_b) = \text{minimum} \tag{7.2}$$

$$PRF = P[R \leq R_{cr}] = \text{minimum} \tag{7.3}$$

subjected to the constraints

$$1 \leq r_b \leq nr_b, \ \forall \ b = 1, 2, ..., nb \tag{7.4}$$

where r_b is an integer number reflecting the retrofit technique assigned to bridge b, and nb is the total number of bridges in the network. In this formulation, it is assumed that $r_b = 1$ is associated with *no retrofit* strategy for bridge b. Also, nr_b is the total number of retrofit techniques applicable to bridge b. $\hat{c}_b(r_b)$ and TRC are the cost of retrofitting the bth bridge considering the selected retrofit technique, and the total retrofit cost of all bridges, respectively. PRF is defined as the probabilistic resilience failure of the network computed

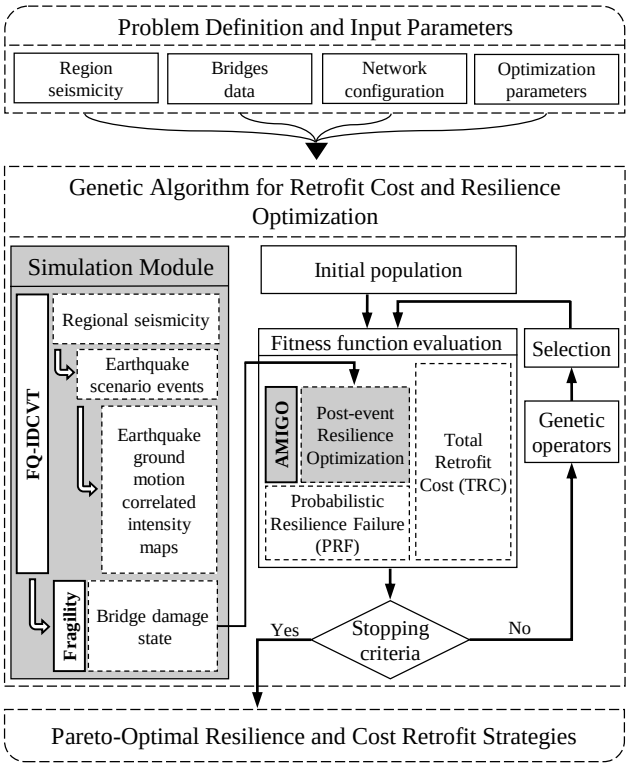

Figure 7.2: Framework for bridge network retrofit cost and resilience optimization

as the probability ($P[\cdots]$) of the post-event optimal resilience (R) being less than a specified critical threshold (R_{cr}). More details about the computation of these values are provided in the next section.

To solve this bi-objective optimization problem, a Genetic Algorithm with Elitist Non-Dominated Sorting (NSGA-II) has been utilized (Deb et al., 2002). The customized genetic operators, namely initial population generator, mutation, and crossover have been utilized to operate the integer-valued design variables (i.e., r_b) of the problem (Deep et al., 2009).

Figure 7.2 shows the flowchart of this framework and its corresponding stages. To find the Pareto-optimal solutions, the Genetic Algorithm continuously searches the design domain by generating new retrofit strategies (i.e., $\{r_1, r_2, ..., r_{nb}\}$) using the genetic operators. At each stage, the generated and selected trial solutions are passed to the fitness function to compute the values of the objectives. TRC is computed using Equation 7.2. The compu-

tation of *PRF* is carried out using a simulation-based optimization scheme as discussed in the following.

In order to take into account the uncertainties in the damage level of bridges, a simulation module is included in the optimization framework to generate the potential damage states of each bridge in the network considering the assigned retrofit strategy, bridge fragility, and seismicity of the region (Figure 7.2). To this respect, first the regional hazard is quantified by generating intensity measure maps (*IMmaps*) as realizations of a two-dimensional random field (Christou and Bocchini, 2015; Bocchini et al., 2016). For the optimal representation of the ground motion intensity with a small number of *IMmaps*, a technique called Functional Quantization by Infinite-Dimensional Centroidal Voronoi Tessellation (FQ-IDCVT) is considered, as presented by Christou et al. (2015). Then, the values of the intensity measure (e.g., PGA) at the location of the bridges of the network are generated. In contrast to individual structures, in the case of loss estimation of spatially distributed infrastructures, such as transportation networks, the quantification of the ground motion intensities should be carried out considering the spatial correlation between the intensities at different sites (Jayaram and Baker, 2009). For each *IMmap*, the values of the ground motion intensity at the location of each bridge is utilized to generate the damage state of the bridges, using the seismic fragilities generated considering the bridge type and its assigned retrofit methodology. The best post-event restoration strategy for each set of bridge damage state scenarios is computed through another round of optimization, considering the transportation network resilience as the single objective of this lower-level optimization problem. *AMIGO* (as presented in Chapter 6), is used to solve this optimization problem. For each retrofit strategy selected by *AMIGO*, the value of *PRF* is computed by constructing the CDF of the resilience values (i.e., *R*). The metrics, formulations, and methodologies used for post-event network resilience optimization are briefly discussed in the next section. It is worth mentioning that although *TRC* and *PRF* has been chosen as

the objectives of the proposed framework, the presented optimization methodologies can accept other objectives, such as restoration cost and duration.

7.3 A New Metric for Post-Event Transportation Network Resilience

In Chapter 6, the methodology and formulations proposed by Bocchini and Frangopol (2012a,b) were used to computed the resilience of transportation networks considering the long-term criterion of disaster management activities (i.e., complete restoration of damages). As reviewed in Section 2.4, Bocchini and Frangopol (2012a,b) expressed the functionality and resilience of transportation networks as a function of the total time (TTT) spent and the total distance (TTD) traveled by all the passengers in the network in one hour. The functionality computed by such formulations tends to reflect an accurate picture of the performance of the transportation network, as it is calculated by rigorous computations. However, solving the traffic distribution and assignment problems for large networks with several links and vertexes is a computationally expensive task. Performing such computations for the post-event restoration and resilience optimization of large transportation networks is still feasible, since typically only one initial damage scenario is considered for the study (as presented in Chapter 6). However, the application of this functionality metric is limited in the current simulation-based retrofit framework due to the computational cost, because the values of TTT and TTD need to be computed several times for different network damage configurations.

To this respect and to overcome the mentioned shortcoming, a new functionality metric is introduced in this chapter, as shown in the following equation:

$$Q(t) = \sum_{i \in I} \sum_{j \in J} \acute{Q}_{ij}(t) \tag{7.5}$$

where I is the set of all nodes in the network. J is the subset of nodes connected to node i. $\acute{Q}_{ij}(t)$ is the contribution of the segment ij to the functionality of the system $Q(t)$, computed by the following equation:

$$\acute{Q}_{ij}(t) = \frac{IF_{ij} \cdot QS_{ij}(t)}{IF_{total}} \tag{7.6}$$

in which $QS_{ij}(t)$ is the functionality of segment ij. IF_{ij} and IF_{total} are the influence factor of the segment ij and the total influence factor, respectively. For each segment ij, the value $QS_{ij}(t)$ can be expressed as the fraction of the total number of lanes of ij which is open to traffic at time t. This value can be influenced by land sliding or accumulation of debris in the aftermath of an event. Regarding the bridges, the damage induced by the event might require the bridge to be partially or fully closed. This functionality reduction is reflected on the value of QS_{ij} for the segment ij which is carried or crossed by the bridge. Additionally, the traffic disruptions caused by construction activities during the restoration are considered in $QS_{ij}(t)$. In the cases where there is more than one bridge along a segment, $QS_{ij}(t)$ is set as the minimum of the functionalities of all bridges of segment ij.

The value of the segment influence factor IF_{ij} is computed as follows:

$$IF_{ij} = \begin{cases} f_{ij} \cdot \bar{l}_{ij} & \text{if bridge } b \text{ is in link } ij \\ f_{ij} \cdot l_{ij} & \text{otherwise} \end{cases} \tag{7.7}$$

where f_{ij} is the traffic flow of the segment ij in $\frac{car\text{-}equivalent}{hour}$, computed by solving the traffic distribution and assignment problems, considering the pre-event traffic demands. The first term of Equation 7.7 is associated with the segments which include at least one bridge. In such cases, IF_{ij} is computed by multiplying f_{ij} by $\bar{l}_{ij}$, which is the length of the segment influenced by the functionality of its bridges. In this study, this length is considered to be the distance between the closest exits before and after the bridges of segment ij. For the segments with no bridges, the flow is multiplied by l_{ij} which is the total length of the

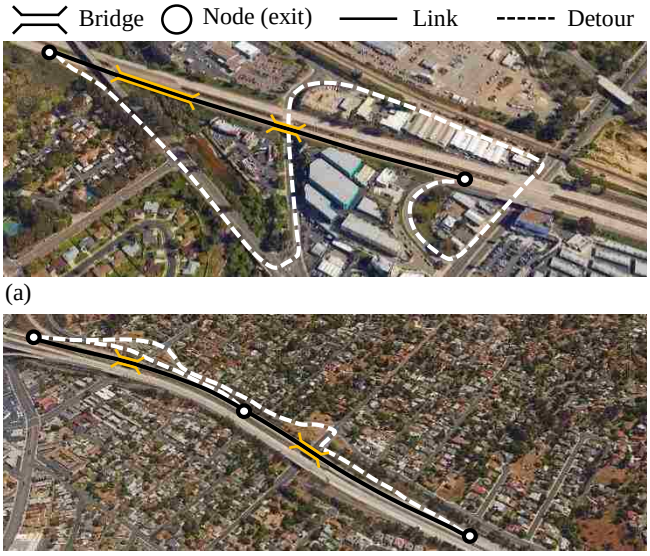

Figure 7.3: Modeling considerations based on the configuration of bridge exits, photos from Google Inc. (2015).

segment. Care should be taken in modeling the network, considering the configuration of the bridges and exits of road segments. For example, in case there is no exit between two bridges, they should be included in one link of the network graph (Figure 7.3a), which connects the exit before the first and after the second bridge. Otherwise, additional nodes should be used to model exits of each bridge (Figure 7.3b). Models of this type can be easily built for any city in the US and other countries, using the available public data (Elsayed and Bocchini, 2014). Finally, IF_{total} is computed by summing all influence factors of all segments of the network as shown bellow:

$$IF_{total} = \sum_{i \in I} \sum_{j \in J} IF_{ij} \tag{7.8}$$

Based on Equations 7.5-7.8, the contribution of each bridge (or road segment) of the network in the functionality of the system is weighted by its traffic flow. The traffic flows are computed only once at the beginning of the algorithm, which improves computational efficiency considerably.

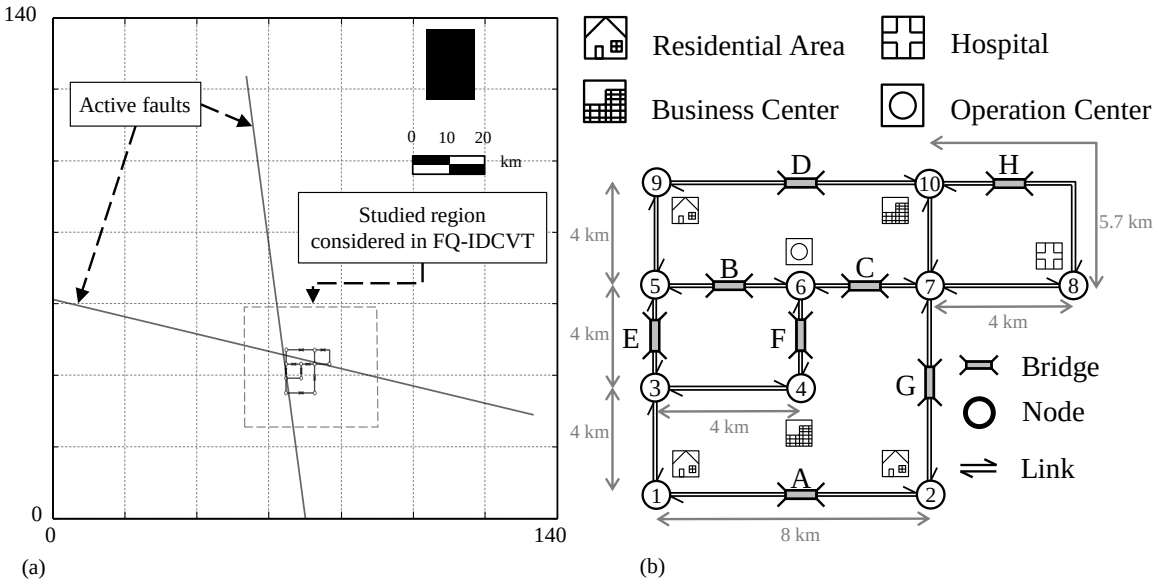

Figure 7.4: Example transportation network: (a) position of the network in the studied seismic region as considered in FQ-IDCVT, (b) network topology and bridges.

It is worth noting that computation of f_{ij} requires accurate information about the traffic demand (travelers' origin and destination) of the studied region. However, since such data is typically unavailable for post-event condition, only the traffic demand associated with the normal pre-event condition is being used. Thus, the resilience computed by using Equations 7.5-7.8 and 2.9 tends to reflect the long-term losses of the transportation network.

7.4 Application

The application of the proposed framework for the computation of the optimal retrofit strategies is presented in this section through a numerical example. To this purpose, the schematic transportation network shown in Figure 7.4 is used. As shown in the figure, the network has 10 nodes, 26 edges, and 8 bridges. Table 7.1 shows the traffic characteristics of each node. The amount of traffic generated and attracted shown in the table are related to the morning traffic before the disaster. In such condition, most of the traffic is directed from residential areas towards business centers. The nodes with zero traffic demand are nodes

Table 7.1: Traffic characteristics of nodes of the example network

Node	Traffic generated ($cars/hour$)	Traffic attracted ($cars/hour$)	Node	Traffic generated ($cars/hour$)	Traffic attracted ($cars/hour$)
1	8000	2000	6	3000	7000
2	8000	2000	7	0	0
3	0	0	8	3000	7000
4	3000	8000	9	8000	2000
5	0	0	10	3000	8000

that are placed in the network to model the intersections. The pre-event link flows (computed by means of traffic analysis), and links effective length needed for the computation of the influence factors in Equation 7.7, are presented in Table 7.2. This table also shows the types of bridges in the network, selected among those common in CSUS, as categorized by Nielson (2005).

The regional seismic hazard and its spatial distribution are probabilistically considered through the "quantizer". In this application, the quantizer is a set of 50 representative *IMmaps* ("quanta") and their associated weights. In particular, the quanta are samples of ground motion intensity maps, which provide a mean-square optimal representation of the entire sample space of the regional seismic hazard (Christou and Bocchini, 2015). For the assessment of the earthquake intensity, the peak ground acceleration (PGA) has been considered as a representative metric and values of the PGA are determined throughout the studied region. To illustrate the variation of PGA throughout the studied network, Figure 7.5 shows four selected ground motion *IMmaps* generated by FQ-IDCVT. As it can be seen, not only there is a considerable amount of variation in the PGA at different locations throughout one map, but also among different samples. The value of PGA at the location of the bridges of the network is extracted and used for the simulation of bridge damage states as illustrated in Figure 7.2.

For this application, only the impact of the damaged bridges on the functionality of the road segments have been considered. Therefore, the value of $\acute{Q}_{ij}(t)$ for the links with no

Table 7.2: Network link and bridge information.

Link No.	Link nodes	f_{ij} ($\frac{car-eq}{h}$)	$l_{ij}, \bar{l}_{ij}$ (km)	Bridge name	Bridge type
1	$1-2$	2.51E+03	8	A	MSSS[1]-Steel Girder
2	$2-1$	2.74E+03	8	A	MSSS-Steel Girder
3	$3-4$	4.77E+03	4	-	-
4	$4-3$	3.18E+02	4	-	-
5	$5-6$	4.49E+03	4	B	MSC[2]-Steel Girder
6	$6-5$	4.57E+02	4	B	MSC-Steel Girder
7	$6-7$	2.98E+03	4	C	MSSS-Concrete Girder
8	$7-6$	3.49E+03	4	C	MSSS-Concrete Girder
9	$7-8$	4.11E+03	4	-	-
10	$8-7$	1.32E+03	4	-	-
11	$9-10$	4.25E+03	8	D	MSC-Concrete Girder
12	$10-9$	5.03E+02	8	D	MSC-Concrete Girder
13	$1-3$	6.91E+03	4	-	-
14	$3-1$	6.77E+02	4	-	-
15	$3-5$	2.68E+03	4	E	MSSS-Steel Girder
16	$5-3$	9.02E+02	4	E	MSSS-Steel Girder
17	$5-9$	1.52E+03	4	-	-
18	$9-5$	3.77E+03	4	-	-
19	$4-6$	2.68E+03	4	F	MSC-Steel Girder
20	$6-4$	3.24E+03	4	F	MSC-Steel Girder
21	$2-7$	6.08E+03	8	G	MSSS-Concrete Girder
22	$7-2$	3.17E+02	8	G	MSSS-Concrete Girder
23	$7-10$	3.62E+03	4	-	-
24	$10-7$	1.16E+03	4	-	-
25	$8-10$	1.68E+03	5.7	H	MSC-Concrete Girder
26	$10-8$	2.89E+03	5.7	H	MSC-Concrete Girder

[1]Multi-Span Simply Supported; [2]Multi-Span Continuous

bridges remains 100% at all time steps.

Several studies have focused on different bridge retrofit methodologies and their impact on the vulnerability and performance of individual bridges, as well as transportation networks. Padgett and DesRoches (2009) presented a methodology to develop seismic fragility curves for retrofitted bridges, and computed the fragility curves for bridges typical of CSUS. Several retrofit measures were included in the study such as strengthening columns with steel jackets and replacing high-type bearings with elastomeric isolation bearings. The use of Carbon Fiber-Reinforced Polymers in retrofitting the flexural members of bridges has been the focus of several other studies (Morbin et al., 2015; Tabandeh and Gardoni, 2014; Okeil et al., 2002, among others). A review of the studies on different bridge

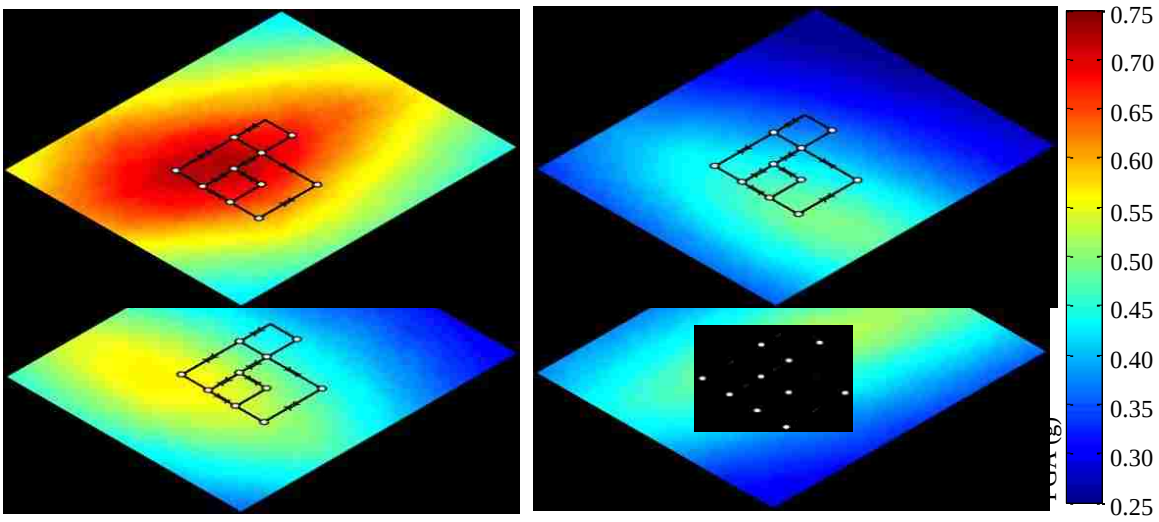

Figure 7.5: Selected ground motion *IMmap* realizations (here PGA) generated by FQ-IDCVT.

retrofit techniques is presented by Billah and Alam (2014). This study uses the fragility curves computed by Nielson (2005) and Padgett and DesRoches (2009) for original and retrofitted bridges, respectively. These fragility curves are presented in the form of log-normal CDFs for four damage states, namely slight, moderate, extensive, and complete damage. The damage state of bridges ($DS0$) of the network has been simulated using these fragility curves and considering the value of the samples of ground motion intensities at the location of each bridge, taken from *IMmaps* (simulation module in Figure 7.2). The simulation is carried out by following the technique presented by Zhou et al. (2010). To this respect, a uniformly distributed random number rn_i between 0-1 is generated for bridge i of the network. The occurrence probabilities of each bridge damage state at the ground motion intensity level generated by FQ-IDCVT ($P[DS|im]$) are also computed using bridge fragility curves and considering the retrofit solution selected for bridge i. The damage states considered in this application are slight, moderate, extensive, and complete damage. The

Table 7.3: Bridge retrofit measures and costs (Padgett, 2007)

r_b	Retrofit measure	$\hat{c}_b(r_b)$[1]	r_b	Retrofit measure	$\hat{c}_b(r_b)$
1	No retrofit	0.0	5	Restrainer cables	16.5
2	Steel jackets	36.0	6	Seat extenders	12.0
3	Elastomeric bearings	70.4	7	Shear keys & restrainer cables	28.5
4	Shear keys	12.0	8	Shear keys & seat extenders	24.0

[1]In thousand US dollars

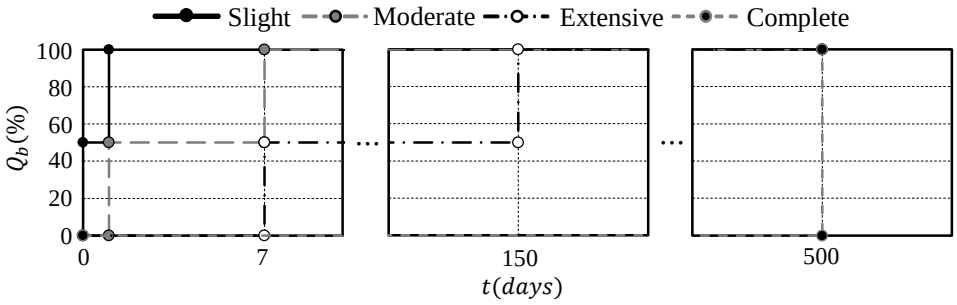

Figure 7.6: Bridge restoration functions.

damage state of bridge *i* is determined using the following equation:

$$DS0 = \begin{cases} complete & \text{if } rn_i \leq P[complete|im] \\ extensive & \text{else if } P[complete|im] < rn_i \leq P[extensive|im] \\ moderate & \text{else if } P[extensive|im] < rn_i \leq P[moderate|im] \\ slight & \text{else if } P[moderate|im] < rn_i \leq P[slight|im] \\ no\ damage & P[slight|im] < rn_i \end{cases} \tag{7.9}$$

Different retrofit techniques (or measures) for individual bridges and the corresponding retrofit costs are shown in Table 7.3.

In order to capture the evolution of the functionality during the restoration of bridges, the restoration functions shown in Figure 7.6 have been used. The values of these functions have been taken from the data presented by Padgett and DesRoches (2007) and HAZUS (DHS, 2009).

It is assumed that the network is located in a critical region. Therefore, its post-event immediate functionality and prompt recovery is of great importance. For this reason, a resilience threshold of $R_{cr} = 98\%$ is assigned for the computation of the *PRF* objective shown in Equation 7.3.

The combinatorial formulation of both optimization problems allows to evaluate the size of the design space by computation of all possible solutions. Considering 8 bridges and 8 retrofit solutions for each bridge, the design space of the upper-level optimization problem includes $8^8 (= 16{,}777{,}216)$ distinct network retrofit strategies. In the case of the lower-level optimization problem, considering 5 damage states for each bridge, the number of all possible damage scenarios for the transportation network is equal to $5^8 (= 390{,}625)$. Therefore, even for this simple example, the computation of the optimal retrofit solutions by complete search of the design domains might take a considerable amount of time and computational effort. Thus, the application of an efficient optimization methodology is inevitable.

The analysis has been performed using the proposed technique, considering 100 individuals for each population and the maximum number of 100 generations for the upper-level optimization problem. The same values have been set for number of populations and generations of the lower-level optimization problem. The upper-level problem converged after 51 generations and the evaluation of 5100 network retrofit solutions, which is less than 0.1% of all possible retrofit solutions. Figure 7.7 illustrates the resulting Pareto optimal solutions. As shown in the figure, the Pareto front includes 14 retrofit solutions, each with distinct values of the network TRC and PRF. These retrofit strategies along with their corresponding values of the objectives are presented in Table 7.4. In this table the numbers shown underneath the bridge labels are associated with the retrofit measures presented in Table 7.3.

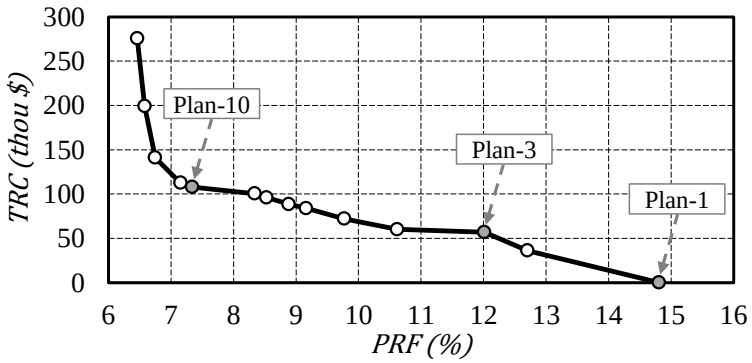

Figure 7.7: Pareto front of optimal retrofit solutions.

Table 7.4: Optimal retrofit strategies for the bridges of the network.

Plan no.	Retrofit solutions for bridges: {A	B	C	D	E	F	G	H}	TRC (thou $)	*PRF* (%)
1	1	1	1	1	1	1	1	1	0.0	14.81
2	1	1	1	1	1	2	1	1	36.0	12.71
3	1	1	6	1	1	4	4	5	57.0	12.01
4	1	6	5	1	5	5	5	1	60.0	10.62
5	5	1	1	1	5	5	2	1	72.0	9.77
6	5	6	5	1	5	5	5	5	84.0	9.16
7	4	5	5	1	5	5	5	5	88.5	8.89
8	5	6	5	5	5	5	5	5	96.0	8.53
9	4	5	5	5	5	5	5	5	100.5	8.34
10	5	5	5	5	5	8	5	5	108.0	7.34
11	5	6	5	4	5	8	5	5	112.5	7.15
12	4	6	5	5	2	8	5	4	141.0	6.75
13	2	6	5	4	4	8	3	5	199.4	6.58
14	3	7	2	4	2	8	2	7	275.9	6.46

The first network retrofit strategy shown in Table 7.4 is a trivial solution associated with not retrofitting any bridge in the network (i.e., $TRC = 0.0\$$). According to this solution, there is about 14.81% probability that the resilience of the network is less than 98% (i.e., $PRF = 14.81\%$), if the restoration of the damage is carried out by following the optimal strategy computed by the lower-level optimization. The next 6 solutions (retrofit plans no. 2 to 7) are associated with retrofitting a subset of bridges of the network. Finally, optimal plans 8 to 14 are associated with performing retrofit actions on all bridges of the network. Also, the Pareto solutions can be divided into two groups. In the first group, ranging from

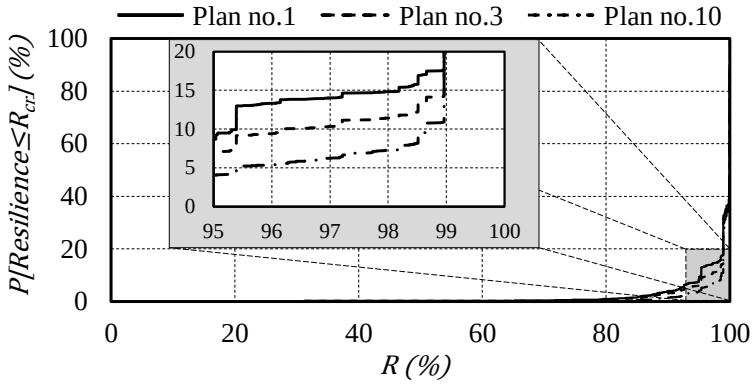

Figure 7.8: CDFs of the optimal post-event resilience, associated with retrofit plan numbers 1, 3, and 10.

plan no. 1 to 11, the relationship between the *PRF* and *TRC* is approximately linear and with a unit slope. This indicates that a percentage decrease in the amount of *PRF* would result in the same percentage increase in *TRC* of the network. In the rest of the solutions, the slope of the Pareto-front increases extensively, so that the decrease in *PRF* is marginal compared to the increase in *TRC*. Finally, it seems that the most efficient and effective retrofit measure is technique 5, which is associated with retrofitting with restrainer cables (Table 7.3), as it is selected for most of the bridges in most of the network retrofit plans.

In order to compare the probabilistic characteristics of the optimal post-event resilience and *PRF* for different Pareto optimal solutions, Figure 7.8 shows the CDFs of the optimal post-event resilience, associated with retrofit plans number 1, 3, and 10. These solutions have been distinguished by highlighted circular markers and rows in Figure 7.7 and Table 7.4, respectively. As it can be seen, the value of the CDFs at all levels of post-event resilience have been reduced going from retrofit plan no. 1 to 10. This includes the value of CDFs at the critical resilience level (i.e., $P[R \leq R_{cr} = 98\%]$).

7.5 Concluding Remarks

A bi-objective two-level simulation-based optimization framework is presented for pre-event retrofit prioritization of bridges in transportation networks. The problem is formulated in the form of a combinatorial optimization with integer-valued design variables. A multi-objective Genetic Algorithm is utilized to solve the problem and provide different tradeoffs between the objectives. These include the minimization of the total cost of bridge retrofit, as well as the probability of the post-event optimal resilience being less than a critical threshold. The computation of the second objective is carried out by a simulation-optimization procedure, through which the optimal post-event resilience of the transportation network is computed for the simulated bridge damage scenarios, considering the uncertainties in the extreme event intensity and bridge fragility. The quantification of hazard uncertainty is carried out by FQ-IDCVT technique, which efficiently provides a set of maps reflecting the variability of the ground motion intensity throughout the studied region.

For more efficiency in the computation of post-event resilience, a new transportation network functionality metric is proposed which takes into account the relative importance of road segments and bridges based on their pre-event traffic demands.

The proposed framework has been used to compute the optimal retrofit cost and post-event resilience of a schematic transportation network with 26 road segments and 8 bridges. The algorithm efficiently provided a set of Pareto optimal solutions after the evaluation of 5100 network retrofit strategies, which is less than 0.1% of the total number of possible retrofit strategies.

Chapter 8

Summary and Contributions

8.1 Summary

Critical lifelines and infrastructures, such as healthcare facilities, water and electric suppliers, and transportation networks play vital roles in modern societies and deeply affect the quality of life of their citizens. In the case of an extreme event (such as earthquake or hurricane), the long lasting loss of functionality of these vital elements contributes considerably to the reduction of habitability of the impacted regions. The consequent gradual (large-scale) migration of the population is one of the major threats to the community's recovery process and its social and economic integrity (Poland, 2009a; Kim and Oh, 2014). In order to minimize the negative impacts of both direct and indirect physical and social losses, it is imperative for the communities located in disaster prone regions to have a comprehensive pre-disaster mitigation and post-event restoration plan, which allows to retrofit the most vulnerable components and recover efficiently from the unavoidable damage. This observation encouraged researchers from several academic fields, as well as disaster officials, to pay a paramount attention to the topics of disaster mitigation, emergency management, and restoration planning. In this context, resilience has became a popular concept and metric for evaluating the response of structures, infrastructure systems, and communities to natural (e.g., earthquake and hurricane) and human induced (e.g., fire spread and terrorist attacks) disasters.

The focus of this research is to develop frameworks, methodologies, and formulations

to quantify, evaluate, improve, and optimize resilience of structures and infrastructure systems. In this dissertation, emphasis has been put on the transportation infrastructure as it is among the most critical, and yet vulnerable infrastructures of the community. In particular, research has been carried out on the transportation infrastructure at both component and system levels. Regarding the component level analysis, techniques and frameworks were proposed for more accurate computation and realistic estimation of the damage, restoration, functionality, and resilience of individual or classes of bridges, considering the underlying variabilities and uncertainties in the response, damage, construction scheduling, and restoration resource availability. At the system level, metrics and methodologies were proposed to realistically quantify and efficiently optimize the resilience of transportation networks, considering the damage caused to the components of the network (i.e., bridges) by extreme events. The contributions of the research are highlighted in the following section.

8.2 Major Contributions

The original contributions of this research are the followings.

1. This study shows how simulation-based techniques and contemporary computing resources can be used to assess probabilistic seismic demand characteristics, fragility curves, resilience and life-cycle loss of various types of structural components and systems, accurately and in a computationally efficient way.

2. The error introduced by the common assumptions on the structural demand for classes of highway bridges is quantified, its propagation is analyzed and the impact on the final results in terms of probability of failure and resilience is estimated. Based on the numerical results and observations, general guidelines are provided on the use of these assumptions for practical applications. This research presents a systematic

and quantitative study of the effect of each of these assumptions on the results of probabilistic seismic demand, fragility, and particularly seismic resilience.

3. For more accurate estimation of resilience, a methodology is proposed to compute the restoration functions of individual bridges. To the best of the author's knowledge, the proposed methodology is the first simulation-based technique to compute sample stepwise restoration functions for individual bridges, considering the (partial or complete) temporary reopenings of the bridge during the restoration process. The results can be used to estimate the post-event time-variant probabilistic characteristics of functionality of bridges. Moreover, this methodology allows removing the difficulties typically involved in defining and validating the system level damage states for bridges, as it only relies on repair-based damage states of the components.

4. Two scheduling schemes are proposed to take into account the uncertainty in the flow of information about the construction process and its variability before and after the extreme event. The proposed scheduling schemes provide a more realistic picture of the effect of uncertainties in the functionality evaluation. The resulting functionality probability bounds can assist disaster officials to make informed decisions on planning post-event emergency management or proactive mitigation policies.

5. *Functionality-Fragility Surface (FFS)* is introduced as a concept and a convenient tool for probabilistic functionality and resilience assessment and communication for structures and infrastructure systems. A technique is presented to compute *FFS*s by combining fragility and restoration functions.

6. *Algorithm with Multiple-Input Genetic Operators* (*AMIGO*) is proposed, which is a new evolutionary optimization algorithm for efficiently addressing resource and time constrained scheduling of large-scale problems. Novel genetic operators for efficient searching of the design space are developed. The application of the proposed

methodology to post-event restoration and resilience optimization of damaged bridge networks is presented. The results show the superior performance of the proposed technique compared to a number of other methodologies.

7. A comprehensive simulation-based framework is presented for pre-event resilience and retrofit optimization of damaged bridges in transportation networks, taking into account the uncertainties in the intensity of the hazard, its spatial distribution, bridge damage, and post-event resilience of the system.

8. Regarding the system level (i.e., transportation network) functionality and resilience analysis, new formulations and models are developed, capable of properly integrating the impact of all critical components (here bridges), capturing the characteristics and properties of the system, and reflecting the restoration goals in different phases of disaster response. The connectivity-based network functionality and resilience metrics proposed in this study reflect the restoration policies typically followed in the medium-term recovery plans, by considering the level of accessibility between the critical regions of the transportation system. Also, network functionality and resilience metrics are proposed based on the level of serviceability of highway segments and bridges. These metrics are developed to match the accuracy provided by congestion-based metrics, while keeping the computational costs reasonable. This makes them suitable for large scale, real world, pre-event and post-event analyses.

Overall, the current dissertation covers different aspects of transportation resilience analysis, including resilience assessment, prediction, enhancement, and optimization. Moreover, the proposed techniques and methodologies encompass a broad time interval considering different phases of disaster management activities, ranging from pre-event predictive studies, to post-disaster short-term emergency, and medium- and long-term recovery phases. Analyses are carried out in a probabilistic fashion, considering different sources of uncer-

tainty in the estimation of seismic hazard, damage, recovery process, and functionality. The studies are performed in a multi-scale fashion, starting from assessing the damage, restoration, and functionality of the smallest critical components of the system, namely bridge structural members (e.g., columns, bearings, abutments, etc.), to evaluating the functionality and resilience of bridge structures, and finally transportation networks. The difficulties involved in defining system level damage states to assess the functionality, restoration time, and other loss measures of bridges have challenged the research community. This research addresses this issue by bypassing system level damage states and directly evaluating the restoration process and functionality of bridge structures, using the proposed methodology.

The accurate and realistic prediction of restoration functions for resilience assessment of different structures and infrastructure systems is one of the challenges the research community is currently facing. In fact, there is a growing consensus about the lack of such restoration functions and of a general procedure to assess the functionality during the recovery process by statistical analyses of the past events or other rigorous analytical techniques. The methodology proposed in this dissertation opens up new horizons in modeling restoration functions not only for bridges, but also other critical structures and infrastructure systems.

8.3 Future Studies

The probabilistic disaster response analysis, and loss and resilience assessment of human societies and communities are among the main themes of research for different fields, including Civil Engineering. While the earlier efforts have been mostly focused on studying the response of the individual structures (such as single buildings, pipelines, and power plants), the more recent developments and methodologies are targeting the analysis of complex units, "systems" and "systems of systems" (such as transportation networks, water

distribution systems, and power grids). However, to perform a study at a regional scale, the transition from component- to system-level and combining the role of all heterogeneous elements of the community, is not a straightforward step. The methodology presented in Chapter 4 is one way of addressing such transition from component damage to system functionality for the case of individual bridges. Similar research needs to be conducted on other types of structures and infrastructure systems such as power grids, water supplies, and telecommunication systems.

Consideration of the interdependencies among the performance and restoration of different components of the community is another topic to which more attention should be paid. The data associated with the restoration and functionality of different components and systems after the past catastrophic events needs to be collected and analyzed carefully. Mathematical models capable of capturing the characteristics of the interdependencies among different infrastructure systems should be developed and possibly validated using the available data.

The social and economic considerations and their impact on the restoration and disaster management activities are other aspects of resilience analysis which have not been investigated extensively and need to be studied in a rigorous way. The behavior of the impacted populations, as well as decision makers and disaster managers are highly interconnected with the economy and historical status of the stricken community. Such factors are among the major determinants of the recovery investment, policies, and pace.

Appendix A

Bridge Component Restoration Information

In this appendix, a complete list of bridge component restoration data needed to compute probabilistic restoration functions and *FFS*s following the techniques presented in Chapters 4 and 5 is presented. In particular, the complete list of the restoration tasks, their duration distribution, and resource requirements are provided. Also, tasks required for the restoration of each component at the relevant repair-based damage states and their precedence relations are presented in this appendix. The data provided here has been collected from multiple scientific papers, archival publications, and interviews with field experts (Barker and Hartnagel, 1998; Mander et al., 1996; Nielson, 2005; Hwang et al., 2001; Mackie et al., 2008; Aygün et al., 2010; Ledezma and Bray, 2008; Girondo, 2014; Sause, 2014).

Table A.1 presents the list of all restoration tasks used in this study, along with their type (i.e., *Prep*, *Temp*, *Reg*). For the discussion on the type of each task refer to Chapter 4. The functionality of the bridge during the execution of each task (qA) and the parameters of the probabilistic distributions describing their duration are presented in Table A.2. Table A.3 presents the amount of resource requirements for each task, considering four resource types, namely manpower, Geo-machinery, crane, and concrete machinery.

Figures A.1-A.12 illustrate the tasks required for the restoration of each component considering their relevant damage states. The arrows show the precedence relations among the tasks. In these figures, the red, blue, and black bars represent the *Prep* tasks, *Temp*

Table A.1: Restoration tasks and their type.

Task no.	Restoration tasks	Type	Task no.	Restoration tasks	Type
1	Repair minor spall	*Reg*	27	Construct 1/2 approach slab	*Reg*
2	Repair column cracks with epoxy	*Reg*	28	Construct 1/2 backwall and approach slab	*Reg*
3	Submit/review bridge removal plan	*Prep*	29	AC overlay	*Reg*
4	Submit/review temporaty support	*Prep*	30	Mudjacking	*Reg*
5	Install column (bent) left temporary support	*Temp*	31	Install abutment temporary support	*Temp*
6	Install column (bent) right temporary support	*Temp*	32	Fabricate/procure pipe piles	*Prep*
7	Remove existing column	*Reg*	33	Excavate bent	*Reg*
8	Place column reinforcement	*Reg*	34	Drive column piles	*Reg*
9	Place column forms	*Reg*	35	Place pile forms	*Reg*
10	Pour column concrete	*Reg*	36	Place foundation reinforcement	*Reg*
11	Cure concrete	*Reg*	37	Pour foundation concrete	*Reg*
12	Remove column forms	*Reg*	38	Backfill	*Reg*
13	Remove the left temporary support	*Temp*	39	Submit/review demo plan for abutment	*Prep*
14	Remove the right temporary support	*Temp*	40	Excavate abutment/demo wing walls	*Reg*
15	Remove abutment temporary support	*Temp*	41	Drive abutment piles	*Reg*
16	Resetting the bearings	*Reg*	42	Drill and bond dowels	*Reg*
17	Remove/construct new pedestals	*Reg*	43	Construct wing walls	*Reg*
18	Cure pedestal concrete	*Reg*	44	Cure abutment footing	*Reg*
19	Install new bearings	*Reg*	45	Cure wing walls	*Reg*
20	Install abutment joint seal assembly	*Reg*	46	Place bent beam reinforcement	*Reg*
21	Excavate abutment	*Reg*	47	Place bent beam forms	*Reg*
22	Repair abutment cracks with epoxy	*Reg*	48	Pour bent beam concrete	*Reg*
23	Repair abutment spalls	*Reg*	49	Remove bent forms	*Reg*
24	Abutment backfill	*Reg*	50	Demolish the multicolumn bent	*Reg*
25	Remove 1/2 backwall and appoach slab	*Reg*	51	Cure bent beam	*Reg*
26	Construct 1/2 backwall	*Reg*	52	Demolition and reconstruction	*Reg*

Table A.2: Restoration task functionality and duration probabilistic distributions

Task no.	$qA(\%)$	Duration				Task no.	$qA(\%)$	Duration			
		$P1$[1]	$P2$	$P3$	Distribution			$P1$	$P2$	$P3$	Distribution
1	100	3	9	6	Trg[2]	27	50	1	2	2	Unif
2	100	3	9	6	Trg	28	50	1	3	2	Trg
3	100	10	20	15	Trg	29	50	1	3	2	Trg
4	100	20	40	30	Trg	30	50	1	3	2	Trg
5	0	1	3	2	Trg	31	0	1	3	2	Trg
6	0	1	3	2	Trg	32	100	30	40	35	Trg
7	100	3	6	-	Unif3	33	50	3	6	-	Unif
8	100	3	6	-	Unif	34	100	3	9	2	Trg
9	100	3	3	-	Unif	35	100	3	3	-	Unif
10	100	3	6	-	Unif	36	100	3	6	-	Unif
11	100	7	10	12	Trg	37	100	3	6	-	Unif
12	100	1	1	-	Unif	38	100	3	12	2	Trg
13	0	1	1	-	Unif	39	100	10	20	15	Trg
14	0	1	1	-	Unif	40	100	1	3	-	Unif
15	0	1	1	-	Unif	41	100	2	4	3	Trg
16	50	1	2	-	Unif	42	100	1	2	1	Unif
17	100	1	3	2	Trg	43	100	2	6	4	Trg
18	100	7	12	10	Trg	44	100	7	10	12	Trg
19	100	1	2	-	Unif	45	100	7	10	12	Trg
20	50	1	3	2	Trg	46	100	1	2	-	Unif
21	50	1	2	-	Unif	47	100	1	2	-	Unif
22	100	1	3	2	Trg	48	100	2	3	-	Unif
23	100	1	3	2	Trg	49	100	1	1	-	Unif
24	50	1	4	2	Trg	50	100	3	6	-	Unif
25	50	1	3	2	Trg	51	100	7	10	12	Trg
26	50	1	3	2	Trg	52	0	75	188	300	Trg

[1]P1 and P2 are the minimum and maximum values of the distributions, respectively. For triangular distributions, P3 is the mode value, [2]Triangular distribution, [3]Uniform distribution

Table A.3: Tasks resource requirements

Task no.	Resource requirements				Task no.	Resource requirements			
	Man-power	Geo-Machine	Crane	Con-Machine		Man-power	Geo-Machine	Crane	Conc-Machine
1	2	0	0	1	27	5	1	0	1
2	2	0	0	1	28	5	0	1	2
3	0	0	0	0	29	3	0	0	1
4	0	0	0	0	30	3	0	0	1
5	5	0	1	0	31	5	0	1	0
6	5	0	1	0	32	0	0	0	0
7	5	0	1	0	33	3	1	0	0
8	5	0	1	0	34	3	1	0	0
9	5	0	1	0	35	5	0	1	0
10	5	0	1	2	36	5	0	0	0
11	2	0	0	0	37	5	0	0	2
12	2	0	1	0	38	5	1	0	0
13	5	0	1	0	39	0	0	0	0
14	5	0	1	0	40	5	2	0	0
15	5	0	1	0	41	3	1	0	0
16	5	0	1	0	42	3	0	0	0
17	5	0	0	1	43	5	0	0	2
18	1	0	0	0	44	2	0	0	0
19	5	0	0	0	45	2	0	0	0
20	3	0	0	1	46	5	0	1	0
21	5	2	0	0	47	5	0	1	0
22	2	0	0	1	48	5	0	1	2
23	2	0	0	1	49	2	0	1	0
24	5	2	0	0	50	5	0	1	0
25	5	1	1	0	51	2	0	0	0
26	5	0	1	2	52	0	0	0	0

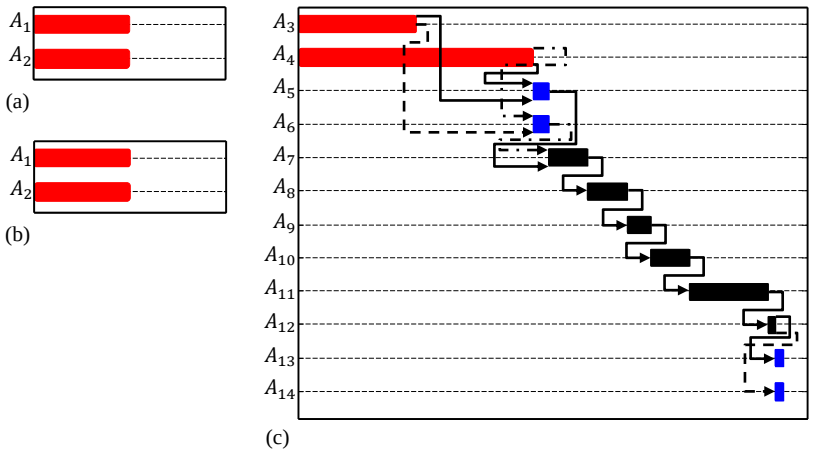

Figure A.1: Left and right columns restoration task precedence relations for (a) DS1, (b) DS2, and (c) DS3

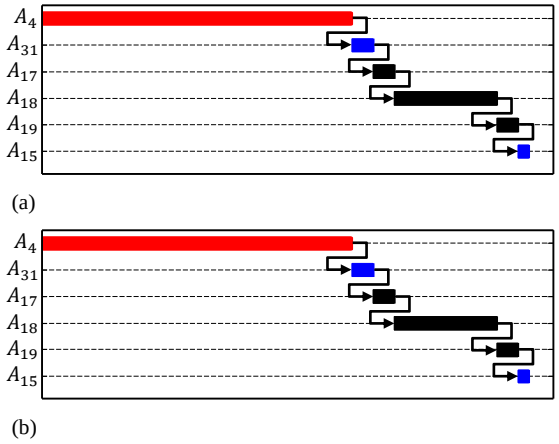

Figure A.2: Left fix bearings restoration task precedence relations for (a) DS1, and (b) DS2

tasks, and *Reg* tasks, respectively. It is worth noting that the figures are schematic and the lengths of the bars do not represent the duration of the tasks. Also, for some components (e.g., *LF* at DS1 and DS2), the tasks and their precedence relations defined for the restoration of different damage states are the same. However, the functionality of the bridge during the restoration of such components is different for the case different initial damage states. This is because different bridge safety requirements (see Section 4.3.5 and Table 5.4) are considered for different damage states of such components. Thus, although the restoration processes are the same, the associated functionality profiles are different for these components.

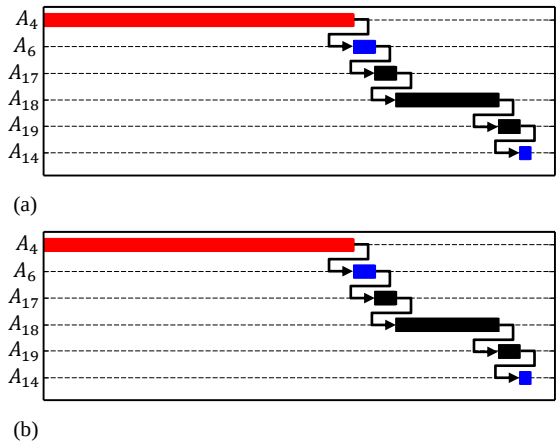

Figure A.3: Middle and right fix bearings restoration task precedence relations for (a) DS1, and (b) DS2

Figure A.13 shows the precedence relations among the components. These relations are defined for each component group, namely left abutment group, right abutment group, left bent group, and right bent group.

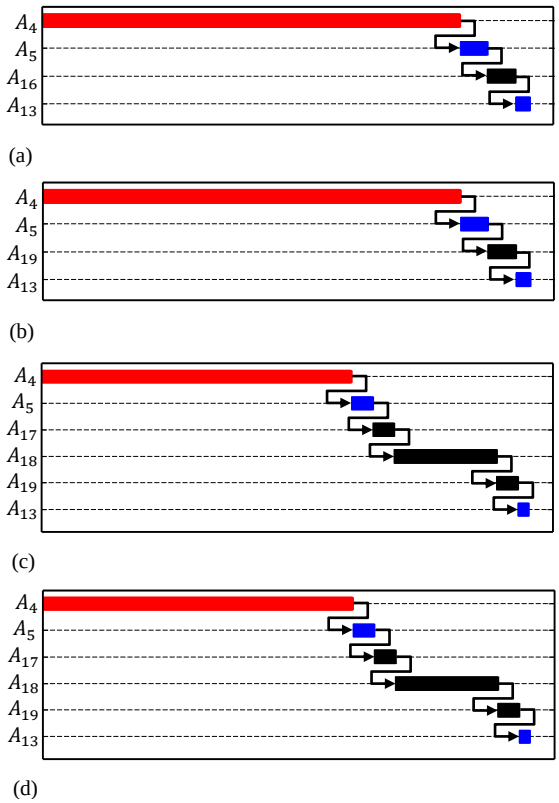

Figure A.4: Left and middle rocker bearings restoration task precedence relations for (a) DS1, (b) DS2, (c) DS3, and (d) DS4

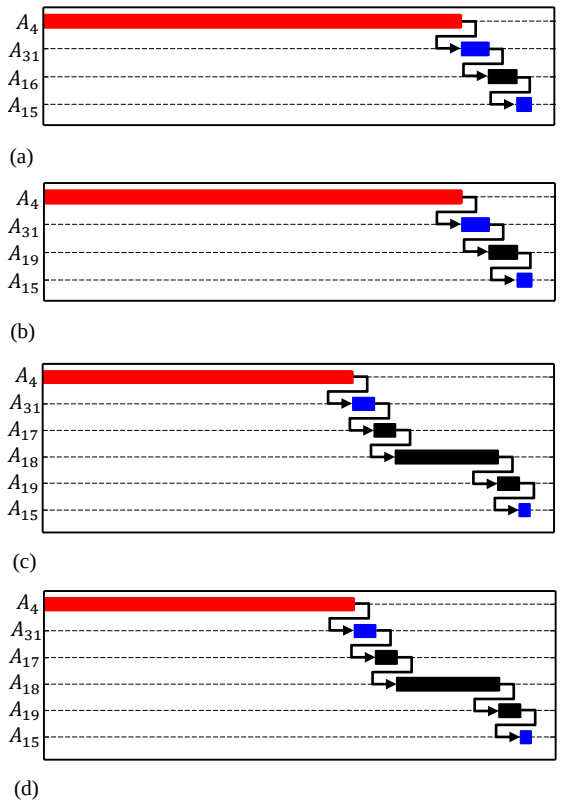

Figure A.5: Right rocker bearings restoration task precedence relations for (a) DS1, (b) DS2, (c) DS3, and (d) DS4

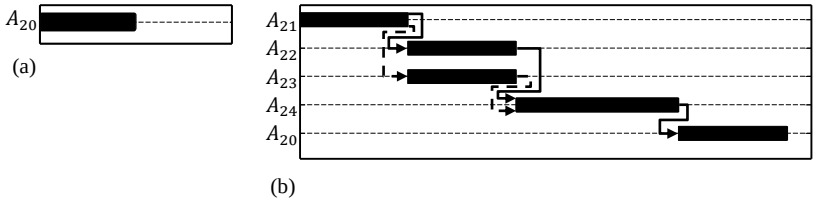

Figure A.6: Left and right abutments restoration task precedence relations for (a) DS1, and (b) DS2

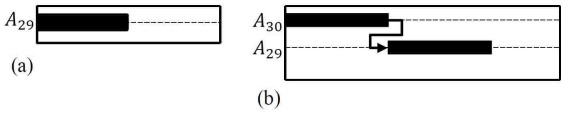

Figure A.7: Left and right approach slabs restoration task precedence relations for (a) DS1, and (b) DS2

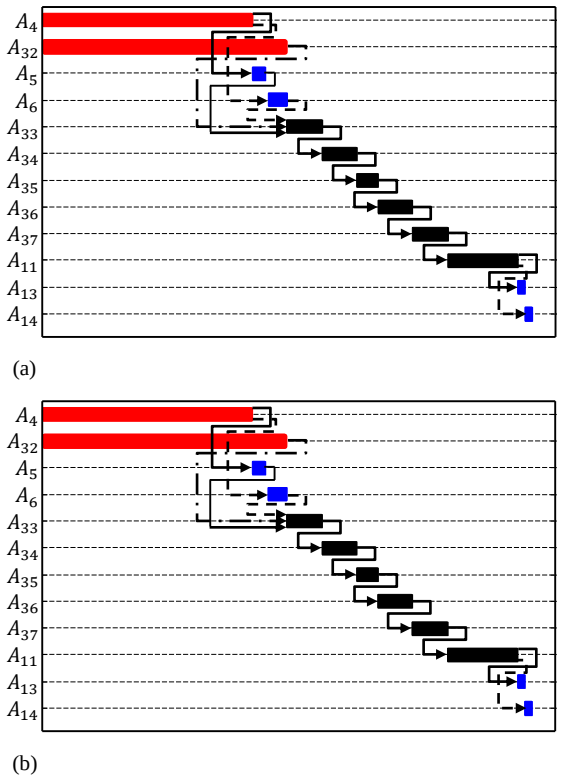

Figure A.8: Left and right column foundations restoration task precedence relations for (a) DS1, and (b) DS2

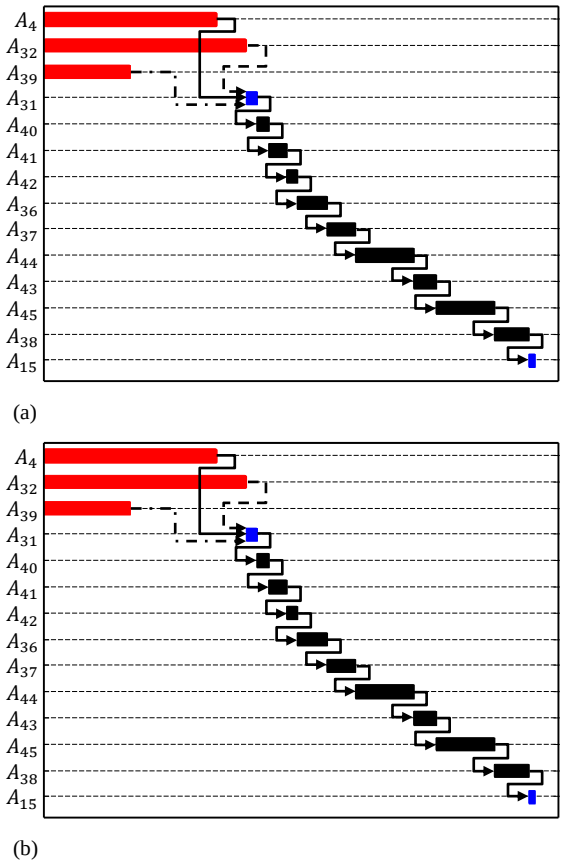

Figure A.9: Left and right abutment foundations restoration task precedence relations for (a) DS1, and (b) DS2

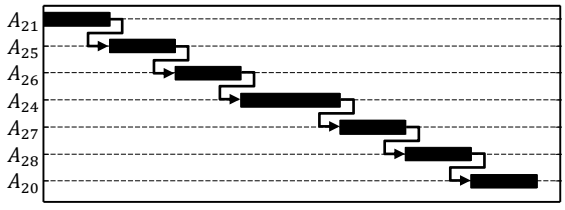

Figure A.10: *LAbAp* and *RAbAp Meta-Components* restoration task precedence relations for DS1

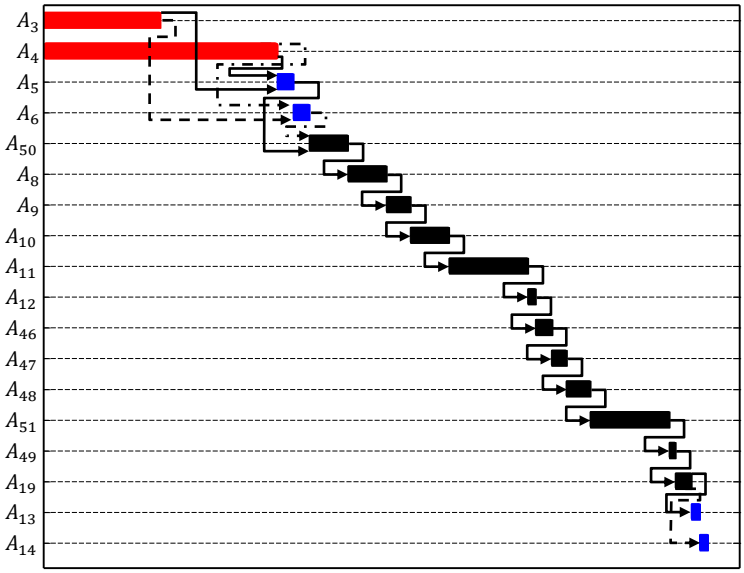

Figure A.11: *LBnt* and *RBnt Meta-Components* restoration task precedence relations for DS1

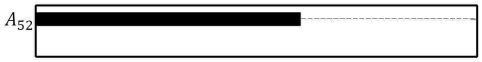

Figure A.12: *Brdg Meta-Components* restoration task precedence relations for DS1

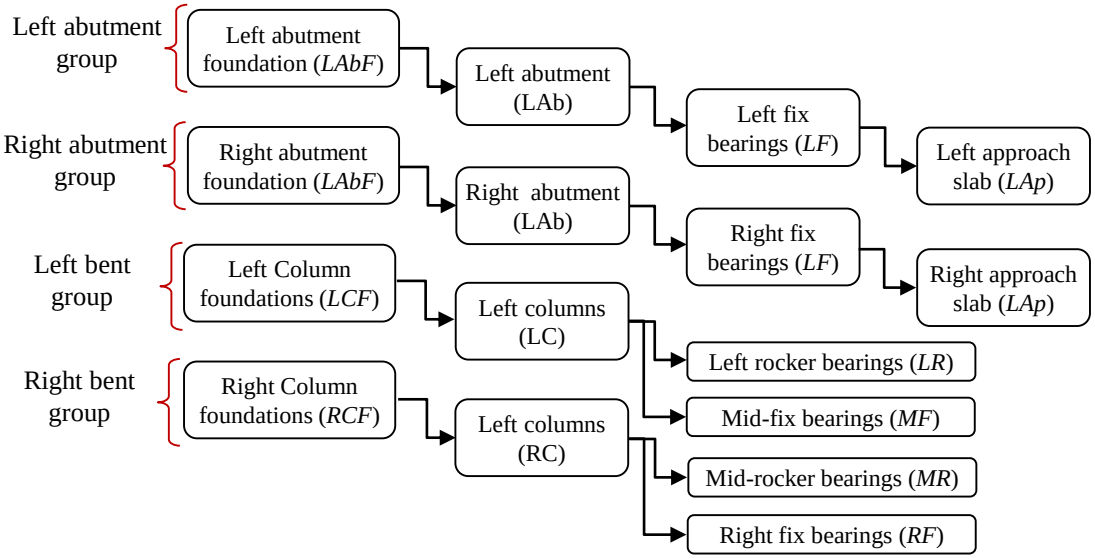

Figure A.13: Component restoration precedence within component groups

References

AAPA [2013]. *U.S. Port Waterborne Foreign Trade*. American Association of Port Authorities, available at: http://www.aapa-ports.org/Industry/content.cfm?ItemNumber=900.

Adger, W. N., Hughes, T. P., Folke, C., Carpenter, S. R., and Rockström, J. [2005]. "Social-ecological resilience to coastal disasters." *Science*, 309(5737), 1036–1039.

Ahuja, R. K., Magnanti, T. L., and Orlin, J. B. [1993]. *Network flows : theory, algorithms, and applications*. Prentice Hall, Englewood Cliffs, N.J.

AmiriHormozaki, E., Pekcan, G., and Itani, A. [2015]. "Analytical fragility functions for horizontally curved steel i-girder highway bridges." *Earthquake Spectra*, 31(4), 2235–2254.

Ang, A. H. and Tang, W. H. [2006]. *Probability concepts in engineering: emphasis on applications to civil and environmental engineering*. John Wiley & Sons, NY.

Artigues, C., Demassey, S., and Neron, E. [2013]. *Resource-constrained project scheduling: models, algorithms, extensions and applications*. John Wiley & Sons, Hoboken, NJ.

Asprone, D. and Manfredi, G. [2013]. "Linking disaster resilience and urban sustainability: A glocal approach for future cities." *SSRN Scholarly Paper ID 2298652*, Social Science Research Network, Rochester, NY (February).

ATC [1985]. "Earthquake damage evaluation data for California." *Report no.*, Applied Technology Council, ATC-13, Redwood City, CA.

Aygün, B., Dueñas-Osorio, L., Padgett, J. E., and DesRoches, R. [2010]. "Efficient longitudinal seismic fragility assessment of a multispan continuous steel bridge on liquefiable soils." *Journal of Bridge Engineering*, 16(1), 93–107.

Baker, J. W. and Allin Cornell, C. [2005]. "A vector-valued ground motion intensity measure consisting of spectral acceleration and epsilon." *Earthquake Engineering & Structural Dynamics*, 34(10), 1193–1217.

Banerjee, S. and Ganesh Prasad, G. [2013]. "Seismic risk assessment of reinforced concrete bridges in flood-prone regions." *Structure and Infrastructure Engineering*, 9(9), 952–968.

Banerjee Basu, S. and Shinozuka, M. [2011]. "Effect of ground motion directionality on fragility characteristics of a highway bridge." *Advances in Civil Engineering*, 2011 doi:10.1155/2011/536171.

Barker, M. and Hartnagel, B. [1998]. "Longitudinal restraint response of existing bridge bearings." *Transportation Research Record: Journal of the Transportation Research Board*, 1624, 28–35.

Bausch, A. W., Faria, J. R., and Zeitzoff, T. [2013]. "Warnings, terrorist threats and resilience: A laboratory experiment." *Conflict Management and Peace Science*, 30, 433–451.

Bazzurro, P. and Cornell, C. [2002]. "Vector-valued probabilistic seismic hazard analysis (vpsha)." *Proceedings of the 7th US national conference on earthquake engineering*, Boston, MA, 21–25.

Bergström, J., van Winsen, R., and Henriqson, E. [2015]. "On the rationale of resilience in the domain of safety: A literature review." *Reliability Engineering & System Safety*, 141, 131–141.

Bhatt, S., Barnhart, N., Wright, J., and Benton, B. [2012]. *Bridge Manual 2012*. Delaware Department of Transportation.

Billah, A., Alam, M., and Bhuiyan, M. [2013]. "Fragility analysis of retrofitted multicolumn bridge bent subjected to near-fault and far-field ground motion." *Journal of Bridge Engineering*, 18, 992–1004.

Billah, A. M. and Alam, M. S. [2014]. "Seismic performance evaluation of multi-column bridge bents retrofitted with different alternatives using incremental dynamic analysis." *Engineering Structures*, 62, 105–117.

Billah, A. M. and Alam, M. S. [2015]. "Seismic fragility assessment of highway bridges: a state-of-the-art review." *Structure and Infrastructure Engineering*, 11(6), 804–832.

Biondini, F., Camnasio, E., and Titi, A. [2015]. "Seismic resilience of concrete structures under corrosion." *Earthquake Engineering & Structural Dynamics*, 44(14), 2445–2466.

Bocchini, P. [2013]. "Computational procedure for the assisted resilience-oriented disaster management of transportation systems." *Safety, Reliability, Risk and Life-Cycle Performance of Structures and Infrastructures*, G. Deodatis, B. R. Ellingwood, and D. M. Frangopol, eds., Colombia University, NY, CRC Press, Taylor and Francis Group (June).

Bocchini, P., Christou, V., and Miranda, M. J. [2016]. "Correlated maps for regional multihazard analysis: Ideas for a novel approach." *Multi-hazard Approaches to Civil Infrastructure Engineering*, Springer, 15–39.

Bocchini, P., Decò, A., and Frangopol, D. M. [2012]. "Probabilistic functionality recovery model for resilience analysis." *Biondini, F. and Frangopol, D.M. (eds.), Bridge Mainte-*

nance, Safety, Management, Resilience and Sustainability, Lake Como, Italy July 8–12, CRC Press, Taylor and Francis, UK, 1920–1927.

Bocchini, P. and Frangopol, D. M. [2011]. "A stochastic computational framework for the joint transportation network fragility analysis and traffic flow distribution under extreme events." *Probabilistic Engineering Mechanics*, 26(2), 182–193.

Bocchini, P. and Frangopol, D. M. [2012a]. "Optimal resilience- and cost-based postdisaster intervention prioritization for bridges along a highway segment." *Journal of Bridge Engineering*, 17(1), 117–129.

Bocchini, P. and Frangopol, D. M. [2012b]. "Restoration of bridge networks after an earthquake: Multicriteria intervention optimization." *Earthquake Spectra*, 28(2), 426–455.

Bocchini, P. and Frangopol, D. M. [2013]. "Connectivity-based optimal scheduling for maintenance of bridge networks." 139(6), 760–769.

Bocchini, P., Frangopol, D. M., Ummenhofer, T., and Zinke, T. [2013]. "Resilience and sustainability of civil infrastructure: Toward a unified approach." *Journal of Infrastructure Systems*, 20(2), 04014004.

Bojórquez, E., Iervolino, I., Reyes-Salazar, A., and Ruiz, S. E. [2012]. "Comparing vector-valued intensity measures for fragility analysis of steel frames in the case of narrow-band ground motions." *Engineering Structures*, 45, 472–480.

Boon, H. J. [2014]. "Disaster resilience in a flood-impacted rural australian town." *Natural Hazards*, 71, 683–701.

Bowman, A. W. and Azzalini, A. [1997]. *Applied smoothing techniques for data analysis: the kernel approach with S-Plus illustrations*. Clarendon Press ; Oxford University Press, Oxford; New York.

Broccardo, M., Galanis, P., Esposito, S., and Stojadinovic, B. [2015]. "Resilience-based risk assessment of civil systems using peer framework for seismic hazard." *Safery and Reliability of Complex engineering Systems: ESREL*, L. Podofillini, B. Sudret, B. Stojadinovic, E. Zio, and W. Kröger, eds., Zurich, Switzerland, CRC Press, Taylor and Francis Group, 331–339 (September).

Brucker, P. [2002]. "Scheduling and constraint propagation." *Discrete Applied Mathematics*, 123(1), 227–256.

Brucker, P., Drexl, A., Möhring, R., Neumann, K., and Pesch, E. [1999]. "Resource-constrained project scheduling: Notation, classification, models, and methods." *European journal of operational research*, 112(1), 3–41.

Brucker, P. and Knust, S. [2006]. *Complex scheduling*. Springer, Berlin, Heidelberg.

Bruneau, M., Chang, S. E., Eguchi, R. T., Lee, G. C., ORourke, T. D., Reinhorn, A. M., Shinozuka, M., Tierney, K., Wallace, W. A., and von Winterfeldt, D. [2003]. "A framework to quantitatively assess and enhance the seismic resilience of communities." *Earthquake Spectra*, 19(4), 733–752.

Bruyelle, J.-L., ONeill, C., El-Koursi, E.-M., Hamelin, F., Sartori, N., and Khoudour, L. [2014]. "Improving the resilience of metro vehicle and passengers for an effective emergency response to terrorist attacks." *Safety Science*, 62, 37–45.

Bureau of Public Roads [1964]. *Traffic Assignment Manual*. U.S. Department of Commerce, Urban Planning Division, Washington D.C.

Caltrans [1999]. "Caltrans seismic design criteria." *Report no.*, California Department of Transportation, Sacramento, California.

Chandrasekaran, S. and Banerjee, S. [2015]. "Retrofit optimization for resilience enhance-

ment of bridges under multihazard scenario." *Journal of Structural Engineering*, 142, C4015012.

Chang, L., Elnashai, A. S., and Spencer, B. F. [2012a]. "Post-earthquake modelling of transportation networks." *Structure and Infrastructure Engineering*, 8(10), 893–911.

Chang, L., Peng, F., Ouyang, Y., Elnashai, A., and Spencer, B. [2012b]. "Bridge seismic retrofit program planning to maximize postearthquake transportation network capacity." *Journal of Infrastructure Systems*, 18(2), 75–88.

Chang, S. E. and Nojima, N. [2001]. "Measuring post-disaster transportation system performance: the 1995 kobe earthquake in comparative perspective." *Transportation Research Part A: Policy and Practice*, 35(6), 475–494.

Choi, E. [2002]. "Seismic analysis and retrofit of mid-america bridges." Ph.D. thesis, Georgia Institute of Technology, Atlanta, GA.

Choi, E., DesRoches, R., and Nielson, B. [2004]. "Seismic fragility of typical bridges in moderate seismic zones." *Engineering Structures*, 26(2), 187–199.

Christou, V. and Bocchini, P. [2015]. "Efficient computational models for the optimal representation of correlated regional hazard." *12th International Conference on Applications of Statistics and Probability in Civil Engineering, ICASP12*, Vancouver, Canada, July 12–15, 1–8.

Christou, V., Bocchini, P., and Miranda, M. J. [2015]. "Optimal representation of multi-dimensional random fields with a moderate number of samples: Application to stochastic mechanics." *Probabilistic Engineering Mechanics*, 44, 53–65.

Cimellaro, G. P., Reinhorn, A. M., and Bruneau, M. [2010a]. "Framework for analytical quantification of disaster resilience." *Engineering Structures*, 32(11), 3639–3649.

Cimellaro, G. P., Reinhorn, A. M., and Bruneau, M. [2010b]. "Seismic resilience of a hospital system." *Structure and Infrastructure Engineering*, 6, 127–144.

Cimellaro, G. P., Villa, O., and Bruneau, M. [2014]. "Resilience-based design of natural gas distribution networks." *Journal of Infrastructure Systems*, 21(1), 05014005.

Coello, C. A. C., Van Veldhuizen, D. A., and Lamont, G. B. [2002]. *Evolutionary algorithms for solving multi-objective problems*, Vol. 242. Springer, NY.

Comartin, C. D., Greene, M., and Tubbesing, S. K. [1995]. "The hyogo-ken nanbu earthquake: Great hanshin earthquake disaster, january 17, 1995: Preliminary reconnaissance report." *Report no.*, Earthquake Engineering Research Institute.

Cornell, C. A., Jalayer, F., Hamburger, R. O., and Foutch, D. A. [2002]. "Probabilistic basis for 2000 SAC federal emergency management agency steel moment frame guidelines." *Journal of Structural Engineering*, 128(4), 526–533.

Cornell, C. A. and Krawinkler, H. [2000]. "Progress and challenges in seismic performance assessment." *PEER Center News*, 3(2), 1–3.

Deb, K. and Goel, T. [2001]. "Controlled elitist non-dominated sorting genetic algorithms for better convergence." *Evolutionary Multi-Criterion Optimization*, E. Zitzler, L. Thiele, K. Deb, C. A. C. Coello, and D. Corne, eds., Lecture Notes in Computer Science, Springer Berlin Heidelberg, 67–81.

Deb, K., Pratap, A., Agarwal, S., and Meyarivan, T. [2002]. "A fast and elitist multiobjective genetic algorithm: NSGA-II." *IEEE transactions on evolutionary computation*, 6(2), 182197.

Decò, A., Bocchini, P., and Frangopol, D. M. [2013]. "A probabilistic approach for the prediction of seismic resilience of bridges." *Earthquake Engineering & Structural Dynamics*, 42(10), 1469–1487.

Deep, K., Singh, K. P., Kansal, M. L., and Mohan, C. [2009]. "A real coded genetic algorithm for solving integer and mixed integer optimization problems." *Applied Mathematics and Computation*, 212(2), 505–518.

Demeulemeester, E. and Herroelen, W. [2002]. *Project scheduling: A research handbook*. Kluwer Academic Publishers.

DHS [2009]. *HAZUS-MH MR4 Earthquake Model User Manual*. Department of Homeland Security; Federal Emergency Management Agency; Mitigation Division. Whashington, D.C.

DHS Risk Steering Committee [2008]. *DHS risk Lexicon*. Washington, DC: The Department of Homeland Security.

Dueñas-Osorio, L. and Padgett, J. [2011]. "Seismic reliability assessment of bridges with user defined-system failure events." *Journal of Engineering Mechanics*, 137(10), 680–690.

EERI [1994]. "Loma prieta earthquake, october 17, 1989: Preliminary reconnaissance report." *Report no.*, Earthquake Engineering Research Institute.

Ellingwood, B. and Hwang, H. [1985]. "Probabilistic descriptions of resistance of safety-related structures in nuclear plants." *Nuclear Engineering and Design*, 88(2), 169–178.

Elsayed, H. and Bocchini, P. [2014]. "Seismic resilience of bridges and transportation networks: application to San Francisco." Lehigh Valley Chapter of ASCE, April 2014.

Enright, M. P. and Frangopol, D. M. [1998]. "Probabilistic analysis of resistance degradation of reinforced concrete bridge beams under corrosion." *Engineering Structures*, 20(11), 960–971.

Evans, S. P. [1976]. "Derivation and analysis of some models for combining trip distribution and assignment." *Transportation Research*, 10(1), 37–57.

Fan, X. and McCormick, J. P. [2015]. "Characterisation of the behaviour of steel bridge bearings under cyclic load reversal." *Structure and Infrastructure Engineering*, 11(6), 744–760.

Fang, J., Li, Q., Jeary, A., and Liu, D. [1999]. "Damping of tall buildings: its evaluation and probabilistic characteristics." *The Structural Design of Tall Buildings*, 8(2), 145–153.

Faturechi, R. and Miller-Hooks, E. [2014]. "Measuring the performance of transportation infrastructure systems in disasters: A comprehensive review." *Journal of Infrastructure Systems*, 21(1), 04014025.

FEMA [2006]. *Next-generation performance-based seismic design guidelines*. Number FEMA-445. Federal Emergency Management Agency, Washington, D.C.

FHWA [2002]. *National Bridge Inventory*. Federal HighWay Administration.

FHWA [2013]. *National Bridge Inventory*. Federal HighWay Administration, available on line at http://www.fhwa.dot.gov/bridge/nbi.htm (visited on June 15, 2014).

Franchin, P., Lupoi, A., Pinto, P., and Schotanus, M. I. [2003]. "Seismic fragility of reinforced concrete structures using a response surface approach." *Journal of Earthquake Engineering*, 7, 45–77.

Francis, R. and Bekera, B. [2014]. "A metric and frameworks for resilience analysis of engineered and infrastructure systems." *Reliability Engineering & System Safety*, 121, 90–103.

Gardoni, P., Mosalam, K. M., and der Kiureghian, A. [2003]. "Probabilistic seismic demand models and fragility estimates for RC bridges." *Journal of earthquake engineering*, 7, 79–106.

Gen, M. and Cheng, R. [2000]. *Genetic algorithms and engineering optimization*. John Wiley & Sons, NY.

Ghosh, J. and Padgett, J. [2010]. "Aging considerations in the development of time-dependent seismic fragility curves." *Journal of Structural Engineering*, 136(12), 1497–1511.

Ghosn, M., Dueñas-Osorio, L., Frangopol, D. M., Mcallister, T., Bocchini, P., Manuel, L., Ellingwood, B. R., Arangio, S., Bontempi, F., Shah, M., Akiyama, M., Biondini, F., Hernandez, S., and Tsiatas, G. [2016]. "Performance indicators for structural systems and infrastructure networks." *Journal of Structural Engineering*, 142(9), F4016003.

Giovenale, P., Cornell, C. A., and Esteva, L. [2004]. "Comparing the adequacy of alternative ground motion intensity measures for the estimation of structural responses." *Earthquake engineering & structural dynamics*, 33(8), 951–979.

Giovinazzi, S. and Nicholson, A. [2010]. "Transport network reliability in seismic risk analysis and management.." *Report no.*, University of Canterbury. Civil and Natural Resources Engineering.

Girondo, M. [2014]. Personal communication.

Goldberg, D. E. [1989]. *Genetic Algorithms in Search, Optimization, and Machine Learning*. Addison-Wesley Professional.

Google Inc. [2015]. *Google Earth, release 7.1.5.1557*. Keyhole Inc. & Google Inc., Menlo Park, California.

Grigoriu, M. [1998]. "Simulation of stationary non-gaussian translation processes." *Journal of Engineering Mechanics*, 124(2), 121–126.

Gurobi [2015]. *Gurobi Optimizer Reference Manual*. Gurobi Optimization, Inc., available at: http://www.gurobi.com.

Hall, J. [1994]. "Northridge, california earthquake of january 17, 1994: Preliminary reconnaissance report." *Report no.*, Earthquake Engineering Research Institute.

Hartmann, S. and Briskorn, D. [2010]. "A survey of variants and extensions of the resource-constrained project scheduling problem." *European Journal of Operational Research*, 207(1), 1–14.

Henry, D. and Ramirez-Marquez, J. E. [2012]. "Generic metrics and quantitative approaches for system resilience as a function of time." *Reliability Engineering & System Safety*, 99, 114–122.

Holling, C. S. [1973]. "Resilience and stability of ecological systems." *Annual Review of Ecology and Systematics*, 4, 1–23.

Hollnagel, E., Woods, D. D., and Leveson, N. [2007]. *Resilience engineering: Concepts and precepts*. Ashgate Publishing, Ltd.

HOR [2014]. *Bridge Maintenance Manual*. Iowa Department of Transportation, Office of Bridges and Structures.

Hosseini, S., Barker, K., and Ramirez-Marquez, J. E. [2016]. "A review of definitions and measures of system resilience." *Reliability Engineering & System Safety*, 145, 47–61.

Huo, Y. and Zhang, J. [2013]. "Effects of pounding and skewness on seismic responses of typical multispan highway bridges using the fragility function method." *Journal of Bridge Engineering*, 18, 499–515.

Hwang, H., Liu, J. B., and Chiu, Y.-H. [2001]. "Seismic fragility analysis of highway bridges." *Report no.*, Mid-America Earthquake Center, MAEC RR-4 Project.

Hwang, H. H. and Jaw, J.-W. [1990]. "Probabilistic damage analysis of structures." *Journal of Structural Engineering*, 116(7), 1992–2007.

Iman, R. L. and Conover, W.-J. [1982]. "A distribution-free approach to inducing rank correlation among input variables." *Communications in Statistics-Simulation and Computation*, 11(3), 311–334.

Jalayer, F. [2003]. "Direct probabilistic seismic anaysis: implementing non-linear dynamic assessments." Ph.D. thesis, Stanford University, Stanford, CA.

Jayaram, N. and Baker, J. W. [2009]. "Correlation model for spatially distributed ground-motion intensities." *Earthquake Engineering & Structural Dynamics*, 38(15), 1687–1708.

Kafali, C. and Grigoriu, M. [2007]. "Seismic fragility analysis: Application to simple linear and nonlinear systems." *Earthquake Engineering & Structural Dynamics*, 36(13), 1885–1900.

Karamlou, A. and Bocchini, P. "Introducing functionality-fragility surfaces." *under review*.

Karamlou, A. and Bocchini, P. [2014a]. "Optimal bridge restoration sequence for resilient transportation networks." *Structures Congress 2014*, Boston, MA, April 3–5, ASCE, 1437–1447.

Karamlou, A. and Bocchini, P. [2014b]. "Quantification of the approximations introduced by assumptions made on marginal distributions of the demand for highway bridge fragility analysis." *Second international conference on vulnerability and risk analysis and management (ICVRAM 2014)*, Liverpool, UK July 13–16, ASCE, 1321–1330.

Karamlou, A. and Bocchini, P. [2015]. "Computation of the bridge seismic fragility by large-scale simulation for resilience analysis." *Earthquake Engineering & Structural Dynamics*, 44(12), 1959–1978.

Karamlou, A. and Bocchini, P. [2016a]. "From component damage to system-level probabilistic restoration functions for a damaged bridge." *Journal of Infrastructure Systems, in press* doi: 10.1061/(ASCE)IS.1943-555X.0000342.

Karamlou, A. and Bocchini, P. [2016b]. "Sequencing algorithm with multiple-input genetic operators: application to disaster resilience." *Engineering Strucutres*, 117, 591–602.

Karamlou, A., Bocchini, P., and Christou, V. [2016]. "Metrics and algorithm for optimal retrofit strategy of resilient transportation networks." *Maintenance, Monitoring, Safety, Risk and Resilience of Bridges and Bridge Networks*, Foz do Iguau, Brazil, June 26–30, Taylor and Francis, 1121–1128.

Kennedy, R. and Ravindra, M. [1984]. "Seismic fragilities for nuclear power plant risk studies." *Nuclear Engineering and Design*, 79(1), 47–68.

Kennedy, R. P., Cornell, C., Campbell, R., Kaplan, S., and Perla, H. [1980]. "Probabilistic seismic safety study of an existing nuclear power plant." *Nuclear Engineering and Design*, 59(2), 315–338.

Ketchum, M., Chang, V., and Shantz, T. [2004]. "Influence of design ground motion level on highway bridge costs." *Report No. Lifelines 6D01*.

Kim, J. and Oh, S. S. [2014]. "The virtuous circle in disaster recovery: who returns and stays in town after disaster evacuation?." *Journal of Risk Research*, 17, 665–682.

Kolisch, R. [1996]. "Serial and parallel resource-constrained project scheduling methods revisited: Theory and computation." *European Journal of Operational Research*, 90(2), 320–333.

Kolisch, R. and Padman, R. [2001]. "An integrated survey of deterministic project scheduling." *Omega*, 29(3), 249–272.

Lagaros, N. D., Tsompanakis, Y., Psarropoulos, P. N., and Georgopoulos, E. C. [2009]. "Computationally efficient seismic fragility analysis of geostructures." *Computers & Structures*, 87(19), 1195–1203.

Ledezma, C. A. and Bray, J. D. [2008]. *Performance-based earthquake engineering design evaluation procedure for bridge foundations undergoing liquefaction-induced lateral ground displacement*. Pacific Earthquake Engineering Research Center.

Levinson, D. M. and Kumar, A. [1994]. "Multimodal trip distribution: structure and application." *Transportation Research Record*, (1466), 124–124.

Luco, N. and Cornell, C. A. [2007]. "Structure-specific scalar intensity measures for near-source and ordinary earthquake ground motions." *Earthquake Spectra*, 23(2), 357–392.

Ludwig, D., Jones, D. D., and Holling, C. S. [1978]. "Qualitative analysis of insect outbreak systems: The spruce budworm and forest." *Journal of Animal Ecology*, 47(1), 315–332.

Lupoi, G., Franchin, P., Lupoi, A., and Pinto, P. [2006]. "Seismic fragility analysis of structural systems." *Journal of Engineering Mechanics*, 132(4), 385–395.

Mackie, K. and Stojadinovic, B. [2001]. "Probabilistic seismic demand model for california highway bridges." *Journal of Bridge Engineering*, 6(6), 468–481.

Mackie, K. R., Kucukvar, M., Tatari, O., and Elgamal, A. [2015]. "Sustainability metrics for performance-based seismic bridge response." *Journal of Structural Engineering*, 142, C4015001.

Mackie, K. R., Wong, J.-M., and Stojadinović, B. [2008]. *Integrated probabilistic performance-based evaluation of benchmark reinforced concrete bridges*. Pacific Earthquake Engineering Research Center.

Mander, J. B., Kim, D., Chen, S., and Premus, G. [1996]. "Response of steel bridge bearings to reversed cyclic loading." *Report No. NCEER-96-0014*, National Center for Earthquake Engineering Research.

McGuire, R. K., Silva, W. J., and Costantino, C. J. [2001]. "Technical basis for revision of regulatory guidance on design ground motions: Hazard- and risk-consistent ground motion spectra guidelines." *Report no.*, NUREG/CR-6728, U.S. Nuclear Regulatory Commission, Washington, D.C.

McKay, M. D., Beckman, R. J., and Conover, W. J. [2000]. "A comparison of three methods for selecting values of input variables in the analysis of output from a computer code." *Technometrics*, 42(1), 55–61.

McKenna, F., Fenves, G. L., Scott, M. H., and Jeremic, B. [2000]. *Open System for Earthquake Engineering Simulation (OpenSees)*. Pacific Earthquake Engineering Research Center, University of California, Berkeley, CA.

Morbin, R., Zanini, M., Pellegrino, C., Zhang, H., and Modena, C. [2015]. "A probabilistic strategy for seismic assessment and frp retrofitting of existing bridges." *Bulletin of Earthquake Engineering*, 13(8), 2411–2428.

Muthukumar, S. and DesRoches, R. [2005]. "Effect of frame-restoring force characteristics on the pounding response of multiple-frame bridges." *Earthquake Spectra*, 21(4), 1113–1135.

Neumann, K., Schwindt, C., and Zimmermann, J. [2003]. *Project scheduling with time windows and scarce resources: temporal and resource-constrained project scheduling with regular and nonregular objective functions*. Springer, Berlin.

Nielson, B. G. [2005]. "Analytical fragility curves for highway bridges in moderate seismic zones." Ph.D. thesis, Georgia Institute of Technology, Atlanta, GA.

NIST [2015]. "Community resilience planning guide for buildings and infrastructure systems." *Report no.*, National Institute of Standards and Technology (NIST) (October).

O'Brien, J. J. and Plotnick, F. L. [2015]. *CPM in Construction Management*. McGrawHill, NY.

Okeil, A. M., El-Tawil, S., and Shahawy, M. [2002]. "Flexural reliability of reinforced concrete bridge girders strengthened with carbon fiber-reinforced polymer laminates." *Journal of bridge engineering*, 7(5), 290–299.

Omer, M., Mostashari, A., Nilchiani, R., and Mansouri, M. [2012]. "A framework for assessing resiliency of maritime transportation systems." *Maritime Policy & Management*, 39, 685–703.

Omer, M., Nilchiani, R., and Mostashari, A. [2009]. "Measuring the resilience of the trans-oceanic telecommunication cable system." *IEEE Systems Journal*, 3(3), 295–303.

Orabi, W., El-Rayes, K., Senouci, A. B., and Al-Derham, H. [2009]. "Optimizing post-disaster reconstruction planning for damaged transportation networks." *Journal of Construction Engineering and Management*, 135(10), 1039–1048.

Orabi, W., Senouci, A. B., El-Rayes, K., and Al-Derham, H. [2010]. "Optimizing resource utilization during the recovery of civil infrastructure systems." *Journal of Management in Engineering*, 26(4), 237–246.

Ouyang, M. and Dueñas-Osorio, L. [2012]. "Time-dependent resilience assessment and improvement of urban infrastructure systems." *Chaos: An Interdisciplinary Journal of Nonlinear Science*, 22(3), 033122.

Ouyang, M., Dueñas-Osorio, L., and Min, X. [2012]. "A three-stage resilience analysis framework for urban infrastructure systems." *Structural Safety*, 3637, 23–31.

Özdamar, L. and Ulusoy, G. [1995]. "A survey on the resource-constrained project scheduling problem." *IIE transactions*, 27(5), 574–586.

Padgett, J. E. [2007]. "Seismic vulnerability assessment of retrofitted bridges using probabilistic methods." Ph.D. thesis, Georgia Institute of Technology, Atlanta, GA.

Padgett, J. E. and DesRoches, R. [2007]. "Bridge functionality relationships for improved seismic risk assessment of transportation networks." *Earthquake Spectra*, 23(1), 115–130.

Padgett, J. E. and DesRoches, R. [2009]. "Retrofitted bridge fragility analysis for typical classes of multispan bridges." *Earthquake Spectra*, 25(1), 117–141.

Padgett, J. E., Ghosh, J., and Dueñas-Osorio, L. [2013]. "Effects of liquefiable soil and bridge modelling parameters on the seismic reliability of critical structural components." *Structure and Infrastructure Engineering*, 9, 59–77.

Padgett, J. E., Nielson, B. G., and DesRoches, R. [2008]. "Selection of optimal intensity measures in probabilistic seismic demand models of highway bridge portfolios." *Earthquake Engineering & Structural Dynamics*, 37(5), 711–725.

Pang, Y., Wu, X., Shen, G., and Yuan, W. [2014]. "Seismic fragility analysis of cable-stayed bridges considering different sources of uncertainties." *Journal of Bridge Engineering*, 19, 04013015.

Park, R., Priestley, M., and Gill, W. D. [1982]. "Ductility of square-confined concrete columns." *Journal of the Structural Division*, 108(4), 929–950.

PEER. "Strong ground motion database. visited on September 1, 2013.

PennDOT [2010]. *Bridge Maintenance Manual, PUB 55*. Pennsylvania Department of Transportation, available at: http://www.dot.state.pa.us/Internet/Bureaus/pdBOS.nsf /FormsAndPubsHomePage?OpenFrameSet.

Petrini, F., Bontempi, F., and Giuliani, L. [2013]. "RISE: a method for design of resilient infrastructures and structures against emergencies." *Safety, Reliability, Risk and Life-Cycle Performance of Structures and Infrastructures*, G. Deodatis, B. R. Ellingwood, and D. M. Frangopol, eds., NY , June 16–20, CRC Press.

Piratla, K. R. [2016]. "Investigation of sustainable and resilient design alternatives for water distribution networks." *Urban Water Journal*, 13(4), 412–425.

Poland, C. D. [2009a]. *Building Resilient Communities: Fresh Challenges for Earthquake Professionals*. Lawson Lecture Series. UC Berkeley, Berkeley, CA, USA, April 14, 2009, complete video available at: http://seismo.berkeley.edu/news/lawson_lecture.html.

Poland, C. D. [2009b]. *The resilient city: defining what San Francisco needs from its seismic mitigation policies*. San Francisco Planning and Urban Research Association report, San Francisco, CA, USA.

Poland, C. D. [2011]. *Building Disaster Resilient Communities*. Fazlur R. Khan Distinguished Lecture Series. Lehigh University, Bethlehem, PA, USA, April 8, 2011, complete video available at: http://www.lehigh.edu/~infrk.

Porter, K. A. [2004]. "A survey of bridge practitioners to relate damage to closure." *Report EERL 2004-07*.

Presidential Policy Directive [2013]. *Critical Infrastructure Security and Resilience. PPD-21, Released February 12, 2013*. available at: http://www.whitehouse.gov/the-press-office/2013/02/12/presidential-policy-directive-critical-infrastructure-security-and-resil, (visited on August 27, 2015).

Pritsker, A. A. B., Waiters, L. J., and Wolfe, P. M. [1969]. "Multiproject scheduling with limited resources: A zero-one programming approach." *Management Science*, 16(1), 93–108.

Ramirez, J. A., Frosch, R. J., Sozen, M. A., and Turk, A. M. [2000]. *Handbook for the post-earthquake safety evaluation of bridges and roads*. School of Civil Engineering, Purdue University,Prepared for the Indiana Department of Transportation, INDOT.

Reed, D., Kapur, K., and Christie, R. [2009]. "Methodology for assessing the resilience of networked infrastructure." *IEEE Systems Journal*, 3(2), 174–180.

Righi, A. W., Saurin, T. A., and Wachs, P. [2015]. "A systematic literature review of resilience engineering: Research areas and a research agenda proposal." *Reliability Engineering & System Safety*, 141, 142–152.

Rinaldi, S. M., Peerenboom, J. P., and Kelly, T. K. [2001]. "Identifying, understanding, and analyzing critical infrastructure interdependencies." *IEEE Control Systems*, 21(6), 11–25.

Rix, G. and Fernandez-Leon, J. [2004]. "Synthetic ground motions for memphis, tn." *Æ http://www. ce. gatech. edu/research/mae_ground_ motionæ (Jul. 5, 2008)*.

Rodriguez-Nikl, T. [2015]. "Linking disaster resilience and sustainability." *Civil Engineering and Environmental Systems*, 32(1-2), 157–169.

Rose, A. and Liao, S.-Y. [2005]. "Modeling regional economic resilience to disasters: A computable general equilibrium analysis of water service disruptions." *Journal of Regional Science*, 45(1), 75–112.

Rothlauf, D. F. [2006]. "Representations for genetic and evolutionary algorithms." *Representations for Genetic and Evolutionary Algorithms*, Springer Berlin Heidelberg.

Sause, R. [2014]. Personal communication.

Saydam, D., Bocchini, P., and Frangopol, D. M. [2013]. "Time-dependent risk associated with deterioration of highway bridge networks." *Engineering Structures*, 54, 221–233.

Shafieezadeh, A., Ramanathan, K., Padgett, J. E., and DesRoches, R. [2012]. "Fractional order intensity measures for probabilistic seismic demand modeling applied to highway bridges." *Earthquake Engineering & Structural Dynamics*, 41(3), 391–409.

Sheffi, Y. [1985]. *Urban Transportation Networks: Equilibrium Analysis With Mathematical Programming Methods*. Prentice Hall.

Shinozuka, M., Murachi, Y., Dong, X., Zhou, Y., and Orlikowski, M. J. [2003]. "Effect of seismic retrofit of bridges on transportation networks." *Earthquake Engineering and Engineering Vibration*, 2(2), 169–179.

Shome, N. [1999]. "Probabilistic seismic demand analysis of non-linear structures." Ph.D. thesis, Stanford University, Stanford University.

Shome, N. and Cornell, A. [1999]. *Probabilistic Seismic Demand Analysis of Nonlinear Structures. Reliability of Marine Structures*. Department of Civil and Environmental Engineering Stanford University, California Program Report No. RMS-35.

Sohn, J. [2006]. "Evaluating the significance of highway network links under the flood damage: An accessibility approach." *Transportation Research Part A: Policy and Practice*, 40, 491–506.

Soltani-Sobh, A., Heaslip, K., and El Khoury, J. [2015]. "Estimation of road network reliability on resiliency: An uncertain based model." *International Journal of Disaster Risk Reduction*, 14, 536–544.

Soltani-Sobh, A., Heaslip, K., Stevanovic, A., El Khoury, J., and Song, Z. [2016]. "Evaluation of transportation network reliability during unexpected events with multiple uncertainties." *International Journal of Disaster Risk Reduction*, 17, 128–136.

Tabandeh, A. and Gardoni, P. [2014]. "Probabilistic capacity models and fragility estimates for rc columns retrofitted with frp composites." *Engineering Structures*, 74, 13–22.

The Mathworks Inc. [2014]. *Matlab version 8.3 - R2014a*. Natick, Massachusetts.

Tondini, N. and Stojadinovic, B. [2012]. "Probabilistic seismic demand model for curved reinforced concrete bridges." *Bulletin of Earthquake Engineering*, 10(5), 1455–1479.

Torbol, M. and Shinozuka, M. [2014]. "The directionality effect in the seismic risk assessment of highway networks." *Structure and Infrastructure Engineering*, 10(2), 175–188.

Tuzun Aksu, D. and Ozdamar, L. [2014]. "A mathematical model for post-disaster road restoration: Enabling accessibility and evacuation." *Transportation Research Part E: Logistics and Transportation Review*, 61, 56–67.

USGS [2013]. *U.S. Geological hazard science center*. United States Geological Service, available at: http://earthquake.usgs.gov/hazards/?source=sitenav.

Venkittaraman, A. and Banerjee, S. [2014]. "Enhancing resilience of highway bridges through seismic retrofit." *Earthquake Engineering & Structural Dynamics*, 43(8), 1173–1191.

Vogus, T. J. and Sutcliffe, K. M. [2007]. "Organizational resilience: towards a theory and research agenda." *Systems, Man and Cybernetics, 2007. ISIC. IEEE International Conference on*, IEEE, 3418–3422.

Vugrin, E. D., Turnquist, M. A., and Brown, N. J. [2014]. "Optimal recovery sequencing for enhanced resilience and service restoration in transportation networks." *International Journal of Critical Infrastructures*, 10(3), 218–246.

Wang, Z., Dueñas-Osorio, L., and Padgett, J. E. [2013a]. "Seismic response of a bridgesoil-foundation system under the combined effect of vertical and horizontal ground motions." *Earthquake Engineering & Structural Dynamics*, 42, 545–564.

Wang, Z., Padgett, J. E., and Dueñas-Osorio, L. [2013b]. "Influence of vertical ground motions on the seismic fragility modeling of a bridge-soil-foundation system." *Earthquake Spectra*, 29, 937–962.

Wilkinson, S., Free, M., Grant, D., Boon, D., Paganoni, S., Mason, A., Williams, E., Fraser, S., and Haskell, J. [2011]. "The Christchurch, New Zealand earthquake of 22 February 2011." *Report no.*, Earthquake Field Investigation Team, Institution of Structural Engineers.

Yanev, B. [2007]. *Bridge management*. John Wiley & Sons, Inc., Hoboken, NJ.

Zhang, J. and Huo, Y. [2009]. "Evaluating effectiveness and optimum design of isolation devices for highway bridges using the fragility function method." *Engineering Structures*, 31, 1648–1660.

Zhang, J., Huo, Y., Brandenberg, S. J., and Kashighandi, P. [2008]. "Effects of structural characterizations on fragility functions of bridges subject to seismic shaking and lateral spreading." *Earthquake Engineering and Engineering Vibration*, 7(4), 369–382.

Zhou, Y., Banerjee, S., and Shinozuka, M. [2010]. "Socio-economic effect of seismic retrofit of bridges for highway transportation networks: a pilot study." *Structure and Infrastructure Engineering*, 6(1-2), 145–157.

Vita

Aman Karamlou was born in Tehran, Iran in 1983. He received his Bachelor of Science degree in Civil Engineering from Azad University of Tehran (Central Branch) in 2007. In 2010, he completed his Masters of Science degree in Structural Engineering from AmirKabir University of Technology. In his Masters thesis, he worked on the seismic performance of rectangular and L-shaped Insulating Concrete Form (ICF) panels. He performed extensive experimental and numerical studies on the cyclic behavior of ICF shear walls. Aman joined Lehigh University in 2011 to continue his education toward PhD. He will receive his PhD in January 2017.